HZDR-051

SPECTRAL HISTORY MODELING IN THE REACTOR DYNAMICS CODE DYN3D

Yurii Bilodid

Wissenschaftlich-Technische Berichte
HZDR-051· ISSN 2191-8708

WISSENSCHAFTLICH-
TECHNISCHE BERICHTE

HZDR
HELMHOLTZ
ZENTRUM DRESDEN
ROSSENDORF

Wissenschaftlich-Technische Berichte
HZDR-051

Yurii Bilodid

SPECTRAL HISTORY MODELING IN THE REACTOR DYNAMICS CODE DYN3D

HZDR

HELMHOLTZ
ZENTRUM DRESDEN
ROSSENDORF

Druckausgabe: ISSN 2191-8708

Elektronische Ausgabe: ISSN 2191-8716

Qucosa: http://fzd.qucosa.de/startseite/

Die vorliegende Arbeit wurde sowohl als Dissertation an der Fakultät Maschinenwesen der Technischen Universität Dresden sowie als Wissenschaftlich-Technischer Bericht des Helmholtz-Zentrum Dresden – Rossendorf mit der Berichtsnummer **HZDR-051** veröffentlicht.

2014

Herausgegeben vom

Helmholtz-Zentrum Dresden - Rossendorf

Bautzner Landstr. 400

01328 Dresden

Germany

Spectral History Modeling in the Reactor Dynamics Code DYN3D

Der Fakultät Maschinenwesen

der

Technischen Universität Dresden

zur

Erlangung des akademischen Grades

Doktoringenieur (Dr.-Ing.)

angenommene Dissertation

Dipl.-Ing. Yurii Bilodid

Tag der Einreichung:	18.06.2013
Tag der Verteidigung:	16.05.2014
Gutachter:	Herr Prof. Dr.rer.nat. F.-P. Weiß
	Herr Prof. Dr.-Ing.habil. A. Hurtado
Vorsitzender der Promotionskommission:	Herr Prof. Dr.rer.nat.habil. S. Odenbach

To Yuri M. Bilodid the Elder

Abstract

A new method of treating spectral history effects in reactor core calculations was developed and verified in this dissertation. The nature of history effects is a dependence of fuel properties not only on the burnup, but also on the local spectral conditions during burnup. The basic idea of the proposed method is the use of the plutonium-239 concentration as the spectral history indicator. The method was implemented in the reactor dynamics code DYN3D and provides a correction for nodal cross sections according to the local spectral history.

A verification of the new method was performed by single-assembly calculations in comparison with results of the lattice code HELIOS. The application of plutonium-based history correction significantly improves the cross section estimation accuracy both for UOX and MOX fuel, with quadratic and hexagonal geometry.

The new method was applied to evaluate the influence of history effects on full-core calculation results. Analysis of a PWR equilibrium fuel cycle has shown a significant effect on the axial power distribution during a whole cycle, which causes axial temperature and burnup redistributions. The observed neutron flux redistribution improves neutron economy, so the fuel cycle is longer than in calculations without history corrections. Analyses of hypothetical control rod ejection accidents have shown a minor influence of history effects on the transient course and safety relevant parameters.

Zusammenfassung

Eine neue Methode zur Modellierung der Spektralgeschichte als Bestandteil von Kernreaktorberechnungen wurde in dieser Dissertation entwickelt und verifiziert. Die spektrale Abbrandgeschichte hat praktische Bedeutung für die Brennstoffeigenschaften, die nicht nur von der Höhe des Abbrandwertes, sondern auch vom lokalen Neutronenspektrum während des Abbrandprozesses abhängen. Die Grundidee der vorgeschlagenen Methode besteht in der Nutzung der lokalen Plutonium-239-Konzentration als quantitativen Indikator für die spektrale Abbrandgeschichte. Die Methode wurde in das Reaktordynamikprogramm DYN3D implementiert; sie gewährleistet eine Korrektur der nodalen Wirkungsquerschnitte gemäß der lokalen spektralen Abbrandgeschichte.

Eine Verifikation der neuen Methode wurde mit Einzelbrennelementberechnungen im Vergleich zu Ergebnissen des Zellabbrandprogramms HELIOS durchgeführt. Die Korrektur auf der Basis der Plutoniumkonzentration verbessert die Genauigkeit der Wirkungsquerschnitte signifikant, sowohl für UOX als auch für MOX, in quadratischer und hexagonaler Geometrie.

Die neue Methode wurde für die Bestimmung des Einflusses der spektralen Abbrandgeschichte auf die Modellierung ganzer Reaktorkerne angewandt. Die Analyse eines DWR-Gleichgewichtszyklus zeigt eine signifikante Auswirkung auf die axiale Leistungsverteilung während eines ganzen Zyklus. Über die axiale Temperaturverteilung (Rückkopplung) entsteht wiederum eine Rückwirkung auf die Abbrandverteilung selbst. Die beobachtete modifizierte Neutronenflussverteilung verbessert die Neutronenökonomie, sodass der Brennstoffzyklus länger wird, verglichen mit Berechnungen ohne Berücksichtigung der Abbrandgeschichte. Analysen von hypothetischen Stabauswurfszenarien ergaben einen nur geringen Einfluss der Abbrandgeschichte auf Transientenverlauf und sicherheitsrelevante Parameter.

Contents

1 Introduction

Nuclear reactor simulations play a key role in reactor design, operation and safety assurance. The goal of reactor simulations is to predict reactor behavior in normal daily operation and in different types of operational or accidental transient. The state of a nuclear reactor is determined by the distribution of neutrons in the reactor core, so the balance of neutrons production, destruction and leakage is considered by reactor simulation tools.

The set of simulation tools utilizes a number of methods of neutron transport consideration; each of them is applied to its own task accordingly to advantages and limitations of this method.

Monte Carlo methods are widely used for the steady-state modeling of very complex three-dimensional heterogeneous systems, including full reactor cores. Some recent Monte Carlo codes are able to perform burnup calculations [Leppänen, 2009] and steady-state calculation with thermo-hydraulic feedback [Kotlyar, 2009]. The main limitation of Monte Carlo methods is high computational cost, which makes application of Monte Carlo to transient calculations impossible so far.

The state-of-art in transient processes simulations is the usage of three-dimensional (3D) coupled neutron-kinetics – thermo-hydraulics nodal codes [Smith, 2013]. Such codes divide the reactor core volume into nodes which are handled as homogeneous. 3D time-dependent neutron transport is solved using fast and simple diffusion or simplified transport methods with thermo-hydraulic feedback. This approach allows to simulate transients and accidents in the reactor core with high local nonuniformity (e.g. control rod ejection). Some of considered transient are involving not only reactor core but all major equipment on a primary and secondary sides of a power plant (e.g. loss of coolant and steam line break accidents). Simulation of such processes requires coupling of 3D nodal codes with so-called system codes, which describe thermo-hydraulics and operational logic of the whole plant. Consideration of transients with complicated coolant mixing phenomena inside a reactor pressure vessel (e.g. boron dilution) requires coupling of nodal code with Computed Fluid Dynamics (CFD) code.

Lattice codes are used to prepare for nodal codes properties of homogeneous nodes, which usually represent an axial layer of fuel assembly. Lattice codes solve neutron transport in fuel assembly heterogeneous lattice utilizing high-order transport methods with fine spatial and energy discretization. Results are homogenized and compiled into few-group cross sections libraries, which represent dependence of nuclear fuel properties on operational parameters and grade of fuel depletion. Influence of so-called spectral history effects on fuel properties is the topic of this thesis.

As mentioned above, nuclear reactor analysis is a multi-physics task, which involves a set of simulation tools. To insure continuous improvement of simulation tools and provide general

platform for codes interaction and data exchange, the European Platform for Nuclear Simulations (NURESIM and NURISP Projects) is founded by European Commission [Chauliac, 2009].

The NURESIM platform incorporates the latest advances in neutron kinetics, thermal-hydraulics and fuel modeling. The different codes and solvers are coupled by a common data structure. The platform provides generic pre-processing, post-processing, statistical sensitivity and uncertainty analyses tools and informatics environment for testing and comparing different codes. The NURESIM platform and the individual models, solvers and codes has been validated through challenging applications corresponding to nuclear reactor situations, and including reference calculations, experiments and plant data.

18 organizations from 13 countries are involved in the NURESIM project. The contribution of the Helmholtz-Zentrum Dresden-Rossendorf (HZDR) to Core-Physics sub-project of NURESIM is the Advanced Kinetics Code DYN3D.

The goal of this thesis was to develop a new method of accounting for spectral history effects, to implement this method into DYN3D, to validate it and to evaluate the influence of history effect on reactor core parameters, and therefore to enhance the accuracy of the code predictions in steady-state and burnup calculations (power distribution, fuel cycle length) as well as in transient simulations (prediction of safety-relevant parameters).

Chapter 1 briefly outlines the place of reactor dynamics codes in the structure of nuclear reactor analysis and the place of this work in the development of the reactor dynamics code DYN3D.

Chapter 2 reviews the contemporary practice of reactor simulations. The 2-step concept of reactor simulations, cross section libraries approach and codes used for this investigation are described here.

Chapter 3 is focused on spectral history effects. The first part of this chapter describes the nature and physical mechanism of these effects, while the second part reviews existing solutions, implemented in other code systems.

Chapter 4 consists of three sections. The first one presents the idea and methodology of using the plutonium-239 concentration as the spectral history indicator. Section 4.2 describes the implementation of the developed method into the HZDR reactor dynamic code DYN3D. The third section briefly compares the new method with existing solutions.

The verification of the method by single-assembly calculations for various fuel types is a topic of Chapter 5. Cross sections values and multiplication factors calculated using plutonium-correction were compared with those calculated by the lattice transport code HELIOS.

Chapters 6 and 7 is dedicated to full-core calculations applying the new method. Chapter 6 evaluates the influence of modified cross sections on results on steady-state and cycle-burnup calculations, while Chapter 7 considers transient simulations.

Chapter 8 summarizes the current work and presents the main conclusions based on the obtained results.

2 Contemporary practice in reactor simulations

2.1 Chain of calculations

Nuclear reactors are facilities in which a controlled nuclear fission chain reaction is sustained. The produced nuclear energy is extracted for generation of electricity or heat. In such a reactor, neutrons are interacting with the reactor materials inducing nuclear fission and suffering absorption or scattering. The reactor materials are nuclear fuel, coolant/moderator, structural materials, and neutron absorbing materials. The structural arrangement of reactor materials and their content is changing depending on the life-cycle of the fuel or on the operational mode of the reactor.

2.1.1 Basic definitions

The required quantity in nuclear reactor simulations is the **neutron density** as a function of space, energy and time $n(\vec{r},E,t)$. Another important quantity in reactor theory is the **neutron flux**:

$$\phi(\vec{r},E,t) = v \cdot n(\vec{r},E,t), \tag{2.1}$$

where v is the scalar velocity.

The consideration of anisotropic processes requires the introduction of an **angular neutron flux**:

$$\varphi(\vec{r},E,\vec{\Omega},t) = v \cdot n(\vec{r},E,\vec{\Omega},t), \tag{2.2}$$

where the **angular neutron density** $n(\vec{r},E,\vec{\Omega},t)\cdot d\vec{r}\cdot dE\cdot d\vec{\Omega}$ is an expected number of neutrons in the volume $d\vec{r}$ about point $\vec{r}$, in the energy interval dE about E, moving in direction $\vec{\Omega}$ in solid angle $d\vec{\Omega}$ at time t.

The **microscopic cross section** $\sigma_{i,j}$ is a value which characterizes the probability of a certain reaction i (absorption, fission, scattering, etc.) between neutron and nucleus of nuclide j.

Microscopic cross sections are used in determining the nuclear **reaction rate**:

$$R_i = \phi \sum_j \sigma_{i,j} N_j = \phi \Sigma_i, \tag{2.3}$$

where R_i - number of reactions of type i, per (s·cm^3);

ϕ - neutron flux, 1/(s·cm^2);

σ_{ij} - microscopic cross section of nuclei j for reaction i, barns or cm^2;

N_j – number density of nuclide j, atoms/cm^3;

$\Sigma_i = \sum_j \sigma_{i,j} N_j$ - **macroscopic cross-section** for reaction i, 1/cm.

2.1.2 Neutron energy spectrum

Neutrons are born in fission reaction with energy about 2 MeV. In Light Water Reactors (LWR) most of these fast prompt fission neutrons get from the fuel to the water moderator and suffer collisions with light nuclei slowing down to the thermal energy level. Distributions of neutrons by their energy is called **neutron energy spectrum**. A typical LWR neutron spectrum is shown in Fig. 2.1. Usually, in nuclear reactor simulations the neutron energy discretization into energy groups is applied. Lattice codes perform **multi-group** (up to ~200) calculations of cross sections and other lattice parameters, afterwards the group cross sections are collapsed to only a **few groups** (2-16) for the use by coarse-mesh codes.

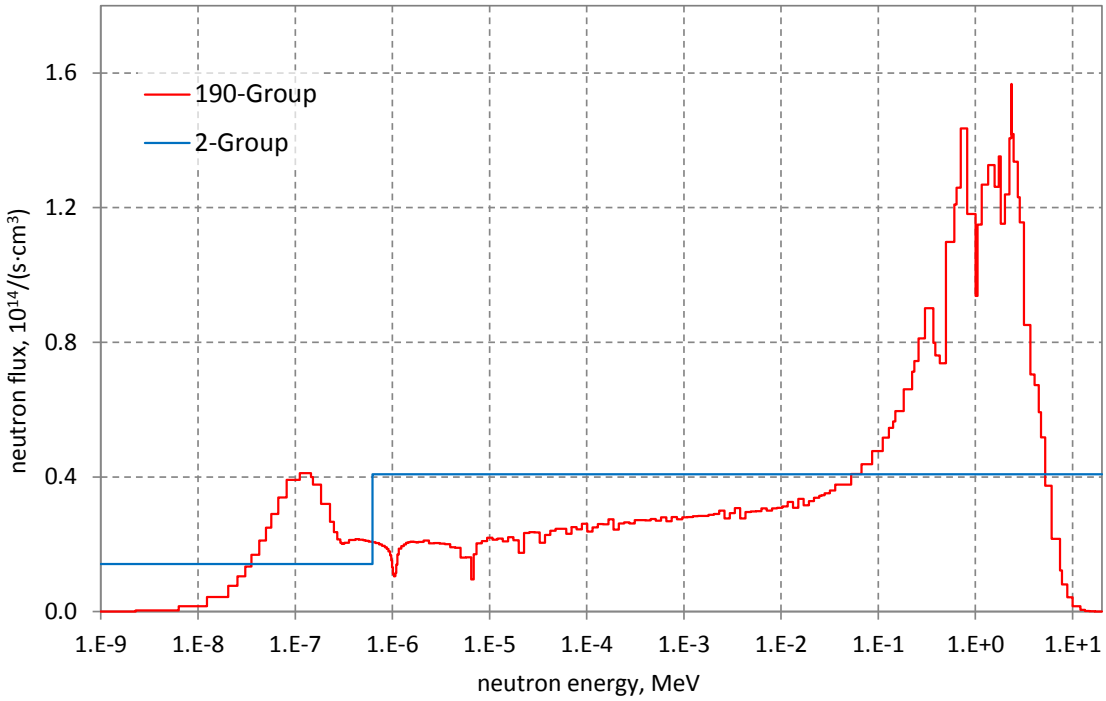

Fig. 2.1 Typical neutron spectrum for LWR.

Changes in operational parameters (water and fuel temperatures, boron concentration, power level, control rod movements etc.) influence the neutron spectrum. Increasing or decreasing of the fast portion of spectrum is called **spectrum hardening** or **softening**, respectively. Spectrum hardening corresponds to increasing average neutron energy.

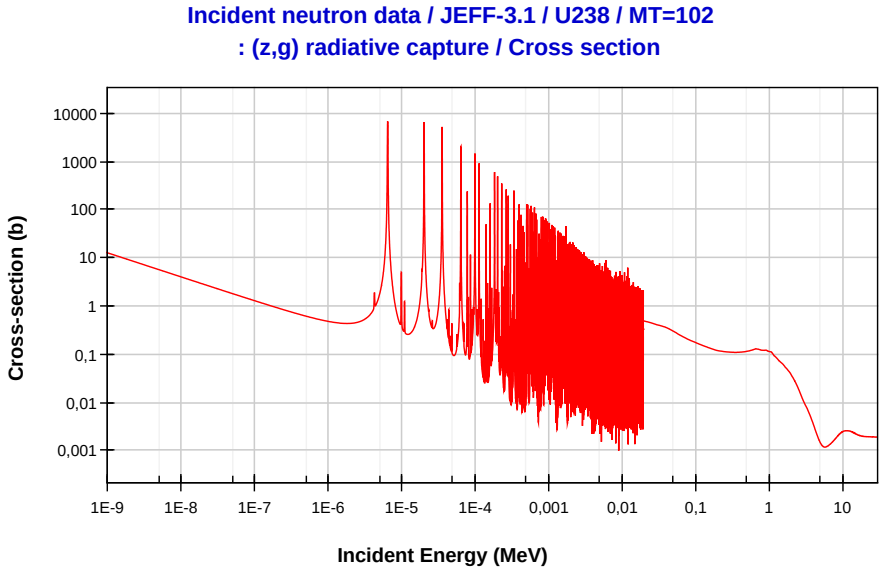

Fig. 2.2 Radiative capture cross section of ^{8}U. [NEA, 2010]

Microscopic cross sections depend on the neutron energy as illustrated by the radiative capture cross section of ^{238}U in Fig. 2.2. Absorption cross section of most nuclides in the low-energy region is inversely proportional to $\sqrt{E}$, i.e. varies as *1/v*. Above *1/v* region, there is a region of resonances – the sharp peaks of cross section values for certain neutron energies. The resonance energies are corresponding to the inner structure of the compound nucleus which is formed in the interaction [Lamarsh, 2001].

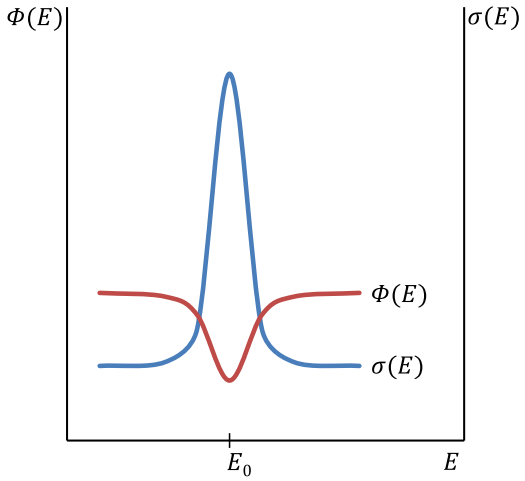

Fig. 2.3 Resonance self-shielding. [Stacey, 2000]

Much higher neutron absorption at resonance energy cause the neutron flux to dip sharply over the range of the resonance (the flux depression), as illustrated in Fig. 2.3. This reduction in the neutron flux in the energy range of the resonance reduces the resonance absorption, since the strong absorption of the resonance tends to shield the absorber nuclei from neutrons with energies around resonance energy E_0, a phenomenon known as energy **self-shielding**. One can see the flux depression in the middle part of the spectrum in Fig. 2.1.

During reactor operation the fuel composition changes as fissile isotopes are consumed and fission products and actinides are produced. The change of fuel composition due to the neutron flux exposure is commonly referred to as fuel **burnup**, which is the amount of energy usually given in Megawatt*day produced in fuel per kilogram of fuel initial heavy metal (MWd/kgHM).

2.1.3 Neutron transport

The main objective of reactor physics is to determine the distribution of the rates of the different nuclear reactions in the reactor. For that, the motion of neutrons and their interactions with the reactor materials of various kinds have to be taken into account.

An accurate model which describes the distribution of neutrons in a medium like a reactor is the Boltzmann transport equation [Nam Zin Cho, 2005]:

$$\begin{aligned}&\frac{1}{v}\frac{\partial}{\partial t}\varphi(\vec{r},E,\vec{\Omega},t)+\vec{\Omega}\cdot\nabla\varphi(\vec{r},E,\vec{\Omega},t)+\Sigma_t(\vec{r},E)\varphi(\vec{r},E,\vec{\Omega},t)\\&=\int_{4\pi}d\vec{\Omega}'\int_0^\infty dE'\Sigma_s(\vec{r},E'\to E,\vec{\Omega}'\cdot\vec{\Omega})\varphi(\vec{r},E',\vec{\Omega}',t)\\&+\frac{\chi(E)}{4\pi}\int_{4\pi}d\vec{\Omega}'\int_0^\infty dE'\nu\Sigma_f(\vec{r},E')\varphi(\vec{r},E',\vec{\Omega}',t)+q(\vec{r},E,\vec{\Omega},t)\end{aligned} \tag{2.4}$$

Here, Σ_t is the macroscopic total cross section, Σ_f is the macroscopic fission cross section, χ is the energy spectrum of the neutrons emerging from fission; Σ_s is the differential macroscopic scattering cross section describing the transfer probability that an incident neutron of initial direction $\vec{\Omega}'$ and energy E' emerges from a possible collision with direction $\vec{\Omega}$ and energy E.

In writing down Eq. (2.4) it is assumed that the medium is isotropic and the fission neutrons are emitted isotropically.

This equation describes the balance of neutrons in an elementary volume. The first term on the left side is the change of the neutron density in time; the second term describes leakage of neutrons outside considered volume; and the third term is the loss of neutrons due to interactions (adsorption and scattering). The right part of Eq. (2.4) describes income of neutrons: the first term is the number of neutrons suffering scattering that changes their energy and direction into $E,\vec{\Omega}$; the second term is the number of neutrons generated by fission; and the third term is the external source of neutrons.

The problem of finding a solution to Eq. (2.4) is nontrivial and requires sophisticated numerical methods. This is due to the complicated energy and space dependency of the cross sections and the angular dependency of the scattering cross section and the neutron flux.

The art of reactor simulations is to simplify the problem to be solvable by numerical methods in reasonable computing time, at the same time taking into account all essential effects playing a role in the reactor performance.

A commonly used simplification is to represent the angular dependency of the scattering cross section in Legendre components [Ronen, 1986]:

$$\Sigma_s(\vec{r}, E' \to E, \mu_0) = \sum_{l=0}^{L} \frac{2l+1}{4\pi} \Sigma_{sl}(\vec{r}, E' \to E) P_l(\mu_0) \tag{2.5}$$

where P_l is the l-th Legendre polynomial and $\mu_0 = \vec{\Omega}' \cdot \vec{\Omega}$ is the cosine of the scattering angle. The truncation index L should be large enough to provide an adequate representation of the differential cross section with the finite Legendre expansion.

Eq. (2.4) is of continuous form of the independent variables. For numerical solution energy and spatial discretizations are applied.

The **energy discretization** is done by the multigroup approximation: the energy range (from zero to maximum energy of neutron) is divided into intervals called energy groups. The group fluxes are defined by integrating of continuous flux over group energy interval g:

$$\phi_g = \int_g \phi(E) dE \tag{2.6}$$

The group-averaged cross sections are defined by [Stacey, 2000]:

$$\Sigma_g = \frac{\int_g \Sigma(E)\phi(E) dE}{\phi_g} \tag{2.7}$$

Spatial discretization divides the whole reactor core volume into finite volume elements V_i. Similar to the energy discretization, the flux in element i is defined by integrating over volume V_i:

$$\phi_i = \int_{V_i} \phi(\vec{r}) d\vec{r} \tag{2.8}$$

and the element-averaged cross sections are:

$$\Sigma_i = \frac{\int_{V_i} \Sigma(\vec{r})\phi(\vec{r}) dE}{\phi_i} \tag{2.9}$$

The total of the volumes V_i creates a mesh. Fig. 2.4 represents typical spatial discretization levels [Nam Zin Cho, 2005]: the **coarse mesh** has the size of a fuel assembly or part of assembly and the **fine mesh** cell is determined e.g. by the fuel rod and surrounding moderator.

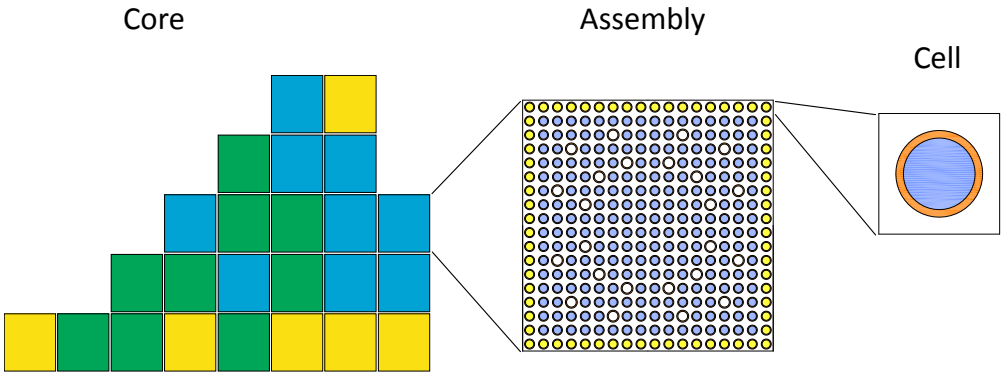

Fig. 2.4 Levels of spatial discretization.

Nodal methods are based on a large coarse mesh (of an assembly size) called “node” whose properties are spatially constant inside the nodes, so homogenization is needed. The **homogenization** provides equivalent homogeneous properties of a node that is physically heterogeneous (see Fig. 2.5). This simplifies the calculation effort but gives an “equivalent” solution for important parameters (such as reactions rates of the node and multiplication factor of the core).

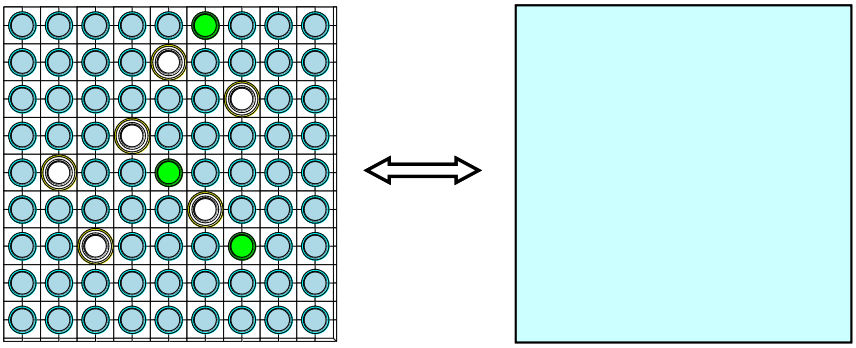

Fig. 2.5 Homogenization of fuel assembly

Even with these approximations modern numerical methods do not allow to solve the time-dependent transport equation for a whole reactor. For reactor dynamics calculation mainly the diffusion approximation is used.

2.1.4 Neutron diffusion

The diffusion equation is derived from Eq. (2.4) by limiting of Legendre components in Eq (2.5) to L=1 (P_1 approximation) and applying Fick’s law:

$$\vec{J}(\vec{r},E) = -D(\vec{r},E)\cdot\nabla\phi(\vec{r},E) \tag{2.10}$$

where the scalar neutron flux is

$$\phi(\vec{r},E) = \int \varphi(\vec{r},E,\vec{\Omega})d\vec{\Omega} \tag{2.11}$$

and the diffusion coefficient

$$D = \frac{1}{3(\Sigma_t - \overline{\mu}_0\Sigma_s)} \tag{2.12}$$

where Σ_t and Σ_s are the total and scattering cross section and $\overline{\mu_0}$ is the mean cosine of the scattering angle.

So, the multigroup diffusion equation can be written in the form:

$$\frac{1}{v_g}\frac{\partial \phi_g(\vec{r},t)}{\partial t} + \nabla \vec{J}_g(\vec{r},t) + \Sigma_{r,g}(\vec{r},t)\phi_g(\vec{r},t) = \sum_{g' \neq g}^{G} \Sigma_{s,g' \to g}(\vec{r},t)\phi_{g'}(\vec{r},t) + \frac{\chi_g}{k}\sum_{g'=1}^{G} \nu\Sigma_{f,g'}(\vec{r},t)\phi_{g'}(\vec{r},t) + S_g(\vec{r},t) \tag{2.13}$$

where $\Sigma_{r,g}$ denotes the removal cross section, consistent of neutron absorption in the group g and neutron scattering from the group g:

$$\Sigma_{r,g} = \Sigma_{a,g} + \sum_{g' \neq g}^{G} \Sigma_{s,g \to g'} \tag{2.14}$$

The diffusion equation (2.13) is much simpler to solve than the transport equation (2.4), but it has significant limitations due to the following assumptions: the probability of neutron absorption is much less than that of scattering, linear spatial variation of the neutron distribution, isotropic scattering [Stacey, 2000]. The first assumption is true for the moderator regions of a reactor, but not for the fuel and control elements; the third assumption is true for heavy nuclei, but false for light ones. However, diffusion theory is widely used in nuclear reactor analysis and provides sufficiently accurate predictions for the most practical tasks. This is possible because complicated heterogeneous structures are replaced in nodal methods by a homogenized mixture with effective averaged "equivalent" cross sections and diffusion coefficients, which are calculated by more accurate transport theory [Ronen, 1986].

2.1.5 Chain of calculations

To perform whole-core dynamics calculations multigroup diffusion equation (2.13) is solved using nodal methods in coarse-mesh spatial discretization with nodes having size of a vertical section of an assembly (or part of assembly). In this case the cross sections and diffusion coefficients of Eq. (2.13) are nodes (i.e. fuel assemblies) properties which are constant inside the nodes.

Thereby reactor simulations are performed in two steps:

- the first step is determining homogenized fuel (nodes) diffusion properties;
- second step – performing core dynamics calculations.

The first step is performed using so-called lattice burnup codes like CASMO [Rhodes, 2006], HELIOS [Ivanov, 2004], APOLLO [Sanchez, 1988], etc. These codes solve the steady-state neutron transport equation for a single fuel assembly (with reflective boundary conditions) in 2-dimensional geometry with fine energy and spatial discretization. Results of these calculations are condensed to few-group assembly-homogenized fuel diffusion properties (cross sections and diffusion

coefficients) [Cacuci, 2010]. These macroscopic cross sections are stored in cross section libraries (XS-libraries).

XS-libraries are used by reactor dynamic codes like DYN3D [Grundmann, 2000], SIMULATE [Croninget, 2005], PARCS [Downar, 2002], etc. to perform the second step of reactor core simulation.

Thereby an XS-library serves as an interface between the lattice and the reactor dynamics codes. The library represents the fuel properties dependence on operational parameters (moderator temperature and density, fuel temperature, boron concentration, control rod presence, etc.) and depletion (burnup).

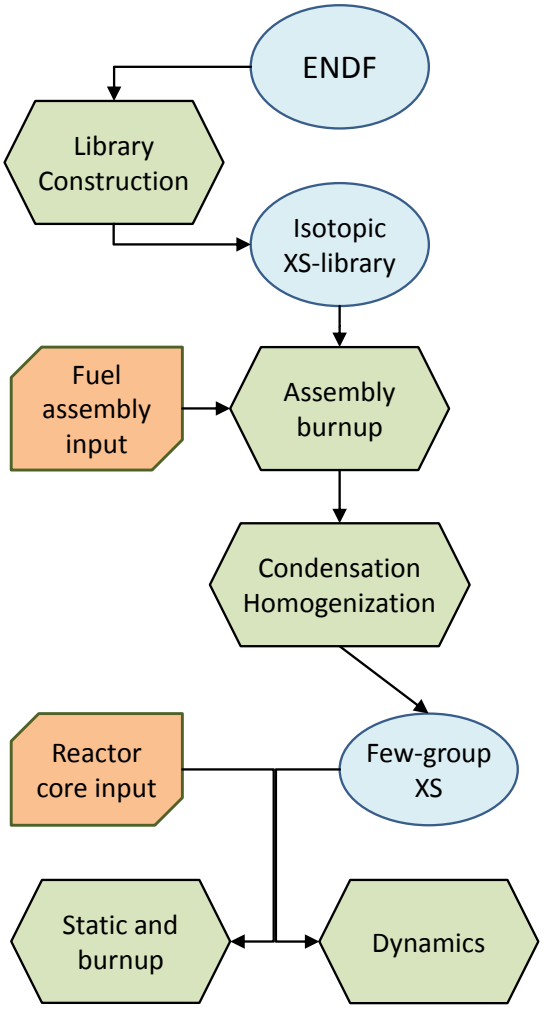

	Groups	Dimensions	Methods
A	1000s	0,1	Transport theory, Monte Carlo
B	40-500	2	Transport theory, Monte Carlo
C	2-16	3	Diffusion theory, SP3

Fig. 2.6 Calculation flow of reactor core design.

Fig. 2.6 shows a typical calculation flow involved in reactor core design and analysis [Stamm'ler, 1983]. Phase A in this figure is the preparation of a multigroup nuclear data library input for lattice codes. This phase is outside the consideration of this study. Phase B corresponds to the first step of reactor simulation, described above, while phase C represents the second step.

2.2 Used codes

In this study, the transport-theory lattice burnup code HELIOS-1 [HELIOS, 2003] (see section 2.2.2) is used to obtain fuel-assembly properties under varying conditions and to produce XS-libraries for the 3D neutron kinetics diffusion code DYN3D [Grundmann, 2005] (see section 2.2.1)

2.2.1 DYN3D

DYN3D is a **DYN**amical **3-D**imensional code for Light Water Reactor (LWR) cores developed in the Institute of Safety Research of Helmholtz-Zentrum Dresden-Rossendorf. The three-dimensional neutronic model utilizes nodal expansion methods (NEM) to solve the two-group neutron diffusion equation for Cartesian [Grundmann, 1995a] and hexagonal [Grundmann, 1999] geometry.

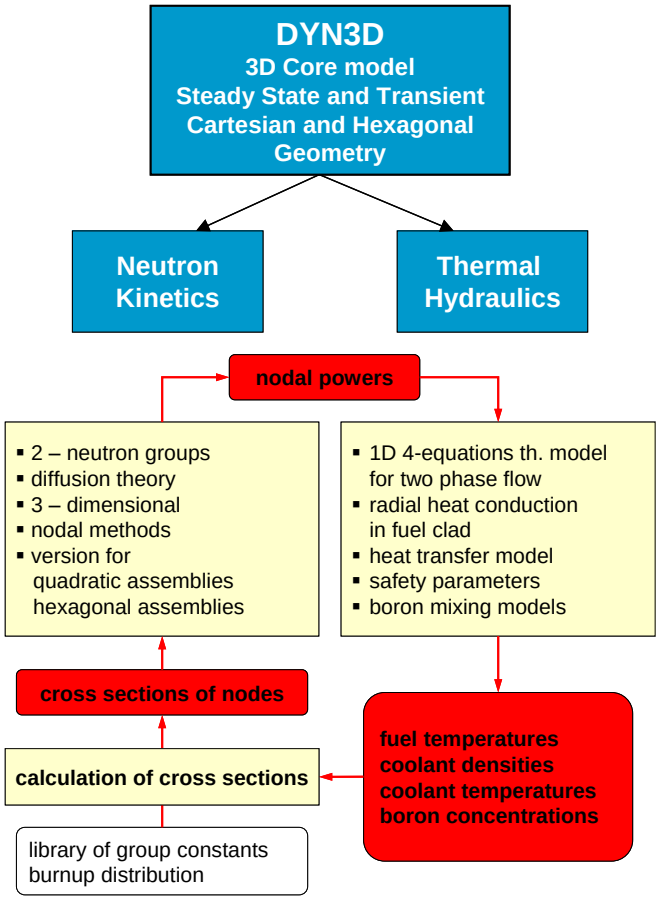

Fig. 2.7 DYN3D structure.

The neutron and heat flux distributions, temperatures fields, reactivity coefficients and other safety-relevant parameters can be calculated in the steady state with eigenvalue, the steady state with fixed source and the transients.

For the solution of the neutron diffusion equations, the reactor core is divided into prism volume elements which are called nodes. The base areas of these prisms are determined by the geometry of the (quadratic or hexagonal) fuel elements. The axial division of the core into layers defines the height of the prisms.

Cross section libraries generated by different lattice codes as CASMO, HELIOS or NESSEL [Heinrich, 1981] are linked to DYN3D (see section 2.3).

The neutron kinetic model is based on the solution of the three-dimensional two-group neutron diffusion equation by nodal expansion methods. It is assumed that the macroscopic cross sections are spatially constant in a node. These cross sections are generated in a homogenization procedure by a lattice code (see section 2.1.3)

In Cartesian geometry, three one-dimensional diffusion equations are solved for the transverse integrated fluxes of the nodes in the three directions x, y, z. In the case of hexagonal-z geometry, a two-dimensional diffusion equation in the hexagonal plane and a one-dimensional equation of the z-direction are solved for the transverse integrated fluxes. In each energy group, the one-dimensional equations are solved with the help of flux expansions in polynomials up to 2^{nd} order and exponential functions being the solutions of the homogeneous Helmholtz equations. The fission source and the scattering source as well as the leakage terms are approximated by the polynomials. Considering the 2-dimensional equation in the hexagonal plane, the side-averaged values (HEXNEM1) or the side-averaged and the corner-point values (HEXNEM2) of flux and current are used for the coupling of nodes in the radial direction.

In the steady state, the homogeneous eigenvalue problem or the heterogeneous problem with given source is solved. An inner and outer iteration strategy is applied. The outer iteration (fission source iteration) is accelerated by Chebychev extrapolation.

The thermal-hydraulic model of DYN3D [Manera, 2005] is based on the solution of a four equation model for the two phase flow in parallel coolant channels. The balance equations for mass, momentum and energy of the mixture and the mass balance of the vapor phase are considered. Each coolant channel represents one or several fuel assemblies corresponding to the mapping scheme given by input. The assembly feedback in an axial layer is calculated from the fuel and coolant properties. Thermohydraulic boundary conditions for the core like coolant inlet temperature, pressure, coolant mass flow rate or pressure drop must be given as input for DYN3D.

Equilibrium concentrations of the reactor poisons can be calculated. The transient behavior of Xe and Sm can be analyzed. The decay heat can be taken into account based on power history in steady state and during a transient.

Concerning reactivity transients an implicit difference scheme with exponential transformation is used for the time integration over the neutronic time step. The exponents in each node are calculated from the previous time step or during the iteration process. The delayed neutrons

precursor equations are analytically solved, assuming the fission rate behaves exponentially over the time step. The heterogeneous equations obtained for each time step are solved by an inner and outer iteration technique similar to the steady state.

A fuel rod model for the calculation of fuel and cladding temperatures is implemented. A thermal-mechanical fuel rod model allows the estimation of the relevant heat transfer behavior of the gas gap between fuel pellets and cladding during the transients and the determination of parameters for fuel rod failure evaluation.

In order to enable DYN3D users to calculate nodal burnup distributions for all possible states occurring during a reactor cycle, a macro-burnup option of the code has been developed. The extension of DYN3D by a macro-burnup option is done by putting a burnup loop around the stationary calculation kernel of the code (see section 4.2.1).

DYN3D was validated by numerous benchmarks and experiments for thermal reactors with hexagonal and quadratic fuel assemblies [Grundmann, 1999; Grundmann, 2004; e.t.c].

To be able to perform simulations of transients, where the behavior of reactor core and plant behavior interact with each other, the code has been coupled to the thermohydraulic plant model ATHLET developed by GRS [Grundmann, 1995; Teschendorff, 1996].

2.2.2 HELIOS

HELIOS-1 is a neutron and gamma transport code for lattice burnup in general 2-dimensional geometry developed by Studsvik Scandpower. It is used to calculate the neutron flux distribution in a specific region of the reactor lattice (fuel assembly sector of symmetry, whole fuel assembly or set of a few assemblies) by solving the neutron transport equation in a discrete energy and spatial mesh. The neutron transport is performed using the current coupling collision probability (CCCP) method [Villarino, 1992]. The calculation model is divided into space elements; the neutron transport within the space element is calculated using collision probabilities. Space elements are coupled using interface current.

The calculated neutron flux is used to obtain macroscopic cross sections homogenized over chosen subregions and in a chosen energy group structure. Homogenization is performed by sophisticated algorithms with resonance treatment. The HELIOS-1 nuclear data libraries are based on ENDF/B-VI [Herman, 2009].

So-called depletion calculations are performed by a series of flux calculations at fixed points in time and solving the burnup chains to get new atom number densities. The material composition changes during a time step are evaluated using constant reaction rates per isotope.

The input consists of the following data types:

- the nuclear-data library with the basic nuclear data, which also defines the energy discretization (group structures) of the neutron transport calculations;
- data that define the (initial) number densities of materials;
- data that define the geometry of the system, including the spatial and angular discretization to be used in the transport calculations;
- data that assign one or more property sets to the geometric system, thus defining one or more "states" of that system;
- data that define the execution sequence of the calculations;
- data that define which output will be saved in the data base;
- optional data that change default iteration parameters, accuracies and methods, and produced outputs.

At each calculation point (also called reactivity point), the essential results are neutron fluxes and currents, and in case of a burnup or a time step, the new material number densities. Together with the nuclear-library data and the User's input, this is all that is needed to obtain an output for XS library generation.

In this study the HELIOS 1.8 version was used with the 47-neutron-energy-group data library.

2.3 Cross sections libraries

2.3.1 General handling of neutronic data in DYN3D

For the neutronic calculation, a set of homogenized nuclear data is needed for each node. Homogenized two-group neutronic data, i.e. flux-weighted, node-averaged neutron diffusion coefficients, cross sections, assembly discontinuity factors (ADFs), as well as data concerning reactor poisons and delayed neutrons are generated by lattice codes and compiled in data libraries that can be used as DYN3D input. These libraries must contain sets of two-group neutronic data for the applied fuel-element types. Data for the reactor-core reflectors that have been homogenized according to the respective fuel-element geometry are also needed. Furthermore, the library has to comprise homogenized data for the presence of control rods in the core. In DYN3D, the neutronic data have to be provided for the given fuel-element composition, nodal burnup, and the actual reactor operation conditions, characterized by the node-averaged values of:

-fuel temperature T_F,

-moderator temperature T_M,

-boron concentration in moderator $C_{B,}$

-moderator density ρ_M,

which are calculated by DYN3D itself.

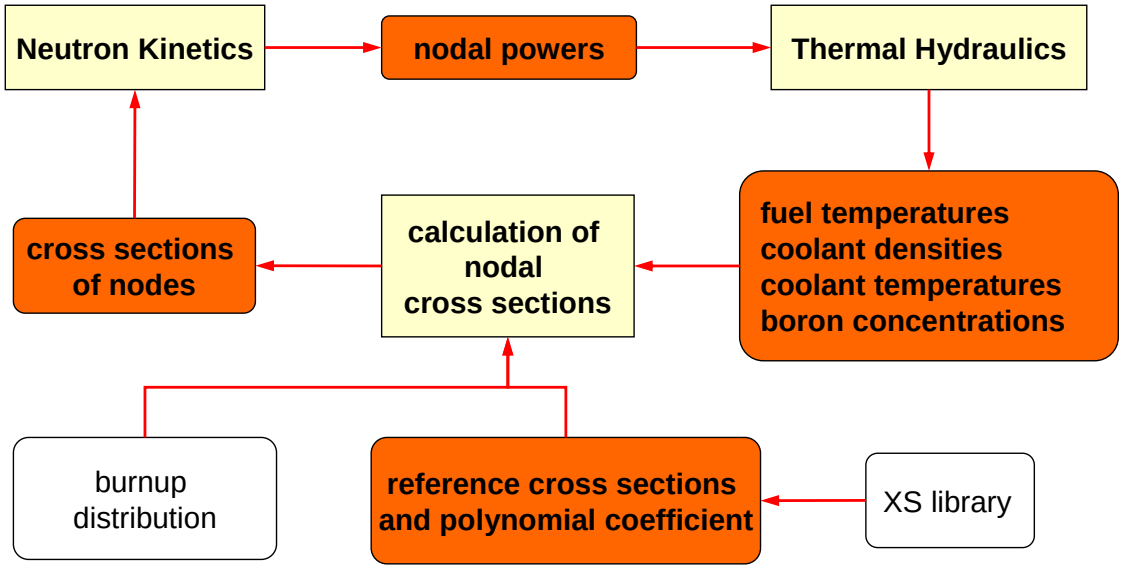

Fig. 2.8 DYN3D cross section calculation scheme.

The records in a library may contain either series of neutronic data, computed for combinations of step-wise varied values („data points"), and/or parameterized data that have been derived from data-point series (see sections 2.3.2-2.3.4). Using such a data basis, DYN3D calculates the actual nuclear data for all nodes (see Fig. 2.8).

In the next three sections the main approaches used for XS libraries generation are described. For this study an approximation-and-interpolation library (see section 2.3.4) for a German Konvoi type PWR and a parametrized data library (see section 2.3.2) for VVER-1000 reactors were used.

2.3.2 Parametrized Data Libraries

When applying a parametrized data library, the neutronic data needed in DYN3D are represented in the form:

$$\Sigma(B,\rho_M,T_F,T_M,C_B)=\Sigma_{ref}(B)\cdot K_{\rho_M}\cdot K_{T_F}\cdot K_{T_M}\cdot K_{C_B} \tag{2.15}$$

or

$$\Sigma(B,\rho_M,T_F,T_M,C_B)=\Sigma_{ref}(B)+\Delta\Sigma_{\rho_M}+\Delta\Sigma_{T_F}+\Delta\Sigma_{T_M}+\Delta\Sigma_{C_B} \tag{2.16}$$

where

$\sum_{ref}$ is the **reference** cross section at the **nominal operation parameters** ρ_M^0, T_M^0, T_F^0, C_B^0, interpolated for the actual burnup B from data points given in the XS library;

$\Delta\sum_i$ and K_i are corrections and correction factors, respectively, which represent the dependence of cross sections on operation parameters. In the XS library they are represented as polynomial coefficients for each of dependencies on ρ_M, T_M, T_F and C_B. These coefficients are also interpolated for the actual burnup from data points given in the library.

2.3.3 Multi-Dimensional-Table Libraries

In the data library described in the section above, interpolation is applied along the burnup steps, the lattice depletion calculation having been carried out at nominal reactor operation conditions. The "instantaneous" operation parameters, such as moderator density and temperature, fuel temperature, and moderator boron concentration have been varied independently one from each other in branching calculations at certain burnup states. Independent variation means that three of the parameters are kept at their reference values while the remaining one is varied. The resulting data records are used as a basis for nuclear-data parameterization.

However, there are effects of neutron spectrum (which changes due to parameter variation) that may perturb the supposed independence of operation-parameter influence on macroscopic cross sections. The problem is tackled by producing multi-dimensional tables of data records, in which all possible combinations of parameter variation are considered. The actual nodal data can then be calculated by multi-dimensional interpolation. The accuracy of this method increases with the density of „data points" produced by the lattice code calculations. Huge tables however will lead to immense computing times.

2.3.4 Approximation-and-Interpolation Libraries

Another type of data library has been proposed in [Petkov, 2002; Petkov, 2003]. In this approach, homogenized two-group neutronic data are provided for DYN3D applying a combination of approximation by polynomials and interpolation in few-dimensional tables.

That means that some (most relevant) dependencies of cross sections on operational parameters are represented in the XS library by few-dimensional tables, while others – by polynomial coefficients. In case of [Petkov, 2002] formula (2.16) turns into:

$$\Sigma(B,\rho_M,T_F,T_M,C_B)=\Sigma_{ref}(B,\rho_M,T_M)+\Delta\Sigma_{T_F}(B,\rho_M,T_M)+\Delta\Sigma_{C_B}(B,\rho_M,T_M), \qquad (2.17)$$

where reference cross sections $\sum_{ref}$ at the nominal values T_F^0, C_B^0 and polynomial coefficients for correction on fuel temperature and boron concentration are given in XS library as 3-dimensional (burnup, moderator density and moderator temperature) tables.

This approach allows a significant reduction of library size in comparison to multi-dimensional-table library while keeping high accuracy of cross sections estimation.

2.3.5 Generation of XS library

Whichever library type is chosen, the preparation procedure, illustrated in Fig. 2.9, consists of neutronic-data set calculations by lattice code and then generation of library-specific reference data points and polynomial coefficients from lattice code data sets by some kind of post-processor.

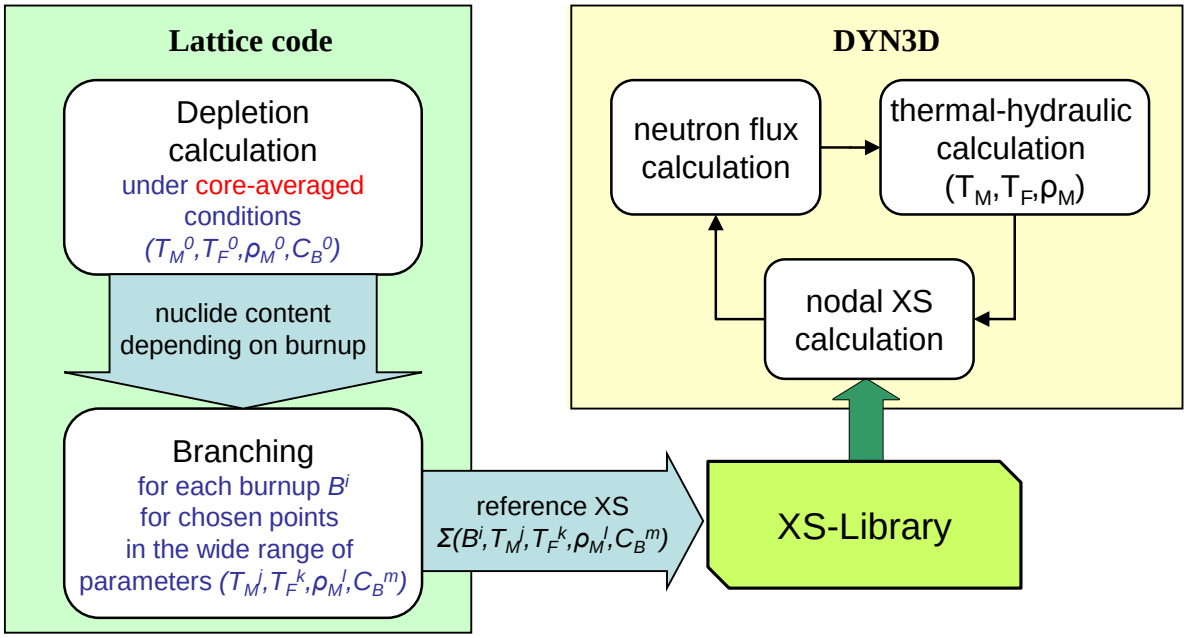

Fig. 2.9 Simplified scheme of XS treatment.

The lattice code user has to specify the fuel assembly geometry and initial nuclide content and then perform a **depletion calculation** to obtain the nuclide content change with burnup. Usually this is a single-assembly (or symmetrical part of assembly) calculation with reflective boundary conditions. **Core averaged values of operation parameters ρ_M^0, T_M^0, T_F^0 and fuel cycle averaged C_B^0 are applied in the depletion calculation.** The values of operation parameters are fixed and do not change during depletion. The result of the depletion calculation is a set of fuel nuclide contents for reference burnup points B^i.

The next step is a set of so-called **branching calculations**: the 2-group assembly-homogenized macroscopic cross sections are computed for a wide range of operation parameters for each burnup step using nuclide contents derived from the depletion calculation. The range of parameters should cover all possible values that can occur in normal operation and transients. Obtained in branching calculations 2-group macroscopic cross sections are stored in a XS-library as **reference cross sections** or, depending on the library format (see sections 2.3.2-2.3.4), used for calculation of parameterization coefficients.

To avoid misunderstanding we will call operation parameters applied in depletion calculations "**historical**", and parameters in branching calculations – "**instantaneous**". In case of whole-core calculations by DYN3D "instantaneous" are actual local parameters of node and "historical" are burnup(B)-averaged parameters, for example the historical fuel temperature:

$$\overline{T}_F = \frac{1}{B}\int_0^B T_F\, dB$$

In the generation of all XS libraries for DYN3D so far only one set of fixed (core- and cycle-averaged or **nominal**) historical operational parameters was used. Thereby the change of fuel

nuclide content was represented only by an overall burnup parameter, measured in megawatt-days produced per kilogram heavy metal (HM) in the (fresh) fuel. However each node in the reactor core has its own burning conditions, which lead to differences in fuel properties. This fact leads to Burnup History Effects described in the next chapter.

2.4 Chapter short summary

The current level of computing methods and techniques does not allow to perform whole-core transient calculations with highest spatial and energy resolutions. Assumptions and simplifications which decrease the problem complexity to a reasonable measure are needed. The commonly accepted approach is to split reactor calculations into two phases (see section 2.1.5):

- fine-mesh lattice codes (typically utilizing the transport method) perform single-assembly calculations with highest possible spatial and energy resolutions, but only in two dimensions, static and depletion, without thermal-hydraulic feedbacks. Results of these calculations are homogenized over the fuel assembly and condensed to few energy groups macroscopic-cross-sections sets that are then used for building a few-group homogenized cross sections library (XS-library);
- data from XS-libraries is used by coarse-mesh reactor dynamic codes (typically utilizing the diffusion method) for simulating reactor core behavior in transient processes in three dimensions and with thermal-hydraulics.

In this approach the XS-library plays the role of an interface which transfers nuclear fuel properties from lattice code to reactor dynamics code. These libraries contain sets of few-group homogenized macroscopic cross sections (and/or polynomial coefficients) depending on instantaneous operational parameters. The change of fuel nuclide content with reactor-operation time is simulated by a single-assembly lattice-code depletion calculation under core-averaged operational parameters and represented in the XS-library as the dependence of fuel properties on the burnup parameter.

3 Burnup history effects

This chapter describes the problem of burnup history effects. The physical background of this phenomenon is explained in section 3.1. Existing methods to take history effects into account, implemented by other code developers are described in section 3.2.

3.1 Physical background

As described in section 2.3, a nodal code estimates local cross sections for each node interpolating reference points from an XS-library, which is compiled from results of single-assembly lattice-code depletion calculations applying core-averaged operational parameters. However, in a reactor core, fuel depletion happens under conditions varying in space and time. Different operation parameters lead to different neutron spectra, depending on the coordinates within the core (node locations) and the degree of depletion.

Moderator density effect

In the upper part of a light-water reactor core the coolant temperature is higher and the water density is lower than core-averaged values. Since in LWR water acts as neutron moderator, less water density leads to less effective neutron moderation and thereby to a harder neutron spectrum.

The radiative capture cross section of ^{8}U has a resonance region (see Fig. 2.2, page 13) with very high cross section values, thus less effective moderation leads to more neutrons to be captured by ^{8}U in this region. Radiative capture of neutrons by ^{8}U leads, after two beta-decays, to the creation of ^{9}Pu (see Eq. (3.1)). So, the hardening of spectrum causes a higher rate of radiative capture by ^{8}U and higher ^{9}Pu production.

$$^{8}U + n \longrightarrow {}^{9}U \xrightarrow{\beta\_ 23.5\,\mathrm{min}} {}^{9}Np \xrightarrow{\beta\_ 2.36 day} {}^{9}Pu \tag{3.1}$$

Since the moderator density in the upper part of core is lower than the core-average during the whole fuel assembly life, ^{9}Pu is built up faster there and the difference in concentration grows with burnup.

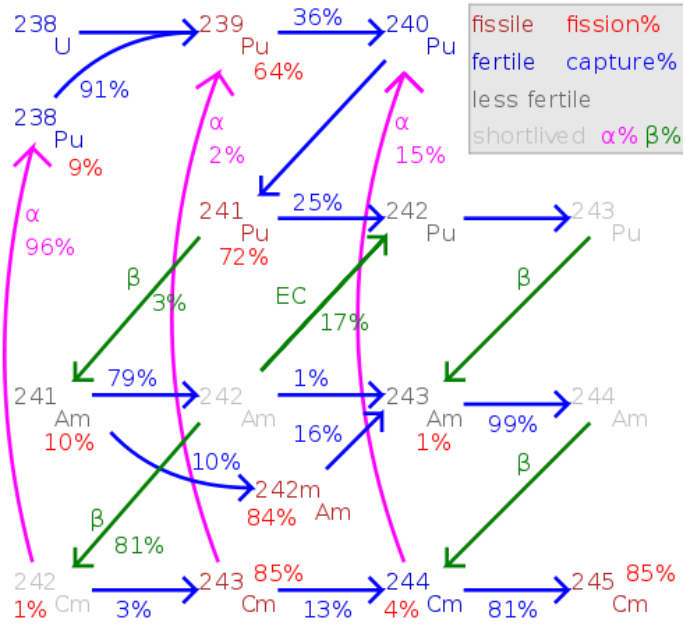

Fig. 3.1 Actinides transmutation flow. [Wikipedia, 2010].

As ^{9}Pu takes part in neutron interactions, its higher concentration leads to a higher rate of these reactions (due to Eq. (2.3)). Consecutive neutron absorptions by ^{9}Pu lead to creation of heavier plutonium isotopes and minor actinides (see Fig. 3.1). So, the higher rate of radiative absorption by ^{9}Pu causes higher build-up of minor actinides.

At the same time, increased concentration of ^{9}Pu leads to higher fission rate of this isotope - more energy is released by fission of ^{9}Pu. Since burnup is measured in energy released per mass of fuel, an increasing energy portion released by fission of ^{9}Pu means a decreasing ^{5}U fission energy portion.

As a result, for the same burnup level the fuel in the upper part of core has higher ^{5}U, ^{9}Pu, and minor-actinide concentrations than fuel which burns in core-averaged conditions. A higher concentration of fissile nuclides causes higher neutron multiplication properties (k_{inf}) of the fuel (see Fig. 3.3).

Results of few single-assembly depletions with different historical operational parameters calculated by HELIOS (calculation model is described in section 4.1) illustrate described above effects in Fig. 3.2 and Fig. 3.3. The influence of a node's history on the ^{8}U and ^{9}Pu concentrations in fuel is shown in Fig. 3.2. Macroscopic cross sections and multiplication factors shown in Fig. 3.3 are calculated using the same instantaneous but different historical operational parameters. Comparing Fig. 3.2 and Fig. 3.3 one can see that differences in fuel properties reflect differences in nuclide content: sequence of curves in figures remains the same, i.e. fuel depleted in hardest spectrum conditions has highest ^{9}Pu and ^{8}U concentrations, highest absorption and fission macroscopic cross sections and the highest multiplication factor.

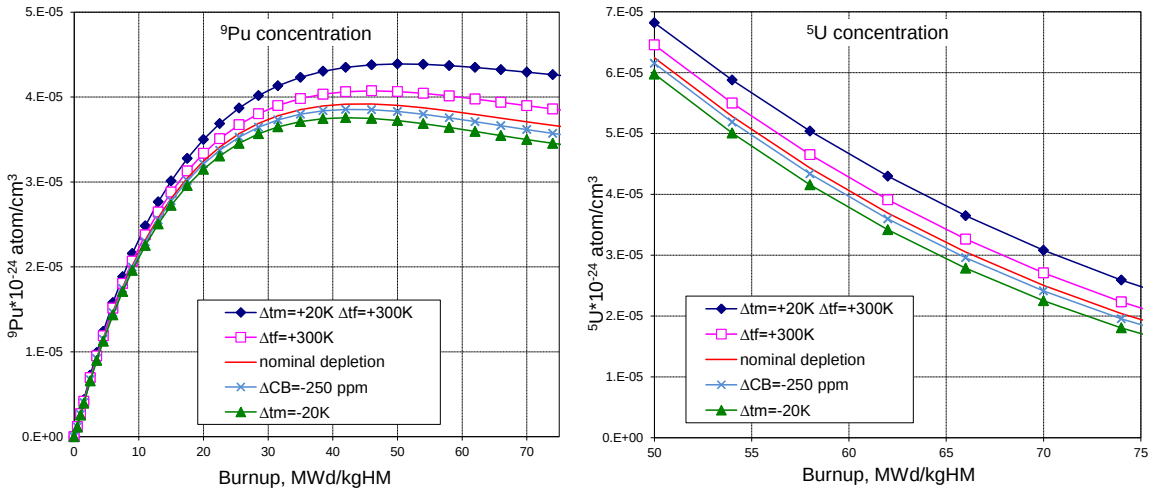

Fig. 3.2 Nuclide concentrations in depletions under varying operation parameters.

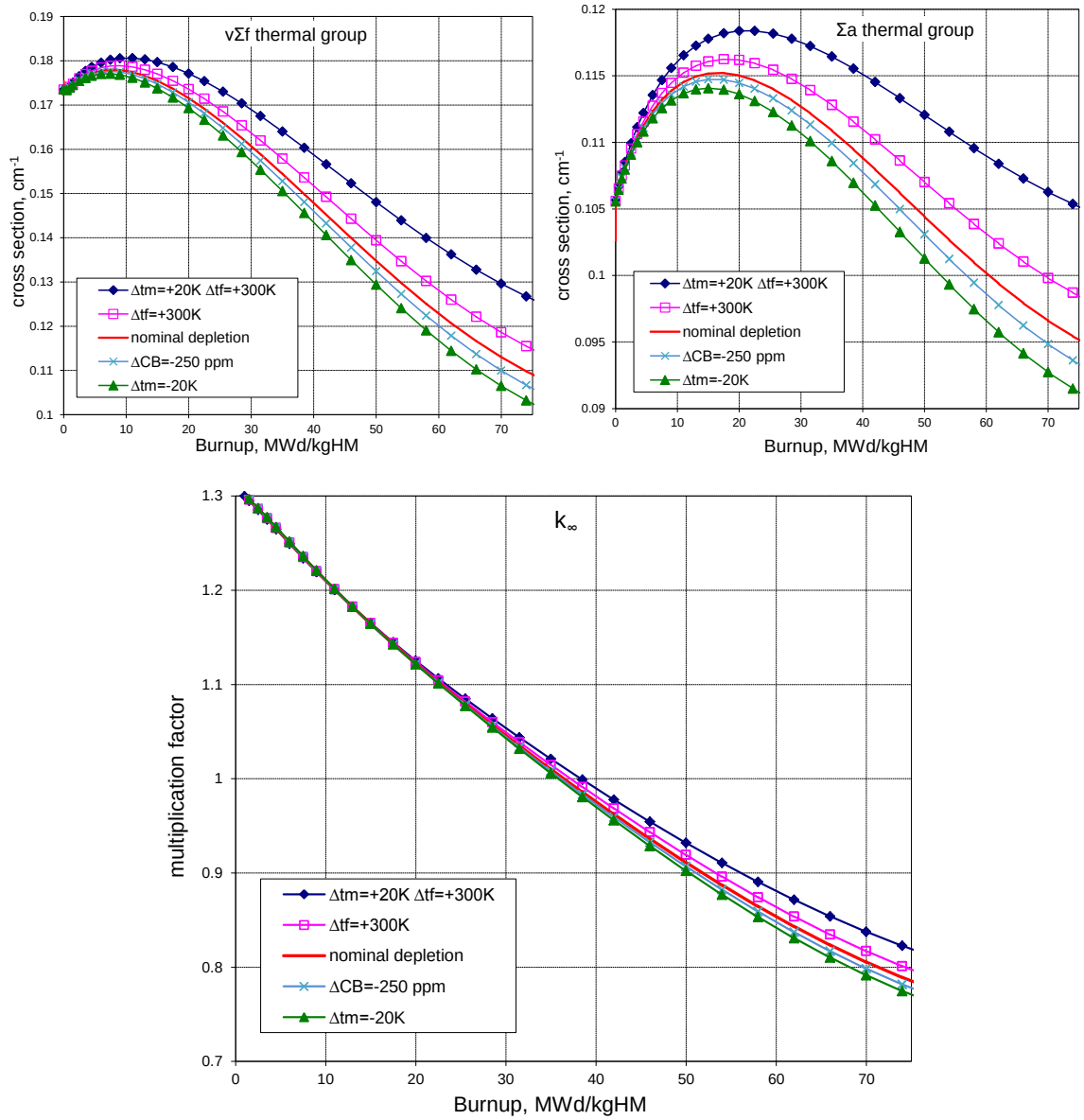

Fig. 3.3 Properties of fuel with different history.

The influence of the neutron spectrum on fuel depletion is described through moderator history effect.

Other operational parameters could also influence neutron spectrum and cause history effects:

Void effect – is a particular case of the moderator density effect. Unlike PWR, in BWR water is boiling and a significant amount of steam is present in the upper part of reactor core. Presence of steam reduces the average moderator density and makes the spectrum harder, just like hotter water in the upper part of PWR.

Fuel temperature effect

In case of deviation of fuel temperature the mechanism is similar to the moderator density effect, but the spectrum is affected by the Doppler Effect.

The phenomenon of the Doppler Effect is caused by a broadening of the absorption resonances due to the thermal motion of nuclei [DOE, 1993] as illustrated in Fig. 3.4. To be absorbed on the resonance by the stationary nucleus, neutron must have energy close to the resonance level E_0. However, nuclei are in continual thermal motion. The nucleus movement toward or away from neutron increases or decreases, respectively, the neutron velocity relative to the nucleus. So, to be absorbed on the resonance, neutron must have velocity (i.e. energy) less or more than E_0. Thereby thermal motion of target nuclei broads width of the resonance and decreases its peak value (see Fig. 3.4), so the total area under resonance remains constant. Increasing fuel temperature leads to faster thermal motion, effectively broadening the energy range of neutrons that may be absorbed on the resonance.

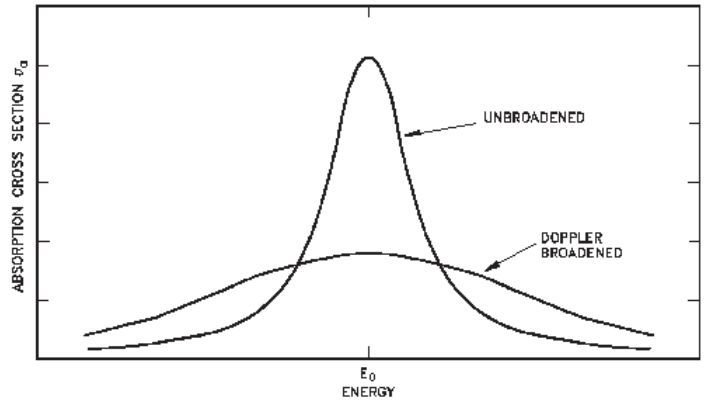

Fig. 3.4 Effect of fuel temperature on resonance absorption peak. [DOE, 1993].

With an increase of fuel temperature, the resonance peaks of the absorption cross section of ^{8}U are affected by Doppler's broadening which causes, due to reduced resonance self-shielding, an increase of the radiative absorption rate by ^{8}U. The probability for a neutron to pass successfully the

resonance region (on its moderation way down to thermal energy) decreases, so the spectrum gets harder.

Just like in the moderator density case, higher absorption rate by ^{8}U leads to higher ^{9}Pu and minor-actinides production and slower depletion of ^{5}U.

Boron concentration effects

The boron acid dissolved in the moderator is used in PWR to compensate the reactivity change due to the fuel burnup during fuel cycle. It contains ^{10}B, which has a very high neutron absorption cross section in the thermal energy region (see Fig. 3.5).

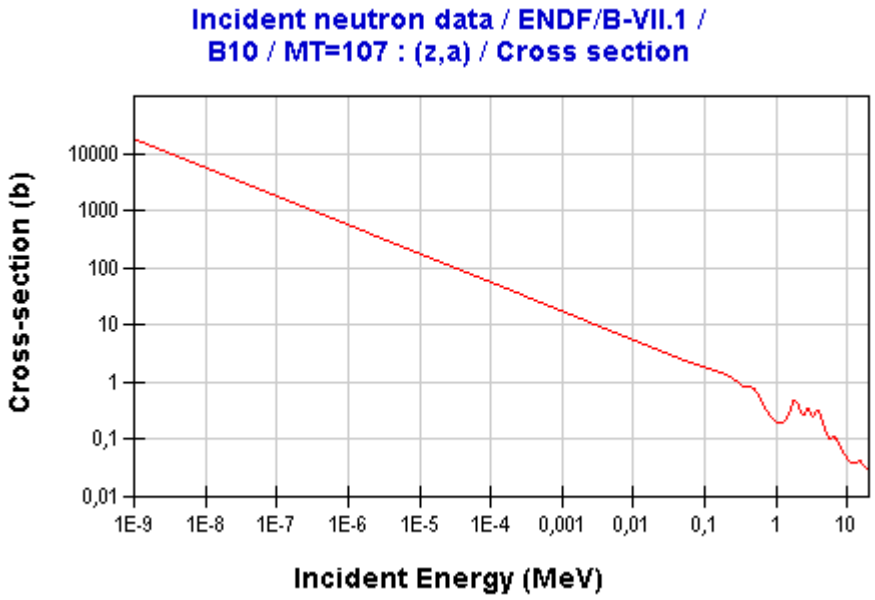

Fig. 3.5 Absorption cross section of ^{10}B. [NEA, 2010]

The boron acid concentration in the moderator is maximum at the beginning of cycle and decreases during cycle, i.e. down to zero at the end of cycle. Usually, for the nominal depletion calculation the cycle-average value ("cycle-middle value": half of the beginning-of-cycle value) is used. However, the average boron concentration which fresh fuel "sees" in its first cycle starts from the maximum value at the beginning of cycle and decreases to the cycle-middle value at the end of cycle. In the first half of the next cycle the boron concentration in the core is higher than average, so the "historical" value for second-year fuel grows – and in the second half of the cycle – decreases back to the cycle-middle value. That means that during the cycle the "historical" boron concentration, especially for fresh fuel, is slightly higher than cycle-average value used in nominal depletion (for generation of XS-library).

Depletion under higher boron concentration means depletion under harder spectrum, which consequences are (as shown for moderator density reduction) higher ^{9}Pu and minor-actinides production rates as well as slower depletion of ^{5}U.

Control rod presence effect

In some cases depletion is happening in the presence of control rods - for example, in a VVER-1000, 6 out of 61 control assemblies are inserted into the core at 20% of their length during fuel cycle. Control rods contain materials (boron, cadmium, hafnium, etc.) with high absorption cross section for thermal neutrons. Their presence suppresses the thermal flux in the rodded and the neighboring nodes and depletion happens in a harder spectrum.

Burnup history effects in general

The change of any operation parameter (fuel and water temperature, water density, boron concentration, control rod presence, etc.) causes a respective change in the neutron spectrum which could be described as spectrum hardening or softening. The neutron spectrum influences nuclide creation/depletion processes in the fuel, in particular radiative absorption rate by ^{8}U and consequently buildup of ^{9}Pu and minor actinides. The difference in nuclide concentrations is accumulating during burnup.

At the same burnup level (in MWd/kgHM), reached under different spectral conditions, the fuel has accumulated different nuclide contents. Fuel with different nuclide content has different properties (2-group homogenized macroscopic cross sections). For this reason, the nodal macroscopic cross sections will depend on the spectral history the node has "seen" in its course of reaching a certain depletion state (see Fig. 3.3). By creating XS libraries using only a single reference depletion calculation (under nominal core-averaged conditions, as described in section 2.3.5) this effect is neglected.

Thus, the specific exposure (burnup) measured in MWd/kgHM is not quite sufficient as a parameter to describe the changes of macroscopic cross sections during depletion. This study proposes a method to take deviations in nuclide content into account and to reduce the inaccuracy of the "standard" treatment applied so far.

3.2 Existing methods

As shown above, cross sections for two nodes having suffered different depletion paths differ even if the instantaneous local conditions are the same. This is mainly due to the differences in the buildup of actinides and uranium depletion rates that change with the spectrum and thus, with the burnup history. Neglecting this effect leads to inaccuracy in nodal cross sections estimation.

An obvious solution seems to be performing a detailed heterogeneous transport calculation for the whole core. However, contemporary lattice burnup codes are able to perform burnup and steady-state calculations in 2-dimentional geometry without thermohydraulics, while 3-D transient

modeling with thermohydraulics is needed. The use of the same models in core kinetics as in the lattice burnup requires unaffordable calculation resources.

Recently, some attempts to develop Monte-Carlo codes capable to perform whole-core burnup calculations with thermohydraulic feedbacks are made [Kotlyar, 2009], but this approach is not applicable to dynamics calculations so far.

That means macroscopic XS libraries (produced by heterogeneous fuel-assembly transport calculations) are necessary for 3-D reactor core kinetics, but it is needed to introduce a consideration of history effects. This section briefly describes existing methods implemented in other codes and described in scientific journals.

3.2.1 Microscopic depletion model

A hybrid macro/micro cross sections estimation model is employed in 3D nodal code SIMULATE-4 [Bahadir, 2005; Bahadir, 2005a], in which the nodal cross sections are estimated as:

$$\Sigma^{actual} = \Sigma^{nom} + \sum_{i=1}^{\sim 50} \sigma_i (N_i^{actual} - N_i^{nom}) \tag{3.2}$$

where the summation is over selected nuclides. The first term on the right side of Eq. (3.2) represents reference macroscopic cross section Σ^{nom} generated in the single assembly lattice code evaluation. The second term in this equation provides a correction to take into account the fact that actual local nodes depletion (represented by number densities N^{actual}) differs from the nominal single assembly depletion conditions (represented by N^{nom}). Approximately 50 nuclides (15 actinides, 30 fission products, Gd and ^{10}B as burnable absorber) have been chosen according to their importance.

Both the macroscopic and microscopic multi-group cross sections appearing in Eq. (3.2) are represented in few-dimensional tables depending on all important instantaneous parameters (e.g., moderator density, control rod, fuel temperature, etc.) and historical effects (e.g., burnup, moderator density history, and control rod history). The N^{nom} are not taken directly from the lattice code CASMO-4 but calculated in the pre-processing code by solving the SIMULATE-4 isotope chains using the single-assembly fluxes and microscopic cross sections. Hence, N^{nom} and N^{actual} are computed in consistent manners.

The actual local number densities appearing in Eq. (3.2) are tracked for each node using the node-average fluxes available from the multi-group nodal solver. In each depletion step as well as for each shutdown cooling period, linearized burnup equations are solved.

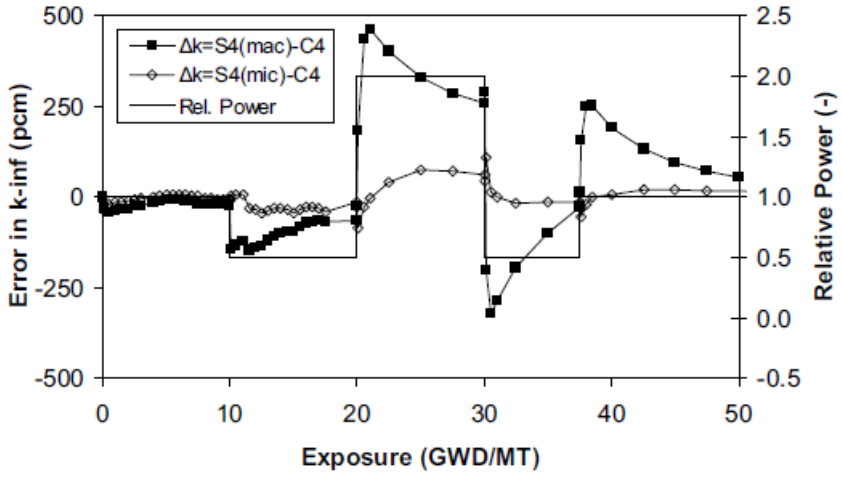

Fig. 3.6 A BWR assembly depletion – 5 step test case. [Bahadir, 2005]

The hybrid depletion model in SIMULATE-4 has been verified against single assembly CASMO-4 calculations and the hybrid model has been compared to traditional macroscopic depletion model.

Deviations of multiplication factor in single-node depletion with power varying over time calculated by SIMULATE-4 using hybrid (S4mic) and macroscopic (S4mac) models from the lattice code results (C4) are shown in Fig. 3.6. Nuclide concentrations, especially those with short half-lives, are sensitive to the power density history. With macroscopic model the maximum error in multiplication factor is 460 pcm. This error is reduced to 110 pcm with the hybrid model.

A hybrid depletion model has been developed as part of the nodal code SIMULATE-4. Single-assembly test problems have demonstrated significant improvements over the traditional macroscopic depletion model.

3.2.2 Spectral history index

Another group of methods utilizes the "historical" correction proportional to a *Spectral History* parameter (*SH*):

$$\Sigma^{actual} = \Sigma^{nom} + \left(\frac{\partial \Sigma}{\partial SH} \right) \Delta SH \tag{3.3}$$

which is defined as the exposure-integrated rate between the nodal spectral index in the actual local conditions SI^{actual} calculated by the nodal code and the spectral index in the single-assembly lattice code calculation in nominal conditions SI^{nom}:

$$SH = \frac{1}{B} \int_0^B \frac{SI^{actual}}{SI^{nom}} dB \tag{3.4}$$

The papers [Lee, 1995; Iwamoto, 1999] define the *Spectral Index SI* as a local ratio between fast and thermal flux:

$$SI = \frac{\phi_1}{\phi_2} \tag{3.5}$$

Investigations described in [Cabellos, 1999; García-Herranz, 1999] have found that parameter (3.5) corrects adequately history effects produced by off-nominal moderator density and boron concentration, but not by off-nominal fuel temperature. The Spectral Index *SI*, proposed in these papers and implemented in 3-D core dynamics code SIMTRAN, is a complex parameter, formulated as resonance absorption probability multiplied by the ratio of fast absorptions to total fissions:

$$SI = \frac{\Sigma_{a1}}{\Sigma_{a1} + \Sigma_{s12}} \frac{\Sigma_{a1}\phi_1}{\Sigma_{f1}\phi_1 + \Sigma_{f2}\phi_2} \tag{3.6}$$

where Σ_a is the absorption cross section in fast group

Σ_f, - the fission cross section

Σ_{s12} - the downscattering cross section

ϕ - the neutron flux,

indexes *1* and *2* denote fast and thermal group, respectively.

The fuel temperature cases are accurately solved in this treatment with a generalized spectral index. The first term represents the resonance absorption probability, which defines ^{9}Pu production by absorption in ^{8}U and depends on fuel temperature. And the second term accounts for the ratio of the total absorption in the fast group to the fission rate that includes the spectral history effects of boron and water density changes.

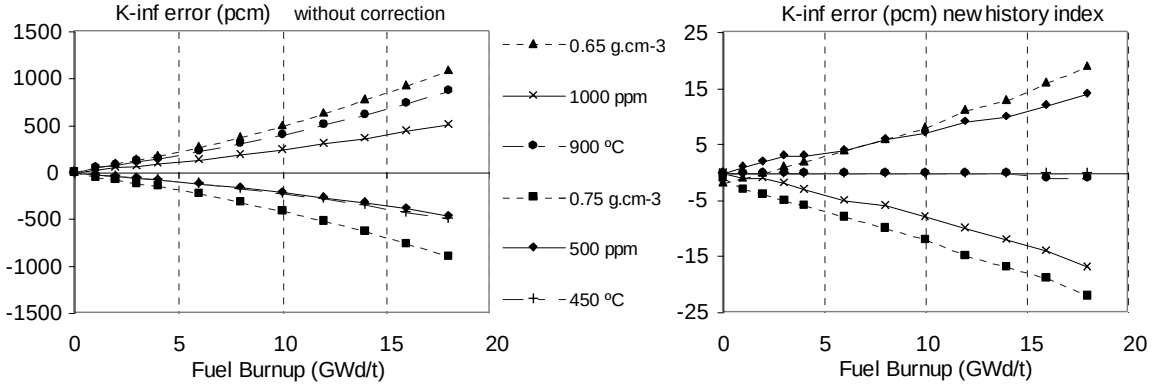

Fig. 3.7 Errors in multiplication factor (pcm) along the burnup for several off-nominal conditions of water density, fuel temperature and boron concentration, without spectral history treatment (left) and considering nodal spectral history index (right). [García-Herranz, 1999]

The spectral history effect for a typical PWR fuel assembly, 17x17 pins with 2.10% enrichment, is summarized in Fig. 3.7. Comparison of several off-nominal calculations (variations in PWR cores around the average nominal values: 0.70 g/cm^3 water density, 100% power and 750

ppm Boron) and corresponding branch cases are performed to quantify history effects. It shows the error in k-infinity without spectral history treatment, as a function of fuel burnup, having errors above 1000 pcm. It can be noticed that the whole scale of errors is reduced with this nodal spectral history correction by almost two orders of magnitude, bringing down the errors to the ± 20 pcm range.

Further development of the spectral index is offered by [Baturin, 2001]. In this paper the spectral index is deduced from the change in the ^{9}Pu concentration:

$$SI = \frac{\Sigma_{c1}}{\Sigma_{a1} + 0.5(\Sigma_{s12} + \Sigma_{s12}^{nom})} \frac{\Sigma_{c1}\phi_1}{\Sigma_{f1}\phi_1 + \Sigma_{f2}\phi_2} \tag{3.7}$$

where Σ_{c1} is the radiative capture cross section in fast group,

index *nom* – for the nominal depletion.

The factors appearing in the Eq. (3.7) for the spectral index have a clear physical meaning: the first factor determines the probability of radiative capture of fast neutrons, while the ratio of the rates of radiative capture by ^{8}U followed by the production of plutonium to fuel burnup is determined by the second factor in this formula.

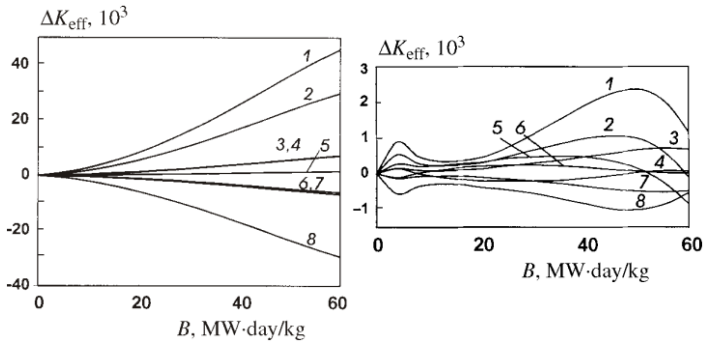

Fig. 3.8 Deviation of the multiplication factor (calculated without (left) and with (right) spectral history treatment) of an infinite lattice of fuel assemblies with variation of burnup conditions. [Baturin, 2001].

1) ρ_M = 0.8 kg/m^3, T_F = 1000 K, C_B = 250 ppm; 2) ρ_M = 0.8 kg/m^3; 3) C_B = 250 ppm; 4) T_F = 1000 K; 5) ρ_M = 0.8 kg/m^3, T_F = 1400 K, C_B = 750 ppm; 6) T_F = 1400 K; 7) C_B = 750 ppm; 8) ρ_M = 0.64 kg/m^3.

Implementation of this correction increases the accuracy of the calculation of the multiplication coefficient by an average factor of 10 (see Fig. 3.8).

3.2.3 Ad-Hoc parameters

In this method the "Ad-Hoc parameters" - exposure-weighted nodal fuel temperature HT_F, moderator density HR_M and boron concentration HC_B are introduced:

$$HT_F = \frac{1}{B}\int T_F dB,\ HR_M = \frac{1}{B}\int \rho_M dB,\ HC_B = \frac{1}{B}\int C_B dB \tag{3.8}$$

The history effects are taken into account by corrections:

$$\Sigma^{actual} = \Sigma^{nom}(B, \rho_M, T_F, T_M, C_B) + \left(\frac{\partial \Sigma}{\partial HT_F}\right)\Delta HT_F + \left(\frac{\partial \Sigma}{\partial HC_B}\right)\Delta HC_B + \left(\frac{\partial \Sigma}{\partial HR_M}\right)\Delta HR_M \quad (3.9)$$

Each correction term is proportional to deviation of respective nodal historical parameter from the value used in nominal depletion calculation. Dependencies on the history variables are determined by performing separate lattice code off-nominal depletion calculations for each of the history effects and represented in XS-libraries by polynomial coefficients.

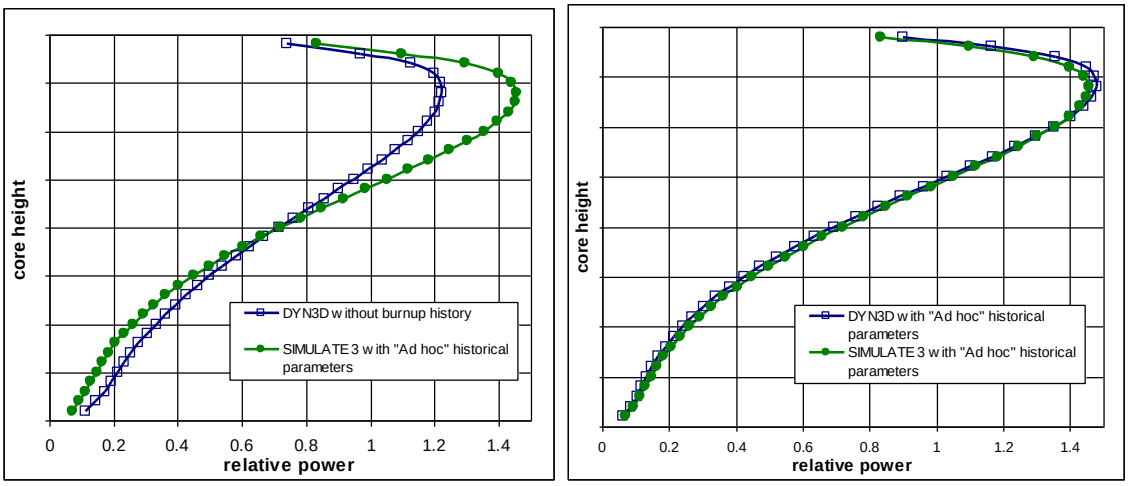

Fig. 3.9 Axial power distribution in the central fuel assembly with high burnup.

This method is implemented in SIMULATE-3 [Bahadir, 2005; Watson, 2002]. The effect of historical correction is demonstrated in Fig. 3.9 (left); the right figure depicts a comparison between DYN3D and SIMULATE-3 calculations for the same case [Mittag, 2006]. For test purposes, this method was partly implemented in DYN3D: a special version of XS-library for PWR fuel was created and the correction (3.9) was introduced into the DYN3D XS calculation scheme. Values of Ad-Hoc parameters and burnup distributions [Mittag, 2006] were taken from the SIMULATE input.

3.3 Chapter short summary

As described in chapter 2, macroscopic XS-libraries are used to transfer fuel properties from a lattice code to a nodal code. The change of fuel properties during depletion is described in the libraries by the dependence on a burnup parameter.

However, the spectral conditions in different parts of reactor core usually differ from those in the lattice code calculation. The variety in local spectral conditions leads to variety in nuclide depletion and build-up and therefore in fuel properties. Therefore, the current nuclide content of fuel should not be described by one burnup parameter alone, because using this parameter in the XS-

library as the only one to describe the change of fuel properties during depletion leads to inaccuracy.

Code developers solve this problem by introducing additional parameters to describe the actual fuel state. Solutions proposed in the literature are:

- consideration of actual nodal nuclide content by calculating nodal concentrations for all important nuclides;
- introduction of parameters which directly (spectral index) or indirectly (historical operational parameters) describe the local spectrum history.

4 Plutonium-239 history indicator

This chapter describes the methodology of using ^{9}Pu as an indicator of a nodal spectral history. The idea of the method is described in section 4.1, while its implementation in the code DYN3D is explained in section 4.2. The description of the proposed method and the results of its verification were published in [Bilodid, 2008; Bilodid, 2010].

4.1 The ^{9}Pu-correction method

History effects were studied in fuel for the German pressurized water reactor (PWR) Konvoi. Three types of 18x18 fuel assemblies (FA) were modeled by HELIOS 1.8:

- Uranium dioxide (UOX) FA with 4.6% enrichment of ^{5}U
- UOX FA with 4.6% enrichment of ^{5}U and gadolinium burnable absorber (BA)
- Mixed oxide (MOX) FA with 4.55% of fissile Pu and 0.23% ^{5}U

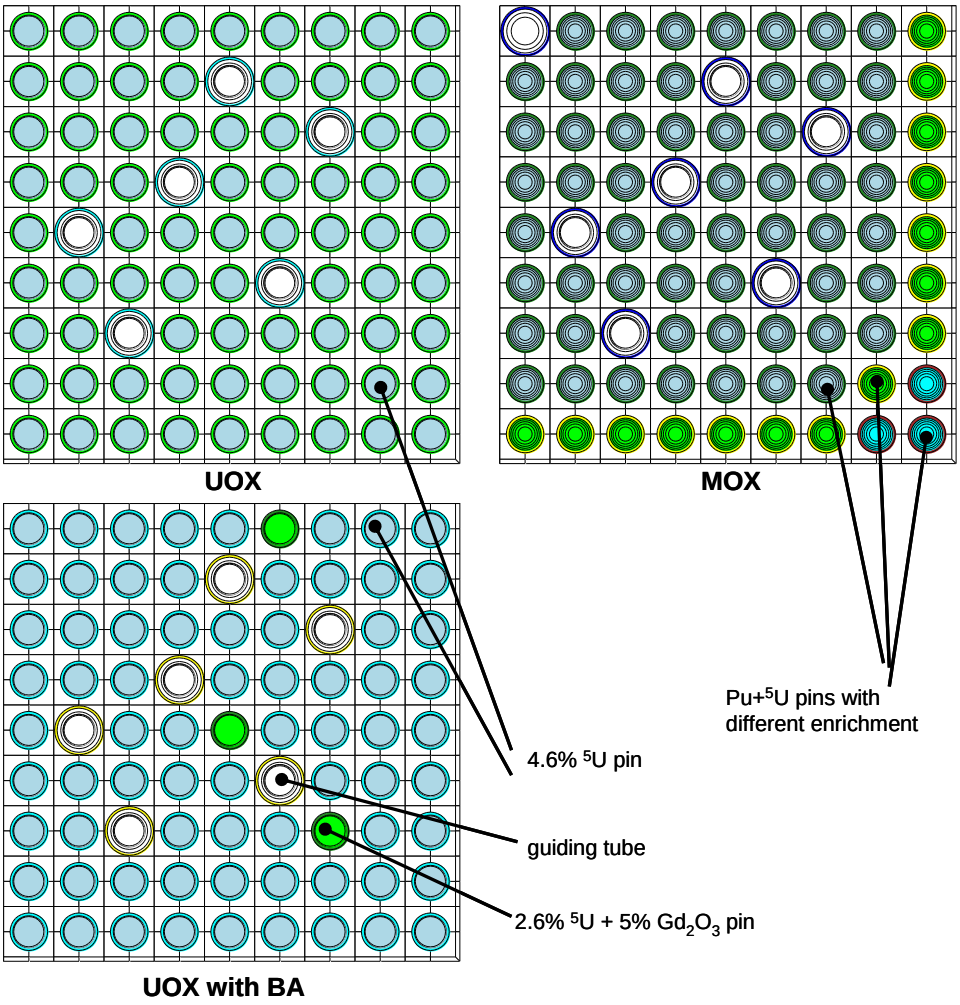

Fig. 4.1 HELIOS ¼ FA models.

The HELIOS models describe a quarter of a (symmetric) FA with reflective boundary conditions, as shown in Fig. 4.1.

A series of HELIOS calculations was performed in order to investigate how depletion under different conditions influences the nuclide content.

Fig. 4.2 and Fig. 4.3 show the comparison of ^{9}Pu and ^{5}U concentrations in **nominal depletion** under core-averaged operation conditions and **off-nominal depletions** with a variation of one or more of the following operation parameters: boron concentration, fuel temperature, moderator temperature (with moderator density depending on temperature and pressure) for UOX FA and for MOX FA.

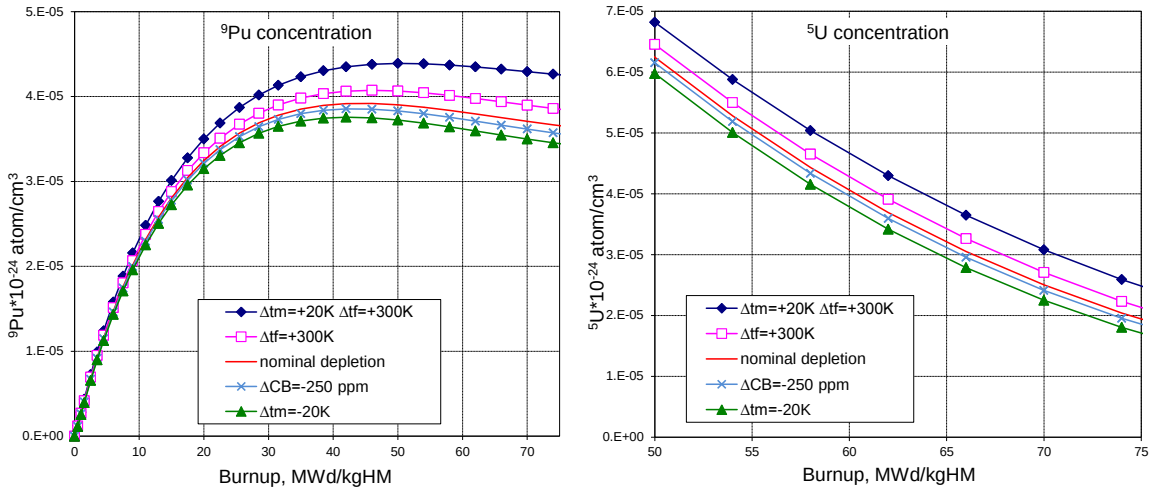

Fig. 4.2 Nuclide concentrations in different depletion conditions, i.e. varying operation parameters for UOX.

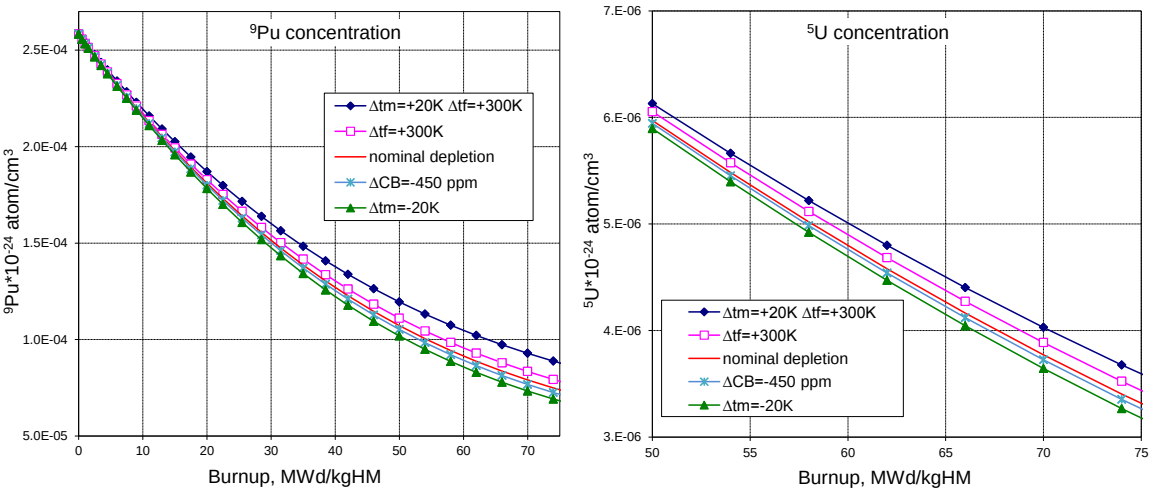

Fig. 4.3 Nuclide concentrations in different depletion conditions, i.e. varying operation parameters for MOX.

Differences in nuclide concentrations are explained by the influence of the neutron spectrum, disturbed by operational parameter variation, on nuclide depletion and build-up processes (see section 3.1).

Fig. 4.4 compares relative deviations of ^{5}U, ^{8}U and ^{9}Pu nuclide concentrations $\delta N = (N - N_{nom}) / N_{nom}$, where N_{nom} is a nuclide concentration in nominal depletion and N is a concentration in one of the off-nominal depletions) for a certain burnup (35 MWd/kgHM in this example). Each data point in this picture represents one of the off-nominal depletion calculations, while the zero-point belongs to the nominal depletion. This comparison shows a correlation between the depletion-history-related changes in the nuclide concentrations. It means that **knowing the concentration for one of the heavy nuclides, the concentrations of others could be estimated**. An important issue is the fact that the correlation in actinide-concentration deviations does not depend on the operational parameter which causes a change in neutron spectrum – so all of them can be treated in the same way.

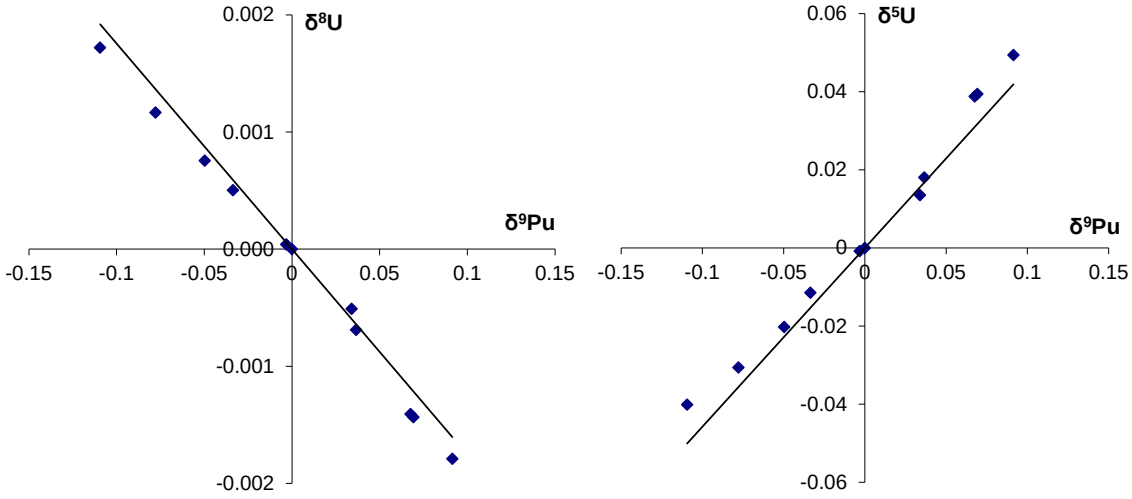

Fig. 4.4 Correlation of the relative change of nuclide concentrations under different depletion conditions.

The next step is to compare normalized deviations of 2-group assembly-homogenized macroscopic cross sections with change of nuclide concentrations. Fig. 4.5 compares absorption and fission cross sections with the ^{9}Pu concentration derived from several calculations, all of them "branching" to the same combination of instantaneous operation parameters, but applying different nuclide contents that had been calculated earlier under varying spectral depletion conditions.

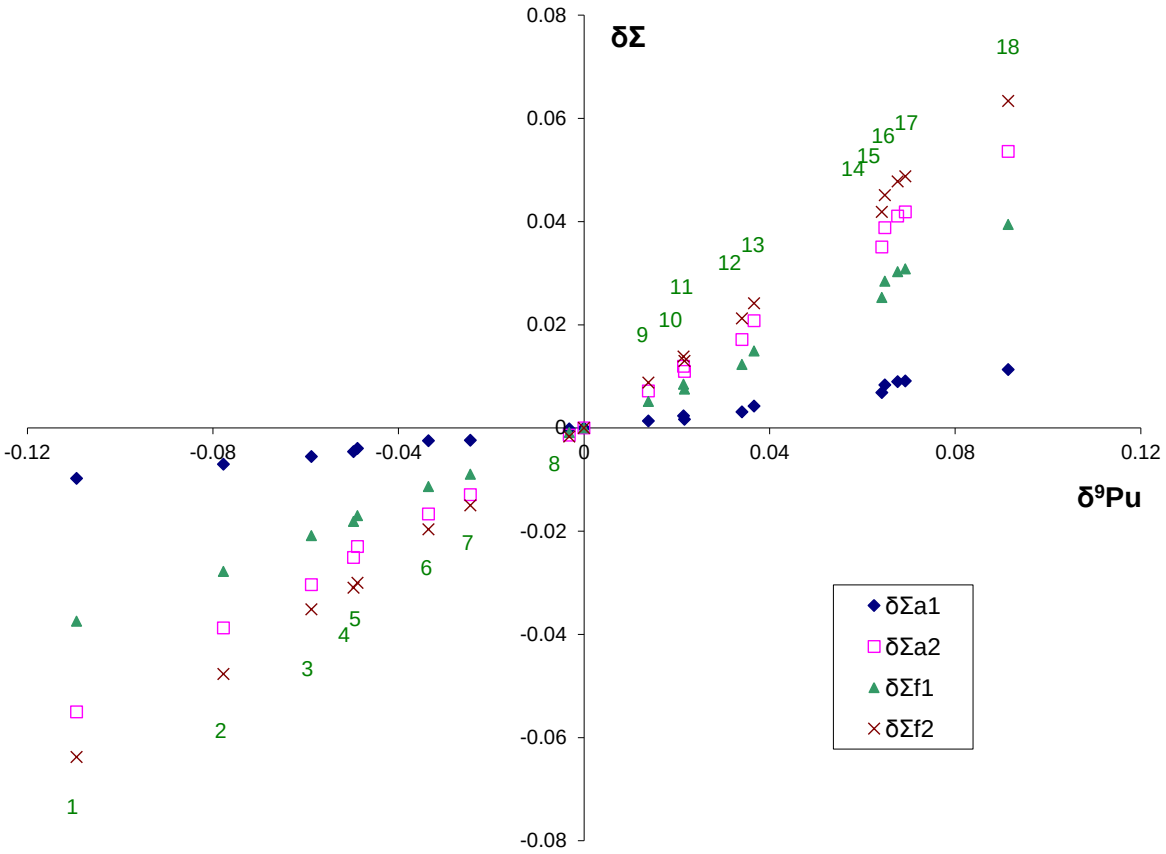

Deviations from nominal values in depletion conditions:

depletion	T_F, K	T_M, K	C_B, ppm	P, MPa
nominal	817	584	500	15.8
1	+58	+29	-	-
2	+683	-	-	-
3	-	+20	-	-
4	+458	-	-	-
5	+883	-20	-	-
6	-	-	+500	-
7	-	+10	-	-
8	-	-	-	14.2
9	+100	-	-	-
10	-	-	-300	-
11	-	-10	-	-
12	-253	-	-	-
13	-	-20	-	-
14	-217	-20	-	-
15	-	-44	-	-
16	-	-49	-	14.2
17	-	-49	-	-
18	-197	-49	-	-

Fig. 4.5 Correlation between the relative change of macroscopic cross sections and ^{9}Pu concentrations at different depletions.

The analysis of the results indicates a correlation between a history-related change of homogenized XS and the history-related change of the nuclide concentration. This means that **having determined the deviation of the local ^{9}Pu concentrations from nominal value** (and knowing the proportionality factor) **it is possible to derive the respective difference in the XS**, thus ^{9}Pu serves as indicator for the actual nuclide content ("burnup history indicator").

In principle, according to conclusion made from Fig. 4.4, any heavy nuclide (^{5}U, ^{8}U or ^{9}Pu) can be used as the burnup history indicator. ^{9}Pu is chosen because its concentration is most sensitive to the burnup history and could be calculated in a nodal code relatively easy.

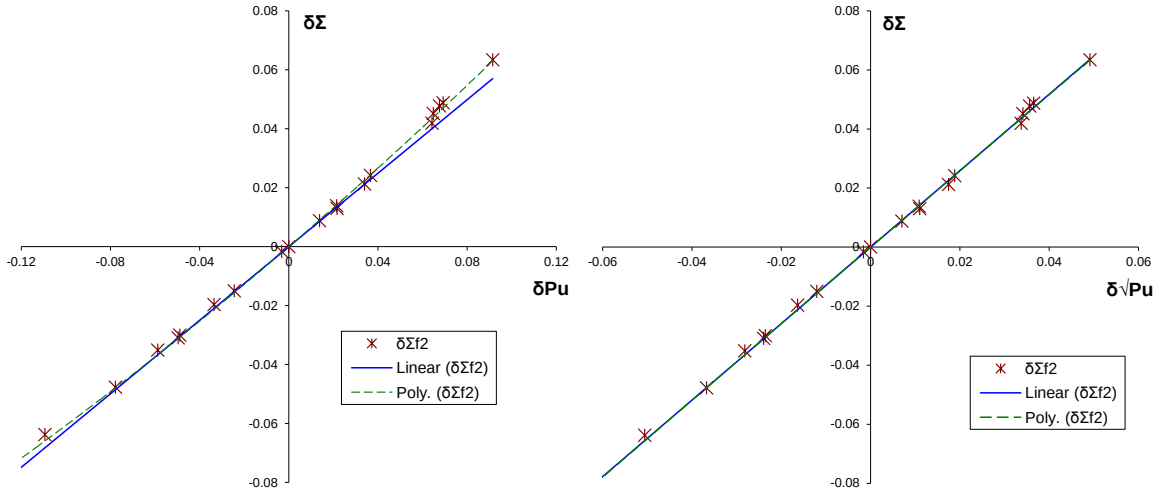

Fig. 4.6 Correlation between the relative change of macroscopic cross sections and ^{9}Pu concentrations in different depletions.

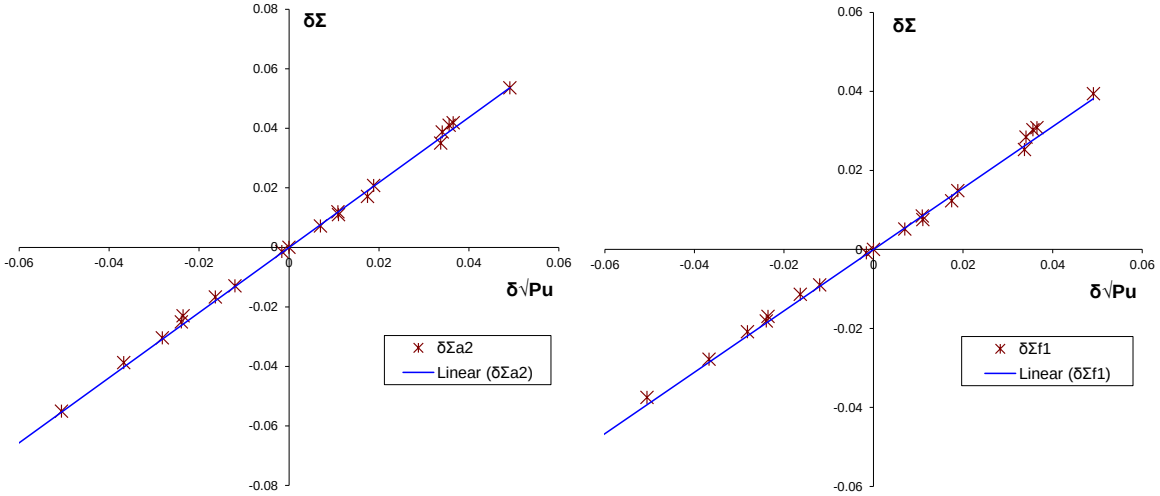

Fig. 4.7 Correlation between the relative change of macroscopic cross sections and square root of ^{9}Pu concentrations in different depletions.

The example of the fission cross section for the thermal group in Fig. 4.6 shows that a 2nd order polynomial describes the correlation better than linear proportionality. To avoid 2nd order coefficients and simplify the relation, the square root of the relative ^{9}Pu concentration

$$\delta\sqrt{Pu} = (\sqrt{Pu} - \sqrt{Pu^{nom}})/\sqrt{Pu^{nom}} = \sqrt{Pu/Pu^{nom}} - 1$$

was used (see Fig. 4.6 and Fig. 4.7). In this case 2nd and 1st order polynomials coincide and the relation can be described by a linear proportionality.

This means that **burnup history effects**, i.e. deviations of homogenized macroscopic cross sections from values of nominal depletion due to local spectral conditions, **may be taken into account by**:

$$\Sigma^{actual} = \Sigma^{nom} \cdot \left[1 + k \left(\sqrt{\frac{N_{Pu}}{N_{Pu}^{nom}}} - 1 \right) \right] \tag{4.1}$$

where Σ^{nom} – nodal macroscopic cross section calculated in the standard way,

N_{Pu}^{nom} – concentration of ^{9}Pu in the nominal depletion,

N_{Pu} – actual local ^{9}Pu concentration,

k – history coefficient, proportionality factor between differences in ^{9}Pu concentrations and differences in macroscopic cross sections.

History coefficients are ratios between the relative change of cross section and the relative change of the history indicator:

$$k = \delta\Sigma / \delta Pu = \frac{\Sigma^{off} - \Sigma^{nom}}{\Sigma^{nom}} \cdot \frac{\sqrt{N_{Pu}^{nom}}}{\sqrt{N_{Pu}^{off}} - \sqrt{N_{Pu}^{nom}}} \tag{4.2}$$

They are calculated for each cross section type and each fuel type as a difference between nominal depletion and, in principle, any of off-nominal depletions. The indexes *nom* and *off* in expression (4.2) indicate cross sections and nuclide concentrations for nominal and chosen off-nominal depletion, respectively.

4.2 Implementation

To implement the above-described method in DYN3D it is needed:

- to calculate the actual ^{9}Pu concentration for each node in the core during the burnup process;
- to calculate history coefficients for each fuel and cross section type;
- to implement the correction of cross sections by Eq. (4.1).

These implementations steps are described in following sections 4.2.1-4.2.3.

4.2.1 Calculation of the local ^{9}Pu concentration

The relevant path of building up ^{9}Pu in the fuel is:

$$^{8}U + n \longrightarrow {}^{9}U \xrightarrow{\beta\_23.5\,\mathrm{min}} {}^{9}Np \xrightarrow{\beta\_2.36day} {}^{9}Pu \tag{4.3}$$

^{8}U captures a neutron and after two β^--decays becomes ^{9}Pu. Due to the short (in burnup time scale) life of ^{9}U, it can be neglected, leading to the differential equations:

$$\frac{d}{dt} N_{^9Np}(t) = N_{^8U} \sum_{g=1}^{2} \sigma_{c,g}^{^8U} \phi_g - N_{^9Np} \left(\lambda_{^9Np} + \sum_{g=1}^{2} \sigma_{a,g}^{^9Np} \phi_g \right) \tag{4.4}$$

$$\frac{d}{dt} N_{^9Pu}(t) = \lambda_{^9Np} N_{^9Np} - N_{^9Pu} \left(\lambda_{^9Pu} + \sum_{g=1}^{2} \sigma_{a,g}^{^9Pu} \phi_g \right) \tag{4.5}$$

where λ – decay constant,

ϕ – neutron flux,

g – number of neutron energy group,

N_i – number densities of ^{8}U, ^{9}Np and ^{9}Pu,

σ_c, σ_a – microscopic cross sections of radiative capture and absorption, respectively.

To simplify expressions, additional variables (with the physical meaning of isotope depletion rate) are introduced:

$$F_{Np} = \lambda_{^9Np} + \sum_{g=1}^{2} \sigma_{a,g}^{^9Np} \phi_g \tag{4.6}$$

$$F_{Pu} = \lambda_{^9Pu} + \sum_{g=1}^{2} \sigma_{a,g}^{^9Pu} \phi_g \tag{4.7}$$

Because only one isotope for each chemical element is present in the following equations, the isotope indexes will be dropped (e.g. *Pu* instead of ^9Pu). Assuming neutron fluxes and microscopic cross sections to be constant during a (small) burnup time step Δt leads to the solution:

$$N_{Np}(t+\Delta t) = N_{Np}(t) e^{-F_{Np}\Delta t} + N_U \sum_{g=1}^{2} \sigma_{c,g}^{U} \phi_g \frac{1 - e^{-F_{Np}\Delta t}}{F_{Np}} \tag{4.8}$$

$$\begin{aligned} N_{Pu}(t+\Delta t) = {} & N_{Pu}(t) e^{-F_{Pu}\Delta t} + \lambda_{Np} N_{Np}(t) \frac{e^{-F_{Np}\Delta t} - e^{-F_{Pu}\Delta t}}{F_{Pu} - F_{Np}} + \\ & \lambda_{Np} \frac{N_U \sum_{g=1}^{2} \sigma_{c,g}^{U} \phi_g}{F_{Np}} \left(\frac{1 - e^{-F_{Pu}\Delta t}}{F_{Pu}} - \frac{e^{-F_{Np}\Delta t} - e^{-F_{Pu}\Delta t}}{F_{Pu} - F_{Np}} \right) \end{aligned} \tag{4.9}$$

This solution has been implemented in a new DYN3D subroutine. The actual ^{9}Pu and ^{9}Np concentrations for each node are calculated in the burnup calculation loop, illustrated in Fig. 4.8, and stored for each burnup step.

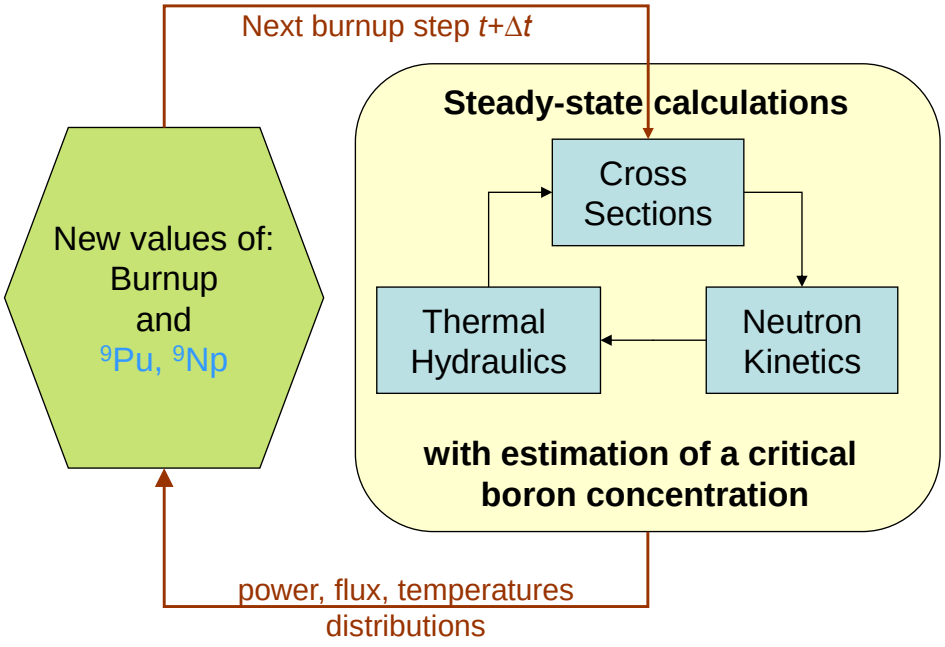

Fig. 4.8 Burnup calculation scheme.

Starting point of the burnup loop is a given material and burnup distribution reflecting the previous reactor-core operational history. For the given state, the code calculates the actual nodal two-group data using the given XS library. Next, the nodal distributions of neutron flux, power density, fuel temperature, coolant density and steady-state concentrations of the reactor poisons xenon and samarium are calculated by an iteration which includes temperature feedback. The calculation of the critical boron concentration (or critical power level) is also a part of the iteration process which finally leads to a stationary core state. The nodal power densities are assumed to be constant for a certain time interval, in which the nodal burnup values increase only little, compared to their increase during a whole reactor cycle. For this burnup time-step interval, DYN3D calculates a burnup growth within each node using the steady-state power densities. Actual ^{9}Np and ^{9}Pu concentrations for each node are calculated by (4.8) and (4.9) using local steady-state neutron fluxes and microscopic cross sections. Now, a new two-group data distribution belonging to the updated nodal burnup and ^{9}Pu values is derived for the next time step. In this way, the burnup calculation proceeds step by step until the end of cycle, or an interesting burnup state is reached, which then can be studied by dynamic DYN3D calculations.

4.2.2 History coefficients

The "history coefficients" *k*, needed for the correction calculation according to Eq. (4.1), are determined for each cross section type and each fuel-material type of the XS library from the results of two HELIOS depletion calculations: under standard (nominal) and modified (off-nominal) conditions.

As the ^{9}Pu-correction method is supposed to equally describe any local history, any off-nominal conditions could be chosen for the second depletion calculation. From the practical point of view it is better to choose conditions with big but reasonable deviations from the core-averaged values. For this study, the depletion calculation with deviations in moderator temperature $\Delta T_M = +20K$ (with moderator density depending on its temperature under nominal pressure) and in fuel temperature $\Delta T_F = +300K$ was used.

The history coefficients are calculated once from results of HELIOS or other lattice code and stored in a special "sub-library" file.

To solve the steady-state diffusion equation DYN3D uses the following (2-group assembly-homogenized) neutronic data from the XS-library:

- $D_{1,2}$ diffusion coefficients for the two neutron groups [cm];
- Σ_{a2} macroscopic absorption cross section (XS) for the thermal group [1/cm];
- Σ_s macroscopic scattering XS from the fast to the thermal group [1/cm];
- $\Sigma_{r=} \Sigma_s + \Sigma_{a1}$ macroscopic removal XS from the fast group [1/cm];
- $\nu\Sigma_{f1,2}$ macroscopic neutron production XS for the two neutron groups [1/cm];
- $E\Sigma_{f1,2}$ macroscopic energy production XS for the two neutron groups [MeV/cm].

The dimensionless history coefficients for these nine cross sections, obtained by (4.2), are shown in Fig. 4.9-4.11. A higher history coefficient means higher sensitivity of the cross section to the deviation in ^{9}Pu concentration, i.e. to the node's history. Thereby, Fig. 4.9-4.11 illustrate that for both UOX and MOX fuels the diffusion coefficients and Σ_r are practically not influenced by the local history; the most sensitive cross sections are Σ_{a2}, $\nu\Sigma_f$, and $E\Sigma_f$. The history coefficients of $\nu\Sigma_f$ and $E\Sigma_f$ are very close, as they are determined by Σ_f.

The high local-history sensitivity of fission cross sections for both groups can be explained by high fission microscopic cross sections of ^{9}Pu and ^{5}U. As shown in Fig. 3.2 (page 29), node history has a strong impact on fissile isotope concentrations, which determine the node-homogenized fission XS in both neutron groups. The high microscopic absorption XS of ^{9}Pu in the thermal group (~ 1100 barn) explains the influence of change in ^{9}Pu concentration on Σ_{a2}. The microscopic absorption XS of ^{9}Pu and ^{5}U in the fast group is relatively small (~14 and ~ 12 barn, respectively) – so Σ_r is almost not sensitive to the local history.

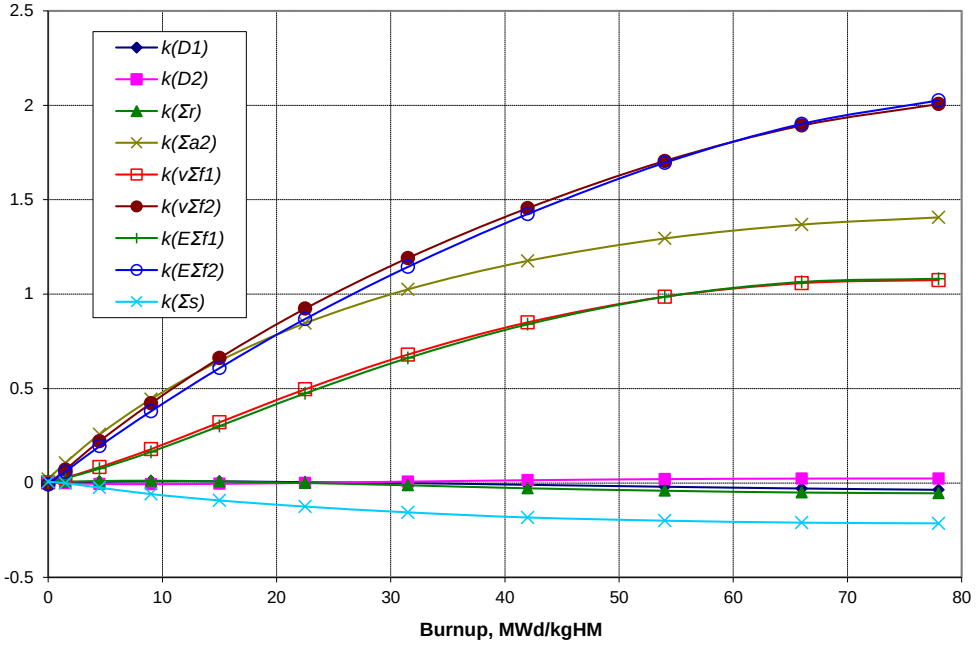

Fig. 4.9 Dependence of history coefficients for UOX fuel on burnup.

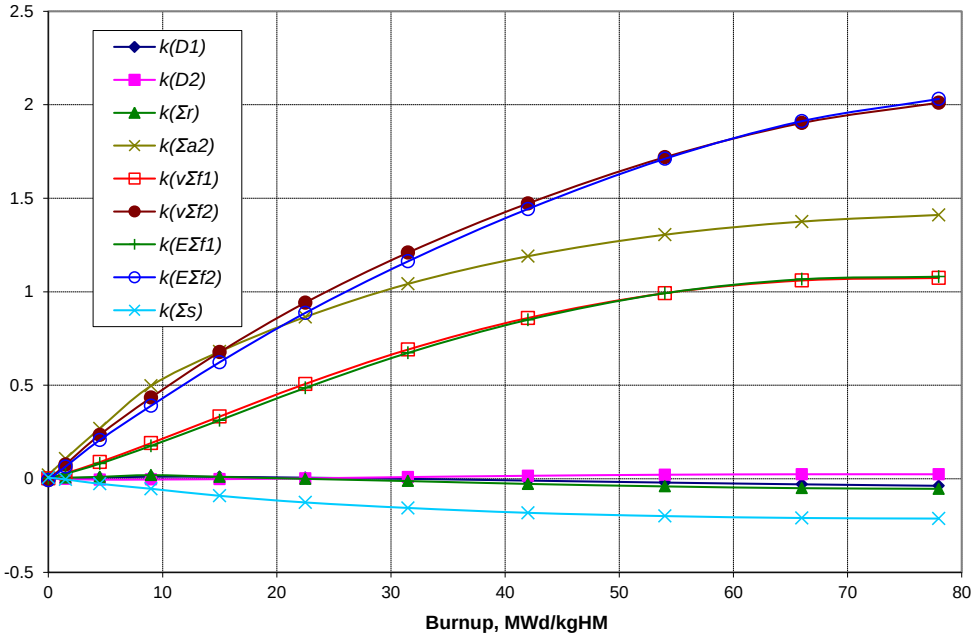

Fig. 4.10 Dependence of history coefficients for UOX fuel with burnable absorber on burnup.

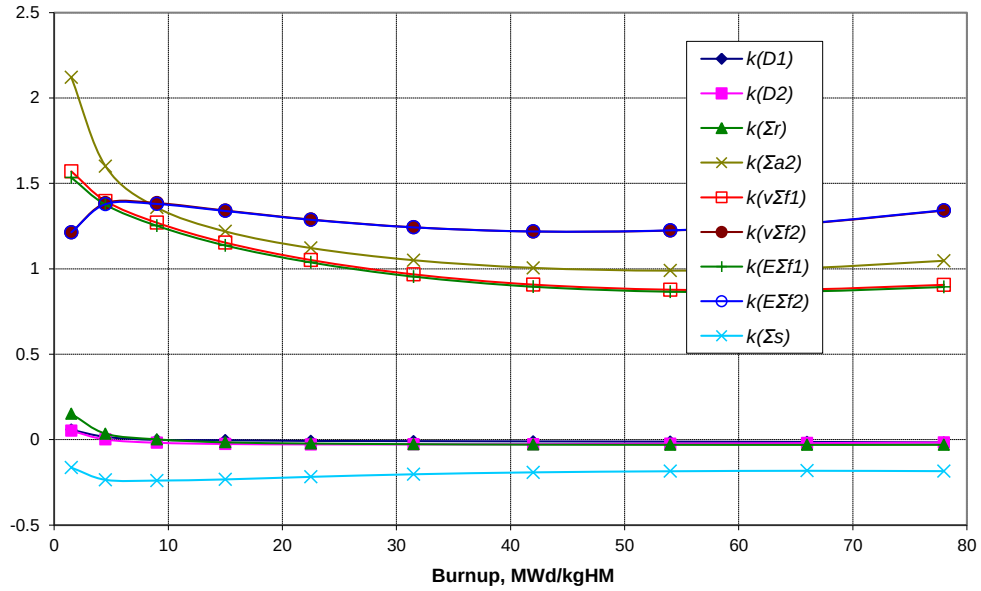

Fig. 4.11 Dependence of history coefficients for MOX fuel on burnup.

The history coefficients (4.2) are inversely proportional to a relative deviation of ^{9}Pu concentrations $\delta\sqrt{Pu} = \sqrt{Pu/Pu^{nom}} - 1$ between nominal and chosen off-nominal depletions. Fresh UOX fuel contains no ^{9}Pu, thus at the beginning of the burnup process, the differences between ^{9}Pu concentrations in two depletion courses are comparable to the absolute values of these concentrations. In case of MOX fuel, however, there is a large amount of ^{9}Pu in fresh fuel, while differences in ^{9}Pu concentrations for low burnup are small. For this reason the δPu parameter for MOX tends to zero at the beginning of the burnup process (see Fig. 4.12).

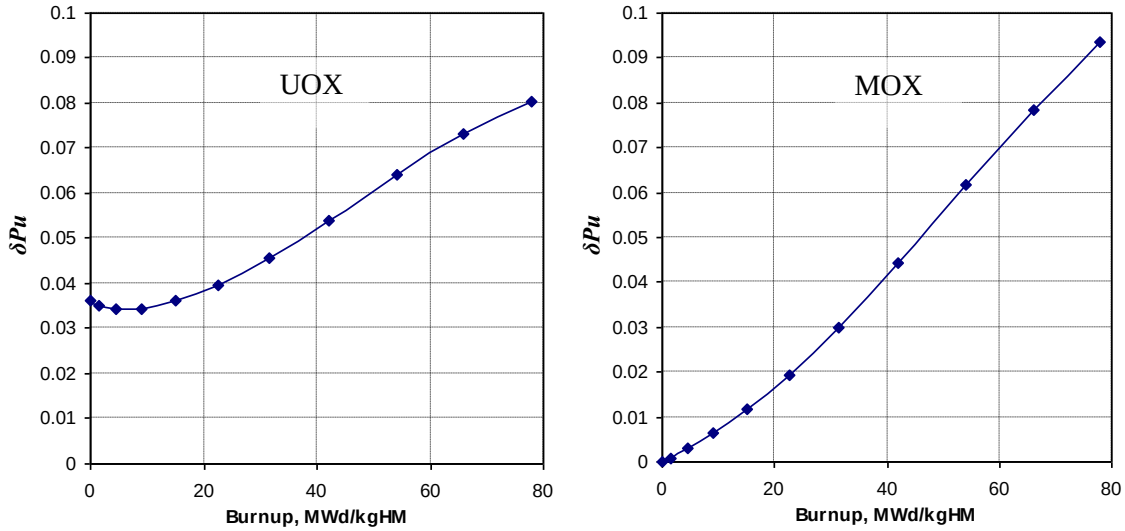

Fig. 4.12 Relative difference in ^{9}Pu concentrations between nominal and modified depletion for UOX (left) and MOX (right).

To avoid division by zero in Eq. (4.2) (calculation of history coefficients) and due to the fact that history effects are considerable only for high burnups the historical correction (4.1) is not applied to nodes with a burnup less than 5 MWd/kgHM.

The analysis of history coefficients obtained by (4.2) shows their dependence on burnup, instantaneous thermohydraulic parameters and boron concentration.

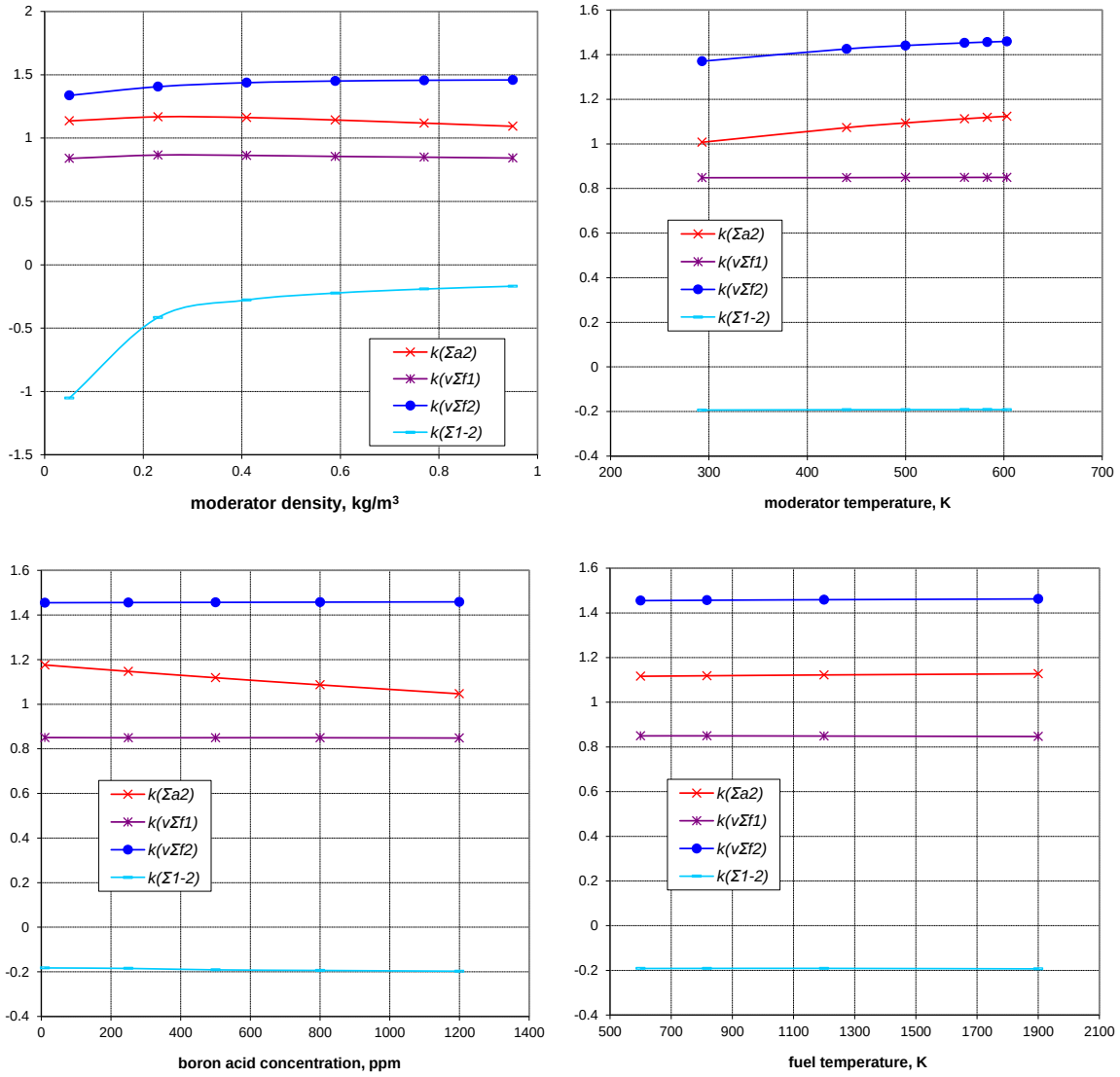

Fig. 4.13 Dependence of history coefficients on instantaneous local thermohydraulic parameters for UOX fuel.

As illustrated for the example of history coefficients for UOX fuel in Fig. 4.13, the dependence on the instantaneous fuel temperature is negligible for all coefficients. The dependence on boron concentration is significant only for the absorption XS in the thermal group, on moderator temperature – for absorption and fission in the thermal group. The dependence on moderator density is weak for all coefficients except downscattering. The outstandingly high sensitivity (to instantaneous moderator density) of the history coefficient for downscattering at very low water

density levels can be explained by poor moderation and growing impact of resonance absorption (i.e. fissile nuclides and actinide concentrations) in the fuel rod.

In the sub-library (see Fig. 4.14), dependencies of historical coefficients on burnup, instantaneous thermohydraulic parameters and boron concentration are given in multidimensional tables.

4.2.3 Cross sections correction

Changes made in the DYN3D nodal XS calculation scheme are shown in Fig. 4.14 in blue color.

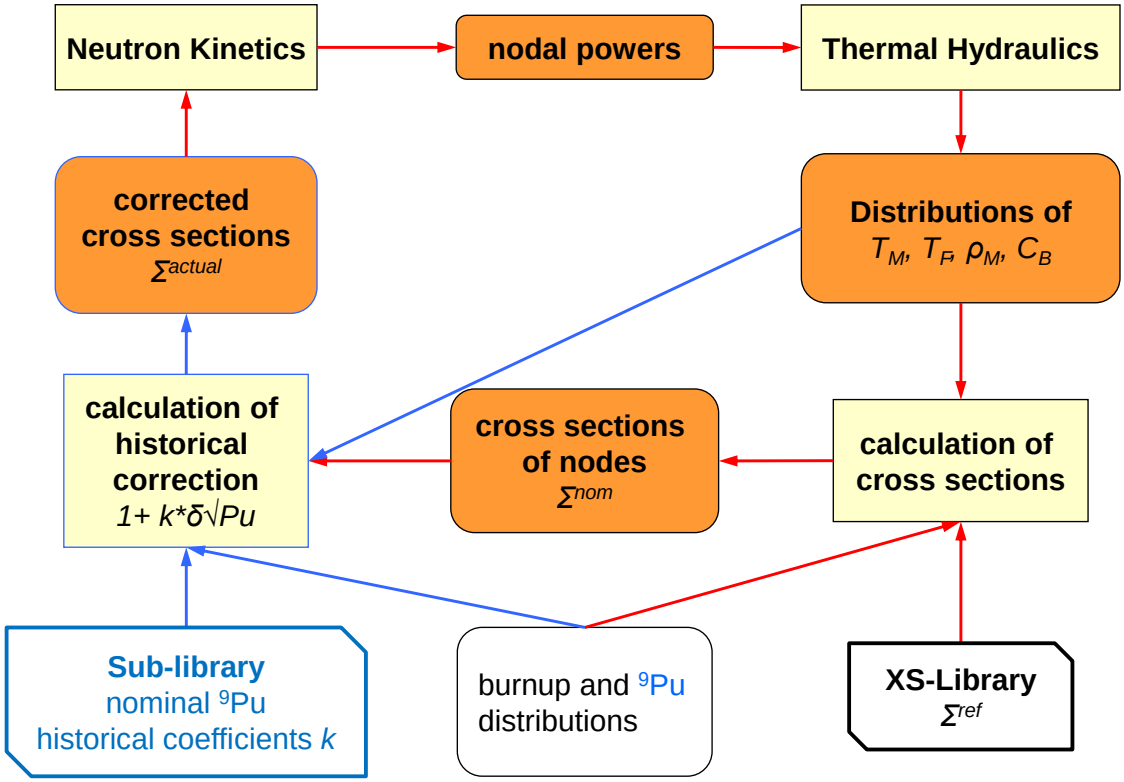

Fig. 4.14 Nodal cross section calculation scheme with historical correction.

Cross sections for each node Σ^{nom} are calculated using reference data from XS library, burnup distribution and actual nodal thermohydraulic parameters as it is described in section 2.3 (see Fig. 2.8). Before the use of cross sections in the neutron kinetics module they are multiplied by a historical correction $1 + k(\sqrt{Pu/Pu^{nom}} - 1)$ (see Eq.(4.1)).

Actual local burnup and ^{9}Pu distributions are obtained in core burnup calculations using the respective option of DYN3D (see Fig. 4.8). History coefficient k is determined by interpolation of the multidimensional table from the sub-library using the actual local burnup and thermohydraulic parameters. Nominal ^{9}Pu concentration is taken from the sub-library.

This scheme allows using existing XS libraries without any changes, because calculation of history correction is separated from calculation of cross sections. Only a historical sub-library has to be generated by a lattice code for each fuel type in a core. If there are few different XS libraries available for the same fuel types, it is possible to use the same sub-library with all of them.

4.2.4 The sub-library

The sub-library contains all the data necessary for the calculation of the historical correction:

- ^{9}Pu and ^{8}U concentrations in nominal depletion,
- microscopic cross sections needed for ^{9}Pu calculation,
- history coefficients.

Equation (4.1) requires the ^{9}Pu concentration in nominal depletion (depletion which was used in preparation of XS library). The comparison of ^{9}Pu concentrations calculated by the new subroutine of DYN3D (using Eq. (4.9)) and HELIOS under nominal conditions (see Fig. 4.15) shows a systematic error (about 1.5% at 50 MWd/kgHM). The reason of this error is the simplified treatment of the ^{9}Pu buildup with 2-group diffusion in DYN3D (see section 4.2.1) in comparison to the detailed burnup chains with multi-group transport in HELIOS.

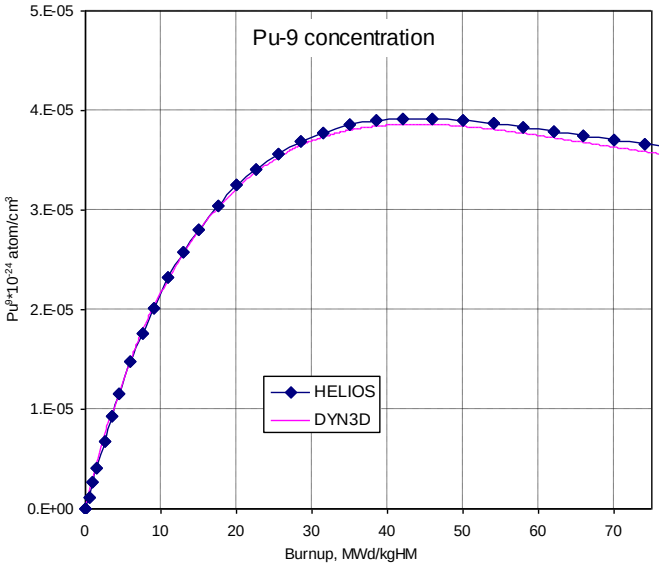

Fig. 4.15 ^{9}Pu concentration at nominal depletion.

For Eq. (4.1) a relative deviation of local ^{9}Pu concentrations from nominal is needed, so local and nominal ^{9}Pu concentrations should be calculated in a consistent way. Therefore nominal ^{9}Pu concentration for the sub-library is not taken from HELIOS depletion calculation but is calculated during sub-library preparation using the same procedure as in DYN3D (Eq. (4.9)) and 2-group condensed neutron fluxes from HELIOS.

2-group absorption for ^{9}Pu and ^{9}Np and radiative capture for ^{8}U microscopic cross sections are needed for the ^{9}Pu concentration calculation according to Eq. (4.4) and Eq. (4.5). They depend on instantaneous local operational parameters and burnup as well as on local history – i.e. a local ^{9}Pu concentration. In the sub-library those cross sections and their historical coefficients are given in multidimensional tables.

The content of a sub-library is calculated once (for each fuel type) from results of HELIOS (as a part of the XS-library preparation procedure or as a separate procedure if a XS-library already exists) and stored in a special DYN3D input file. Then the sub-library is used by DYN3D for any steady-state, burnup or transient calculation.

4.3 Comparison with other methods

Other approaches to the problem of burnup-spectral-history influence on cross sections have been described in section 3.2. In the following, a short estimation is given concerning advantages and disadvantages of the above-described ^{9}Pu-correction methodology in view of other existing solutions. A comparison of accuracies will be possible only by performing suitable benchmark calculations.

4.3.1 Microscopic depletion model.

The description of this method is given in section 3.2.1.

The hybrid micro/macro depletion model is based on “first principles”, but its implementation obviously requires storing of whole-core concentration distributions for 50 nuclides and adding all respective microscopic cross sections to a XS library. However, as shown above (see Fig. 4.4), history-induced deviations of different nuclide concentrations can be estimated by the deviation of a single nuclide such as ^{9}Pu. This assumption dramatically simplifies the method without significant loss of accuracy (see test results in chapter 5).

Besides, the influence of nodal spectral history on some kinetic parameters (for example on the delayed-neutron fraction) cannot be described by Eq. (3.2) (page 33), but needs an additional treatment. The historical correction used in proposed ^{9}Pu-correction method Eq. (4.1) could be easily calculated for any diffusion/kinetic parameter by Eq. (4.2).

4.3.2 Ad-Hoc parameters.

Section 3.2.3 gives a description of this method.

The Ad-Hoc-parameters method considers the history effects related to each of the mentioned exposure-weighted nodal parameters separately, while our studies show that all these effects are caused by the same mechanism – a perturbation of the neutron spectrum.

On the other hand, spectrum disturbances not described directly by the Ad-Hoc parameters (like presence of the control rod, influence of the poisoning and influence of the neighboring nodes on the local spectrum) are neglected. The concentration of ^{9}Pu is sensitive to any spectrum disturbance and, thereby, to any possible history effect. At the same time, the use of only one historical parameter makes ^{9}Pu-correction method simpler and less data need to be stored for each node and burnup step.

4.3.3 Spectral history index.

A description of this method is given in section 3.2.2.

The idea behind the Spectral-Index method is very similar to ^{9}Pu-correction method. Both methods are based on a detection of long-term spectral deviations, only the parameter which indicates a spectrum history is different. The calculation of *SI* by Eq. (3.6) or Eq. (3.7) does not require any additional data, while microscopic cross sections are needed for calculation of the ^{9}Pu concentration (Eq. (4.8) and (4.9)) and that means more data to be stored.

On the other hand the definitions of SI Eq. (3.6) or Eq. (3.7) are valid for 2-group solution and need to be revised for multigroup case. The definition of the ^{9}Pu-correction is exactly the same for a multigroup solution.

4.4 Chapter short summary

As shown in chapter 3, local spectrum conditions during burnup influence local nuclide content and thereby local cross sections. So, the change of cross sections is related to a change of nuclide content. The method described in section 4.1 uses the proven proportionality between the deviation of ^{9}Pu concentration and the deviation of macroscopic cross sections from their values in a single-assembly lattice code calculation.

For the implementation of this method, the nodal ^{9}Pu concentration calculation procedure was integrated into the core-burnup-calculation algorithm of DYN3D. The historical proportionality coefficients for each fuel type together with all necessary microscopic cross sections for ^{9}Pu-calculations make up a “historical sub-library”, i.e. an additional input file for DYN3D, which is prepared using a lattice code.

The main advantages of the proposed method in comparison to other methods described in the literature are:

- relative simplicity, small amount of additional data to be stored for each node;
- universality in terms of described effects;
- independence of methodology on the number of energy groups.

5 Method verification

Since the application of a macroscopic cross section library is a method of an information transfer from a lattice code to a reactor dynamics code, the errors which occur with history effects are consequences of imperfection of this transfer. The proposed ^{9}Pu-correction method was verified showing reduction of errors in cross section estimation.

In this chapter the results of DYN3D nodal cross section calculation with and without application of historical correction are compared with HELIOS single-assembly calculations. To make DYN3D results comparable with HELIOS and to illustrate changes in the nodal cross section estimation, a special DYN3D study was performed:

- the core consists of a single node,
- reflective boundary conditions as applied in HELIOS calculations,
- operational parameters were fixed to the same values as in the HELIOS calculations.

This simplified model allows testing the DYN3D cross sections estimation, using HELIOS results as a reference. As HELIOS is the source of the XS-libraries used by DYN3D – results of HELIOS and DYN3D XS calculations for the same conditions should coincide within the accuracy of interpolation / parameterization of the library. In case of using a standard XS-library for off-nominal depletion, there will be additional error in DYN3D results caused by history effects (as described in section 3.1). According to the physics of these effects, the historical error is equal to zero at the beginning of depletion and grows with the burnup.

5.1 PWR fuel

The HELIOS model of PWR fuel assemblies with rectangular lattice geometry is described in section 4.1.

The comparison for depletion under nominal (core-averaged) operational parameters is shown in Fig. 5.1. In this case there is no difference in ^{9}Pu concentration (historical correction factor (4.1) is equal to 1) and the nodal cross sections calculated by HELIOS and DYN3D agree within the accuracy of the XS library approximations.

Fig. 5.2-5.5 show results for depletion calculations for the same fuel under off-nominal operational parameters. The legend for all figures means: HELIOS – result of HELIOS calculation; DYN3D – result of DYN3D calculation with “standard” library; DYN3D-Pu – result of DYN3D calculation with application of ^{9}Pu-based historical correction. Instantaneous operational parameters in all calculations are equal to historical.

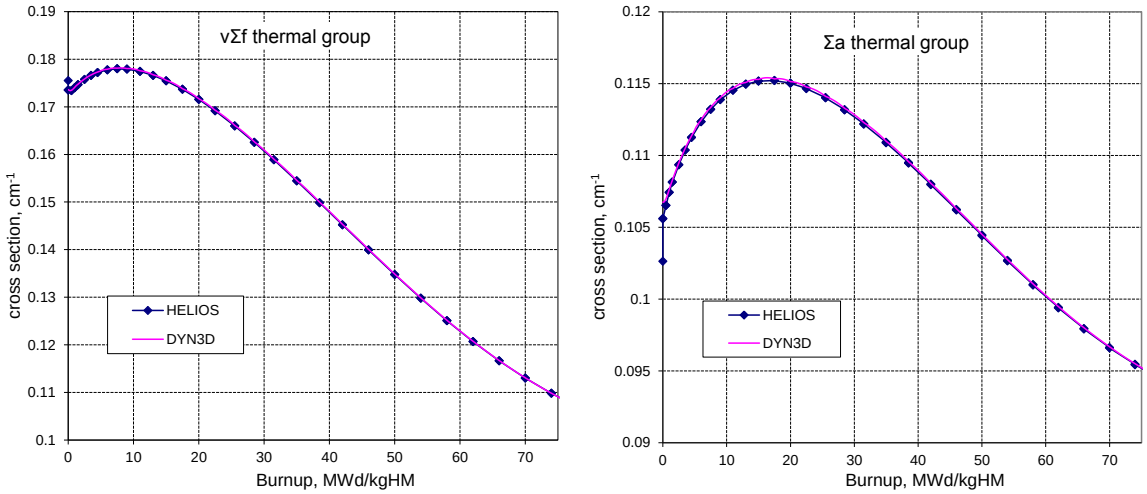

Fig. 5.1 Homogenized macroscopic cross section in nominal depletion.

The growing with burnup deviations between the XS values calculated by DYN3D with standard library and values calculated by HELIOS are caused by spectral history effects. The implementation of the historical correction nearly eliminates these deviations.

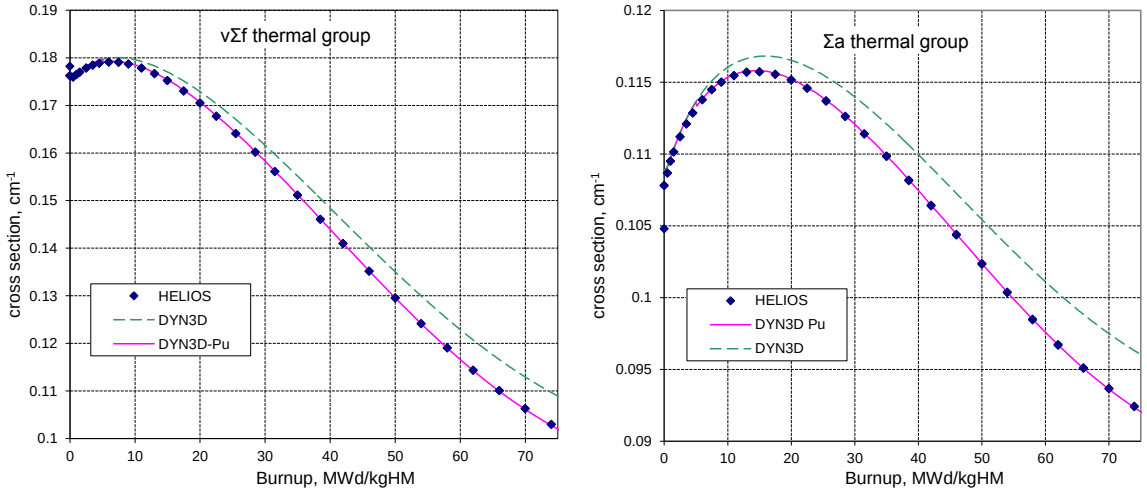

Fig. 5.2 Homogenized macroscopic cross sections for the depletion with deviation in moderator temperature ΔT_M=-20K.

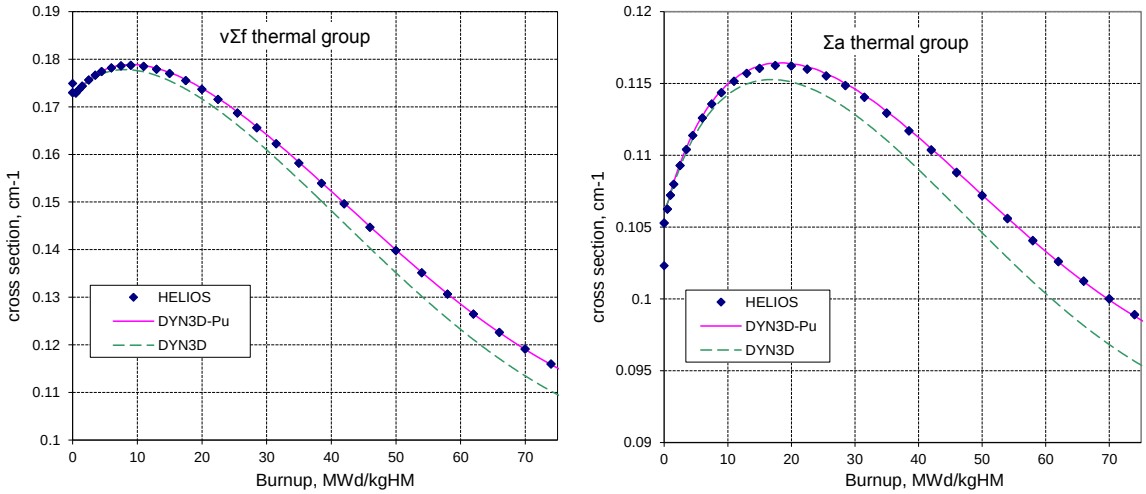

Fig. 5.3 Homogenized macroscopic cross sections for the depletion with deviation in fuel temperature ΔT_F=+300K.

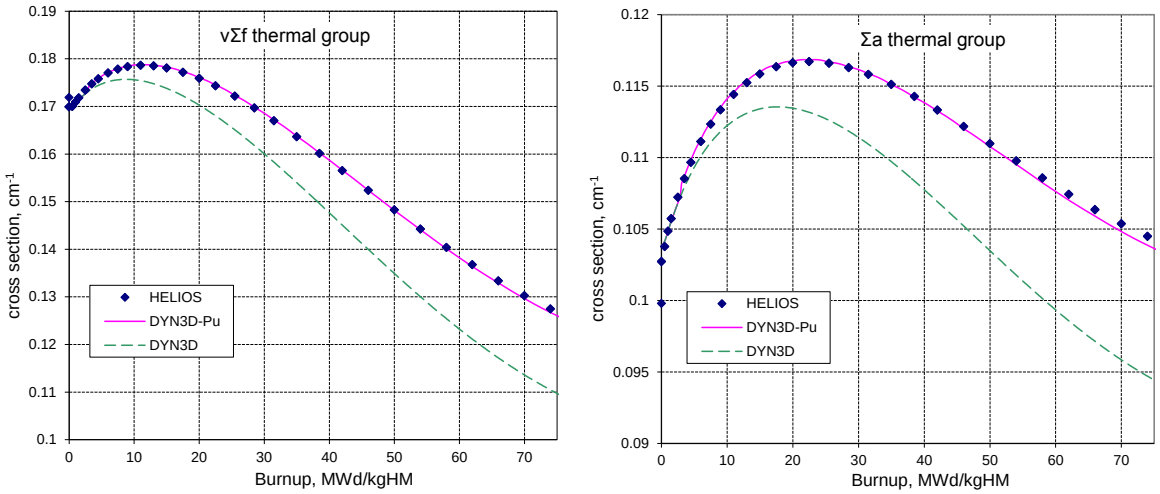

Fig. 5.4 Homogenized macroscopic cross sections for the depletion with deviation in moderator and fuel temperatures ΔT_M=+20K, ΔT_F=+300K.

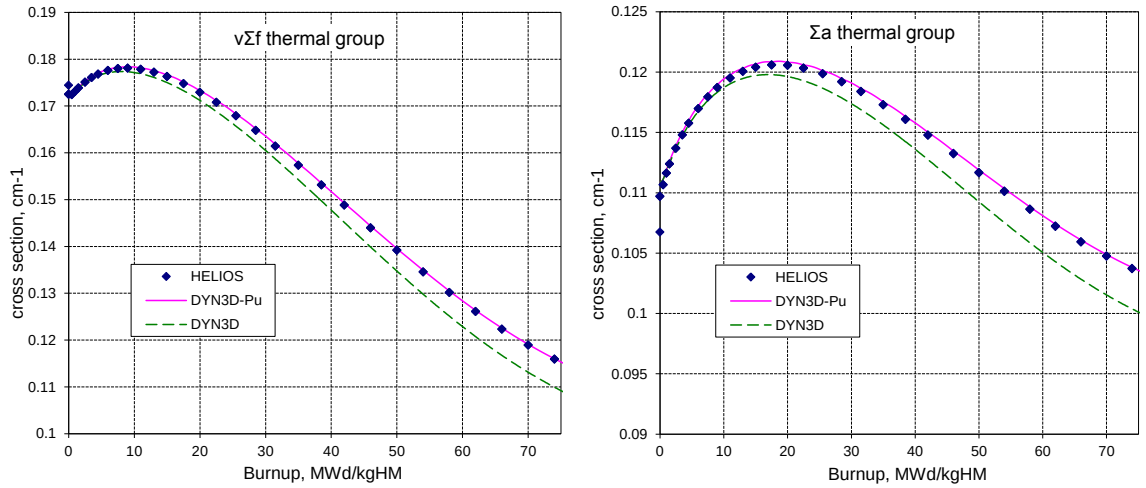

Fig. 5.5 Homogenized macroscopic cross sections for the depletion with deviation in boron acid concentration ΔC_B=+500ppm.

The applicability of the historical correction was also checked for a fuel with burnable absorber and a MOX fuel assembly with the same geometry. The respective results are illustrated in Fig. 5.6 and Fig. 5.7.

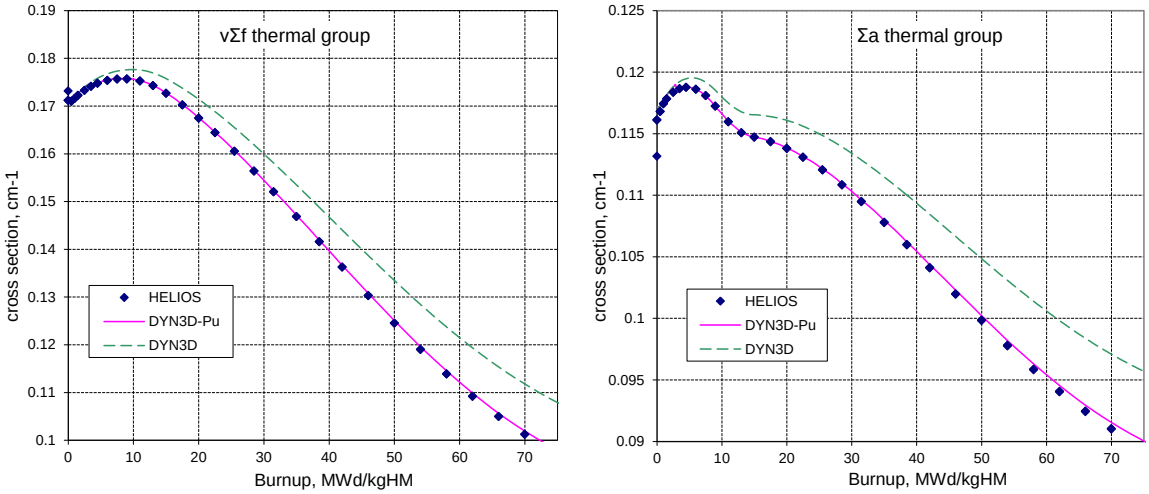

Fig. 5.6 Homogenized macroscopic cross sections of UOX fuel with BA for the depletion with deviation in moderator and fuel temperatures ΔT_M=-20K, ΔT_F=-200K.

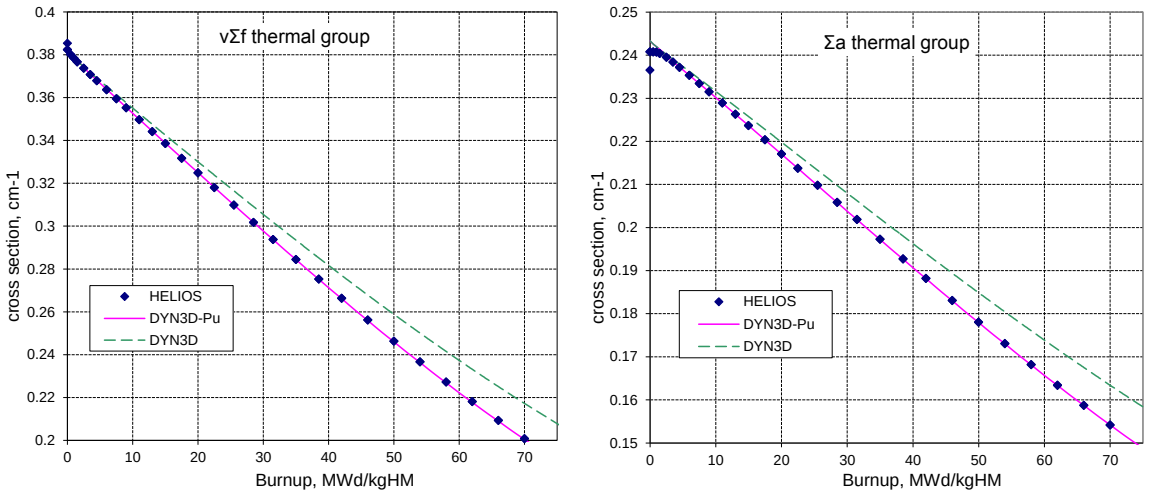

Fig. 5.7 Homogenized macroscopic cross sections of MOX fuel for the depletion with deviation in moderator and fuel temperatures ΔT_M=-20K, ΔT_F=-200K.

Results of various single-assembly depletion calculations are summarized in Fig. 5.8, which illustrates the deviation of multiplication factors calculated by DYN3D from HELIOS values. The application of the historical correction reduces the error by at least one order of magnitude (the difference in graph scales should be noticed).

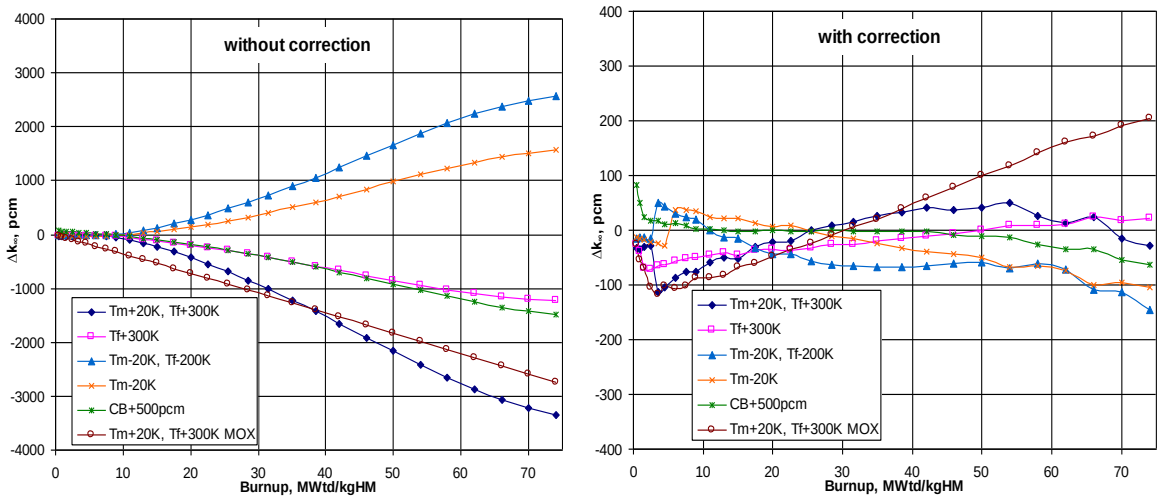

Fig. 5.8 Differences in multiplication factor calculated by HELIOS and DYN3D with and without historical correction.

The application of historical correction significantly improves the cross section estimation accuracy both for UOX and MOX fuel. Thus, the effectiveness of the method – to evaluate spectral-history-related changes of macroscopic cross sections by changes in ^{9}Pu concentrations – has been proved.

5.2 VVER fuel

The method was also verified for VVER-1000 fuel assemblies with hexagonal lattice geometry.

The HELIOS model of the 1/6 TWSA 430GO fuel assembly [Lötsch, 2009; Lötsch, 2010] is shown in Fig. 5.9. This fuel is composed of uranium dioxide fuel pins with different enrichment in ^{5}U and burnable absorber pins with gadolinium.

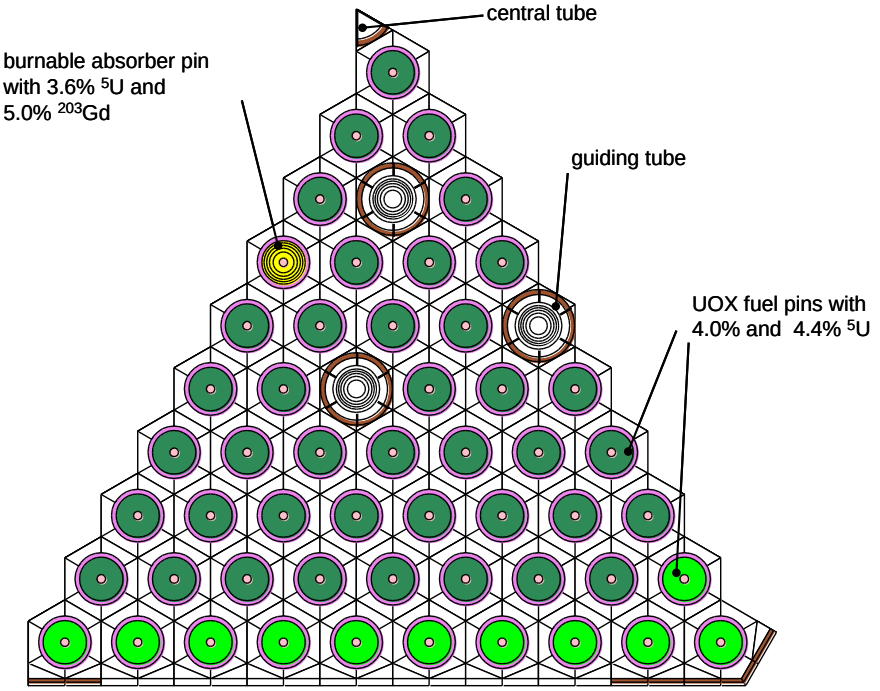

Fig. 5.9 The 60°-model of TWSA fuel.

The dimensionless history coefficients for these nine cross sections, obtained by (4.2), are shown in Fig. 5.10. Just like in the PWR fuel case (see Fig. 4.10) the most spectral-history-sensitive cross sections are the ones of fission in both groups and of absorption in the thermal group.

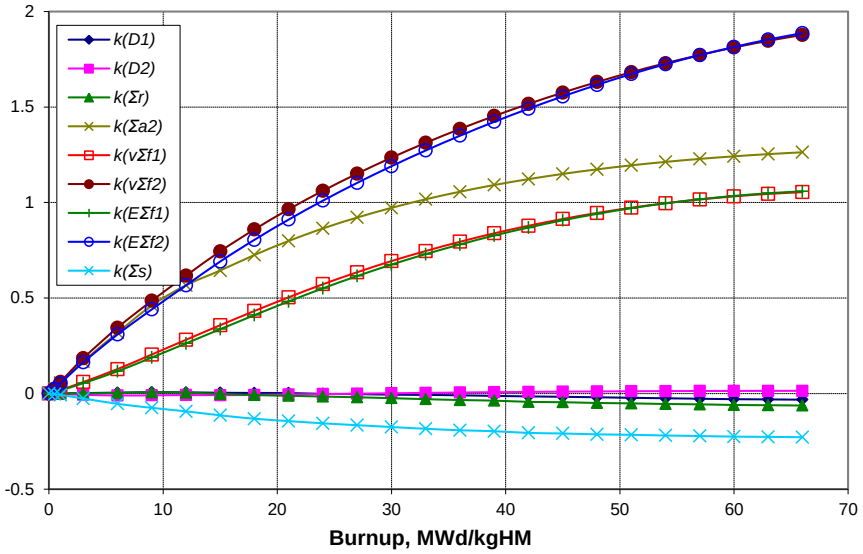

Fig. 5.10 Dependence of history coefficients for TWSA fuel on burnup.

The similar simplified DYN3D model as in the PWR case (see section 5.1) was used to perform single-assembly calculations. The parameterized-data XS-library used for DYN3D calculations was prepared by SSTC NRS (Kyiv, Ukraine) using HELIOS.

Results of the off-nominal depletion calculations are shown in Fig. 5.11-5.13. The legend for the figures is the same as in the PWR case (see Fig. 5.2). DYN3D calculations with the standard

library show growing with burnup errors caused by spectral history effects, which are significantly reduced by the application of historical correction.

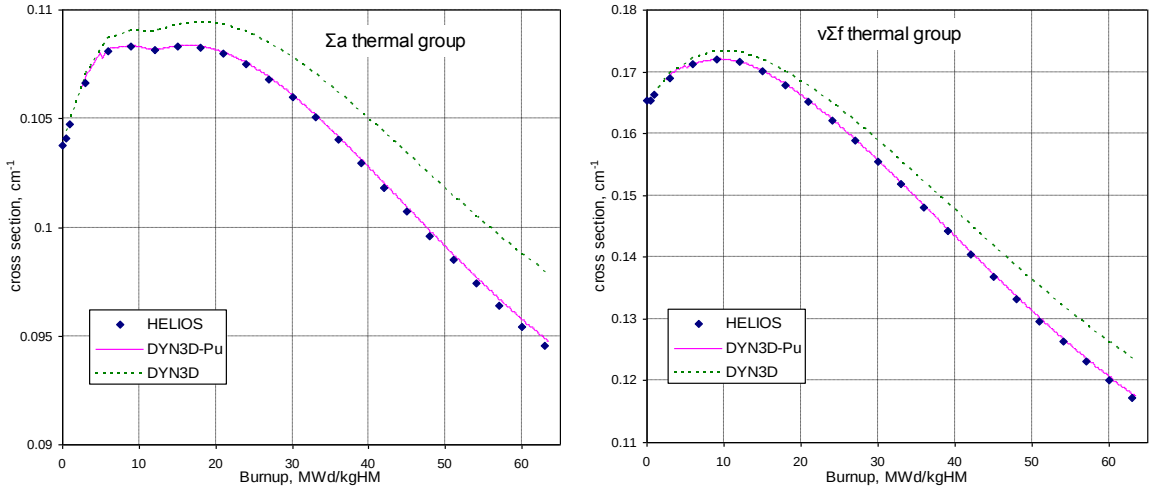

Fig. 5.11 Homogenized macroscopic XS for the depletion with off-nominal moderator temperature ΔT_M=-20K.

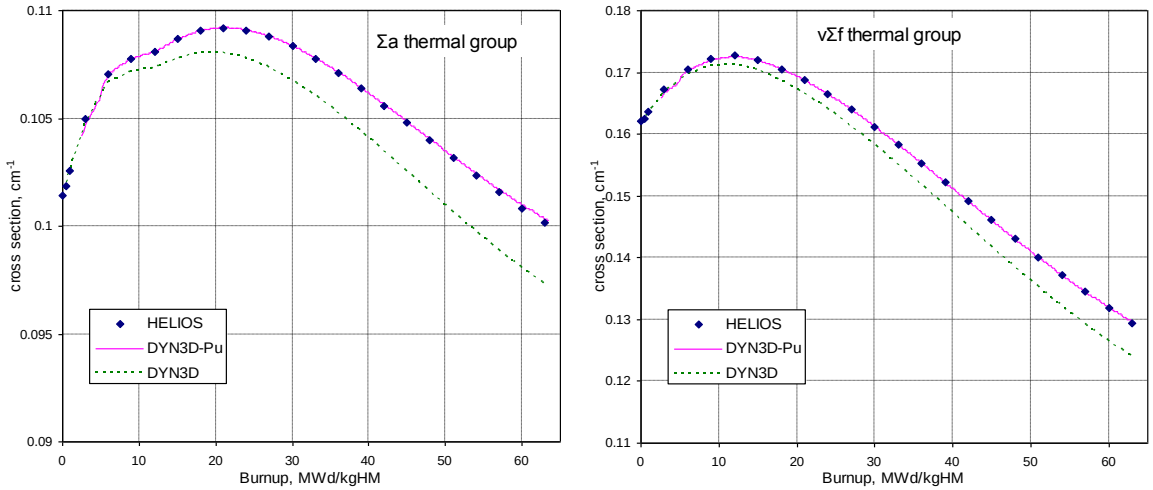

Fig. 5.12 Homogenized macroscopic XS for the depletion with off-nominal fuel temperature ΔT_F=+300K.

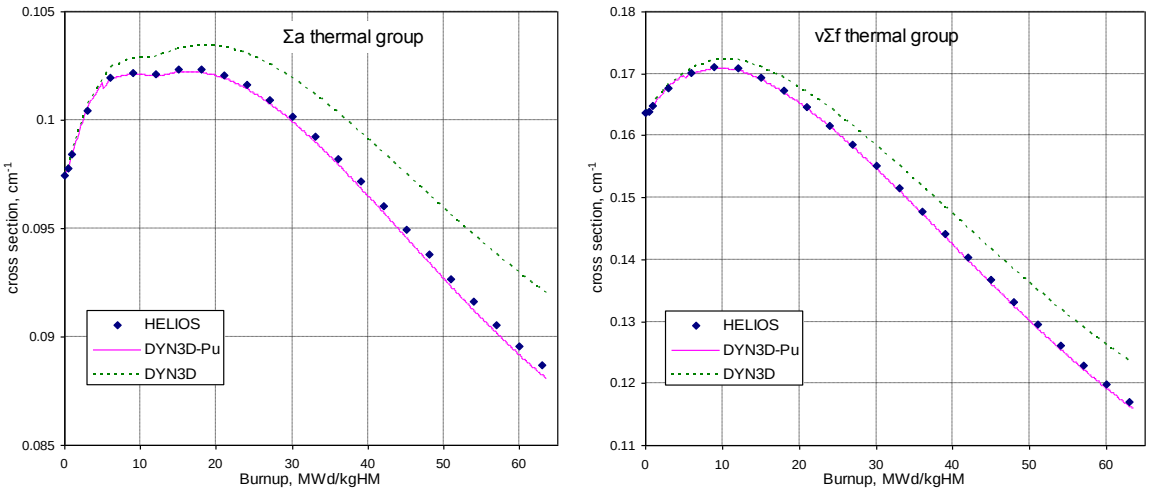

Fig. 5.13 Homogenized macroscopic XS for the depletion with off-nominal boron concentration *CB*=0 g/kg.

Results of the off-nominal depletion calculations are summarized in Fig. 5.14. The application of the historical correction reduces the error in multiplication factor by more than a factor 10.

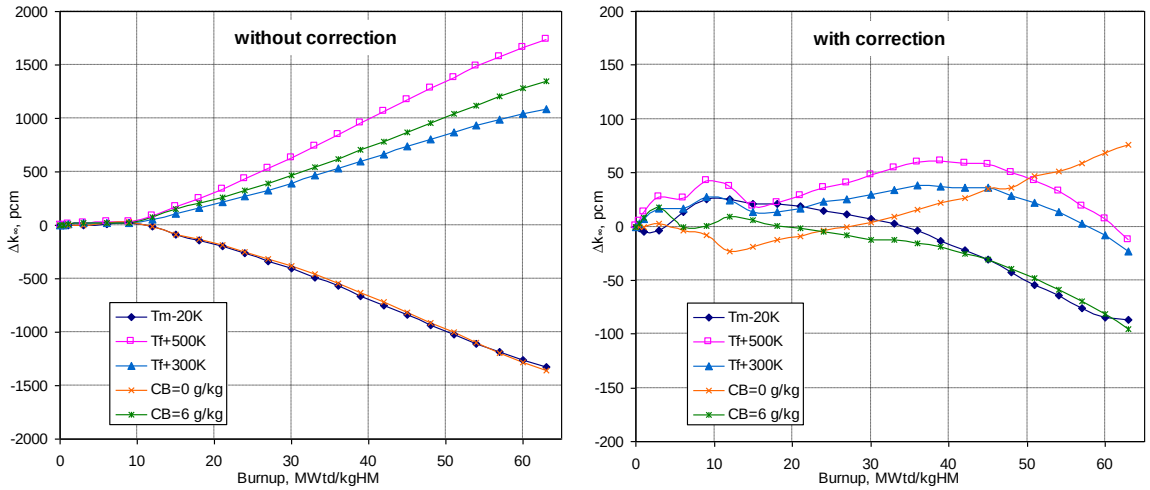

Fig. 5.14 Effect of historical correction on deviation of multiplication factor calculated by DYN3D from HELIOS values.

The results illustrated above proof the effectiveness of the ^{9}Pu-based history correction method for VVER fuel with hexagonal geometry.

5.3 Chapter short summary

The DYN3D cross section calculation procedure is verified in this chapter. Nodal cross sections calculated by the nodal code DYN3D using HELIOS-generated XS-libraries for Western-type PWR and VVER fuels are compared to cross sections calculated by the lattice code HELIOS in different depletion conditions which are present in the cores. The comparison shows a growing with the

burnup error in DYN3D cross sections and multiplication factor estimation, which is caused by spectral history effects.

The application of ^{9}Pu-correction reduces error in multiplication factor from 2-3 thousands pcm to less than 100 pcm for UOX fuel both with quadratic and hexagonal geometries, and to less than 200 pcm in case of MOX fuel.

6 Full-core steady-state and burnup calculations

The purpose of the study described in this chapter is to evaluate the influence of the historical correction on the full-core steady state and burnup calculation results such as 3D power and burnup distributions, critical boron acid concentration, fuel cycle length, fuel temperature distribution, reactivity coefficients and control rod worth. DYN3D results obtained with and without two types of history corrections are compared with each other. Some of these results have been published in [Bilodid, 2011; Bilodid, 2012].

6.1 Equilibrium fuel cycle

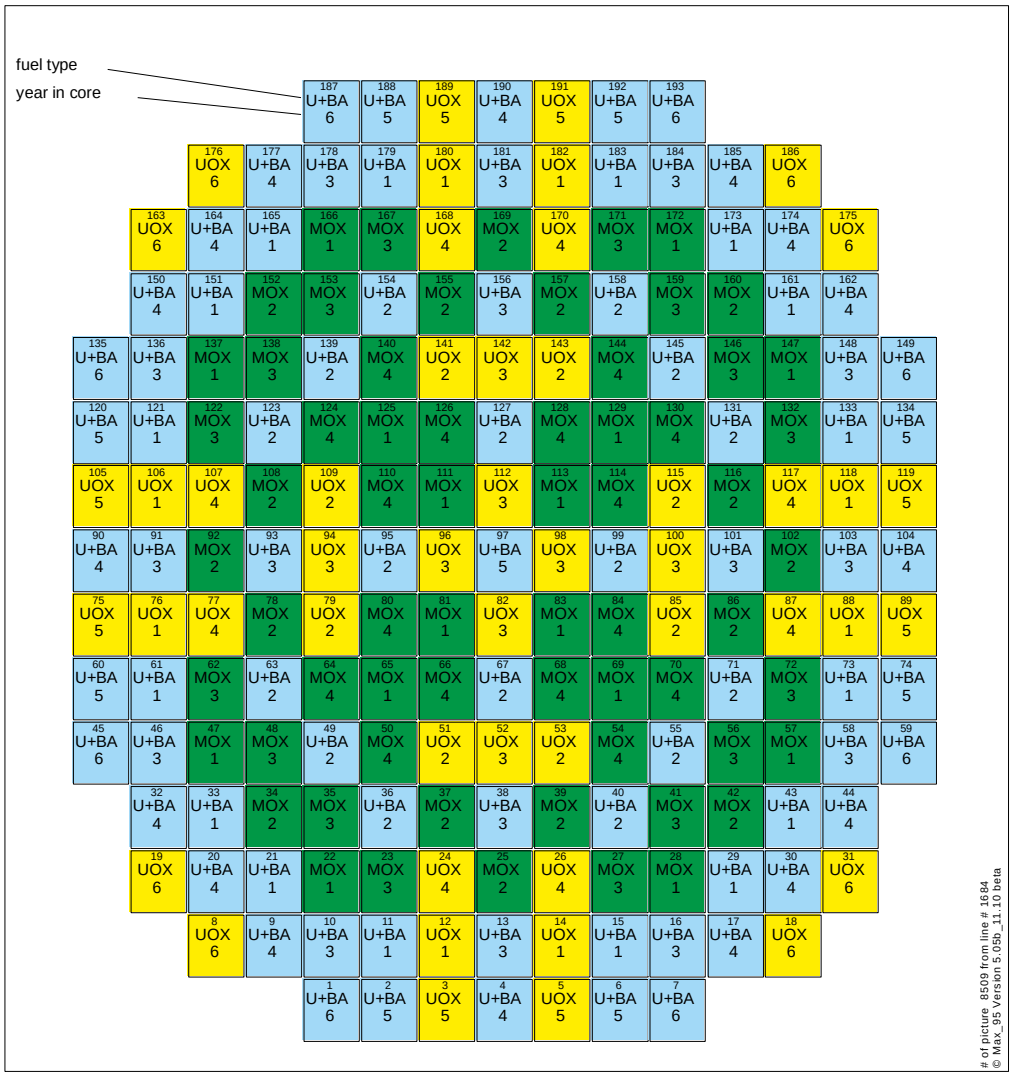

Fig. 6.1 Equilibrium fuel loading.

The influence of the historical correction on results of full-core burnup calculations were studied for a generic equilibrium fuel cycle of a PWR Konvoi. Equilibrium cycle means that the fuel shuffling scheme and the cycle length of the cycle is the same as in the previous one.

The fuel loading (see Fig. 6.1) contains three fuel types: UOX, UOX+BA and MOX (see Fig. 6.1 and Fig. 6.2). A description of the fuel types and their modeling in the lattice code HELIOS is given in section 4.1 (see Fig. 4.1).

The DYN3D model divides the reactor core into nodes: in the radial plane one node per fuel assembly and 14 layers in the axial plane. Additionally, the core is surrounded by a ring of reflector assemblies and top and bottom reflector layers.

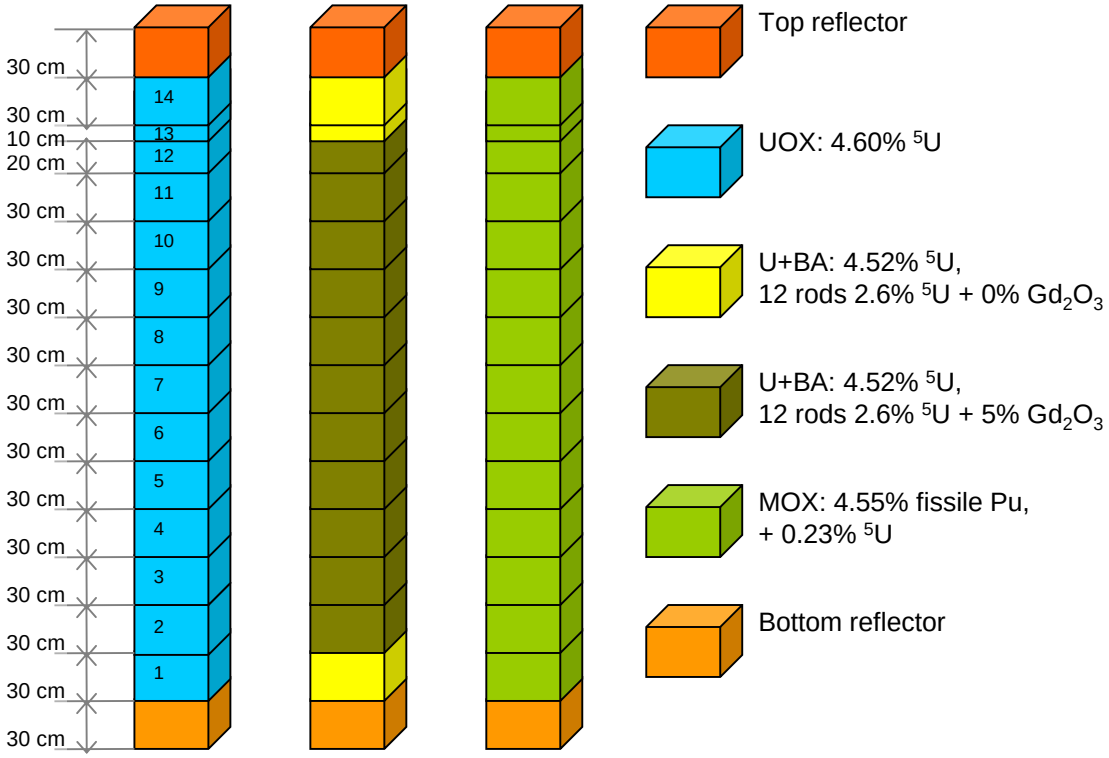

Fig. 6.2 PWR Konvoi fuel model in DYN3D.

For this study the Ad-Hoc parameter method (see chapter 3.2.3) was used for comparison. This method was partly (only steady-state) implemented in DYN3D and a special version of the cross section library was prepared in the frame of a common project with TÜV [Mittag, 2006]. It was not fully validated, but results of steady-state calculations have shown good agreement with SIMULATE-3 results.

For this study the Ad-Hoc-mode of DYN3D was complemented with a core-burnup calculation option. Ad-Hoc parameters are derived in burnup calculations using Eq. (3.8). The comparison of the results of the different methods is useful and allows to judge about general tendencies.

Fig. 6.3-6.16 represents results of the calculations. The legend is the same for all figures:

- DYN3D – is the “standard” DYN3D calculation mode without historical correction,

- DYN3D-Pu – with correction based on ^{9}Pu concentration,
- DYN3D-AdHoc – with correction using Ad-Hoc parameters.

Figures which illustrate radial distributions of burnup and power have been prepared using the visualization tool MAX_CORE. This program compares two radial distributions showing difference in absolute values or in per cent. The upper left corners contain headings of shown distributions; the lower left corners show the numbers of fuel assemblies with the maximum value in each distribution and maximum difference.

For each of the DYN3D modes fuel cycle calculations were repeated until an equilibrium state was reached (no changes in fuel cycle length, boron concentration and power distribution at the beginning of each next cycle). The basic cross section library was the same for all calculations, so any differences in results are determined only by historical corrections.

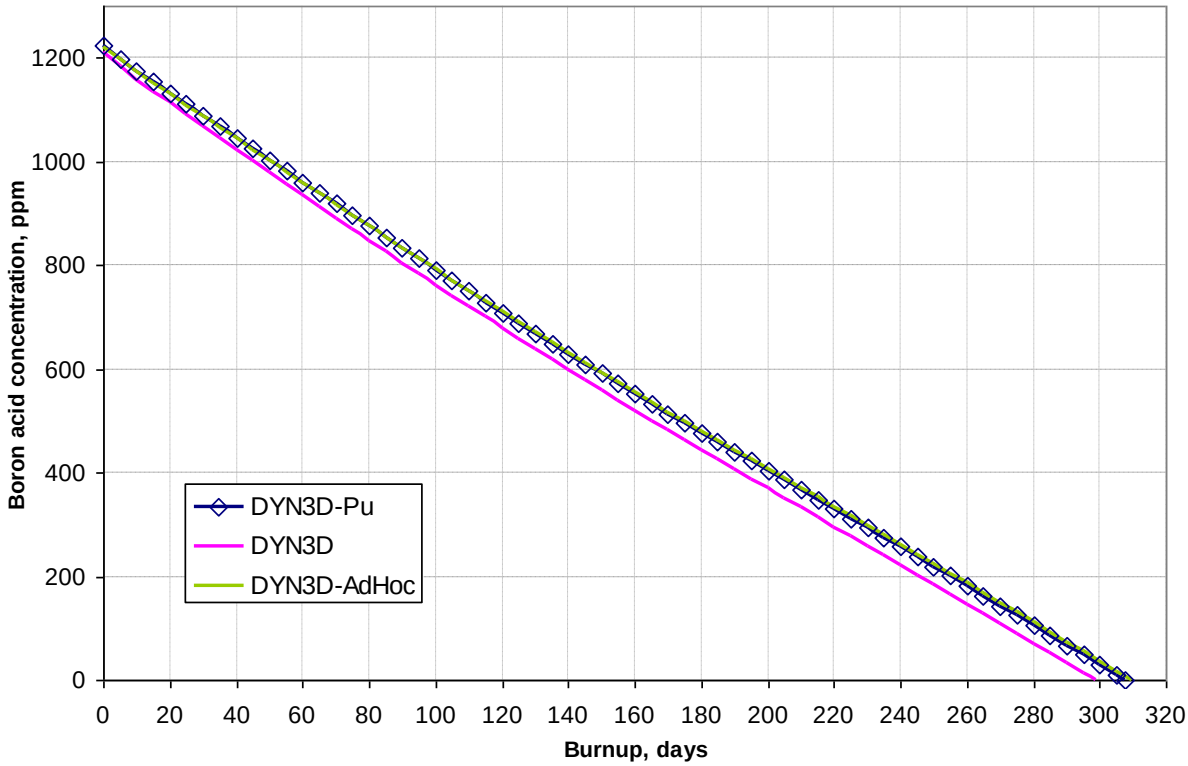

Fig. 6.3 Equilibrium fuel cycle length.

Burnup calculations were carried out up to zero critical boron concentration. The equilibrium fuel cycle lengths (see Fig. 6.3) are: without correction - 298.9 days, for DYN3D-Pu – 307.8 days and for DYN3D-AdHoc – 309.9 days. The results of calculations with corrections show good agreement among themselves but are about 10 days longer than in the standard calculation.

Table 6.1 Equilibrium cycle length

	DYN3D	DYN3D-Pu	DYN3D-AdHoc
Boron concentration at the beginning of cycle, ppm	1205	1220	1218
Cycle length, FPD	298.9	307.8	309.9
Core-averaged burnup at the beginning of cycle, MWd/kgHM	26.58	27.36	27.54
Core-averaged burnup at the end of cycle, MWd/kgHM	37.87	38.99	39.25

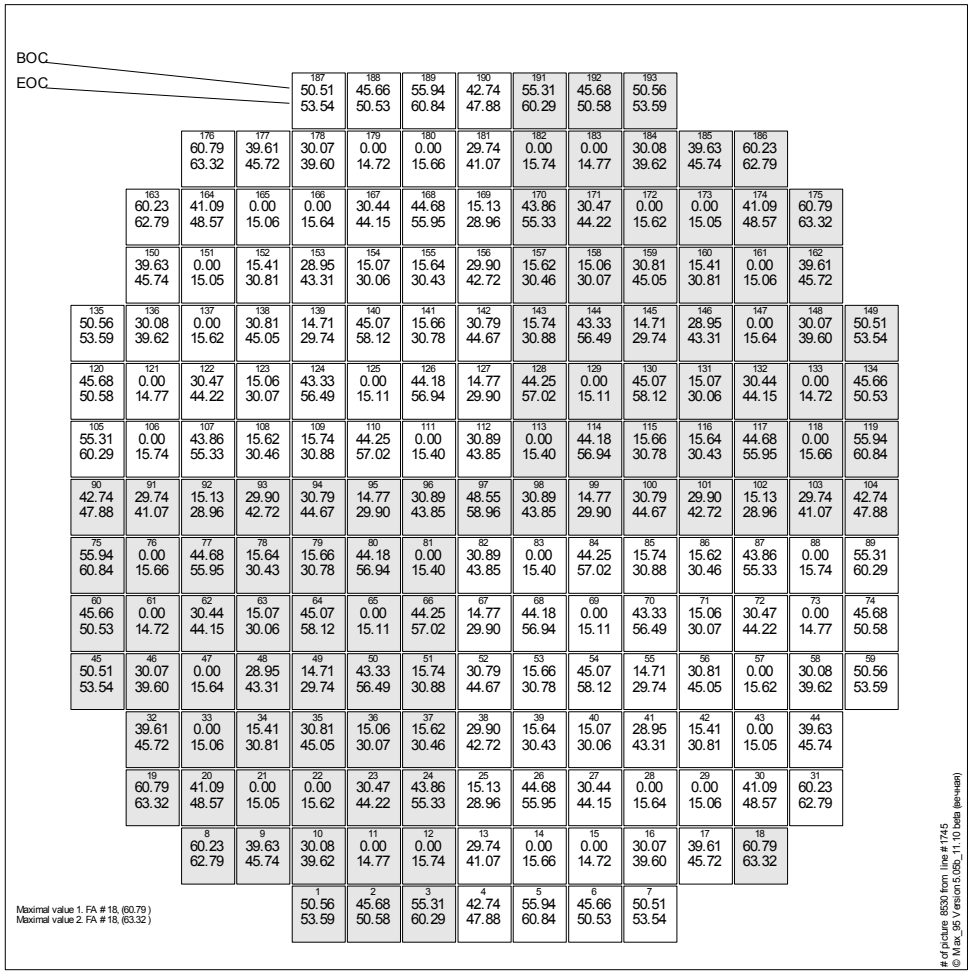

Fig. 6.4 Assembly-averaged burnup distribution in the core by DYN3D-Pu.

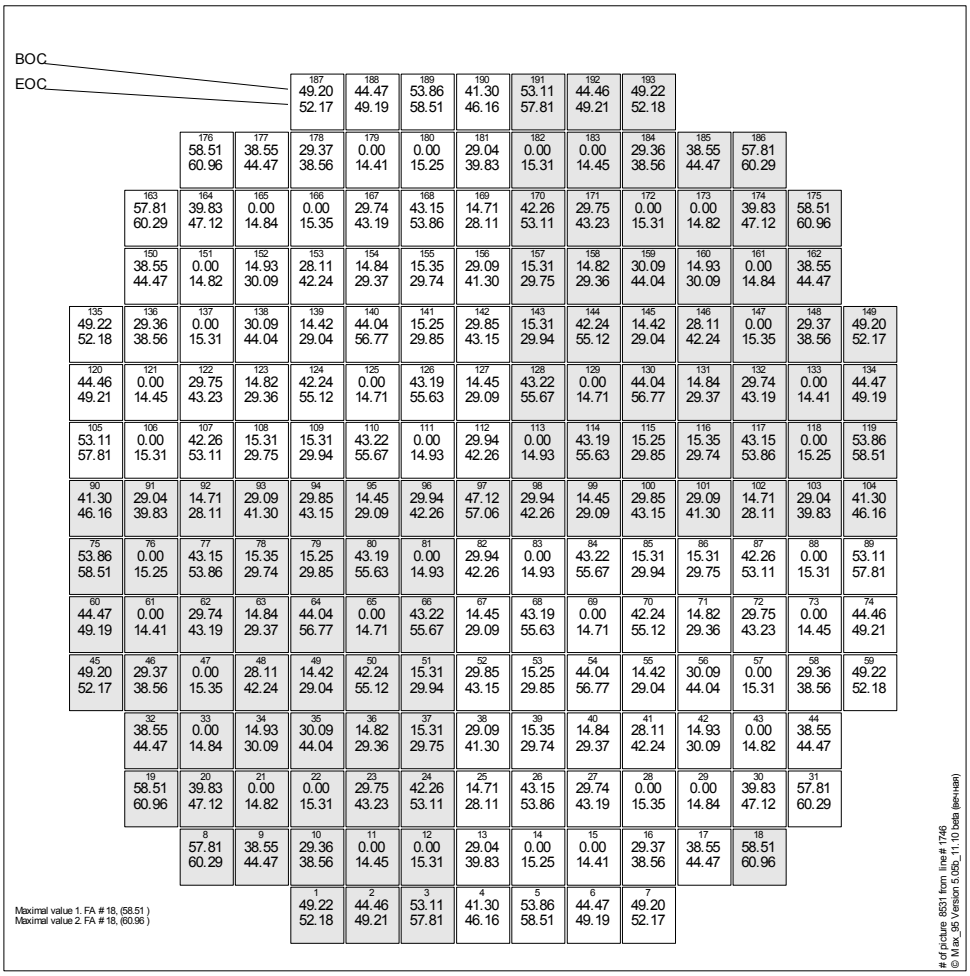

Fig. 6.5 Assembly-averaged burnup distribution in the core by DYN3D.

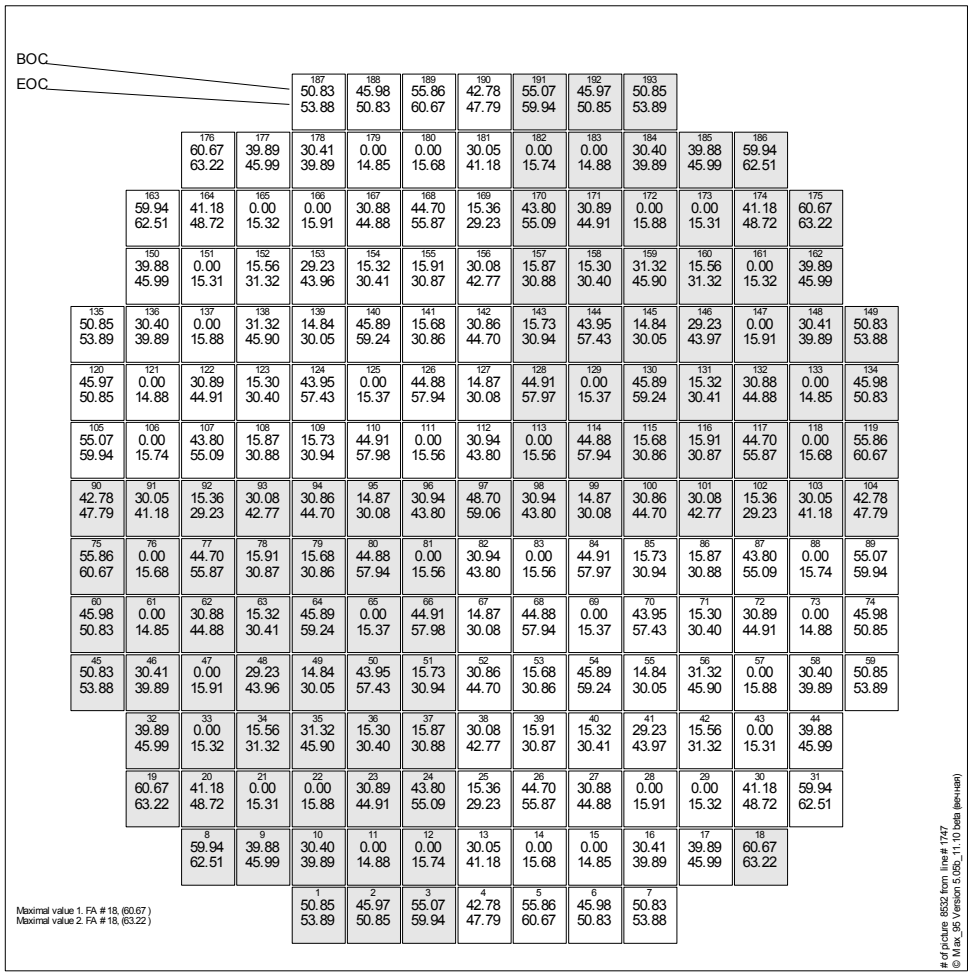

Fig. 6.6 Assembly-averaged burnup distribution in the core by DYN3D-AdHoc.

6.2 Power distributions

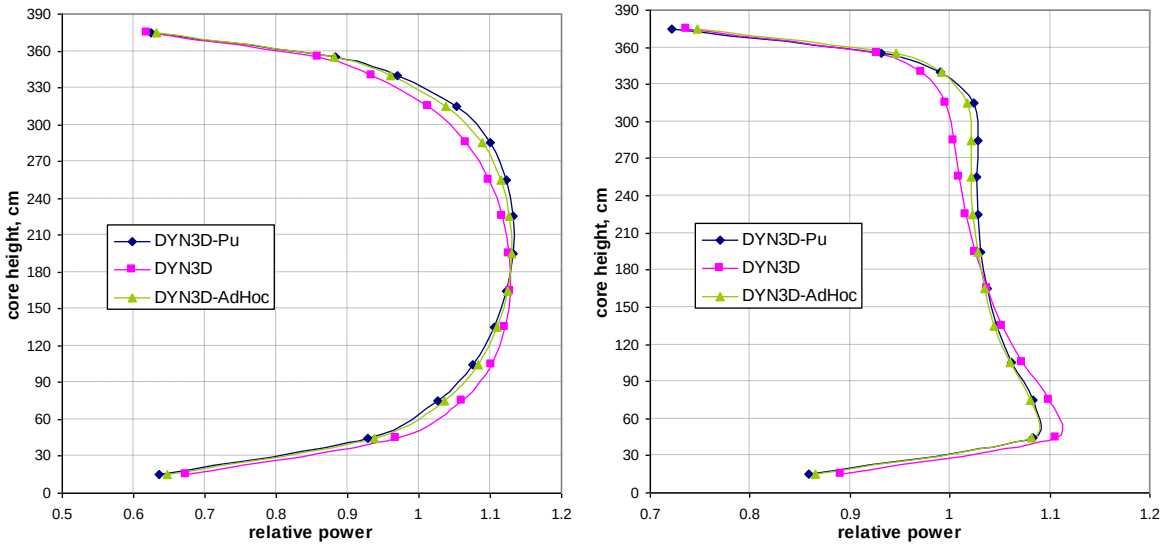

Fig. 6.7 Radially averaged relative power of the core at the beginning (left) and the end (right) of equilibrium cycle.

The 3D power distributions at the beginning and the end of the equilibrium cycle are compared in Fig. 6.7-6.14.

Axial distributions of a radially averaged relative power in core at the beginning and the end of equilibrium cycle are shown in Fig. 6.7. Both methods of historical correction lead to a shift of power generation to the upper part of core during the whole cycle. Increase of relative power in layer 11 and decrease in layer 3 are about 3%.

Assembly-averaged radial power distributions are shown in Fig. 6.8-6.11. The implementation of Ad-Hoc historical correction has a quite minor effect on the radial power distribution, while the results of DYN3D-Pu show a slightly bigger deviation (up to 5% at the beginning of cycle) from standard calculations. As expected, the highest deviations are in the assemblies with the highest burnup.

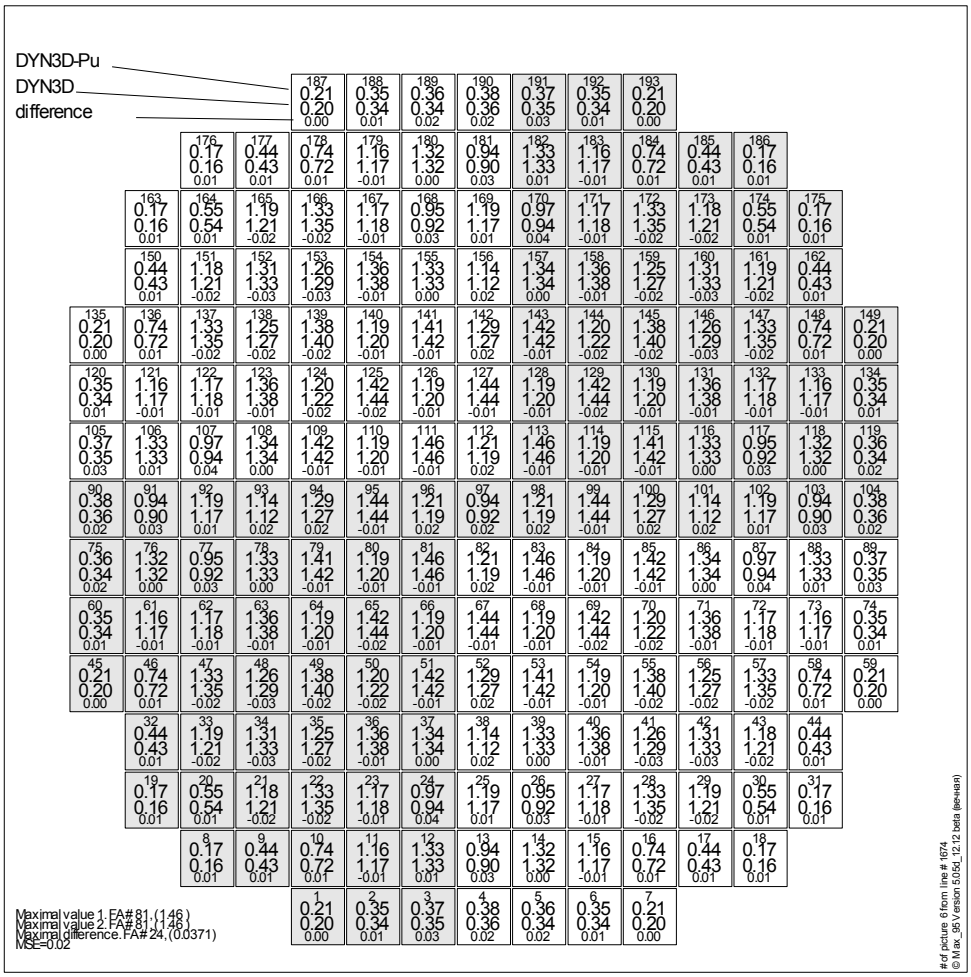

Fig. 6.8 Assembly-averaged relative power distribution in the core at the beginning of equilibrium cycle. Comparison between DYN3D-Pu and DYN3D.

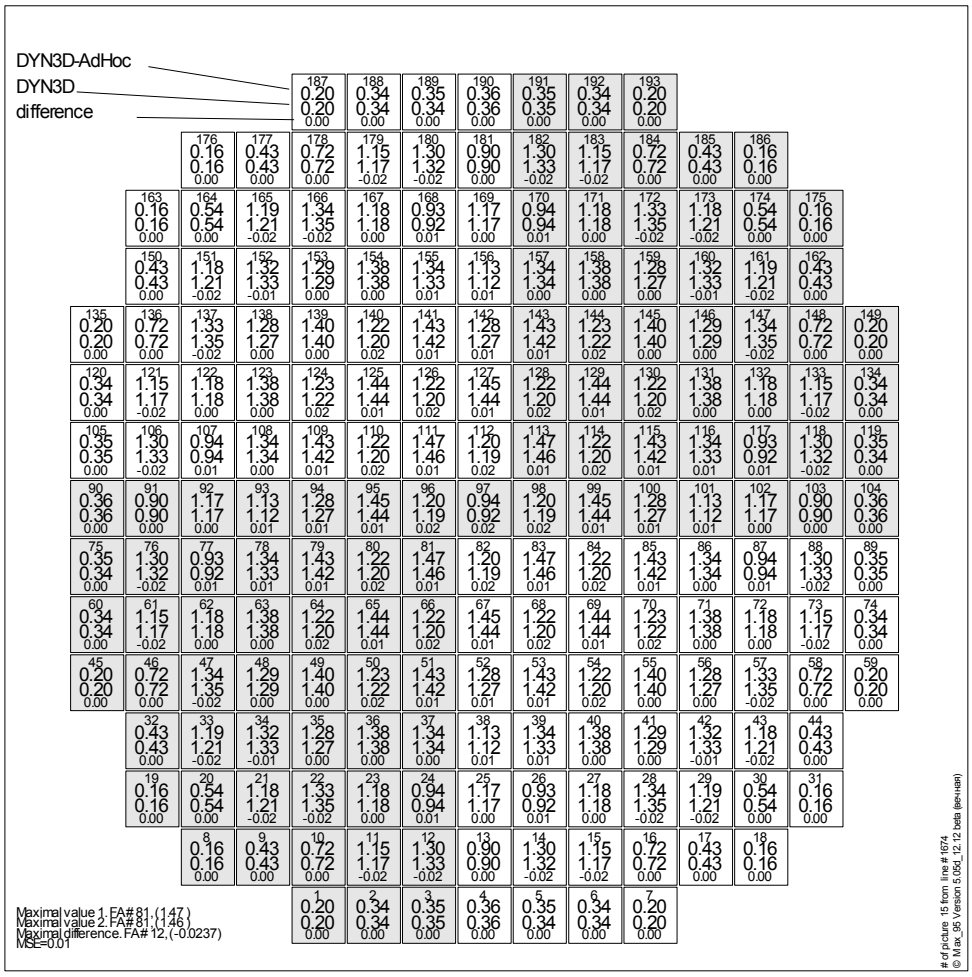

Fig. 6.9 Assembly-averaged relative power distribution in the core at the beginning of equilibrium cycle. Comparison between DYN3D-AdHoc and DYN3D.

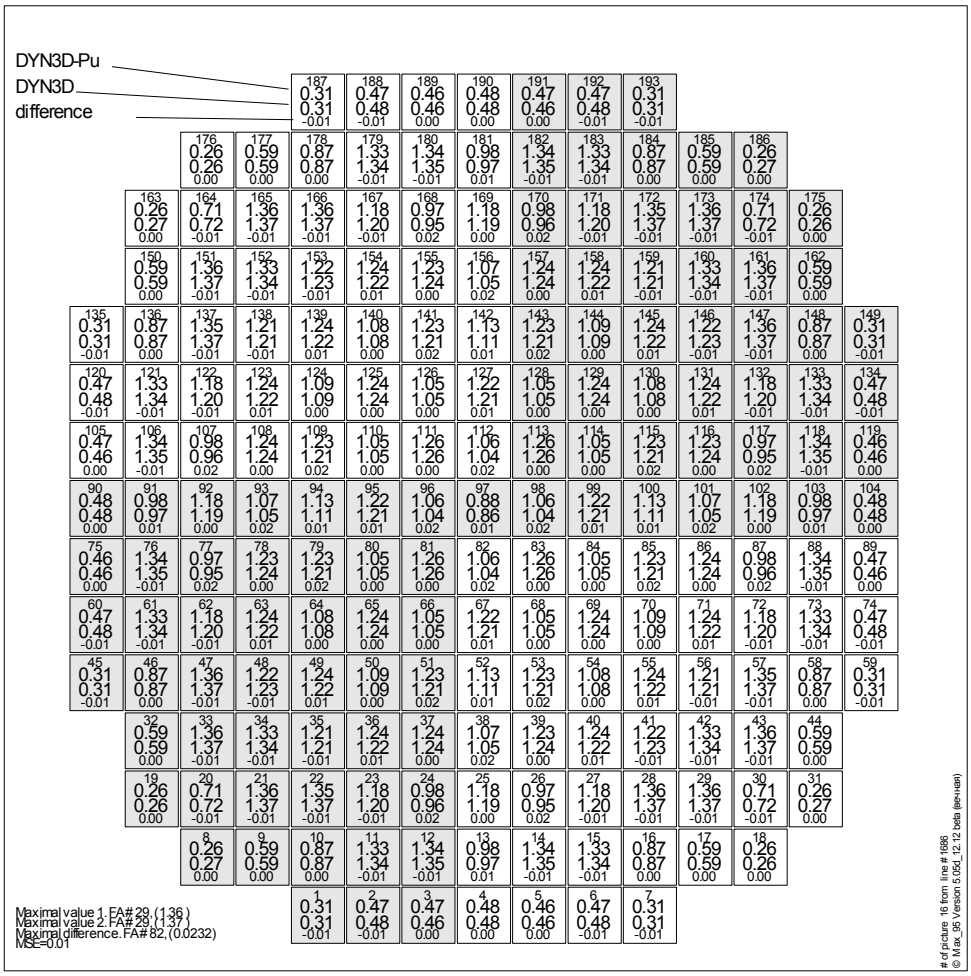

Fig. 6.10 Assembly-averaged relative power distribution in the core at the end of equilibrium cycle. Comparison between DYN3D-Pu and DYN3D.

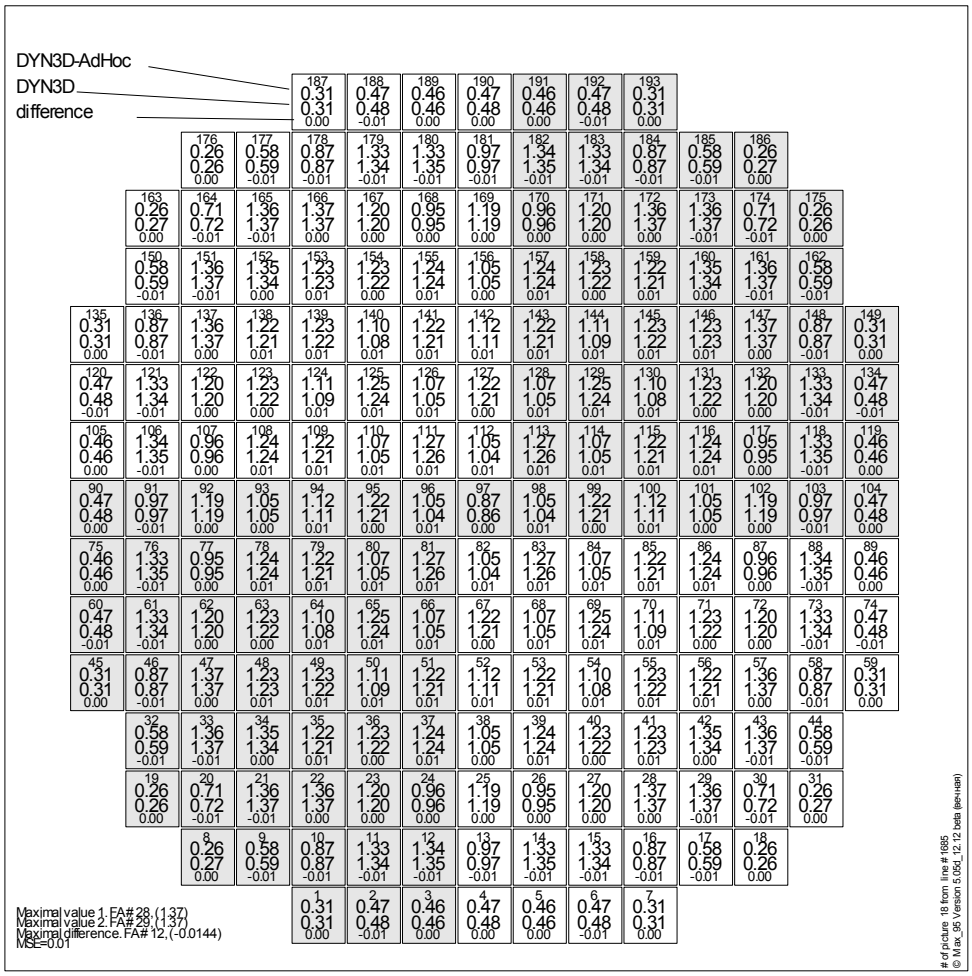

Fig. 6.11 Assembly-averaged relative power distribution in the core at the end of equilibrium cycle. Comparison between DYN3D-AdHoc and DYN3D.

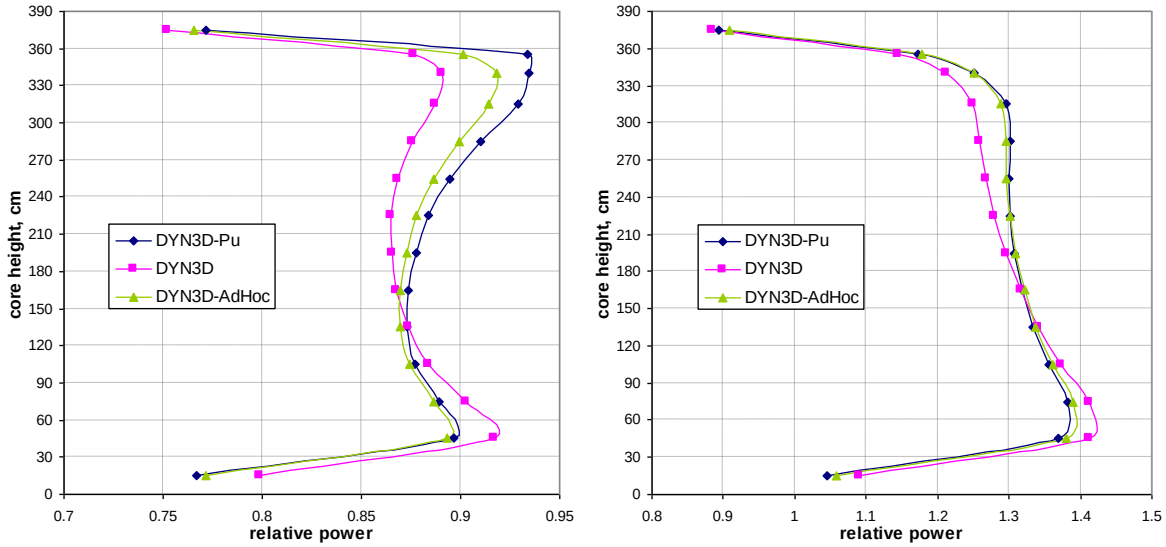

Fig. 6.12 Axial power distribution at the end of cycle in the central fuel assembly (left) and the assembly with the highest power (right).

Fig. 6.12 compares the relative power distributions in the central assembly (#97) and the assembly with the highest relative power (#81). Differences in the calculations with and without corrections reach 5% at the upper part of the central assembly with a high burnup and about 3% at the upper part of assembly #81.

At the hot zero power state (see Fig. 6.15) the difference between corrected and standard calculation reaches 10% for the central assembly. Radial distributions of assembly-average relative powers are shown in Fig. 6.13 and Fig. 6.14. Differences between calculations with and without history corrections is higher in case of hot zero power than in case of full power because power peaks are not suppressed by negative feedbacks.

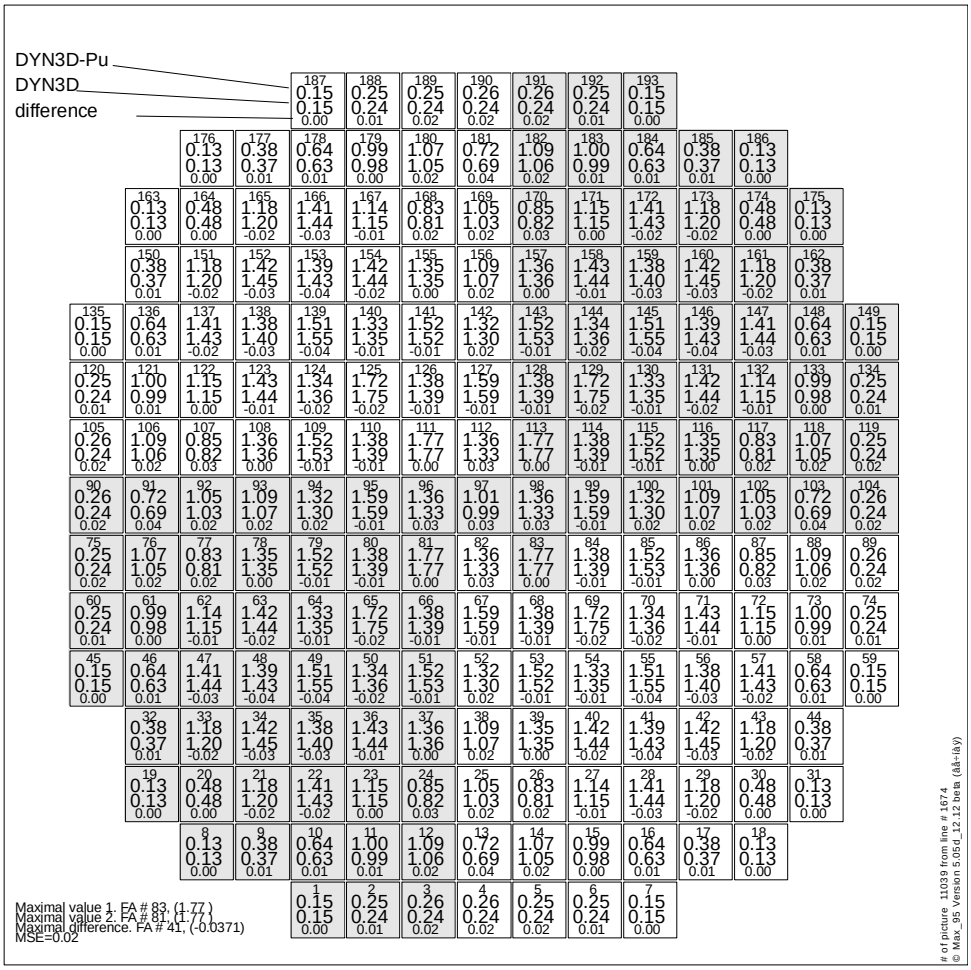

Fig. 6.13 Assembly-averaged relative power distribution in the core at the hot zero power at the beginning of equilibrium cycle. Comparison between DYN3D-Pu and DYN3D.

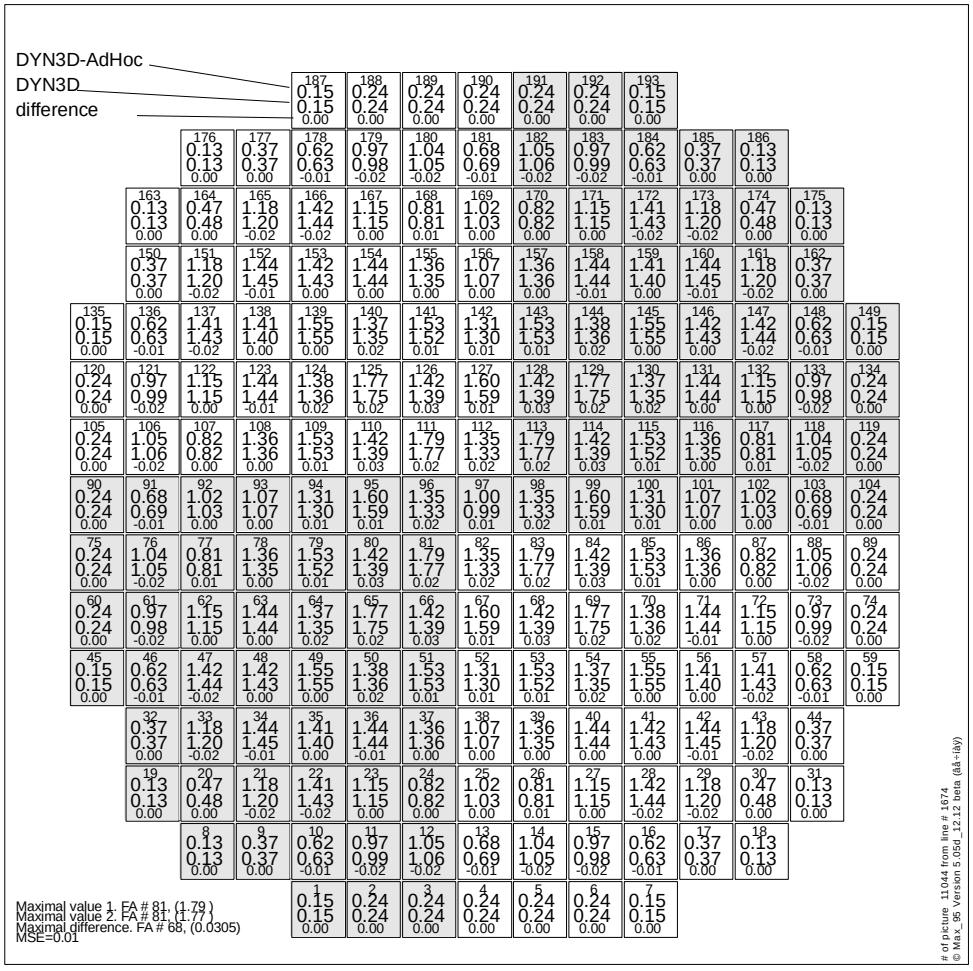

Fig. 6.14 Assembly-averaged relative power distribution in the core at the hot zero power at the beginning equilibrium cycle. Comparison between DYN3D-AdHoc and DYN3D.

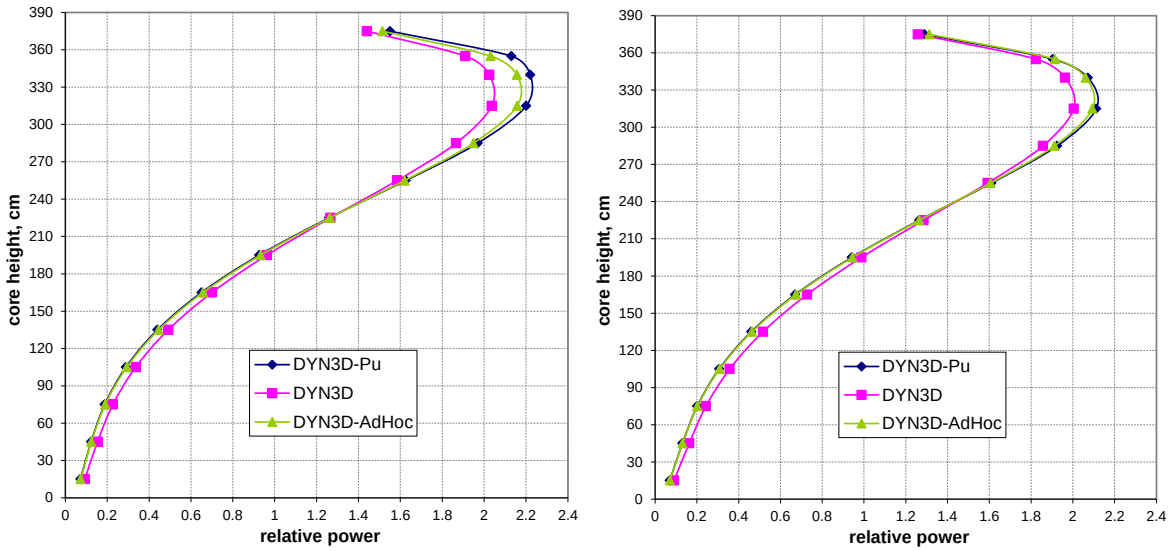

Fig. 6.15 Axial power distribution at hot zero power state at the beginning of cycle in the central fuel assembly (left) and radially averaged for the whole core.

The shift of power generation to the upper part of a core (see Fig. 6.7 and Fig. 6.12) should be quite obvious from the results of single-assembly calculations (see chapter 5, Fig. 5.8). Consideration of the moderator density history effect leads to higher neutron multiplication properties (k_∞) of fuel in the upper part of core which causes neutron flux redistribution.

The upper third of a core is depleting under harder spectrum and fuel there has more ^{9}Pu and ^{5}U for the same burnup level (see section 3.1). Higher fissile nuclides concentration defines higher multiplication properties and leads to neutron flux redistribution from the core bottom to top. The increased power in the upper part of a core make it burn faster. Higher burnup leads to lower multiplication properties, compensating in this way effect of depletion in harder spectrum. This self-compensation explains why the difference between calculations with and without history correction is not as big as in calculations illustrated in Fig. 3.9 (see section 3.2.3). For the study, described in [Mittag, 2006], the same burnup distribution was used in DYN3D calculations with and without Ad-hoc history correction, and thus burnup self-compensation was not taken into account.

The axial burnup redistribution is illustrated in Fig. 6.16 (right): fuel burnup after one cycle calculated by DYN3D-Pu and DYN3D-AdHoc is about 3% higher in upper part and 3% lower in the lower part of assembly than values calculated by standard DYN3D. For the central assembly (see Fig. 6.16, left) the burnup after 5 cycles calculated by DYN3D is lower for the whole assembly because of the shorter cycle length.

The history corrections make calculated axial burnup distribution more uniform. As shown in Fig. 6.7, radially averaged power end the end of cycle is also more uniform in calculations with history corrections. Reduced power peak in the lower part of the core and reduced power at the bottom boundary decrease neutron leakage. Improved neutron economy explains higher boron acid concentration and longer cycle length in calculation with history corrections (see Fig. 6.3).

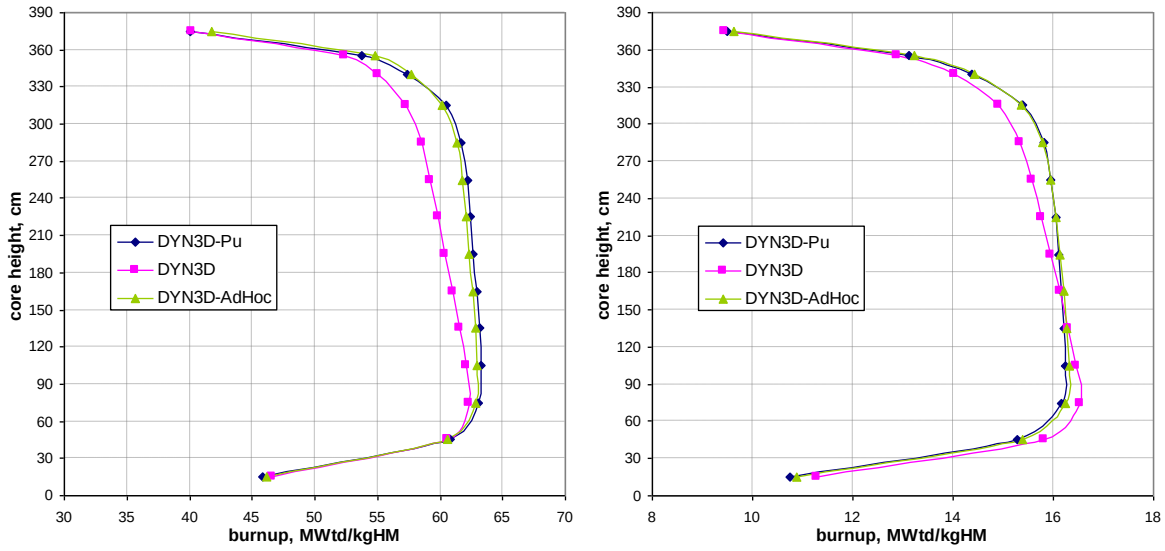

Fig. 6.16 Axial burnup distribution after 295 days of cycle in the central fuel assembly (left) and the first-year assembly with the highest power (right).

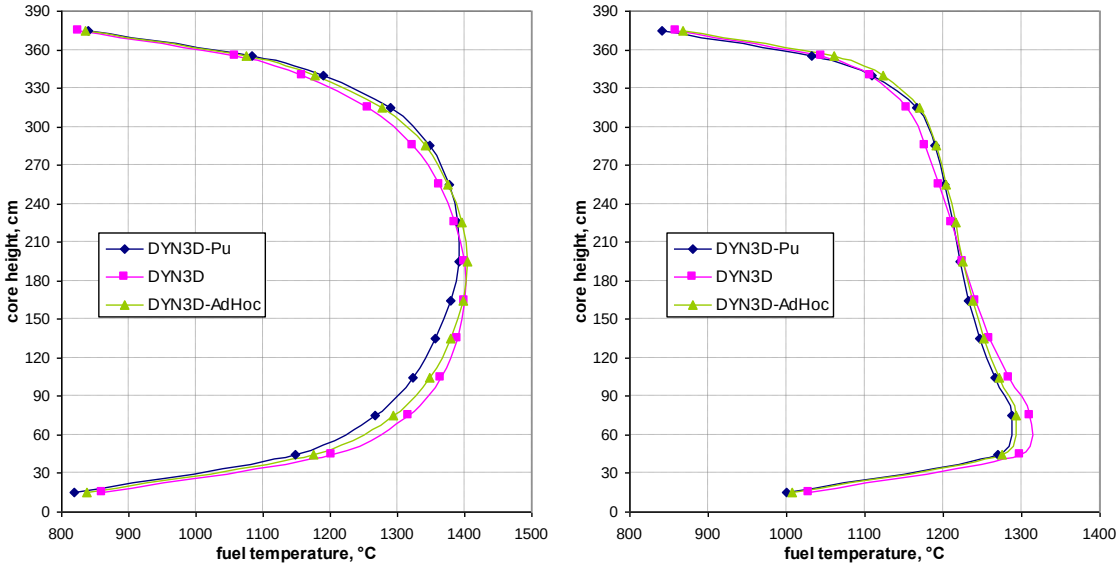

Fig. 6.17 Fuel centerline temperature of the hottest assembly at the beginning (left) and the end (right) of equilibrium cycle.

Redistribution of calculated powers has an effect on predicted values of fuel temperatures. Fig. 6.17 illustrates the axial distribution of the fuel centerline temperature for the hottest assembly #111 at the beginning of the cycle and assembly #28 at the end of the cycle. Application of historical corrections leads to 30-50 K (2-4%) higher temperatures in the upper part of the core and lower temperatures in the lower part.

At the beginning of the cycle the maximum fuel temperature is located in the middle of the core, the results of all three calculations are about the same there. At the end of the cycle the maximum of the fuel temperature is located in the lower part of the core and its value, calculated with historical corrections, is about 30 K (or 2%) lower than in the standard calculation.

6.3 Reactivity coefficients and control rod worth

Critical boron concentration and reactivity coefficients at the beginning and at the end of cycle for a full power state are presented in Table 6.2, for hot zero power – in Table 6.3. The results of DYN3D calculations with and without history consideration show minor deviations in values of reactivity coefficients. History effects have noticeable influence only on the critical boron concentration.

Table 6.4 represents values of SCRAM weight – the negative reactivity introduced by all control rods fully inserted into the core.

Table 6.2 Reactivity coefficients at full power

		BOC			EOC		
		DYN3D	DYN3D-Pu	DYN3D-AdHoc	DYN3D	DYN3D-Pu	DYN3D-AdHoc
CB, ppm		1205	1220	1218	0	0	0
Reactivity coefficients	Moderator temperature, pcm/K	-47.71	-47.68	-48.08	-80.92	-81.37	-81.29
	Fuel temperature, pcm/K	-2.61	-2.59	-2.61	-2.75	-2.72	-2.76
	Boron concentration, pcm/ppm	-5.17	-5.09	-5.10	-6.22	-6.06	-6.08

Table 6.3 Reactivity coefficients at hot zero power

		BOC			EOC		
		DYN3D	DYN3D-Pu	DYN3D-AdHoc	DYN3D	DYN3D-Pu	DYN3D-AdHoc
CB, ppm		2146	2175	2183	595	620	622
Reactivity coefficients	Moderator temperature, pcm/K	-13.13	-13.52	-13.44	-41.00	-40.87	-41.05
	Fuel temperature, pcm/K	-3.40	-3.42	-3.42	-3.49	-3.50	-3.50
	Boron concentration, pcm/ppm	-5.30	-5.17	-5.20	-6.21	-5.95	-5.99

Table 6.4 Scram weight

	SCRAM weight, %			
	BOC		EOC	
	FP	HZP	FP	HZP
DYN3D	6.05	5.60	6.44	6.36
DYN3D-Pu	6.06	5.51	6.45	6.16
DYN3D-AdHoc	6.04	5.53	6.45	6.21

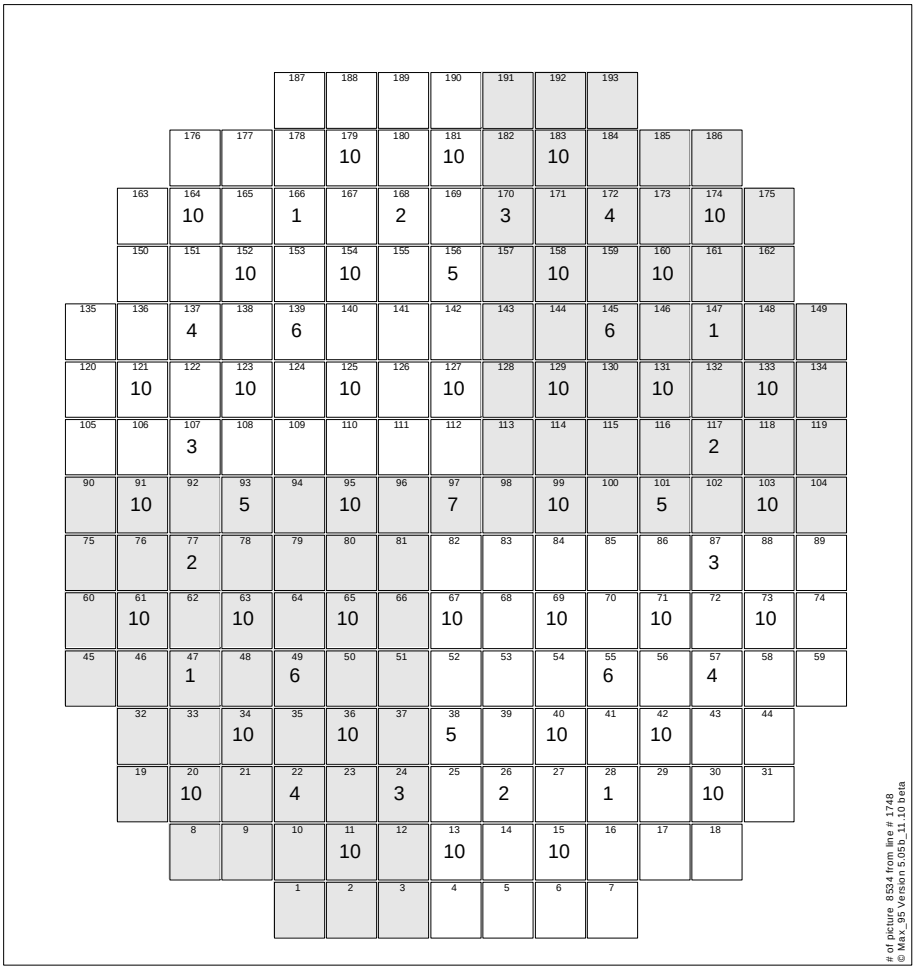

Fig. 6.18 Scheme of control rod banks.

The integral and differential efficiency of the central control rod and control rod banks are illustrated in Fig. 6.19-6.21. The ordinate axis in these figures describes the rod vertical position in percent, 0% meaning fully inserted, 100% - fully withdrawn. The assignment of control rods to rod banks is shown in Fig. 6.18.

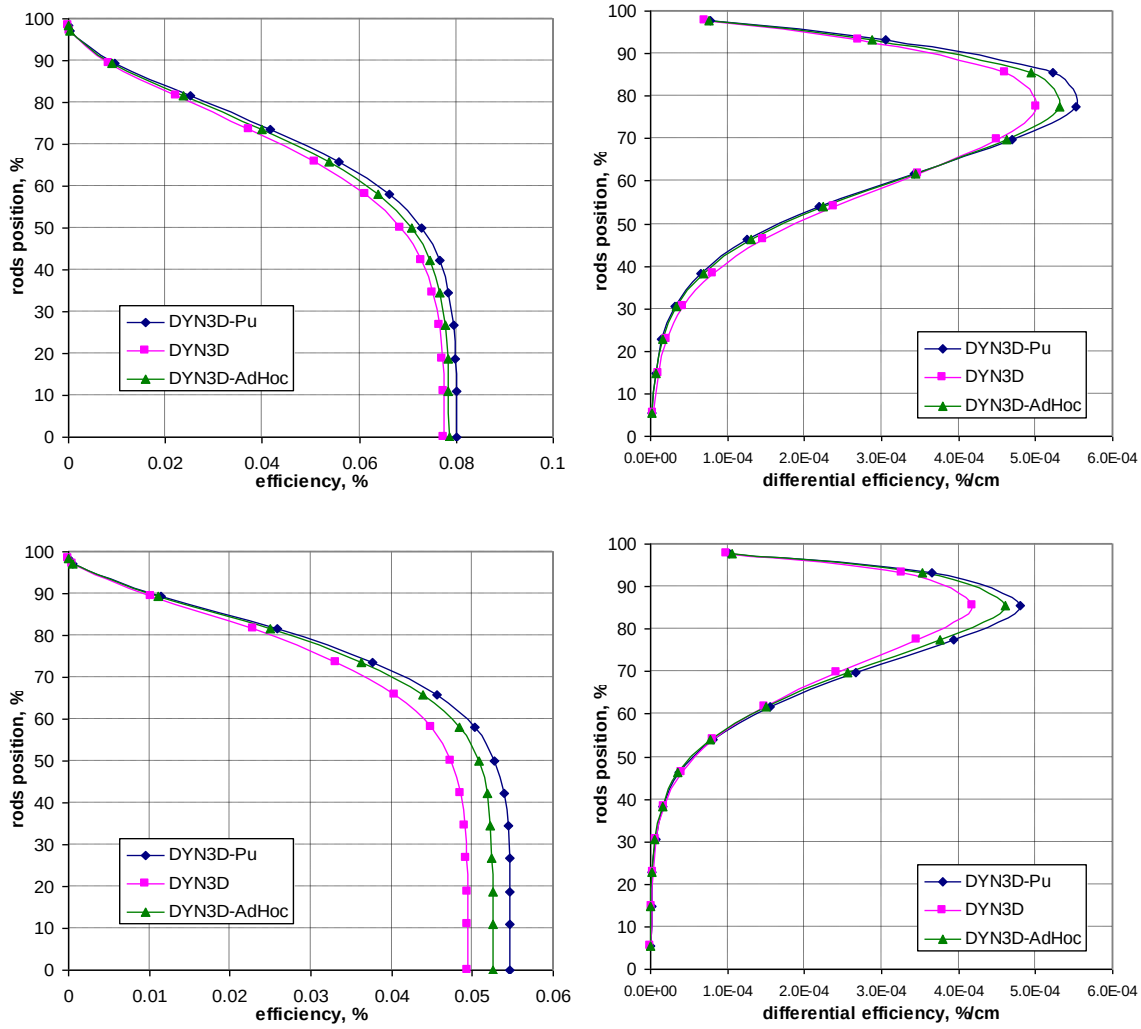

Fig. 6.19 Integral and differential efficiency of the central control rod at the hot zero power state at the beginning (top) and at the end (bottom) of cycle

In all shown cases the effect of history correction is bigger at the end of cycle, because influence of history effects is growing with burnup. At the hot zero power state the differences in values of the integral efficiency of the central rod calculated with and without historical correction reach 10%, and nearly 15% in the differential efficiency. This is an implication of differing neutron flux (power) distributions (see Fig. 6.15).

For the full power state the deviations in differential efficiency with and without historical correction are about 3% (see Fig. 6.21).

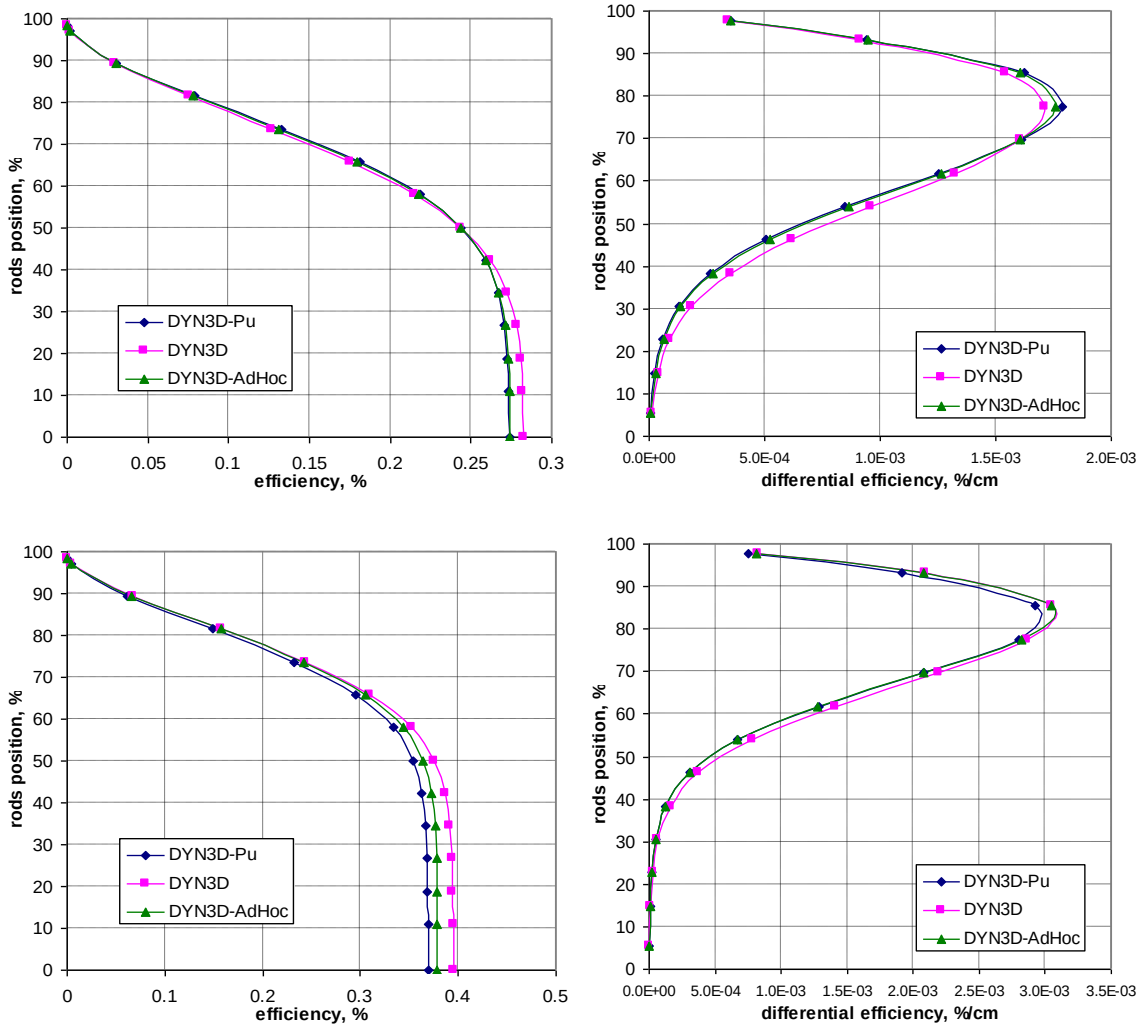

Fig. 6.20 Integral and differential efficiency of the control rod bank #1 at the hot zero power state at the beginning (top) and at the end (bottom) of cycle

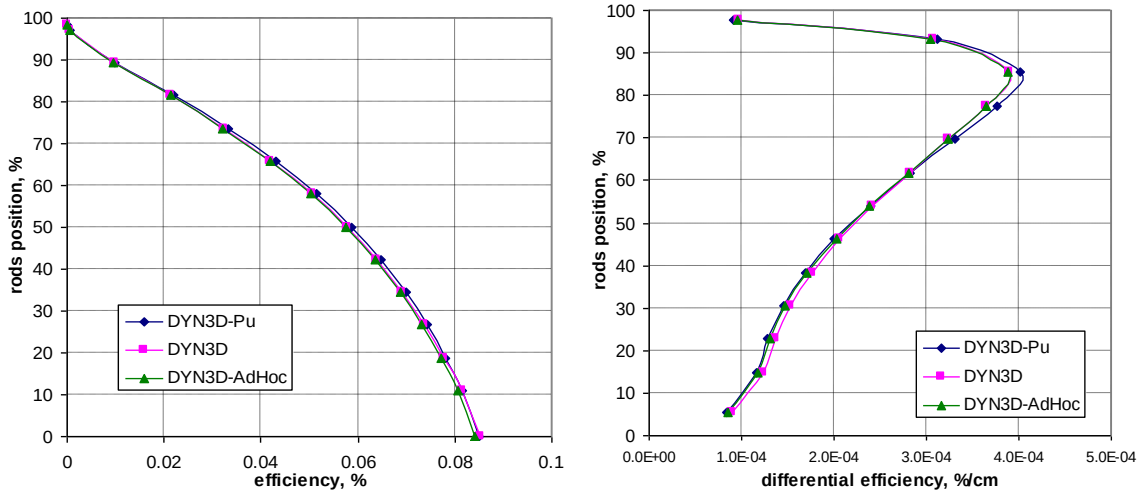

Fig. 6.21 Integral and differential efficiency of the central control rod at the full power state at the end of cycle

6.4 Chapter short summary

Whole core steady-state and burnup calculations of PWR were performed to investigate the influence of history effects on calculation results. Three modes of DYN3D calculation were compared: without history consideration, with ^{9}Pu history indicator and with Ad-Hoc history parameters.

The comparison of 3D power distributions shows a shift of energy release from lower to upper third of reactor during the whole cycle: a 3% increase of radially-averaged relative power at 80% level of core height and a corresponding decrease at 20% level. Respective deviations in the central assembly with high burnup are about 5%, for the hot zero power state deviations reach 10%.

The redistribution in axial power leads to a respective shift in burnup: in calculations with history corrections burnup of the upper part of fuel assemblies is up to 5% higher than in calculation without correction. The equilibrium cycle is about 10 days (~3%) longer in calculations with history corrections.

The fuel temperatures reflect the power redistribution as well: application of historical corrections leads to 30-50 K (about 2-3%) higher temperatures in the upper part of the core and lower temperatures in the lower part.

The influence of historical correction on reactivity coefficients is minor (<3%). Differences in SCRAM weight values at full power state are marginal (about 0.1%). At the hot zero power state historical correction leads to some minor radial redistribution of assembly-averaged powers from fresh to burned fuel assemblies due to more equal axial power distribution. Since the most effective control rod are those which are inserted in fresh assemblies, this radial power redistribution results in about 1.5% lower SCRAM weight at HZP ta the beginning of cycle and about 3% at the end of cycle. Differential and integral weight of control rods and control rod banks are affected by the axial power redistribution. Deviations of these values are about 3-5%.

The results obtained with the two historical correction methods – Pu-correction and Ad-Hoc-parameters – for the fuel cycle length, 3D power, burnup and fuel temperature distributions are closely together and show similar differences to results without correction. However, the results of the two historical corrections do not coincide because of different underlying physical approaches. The differences between both methods are explained by the influence of minor spectral history effects such as poisoning and neighborhood, which are not taken into account by the AdHoc-parameters.

7 Transients

A simulation of transient examples was performed to illustrate the influence of historical correction on safety-relevant parameters calculated by DYN3D such as peak value of introduced positive reactivity, local power peaks, maximum values of fuel and cladding temperatures and minimum value of DNBR. DYN3D results obtained applying ^{9}Pu-historical correction are compared with results obtained without correction.

The cases C1 and C2 defined in the NEACRP Core Transient Benchmark [Finnemann, 1992] – control rod ejection from PWR core at hot zero power (Case C1) and full power (Case C2) were used as the basis for test cases.

In this hypothetical accident the control rod is ejected in 0.1 sec from its initial position to the upper position. The fast rod ejection introduces positive reactivity, which causes power increase and rise of water and fuel temperatures. Due to the negative moderator and fuel temperature feedbacks the reactivity decreases with rise of temperatures and the power stabilizes on a new level.

No SCRAM insertion is considered in these simulations. Flow rate and inlet temperature of coolant are assumed unperturbed during the transient. The analysis is performed for the beginning and the end of generic equilibrium fuel cycle (see section 6.1). Burnup and poisoning distributions as well as ^{9}Pu distribution were derived in respective burnup calculations (see Fig. 6.4-6.6).

In the initial state before control rod ejection reactor is critical with some of control rod banks partly inserted into core (see Fig. 7.21), while equilibrium cycle was modeled with all rods out. To compensate negative reactivity from inserted rods in initial state before transient, zero xenon poisoning was assumed in all cases.

7.1 Case C1 at hot zero power

In the initial state of the reactor before transient the power level is 0.004 MW (HZP) and the inlet temperature is 286°C. The critical boron concentration in the moderator is derived in respective calculations by the DYN3D modes and shown together with reactivity coefficients in Table 7.1. The legend is the same for all pictures and tables:

- DYN3D – is the "standard" DYN3D calculation mode without historical correction,
- DYN3D-Pu – with correction based on ^{9}Pu concentration,

BOC stands for beginning of equilibrium cycle, EOC for end of cycle.

The position of control rods (in percent) in the initial state is shown in Fig. 7.1, where 100% means upper position (rod is fully out), and 0% – lower position (rod is fully in).

Table 7.1 Reactivity coefficients in the C1 hot zero power initial state

		BOC		EOC	
		DYN3D	DYN3D-Pu	DYN3D	DYN3D-Pu
CB, ppm		1797	1821	612	635
Reactivity coefficients	Moderator temperature, pcm/K	-18.62	-19.09	-41.15	-41.31
	Fuel temperature, pcm/K	-3.46	-3.44	-3.56	-3.56
	Boron concentration, pcm/ppm	-5.43	-5.30	-6.41	-6.14

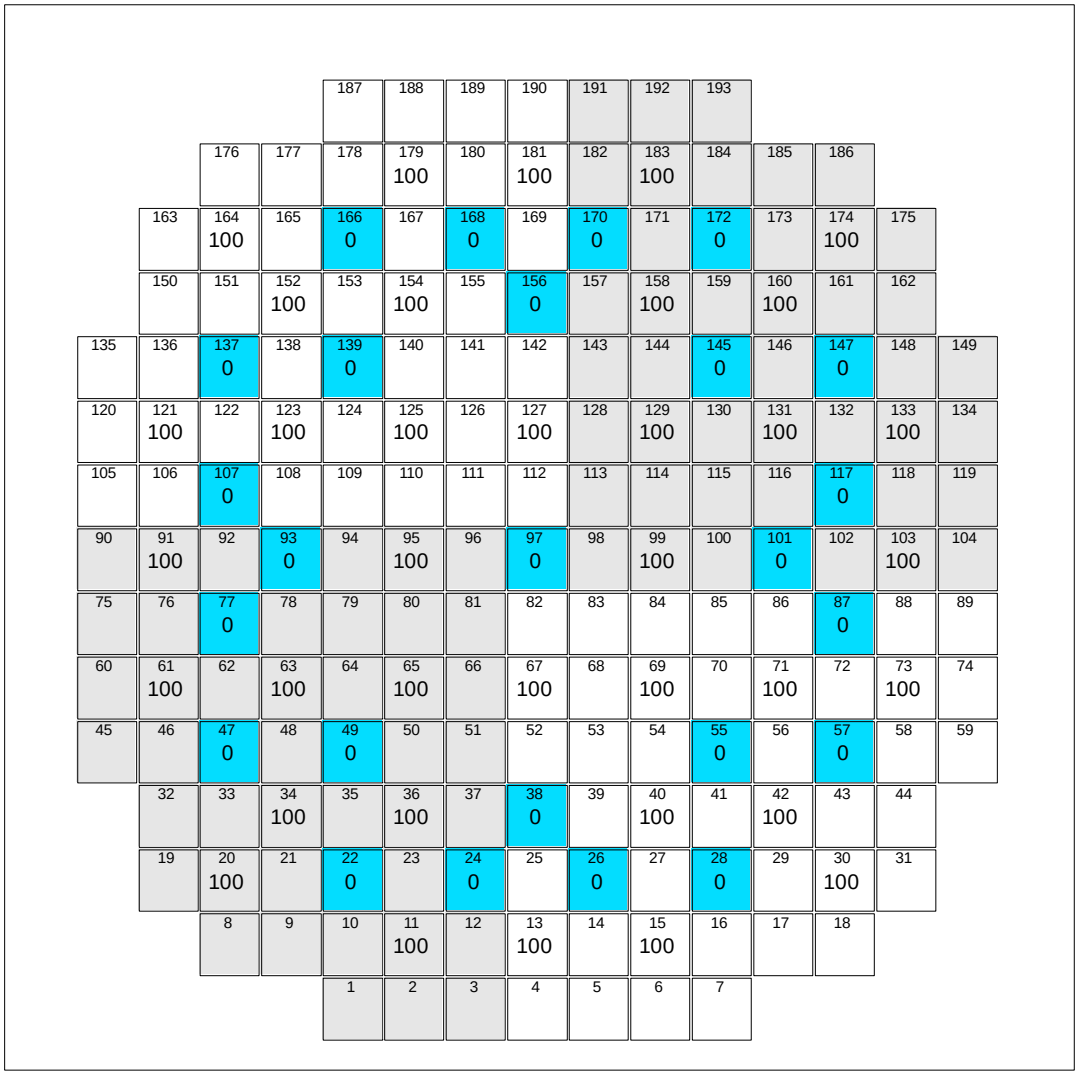

Fig. 7.1 Control rod positions in the C1 HZP initial state.

7.1.1 Beginning of cycle

Hot Zero Power. The initial state

The initial power distribution is illustrated in Fig. 7.2 and Fig. 7.3. Insertion of control rods shifts power generation to the center of core. The most efficient (meaning the highest positive reactivity introduced by its ejection) is the central rod #97. For considering an asymmetrical case, the rod ejection from position #145 was simulated, too. The initial axial power distributions for assemblies #97 and #145 are shown in Fig. 7.3.

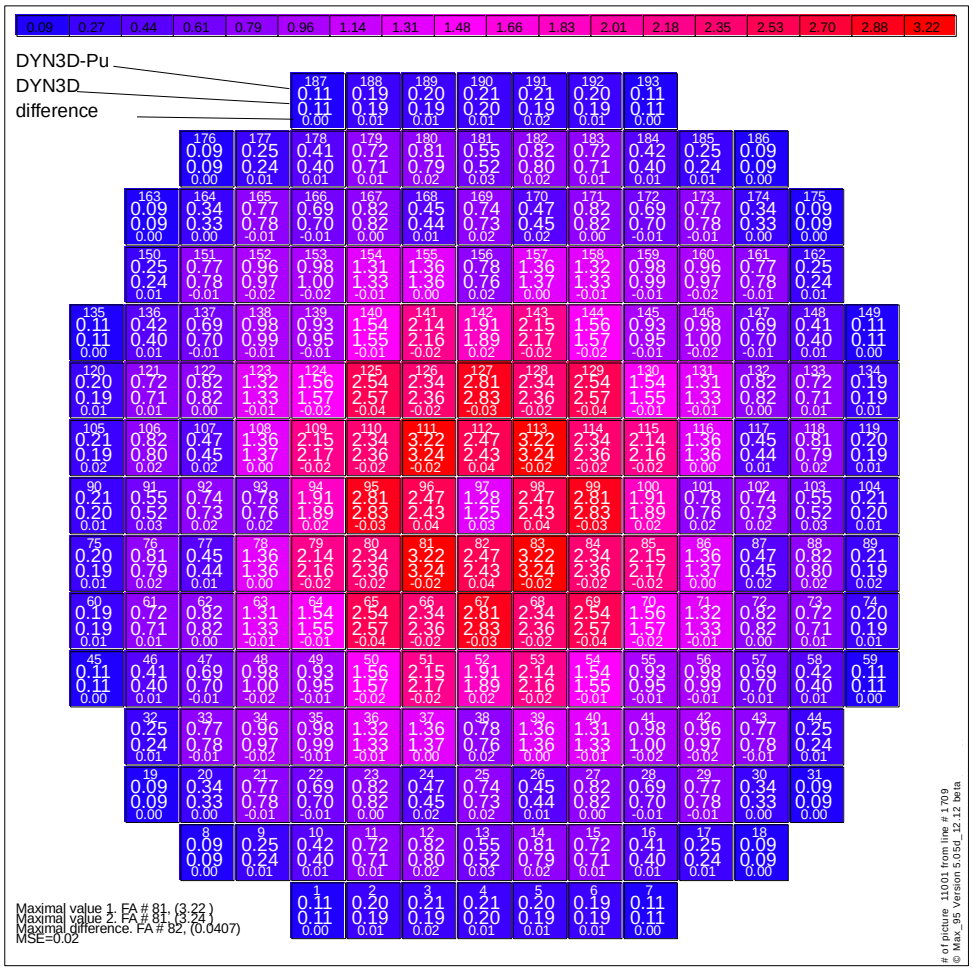

Fig. 7.2 Relative power distribution in the HZP initial state at the beginning of equilibrium cycle.

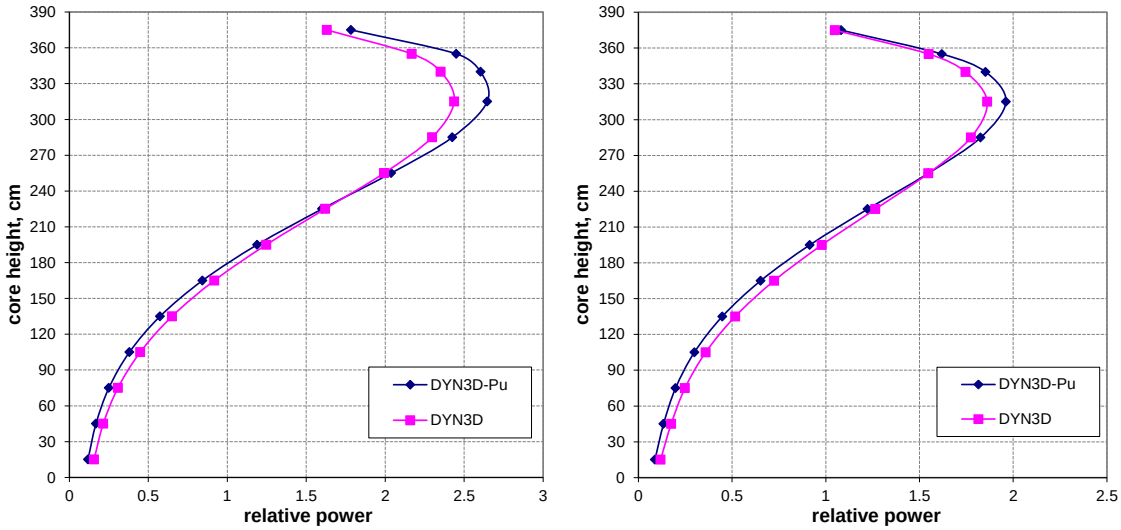

Fig. 7.3 Axial power distribution in the central fuel assembly #97 (left) and assembly #145 (right) in the HZP initial state.

Hot Zero Power. Central-rod ejection.

Results of control rod ejection at the hot zero power level at the beginning of fuel cycle from the central-assembly simulation are illustrated in Fig. 7.4-7.12.

The reactivity increases fast with control-rod ejection until time t = 0.12 sec (see Fig. 7.4, left), when the control rod reaches the upper position. During the next 10 seconds the reactivity is stable, while the reactor power starts to grow. Since the initial power is very low, the power increase (see Fig. 7.5) becomes noticeable only after about 10 sec and causes an increase of core-averaged fuel and coolant temperatures (see Fig. 7.6). The increase of fuel and coolant temperatures introduces negative reactivity (due to negative feedback, see Table 7.1), compensating the effect of control rod ejection (see Fig. 7.4, right). The power increase slows down with the decrease of reactivity, and at the end of the simulation (200 sec) the power nearly approaches a stable level.

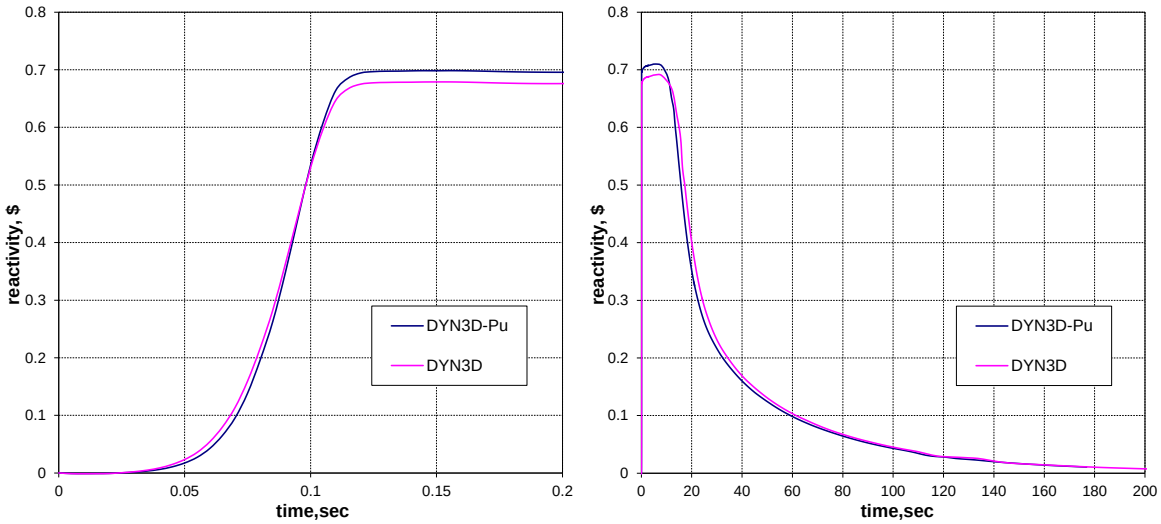

Fig. 7.4 Change of reactivity during the transient.

The introduced reactivity is slightly higher in the calculation with historical correction due to higher power of central fuel assembly in the initial state (see Fig. 7.2) and thus higher worth of the ejected control rod. Due to higher introduced reactivity, reactor power is growing faster and compensation of reactivity by negative temperature feedbacks is stronger and stars earlier in the calculation with history correction.

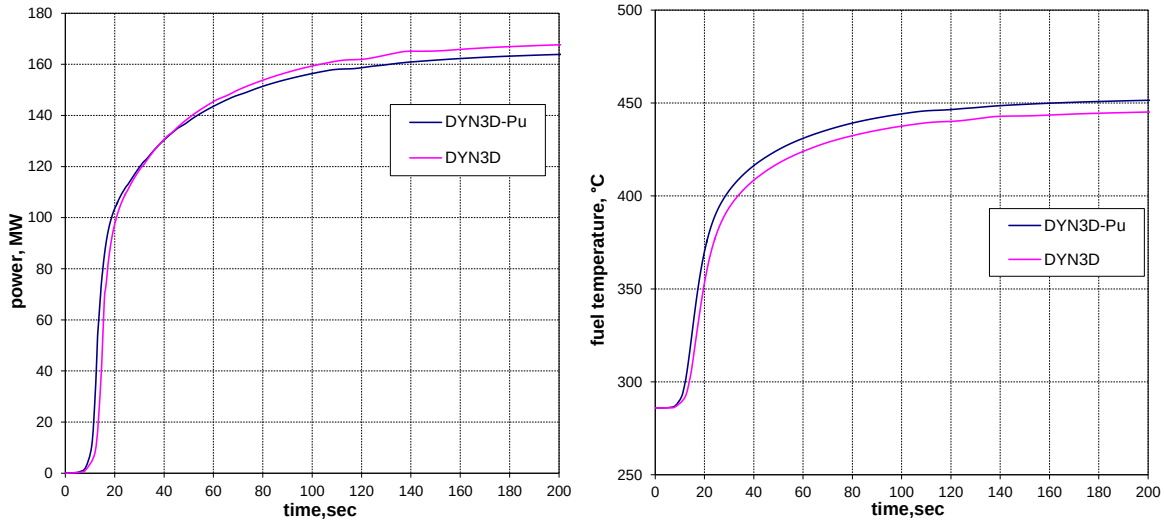

Fig. 7.5 Change of reactor power and maximum fuel center line temperature during the transient.

The maximum fuel center line temperature during the transient occurs in the upper part of the fuel assembly #81 (see Fig. 7.12). As it was discussed in chapter 6, historical correction increases peak value of fuel temperature if it is located in the upper part of a core.

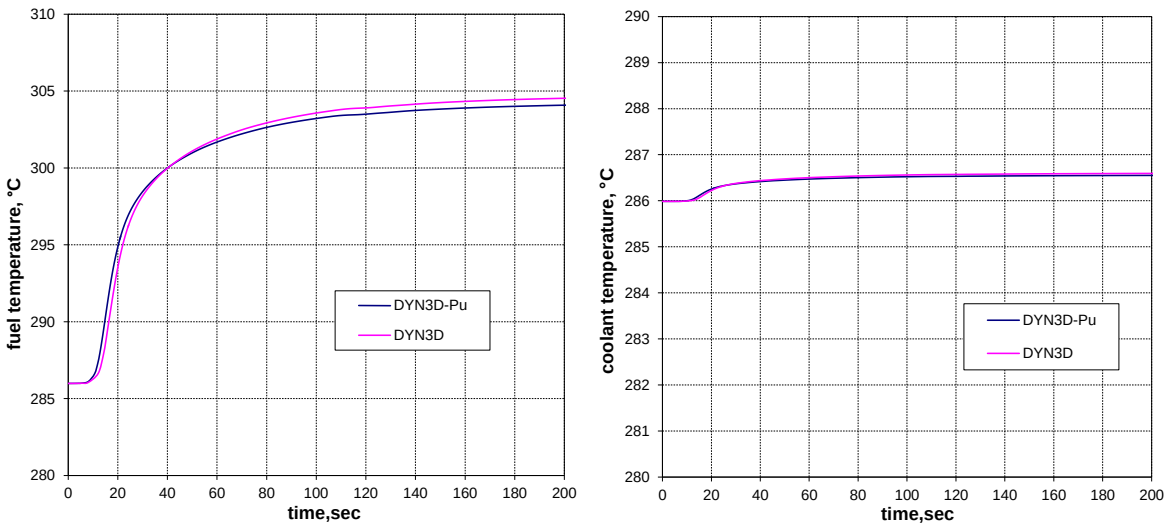

Fig. 7.6 Change of core-averaged fuel and coolant temperatures during the transient.

The maximum value of fuel temperature during the transient is shown in Fig. 7.5. The maximum heat flux on the outer surface of a cladding and the maximum cladding temperature are depicted in Fig. 7.7.

The ejection of the control rod from the central FA causes a symmetrical power increase in the center of core. The radial power distribution at $t = 5.0$ sec (reactivity maximum) is shown in Fig. 7.8 and at $t = 200$ sec (power maximum) – in Fig. 7.10.

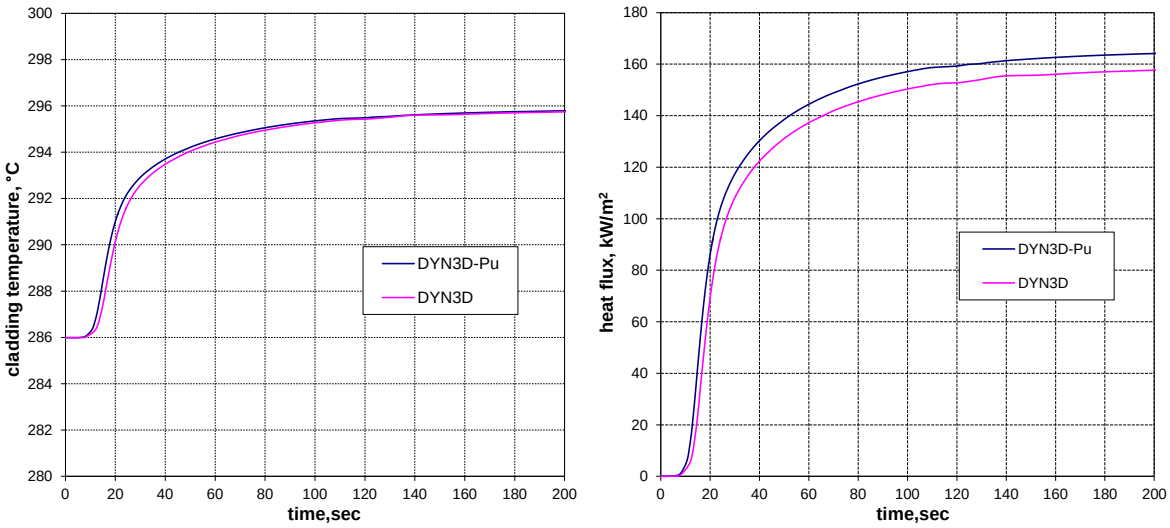

Fig. 7.7 Change of maximum cladding temperature and maximum heat flux on cladding surface during the transient.

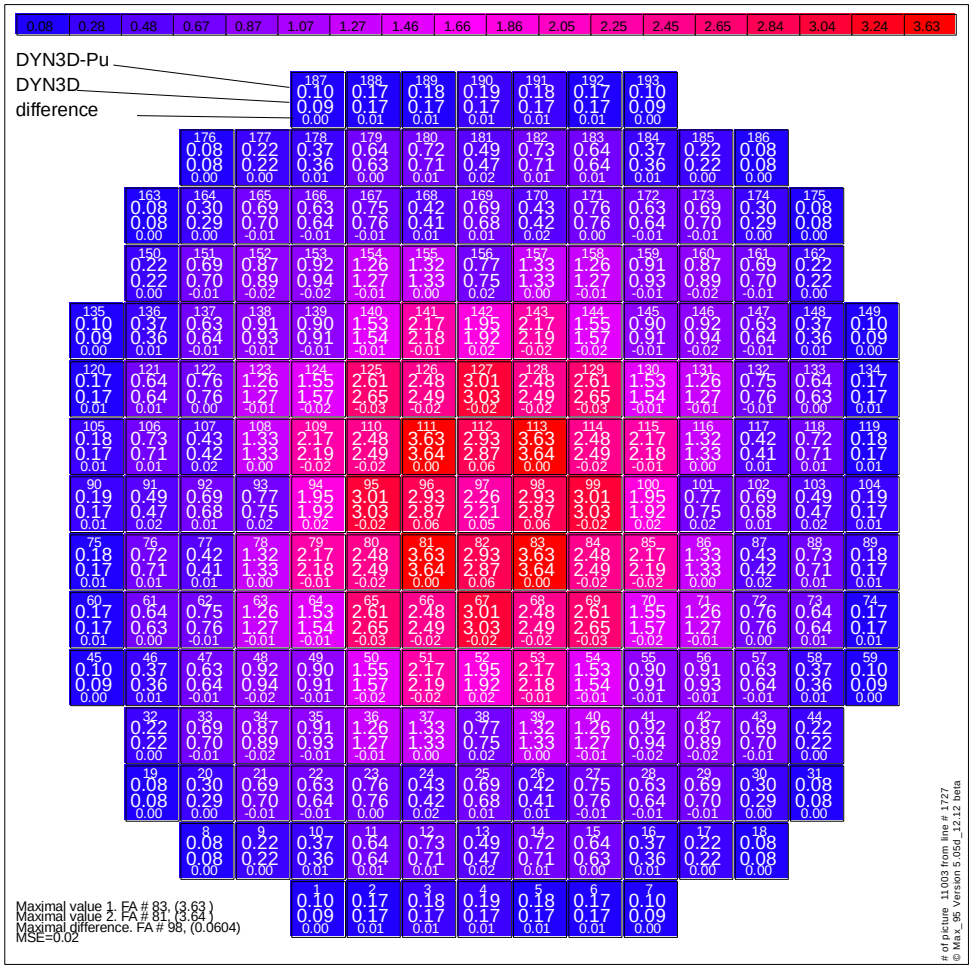

Fig. 7.8 Relative power distribution at 5.0 sec.

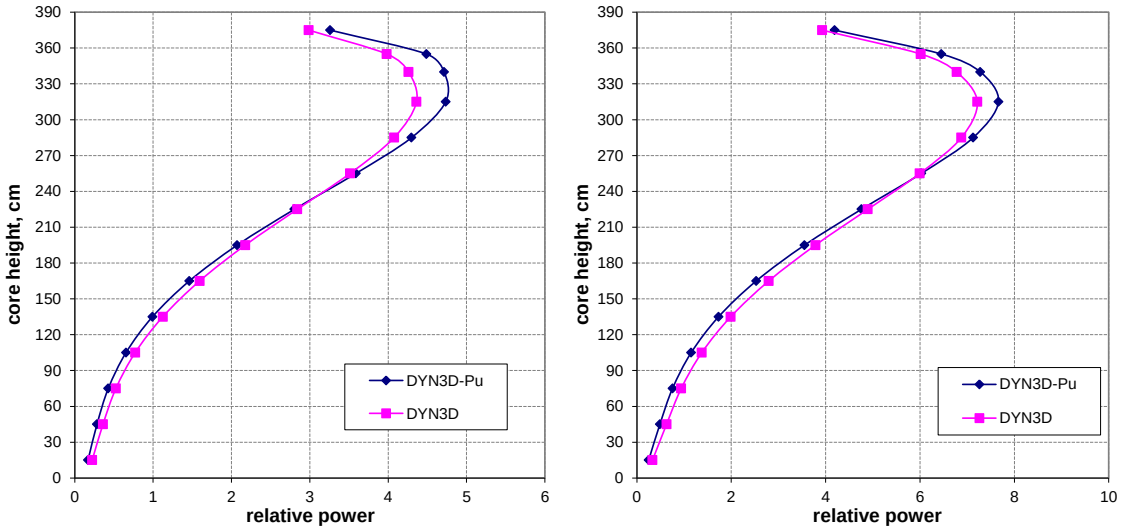

Fig. 7.9 Axial power distribution in the central fuel assembly #97 (left) and assembly #81 (right) at time 5.0 sec.

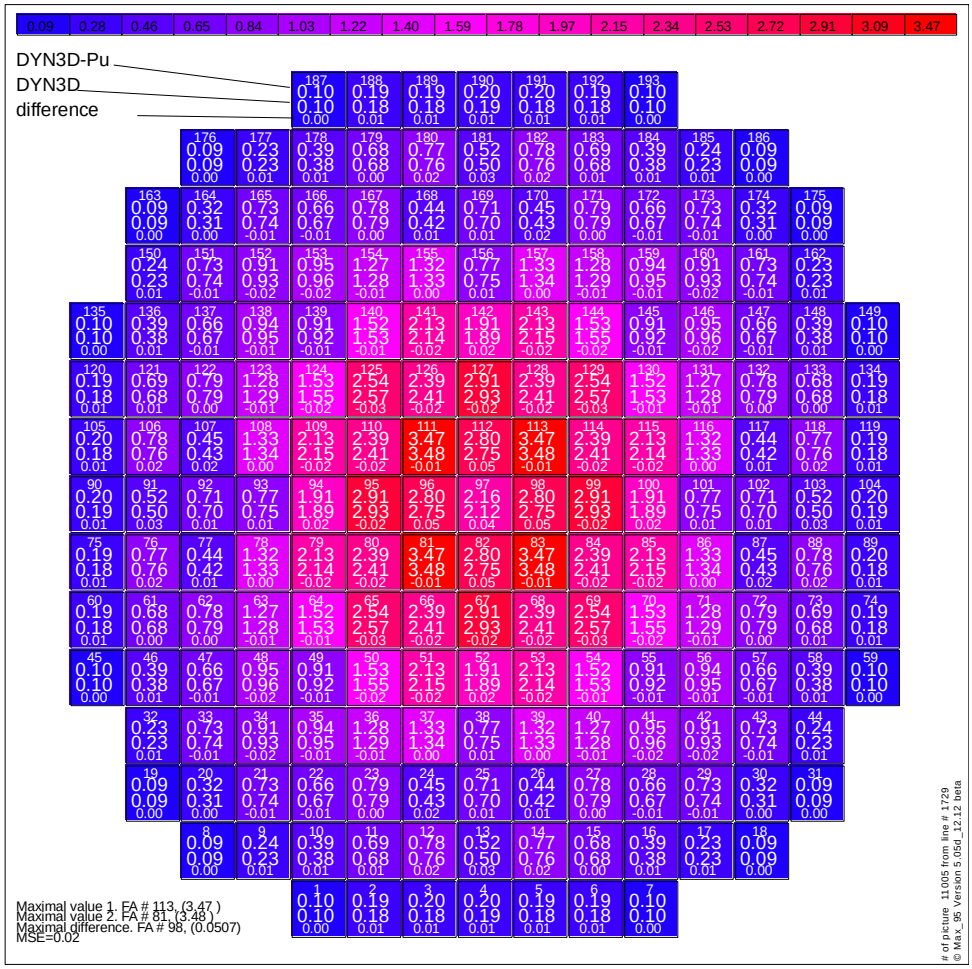

Fig. 7.10 Relative power distribution at 200.0 sec.

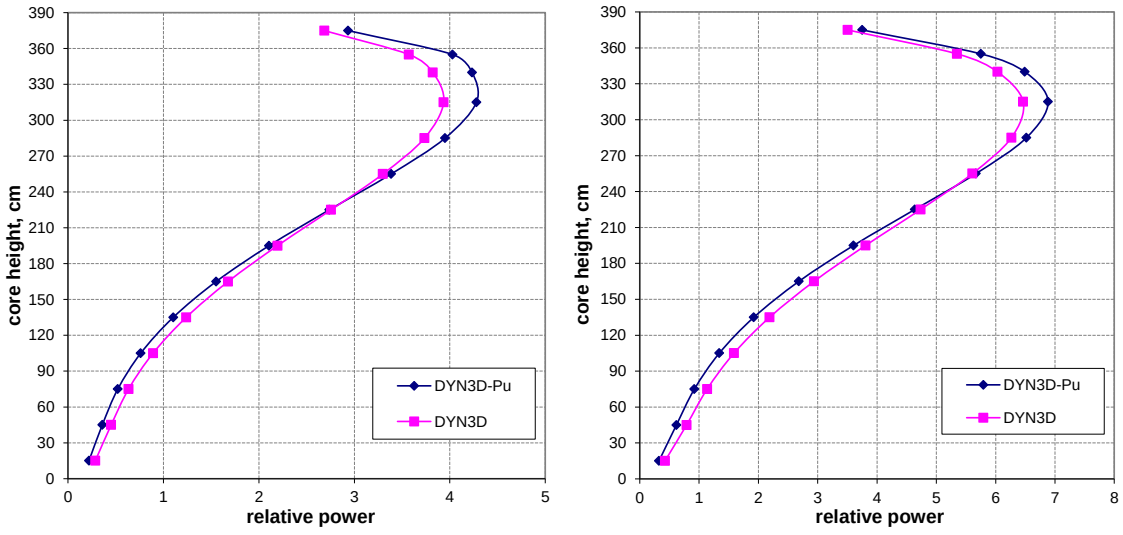

Fig. 7.11 Axial power distribution in the central fuel assembly #97 (left) and assembly #81 (right) at 200.0 sec.

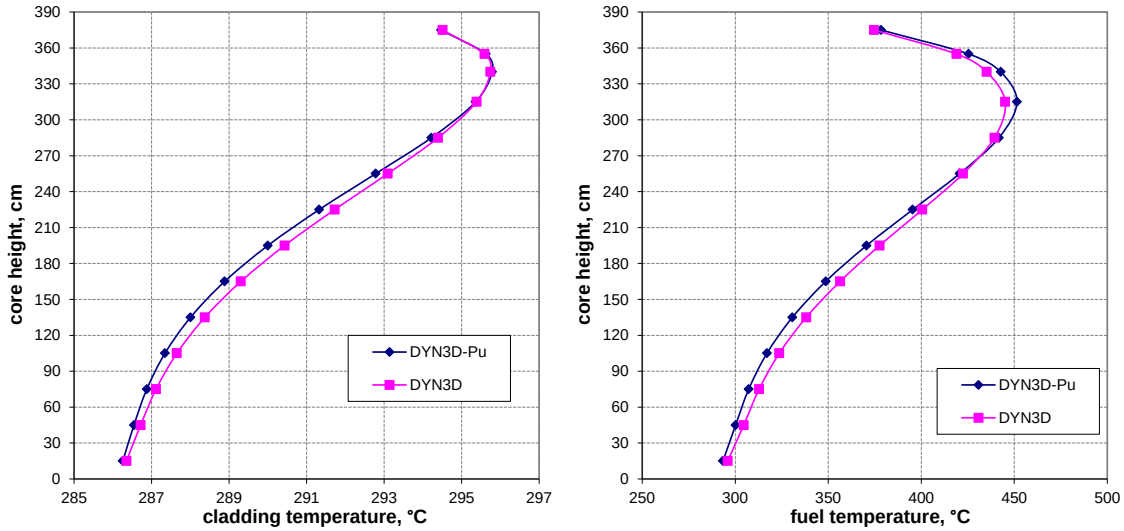

Fig. 7.12 Axial fuel center line (right) and cladding surface temperature (left) distributions in fuel assembly #81 at 200 sec.

The maximum of relative power occur in fuel assembly #81 in initial state and during the whole transient. The maximum value of relative power in assembly #81 is reached at t = 5 sec. Fig. 7.9 represents the axial distribution of relative power in the central assembly #97, wherefrom the rod was ejected, and in hottest assembly #81 at 5 sec; Fig. 7.11 illustrate same axial distributions at 200 sec. These figures reflect the general tendency of the power shift by history corrections, from lower to upper part of core, already discussed in section 6. In the axial layer with maximum power the difference between calculations with and without correction is ≈8%.

Table 7.2 Transient summary

	DYN3D	DYN3D-Pu
Maximum reactivity, $	0.782	0.802
Maximum power, MW	168	164
Maximum fuel temperature, °C	445	451
Maximum cladding temperature, °C	296	296
Maximum heat flux, kW/m^2	158	164

The safety relevant parameters of the PWR core calculated by the two modes of DYN3D are summarized in Table 7.2. The maximum fuel and cladding temperatures and maximum heat flux appear in a fresh fuel assembly, where the influence of history effects is minimal. Therefore deviations in these values are in the range between 1-3%.

The reactor power, fuel and cladding temperatures as well as heat flux are increasing during the transient and do not exactly reach equilibrium values till the end of simulation. Therefore their maximum values in Table 7.2 are given at t = 200 sec.

Hot Zero Power. Periphery-rod ejection

Results of the simulation of a control-rod ejection from a periphery assembly at the hot zero power level at the beginning of fuel cycle are illustrated in Fig. 7.13-7.02. Safety-relevant parameters are summarized in Table 7.3.

The rod is ejected from the assembly #145, which is located in the upper-right quarter of the core (see Fig. 7.1). Therefore, the power generation after ejection is asymmetric (see Fig. 7.16) with its maximum in this quarter. The course of transient is generally the same as in the central-rod ejection case described above. The maximum value of introduced reactivity is smaller than in the previous case due to the smaller weight of the ejected control rod.

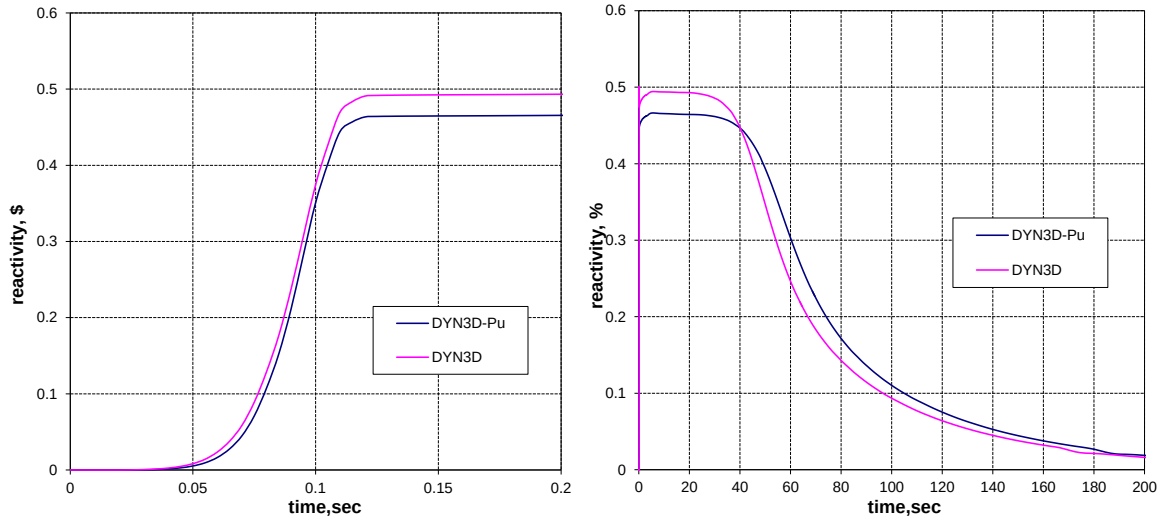

Fig. 7.13 Change of reactivity during the transient.

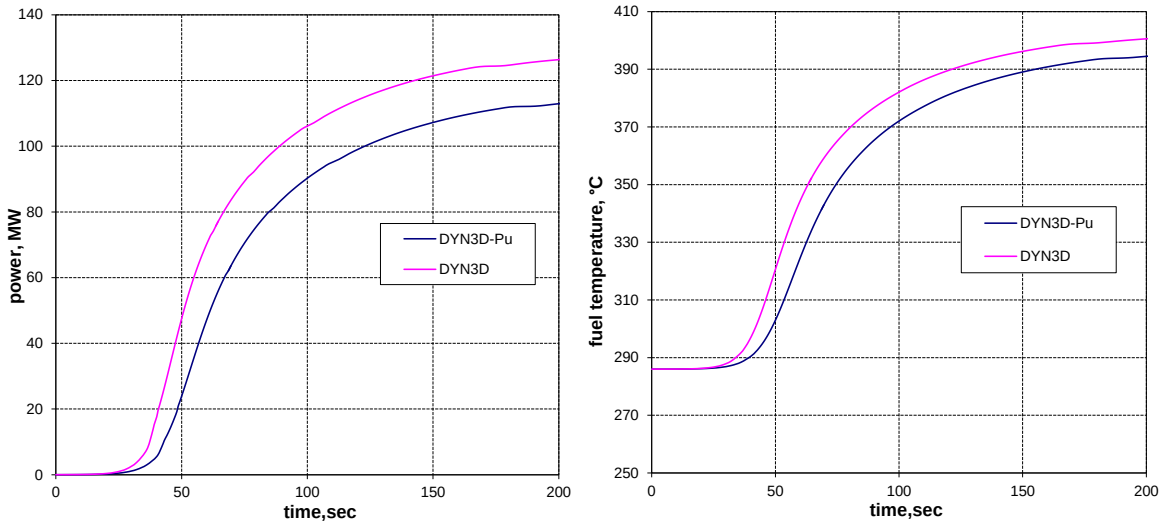

Fig. 7.14 Change of reactor power and maximum fuel center line temperature during the transient.

As opposed to the central rod ejection case, the introduced reactivity is lower in the calculation with historical correction due to the lower power of fuel assembly #145 in the initial state (see

Fig. 7.2). The relative effect of historical correction on reactivity and reactor power is higher in case of periphery rod ejection because fuel assembly #145 is surrounded by assemblies with higher burnup than central assembly. In the initial state all surrounding assemblies (##129-131, 144, 146, 158-160) have lower power in the calculation with historical correction. That significantly decreases worth of the ejected control rod.

The maximum value of fuel temperature during the transient is shown in Fig. 7.14, while maximum values of cladding surface heat flux and cladding temperature are given in Fig. 7.15. Peaks of these values occur in the upper part of the fresh fuel assembly #113 (see Fig. 7.20). Although historical correction increases peak values in the upper part of a core, maximums of fuel and cladding temperatures are higher in the calculation without historical correction because of higher reactor power in this case.

The radial power distribution at t = 15.0 sec (reactivity maximum) is shown in Fig. 7.16 and at t = 200 sec (power maximum) – in Fig. 7.18.

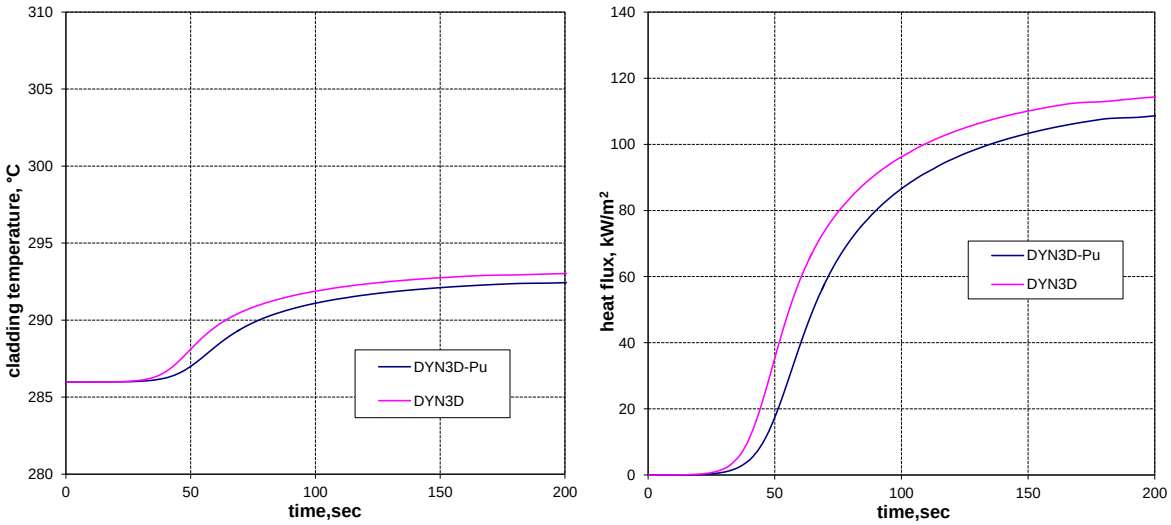

Fig. 7.15 Change of maximum cladding temperature and cladding surface heat flux during the transient.

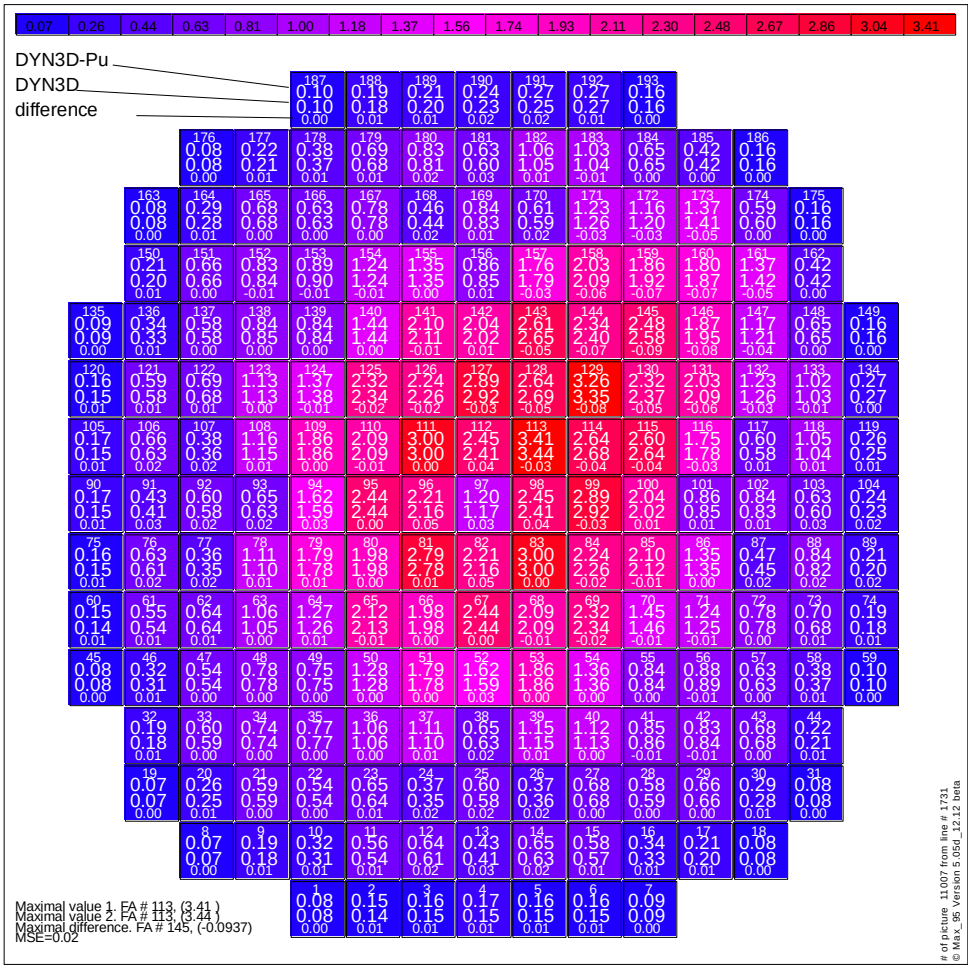

Fig. 7.16 Relative power distribution at 15.0 sec.

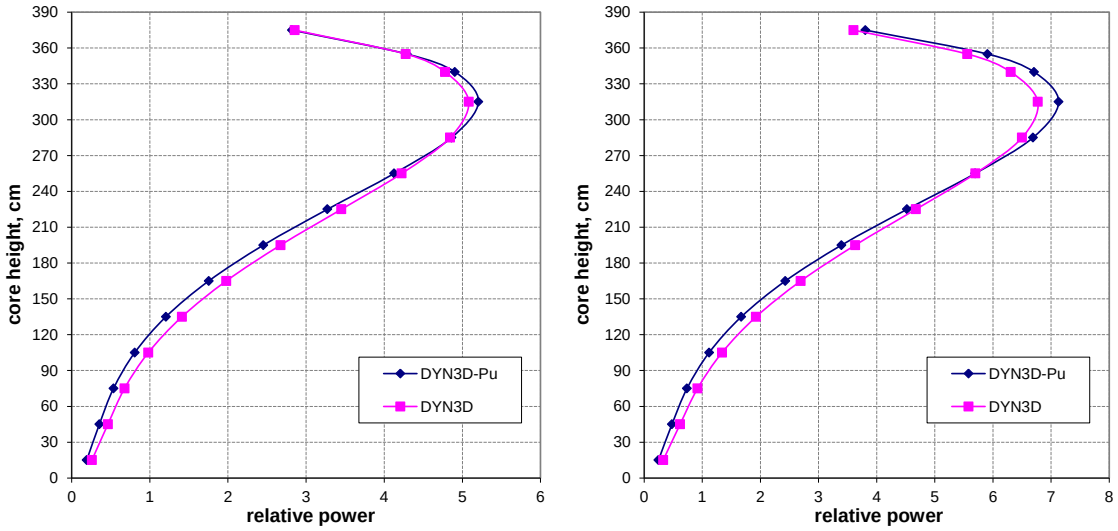

Fig. 7.17 Axial power distribution in assembly #145 (left) and assembly #113 (right) at 15.0 sec.

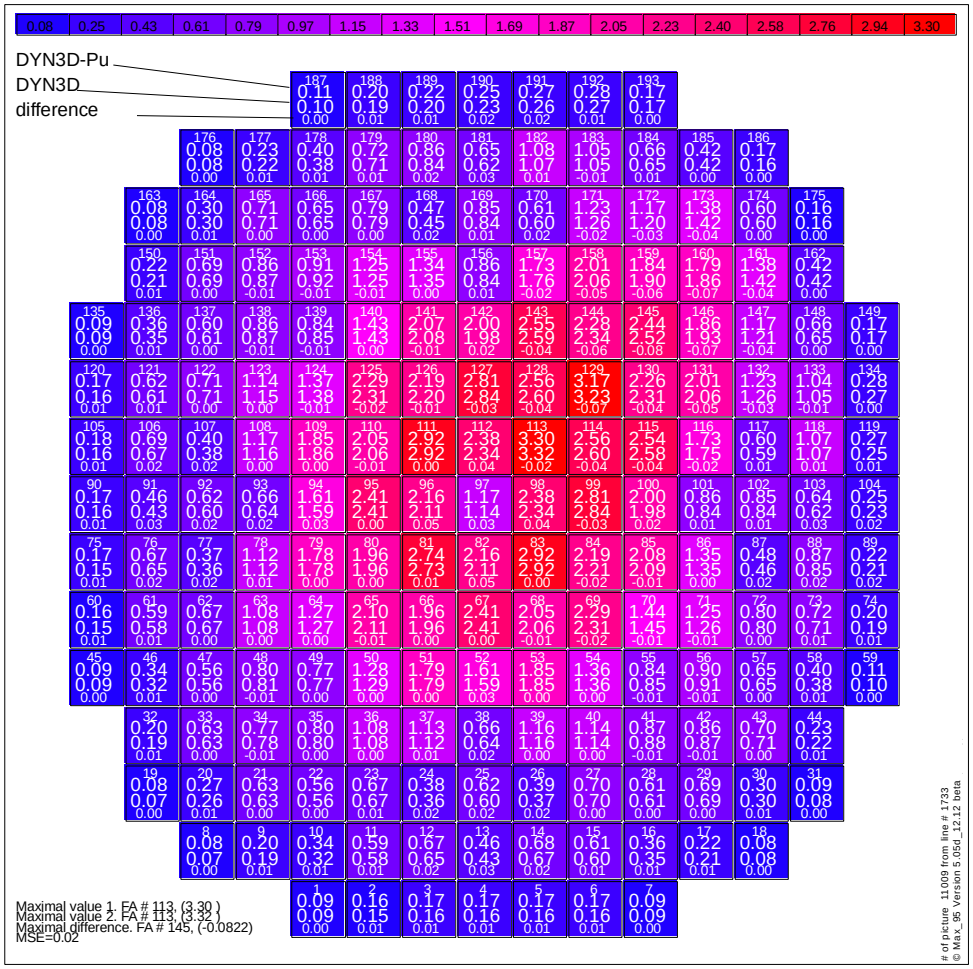

Fig. 7.18 Relative power distribution at 200.0 sec.

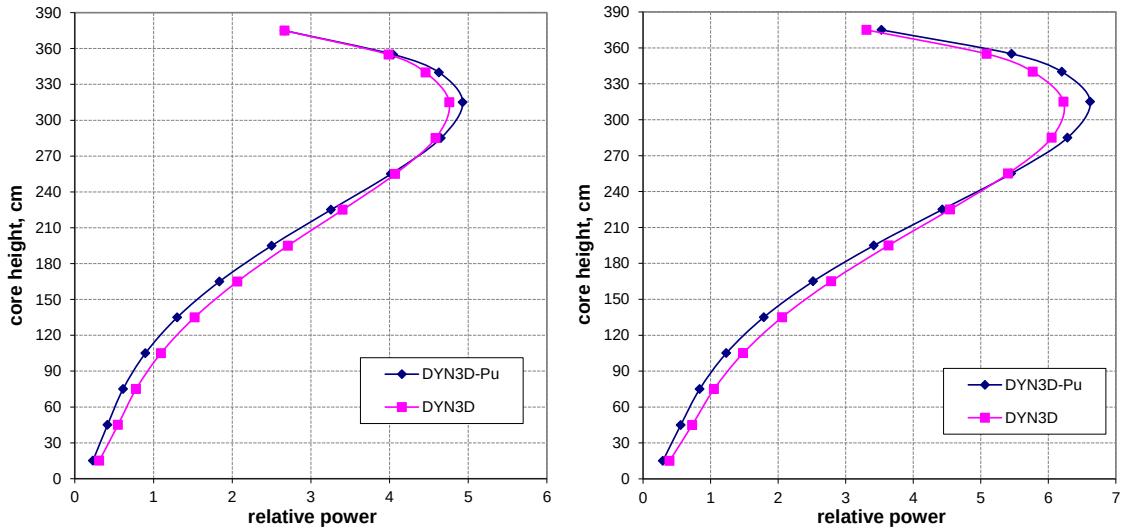

Fig. 7.19 Axial power distribution in assembly #145 (left) and assembly #113 (right) at 200.0 sec.

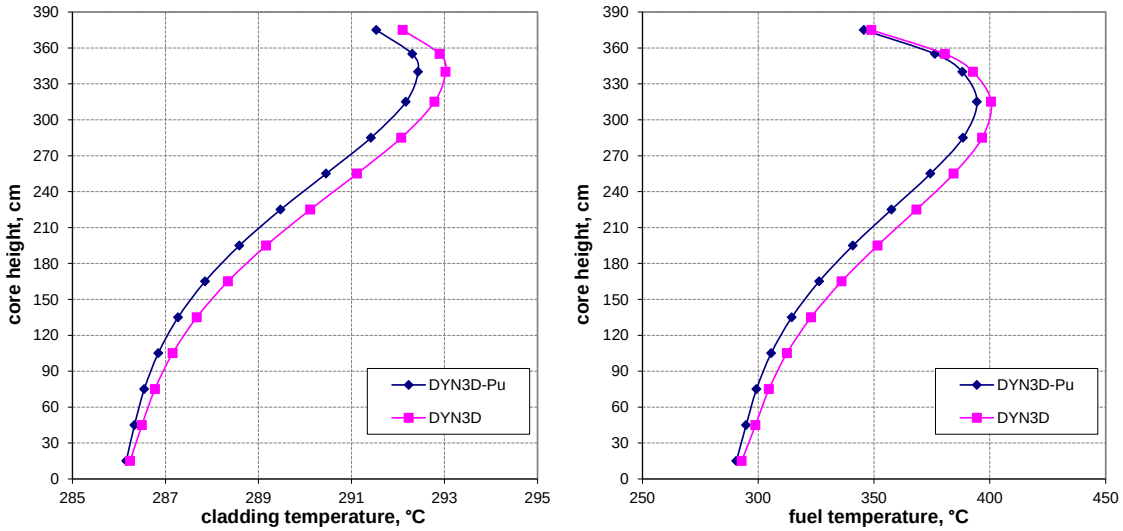

Fig. 7.20 Axial fuel center line (right) and cladding surface temperature (left) distributions in fuel assembly #113 at 200.0 sec.

The maximum of relative power is reached in fuel assembly #113 at t = 5 sec. Fig. 7.17 represents the axial distribution of relative power in assembly #145, wherefrom the rod was ejected, and in hottest assembly #113 at *t* = 15 sec, Fig. 7.19 illustrate same axial distributions at 200 sec. In the axial layer with the power maximum the difference between calculations with and without correction is about 6%.

Table 7.3 Transient summary

	DYN3D	DYN3D-Pu
Maximum reactivity, $	0.516	0.487
Maximum power, MW	126	113
Maximum fuel temperature, °C	401	395
Maximum cladding temperature, °C	293	292
Maximum heat flux, kW/m^2	114.5	108.7

The safety relevant parameters of the reactor core calculated by two modes of DYN3D are summarized in Table 7.3. As in previous case, the maximum fuel and cladding temperatures and maximum heat flux occur in a fresh fuel assembly, where the influence of history effects is minimum. Deviations in these values are about 1-3%.

7.1.2 End of cycle

The same transients were also simulated for the end-of-cycle burnup and poisoning distributions (except xenon poisoning, which was set to zero). The end of cycle state of reactor core is characterized by a more uniform power distribution, higher values of feedback coefficients

(see Table 6.3), higher weight of control rods (see Table 6.4) and deeper fuel burnup. Detailed simulation results are described in section A.1 of Appendix A.

The safety-relevant parameters for the central-rod ejection are summarized in Table 7.4, and for the periphery-rod ejection – in Table 7.5.

Table 7.4 HZP EOC. Central-rod ejection summary

	DYN3D	DYN3D-Pu
Maximum reactivity, $	0.783	0.826
Maximum power, MW	153	151
Maximum fuel temperature, °C	430	438
Maximum cladding temperature, °C	294	294
Maximum heat flux, kW/m^2	144.1	151.3

Table 7.5 HZP EOC. Periphery-rod ejection summary

	DYN3D	DYN3D-Pu
Maximum reactivity, $	0.708	0.661
Maximum power, MW	152	135
Maximum fuel temperature, °C	424	415
Maximum cladding temperature, °C	294	293
Maximum heat flux, kW/m^2	137.7	129.2

The ejection of control rod at the end of cycle introduces higher positive reactivity, because of higher control rod weight. This is partly compensated by stronger temperature and power feedbacks. Influence of historical correction on the transient result at the end of cycle is similar as at the beginning of cycle.

7.2 Case C2 at full power

In the initial state of the reactor before the transient the power level is 3950 MW and the inlet temperature is 293.5°C. Burnup and historical parameters distributions were derived in respective burnup calculations of the generic equilibrium fuel cycle (see section 6). The critical boron concentration in the moderator is derived in respective calculations by each of the two DYN3D modes and shown together with reactivity coefficients in Table 7.6. The boron concentration is above zero at the end of cycle because no xenon poisoning is assumed in all cases.

The position of control rods (in percent) in the initial state is shown in Fig. 7.21, where 100% – upper position (rod fully withdrawn), and 0% – lower position (rod fully inserted). The rod ejections from the central assembly #97 and the periphery assembly #170 were simulated at the beginning and the end of equilibrium fuel cycle.

Table 7.6 reactivity coefficients in the C2 full power initial state

		BOC		EOC	
		DYN3D	DYN3D-Pu	DYN3D	DYN3D-Pu
CB, ppm		1526	1535	259	254
Reactivity coefficients	Moderator temperature, pcm/K	-45.94	-45.70	-81.19	-81.48
	Fuel temperature, pcm/K	-2.58	-2.60	-2.68	-2.69
	Boron concentration, pcm/ppm	-5.25	-5.20	-6.38	-6.29

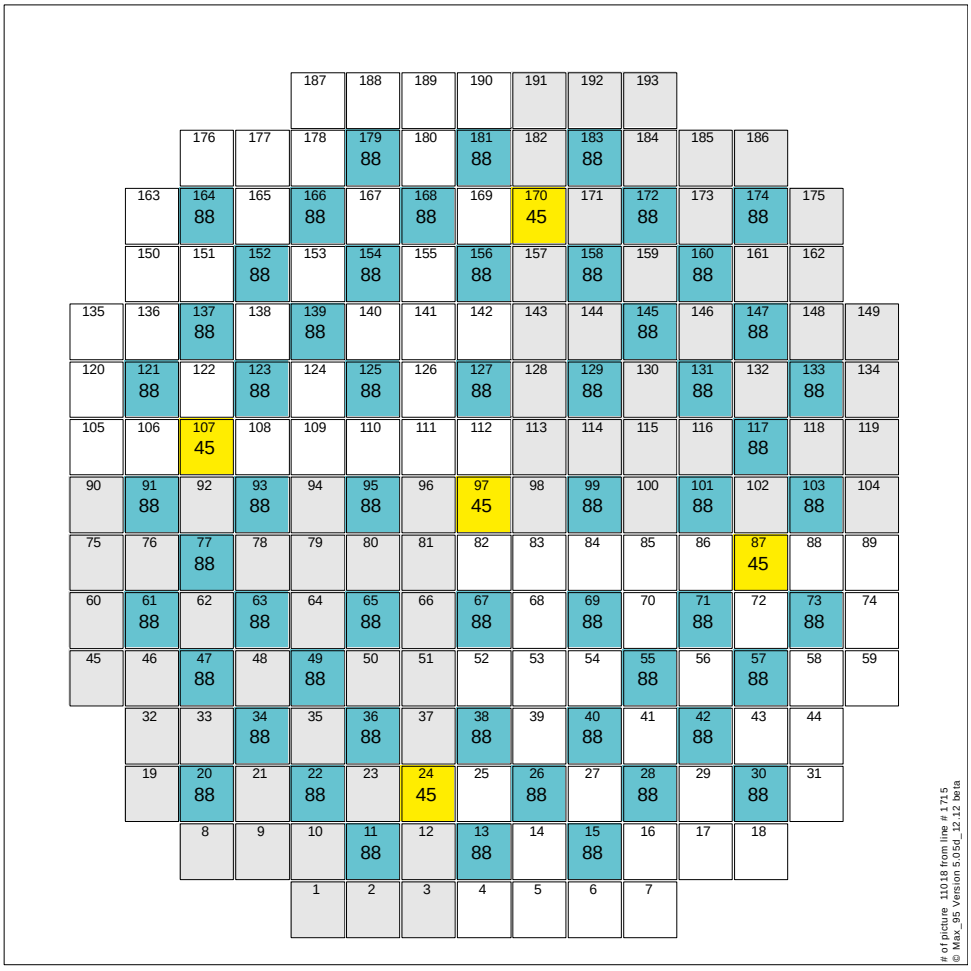

Fig. 7.21 Control rod positions in the C2 full power initial state.

7.2.1 Beginning of cycle

Full Power. The initial state

The initial power distribution is illustrated in Fig. 7.22. The respective axial power distributions for assemblies #97 and #170 are shown in Fig. 7.23. Neutron flux and power production in the upper part of these assemblies are suppressed by partly inserted control rods (see Fig. 7.21).

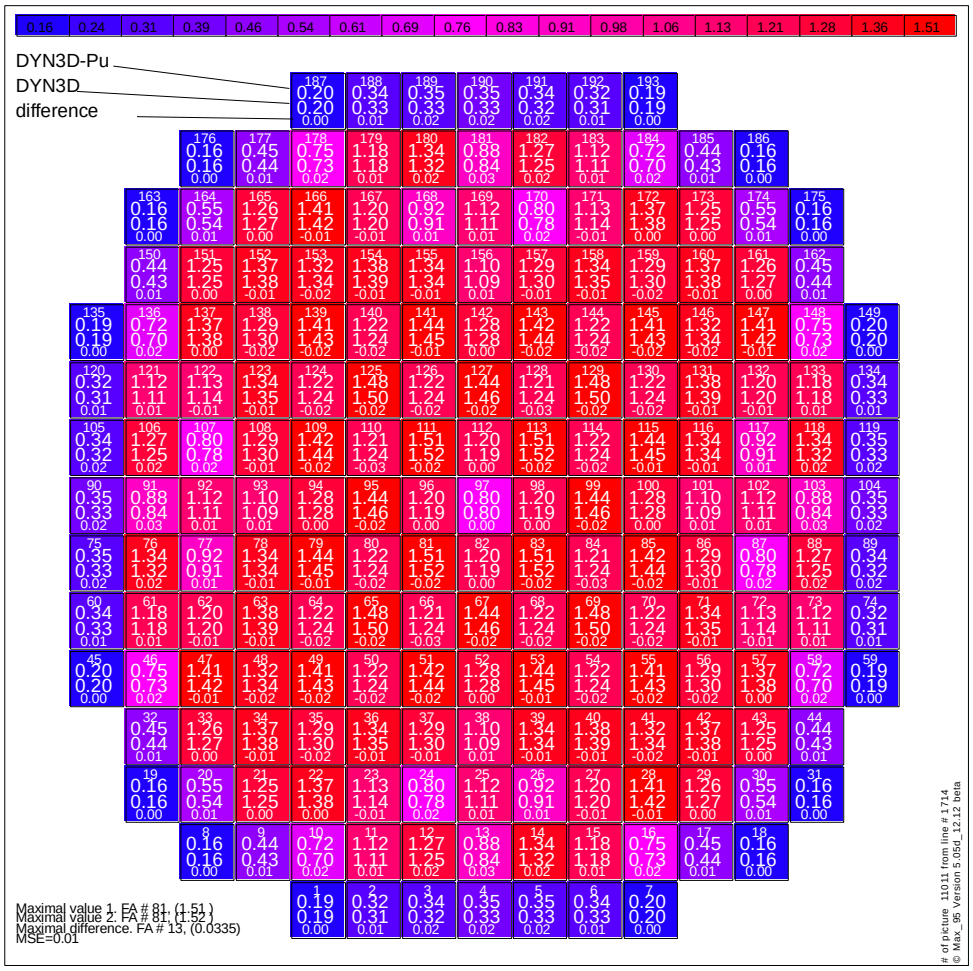

Fig. 7.22 Relative power distribution in the FP initial state at the beginning of equilibrium cycle.

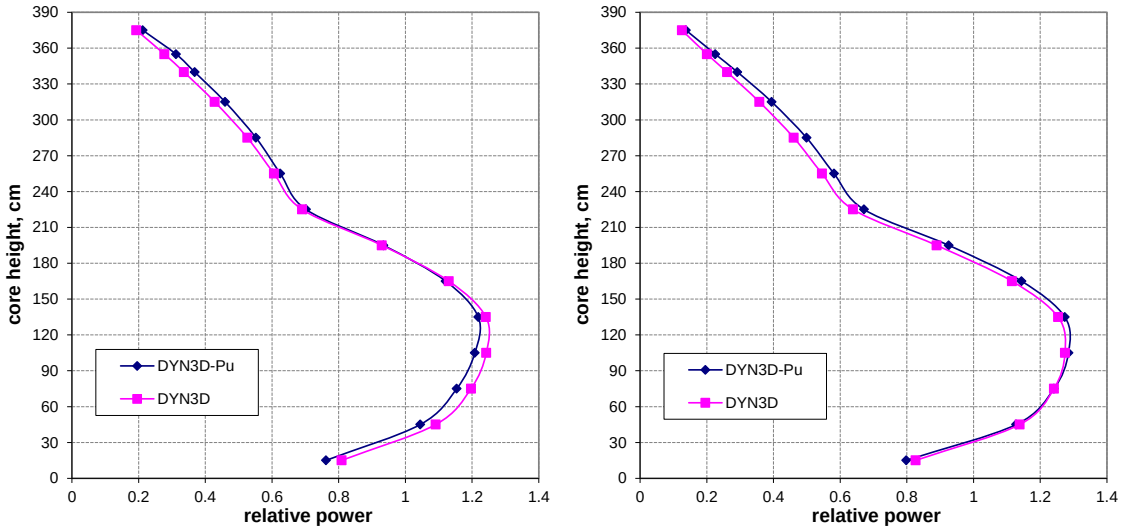

Fig. 7.23 Axial power distribution in the central fuel assembly #97 (left) and assembly #170 (right) in the FP initial state.

Full Power. Central-rod ejection.

Simulation results of control-rod ejection at the full power level at the beginning of fuel cycle from the central assembly are illustrated in Fig. 7.24-7.31.

The reactivity increases with control-rod ejection and reaches its maximum at t = 0.105 sec (see Fig. 7.24), when the ejected control rod is fully withdrawn. In calculations with historical corrections the introduced reactivity is slightly higher than in calculation without correction because the control rod is ejected from the upper part of the core, where differential efficiency of control rods are increased by the historical correction.

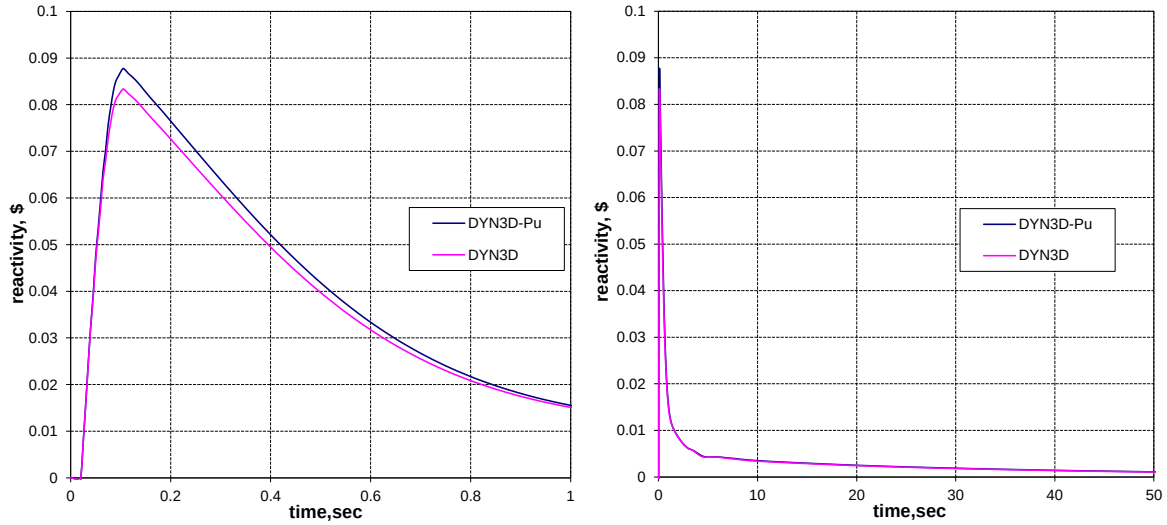

Fig. 7.24 Change of reactivity during the transient.

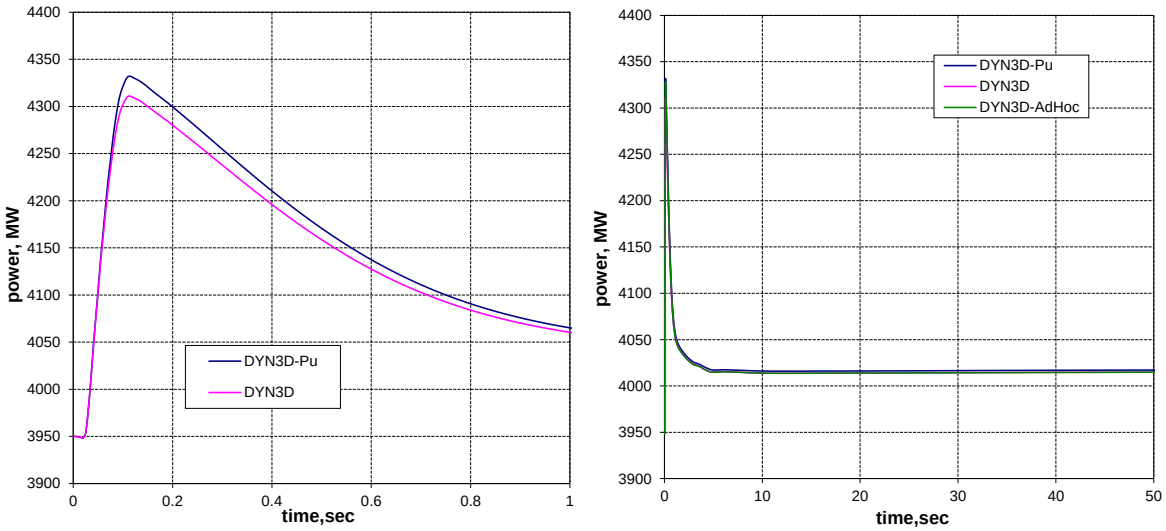

Fig. 7.25 Change of reactor power during the transient.

Introduction of positive reactivity causes an increase of power (see Fig. 7.25) and, thereby, of core-averaged fuel and coolant temperatures (see Fig. 7.26). Due to the negative feedback (see Table 7.6), the increase of fuel and coolant temperatures introduces negative reactivity, compensating the effect of rod ejection. After about 10 sec the reactor stabilizes at the new power level ≈4015 MW. Higher reactivity peak in calculations with historical corrections leads to higher power peak.

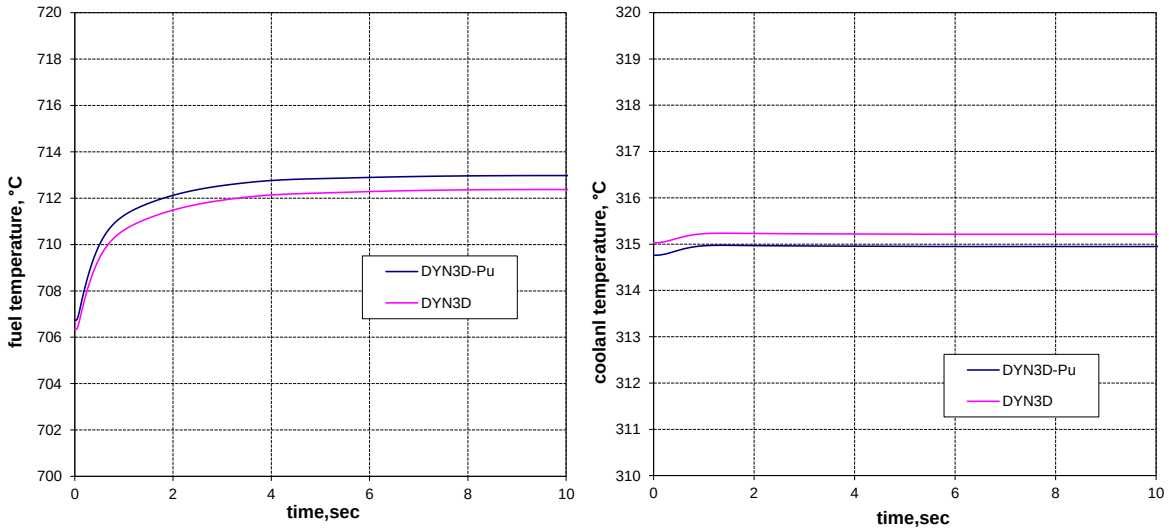

Fig. 7.26 Change of core-averaged fuel and coolant temperatures during the transient.

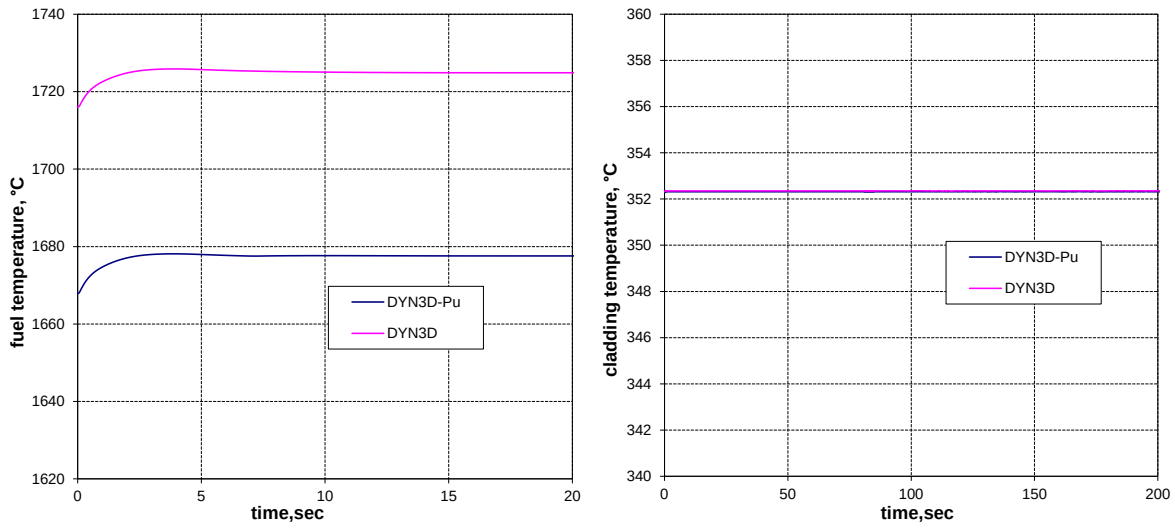

Fig. 7.27 Change of fuel center line (left) and cladding (right) maximum temperatures during the transient.

The maximum fuel and cladding temperatures during the transient are shown in Fig. 7.27. Their axial distributions in the hottest assembly #81 at the moment when temperatures reach maximum values t = 3.95 sec, are depicted in Fig. 7.31. Axial power redistribution due to the historical correction results in lower fuel temperature peak already in the initial state before transient. The maximum temperature increase during the transient is same in both calculations. The maximum cladding temperature coincides in both calculations because its value is limited by sub-cooled boiling.

The maximum heat flux and minimum DNBR (Departure from Nucleate Boiling Ratio) during the transient are shown in Fig. 7.28. The minimum value of DNBR occurs at the upper part of the core, at axial layer #10 (73% of the core height) of fresh fuel assembly #81, while maximum cladding surface heat flux occurs at layer #4 (27% of the core height) of the same assembly. Historical correction slightly decreases the values of the maximum flux and increase minimum DNBR.

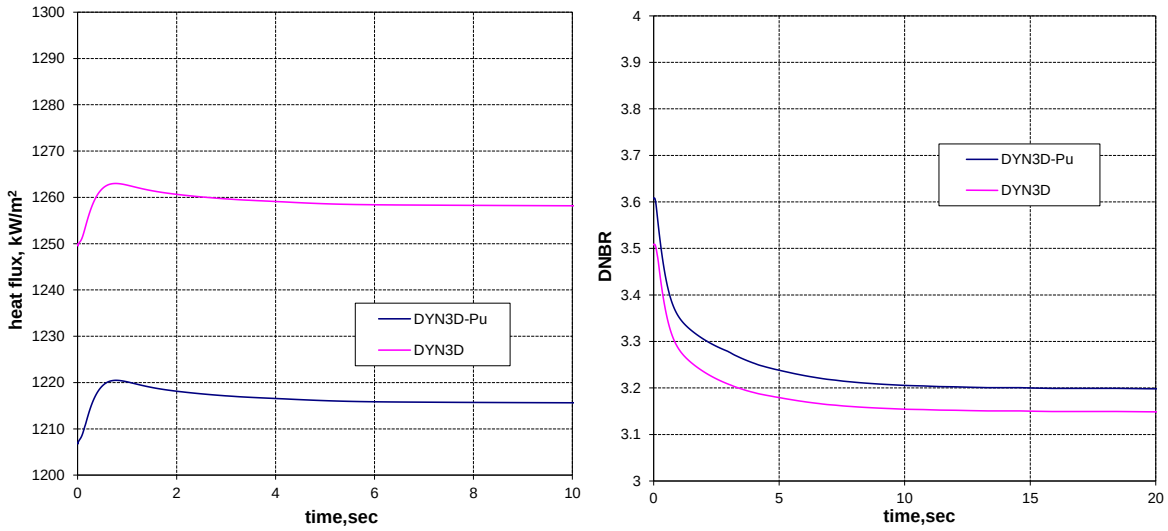

Fig. 7.28 Change of heat flux and DNBR during the transient.

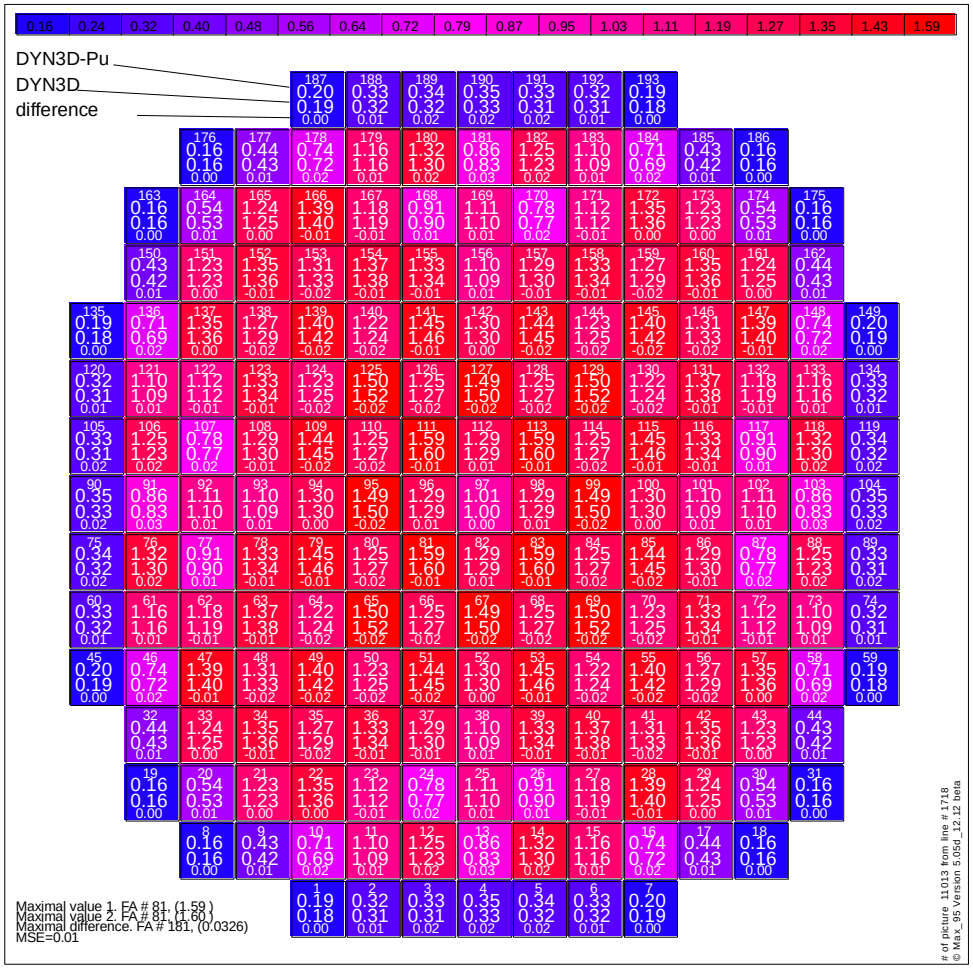

Fig. 7.29 Relative power distribution at 0.12 sec.

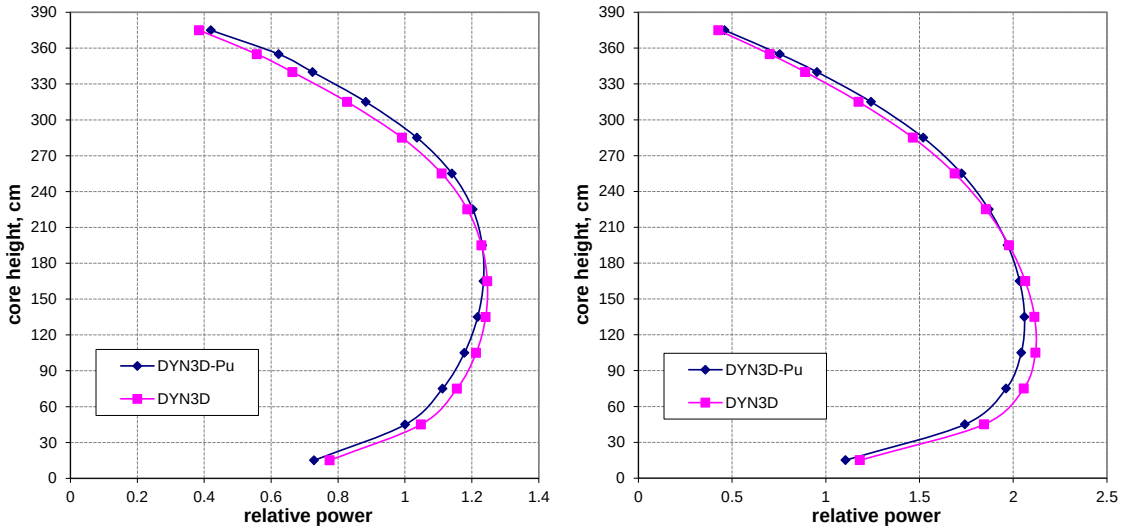

Fig. 7.30 Axial power distribution in the central fuel assembly #97 (left) and assembly #81 at 0.12 sec.

A comparison of radial power distributions at t = 0.12 sec, when the power reaches its maximum, is shown in Fig. 7.29.

Fig. 7.30 represents the axial distribution of the relative power in the central assembly #97, wherefrom the rod was ejected, and in assembly #81, which has its maximum power at t = 0.12 sec. These figures reflect the general tendency of the flux shift, calculated with history corrections, from lower to upper part of the core. In the power-maximum axial layer the difference between calculations with and without correction is about 3%.

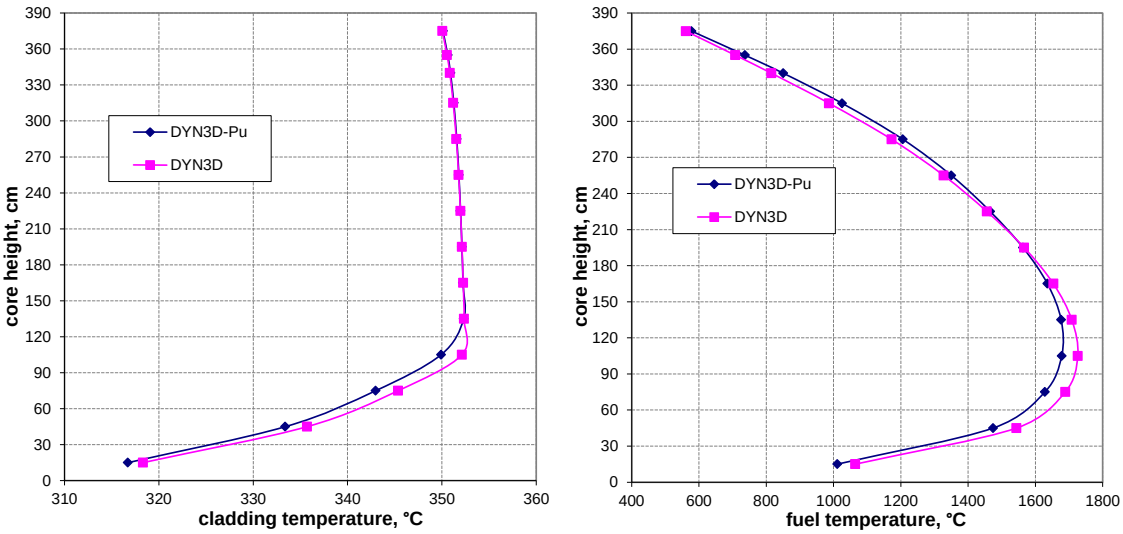

Fig. 7.31 Axial fuel (right) and cladding surface (left) temperatures distributions in fuel assembly #81 at 3.95 sec.

Table 7.7 FP BOC. Central-rod ejection summary.

	DYN3D	DYN3D-Pu
Maximum reactivity, $	0.083	0.088
Maximum power, MW	4311	4332
Maximum fuel temperature, °C	1725.9	1678.1
Maximum cladding temperature, °C	352.4	352.3
Minimum DNBR	3.15	3.19

Safety-relevant core parameters calculated by the two DYN3D modes are summarized in Table 7.7. The maximum fuel temperature and minimum DNBR appear again in a fresh fuel assembly, where the influence of history effects is minimal. History-defined deviations in these parameters are dictated by the axial power redistribution already in the initial state before transient – about 3% for maximum fuel temperature and about 1% for minimum DNBR. The variations during transient of maximum fuel and cladding temperatures and minimum DNBR are the same in calculations with and without historical correction.

The maximum reactivity level calculated by the DYN3D with historical corrections is about 5% higher than without correction. Control rod is ejected from of the upper part of highly burned (see Fig. 6.1) central assembly, where history correction leads to increase of local power (see Fig. 6.7 and Fig. 7.23). Axial power redistribution due to history correction explains higher control rod worth.

Full Power. Periphery-rod ejection.

Results of control-rod ejection at the full power level at the beginning of fuel cycle from a periphery assembly are illustrated in section of Appendix A. Safety-relevant parameters are summarized in Table 7.8.

Table 7.8 FP BOC. Periphery-rod ejection summary

	DYN3D	DYN3D-Pu
Maximum reactivity, $	0.077	0.083
Maximum power, MW	4282	4311
Maximum fuel temperature, °C	1724.4	1676.8
Maximum cladding temperature, °C	352.3	352.3
Minimum DNBR	3.33	3.42

7.2.2 End of cycle

Transient simulation results for the end of cycle are described in section A.3 of Appendix A. The safety-relevant parameters of central-rod ejection are summarized in Table 7.9, and periphery-rod ejection – in Table 7.10.

Table 7.9 FP EOC. Central-rod ejection summary

	DYN3D	DYN3D-Pu
Maximum reactivity, $	0.063	0.067
Maximum power, MW	4214	4232
Maximum fuel temperature, °C	1834.1	1818.2
Maximum cladding temperature, °C	352.3	352.3
Minimum DNBR	4.10	4.18

Table 7.10 FP EOC. Periphery-rod ejection summary

	DYN3D	DYN3D-Pu
Maximum reactivity, $	0.077	0.079
Maximum power, MW	4281	4290
Maximum fuel temperature, °C	1837.0	1821.0
Maximum cladding temperature, °C	352.3	352.3
Minimum DNBR	4.03	4.10

Like in the hot zero power case, the influence of historical correction on the transient result at the end of cycle is similar as at the beginning of cycle.

7.3 Chapter short summary

Control rod ejection transients have been simulated at full and hot zero power levels to illustrate the influence of historical correction on reactor kinetics. The simulation results show that the application of the correction does not change the course of transient, although influencing some core characteristics.

Axial power and burnup redistributions due to historical corrections define respective fuel temperatures and cladding surface heat fluxes redistributions already in the initial steady-state before transient. Generally speaking, if the peak of fuel temperature (heat flux, cladding temperature, minimum of DNBR, etc.) occurs in the bottom of the core, it is reduced in calculation with historical correction; if the peak occurs in the upper part of the core – it is increased by historical correction and peak is not affected if it occurs in the middle level of the core. The change

of these safety-relevant parameters is the same in calculations with and without historical correction.

The peak values of safety-relevant parameters like heat flux, fuel and cladding temperatures, DNBR, etc. appear in “fresh” fuel assemblies with low burnup, where burnup history effects are minimum. For the considered transients the effect of history correction on the introduced reactivity is up to 7%, on the reactor power peak ~1% and on the peak fuel temperature ~3% in full power cases. For hot zero power cases, the difference in the reactivity peak is up to 5%, in the reactor power peak up to 10% and in the peak fuel temperature ~2%.

As described in section 4.2.2, the historical correction is applied to static diffusion parameters (macroscopic cross sections and diffusion coefficients) but not to kinetic parameters (inversed velocities and delayed neutrons data). The obtained results should be revised after the extension of the methodology to kinetic parameters.

8 Summary and Conclusions

The current generation of nuclear reactors (Light Water Reactors, generations 2 and 3 –PWR, BWR, VVER) safety must be ensured with respect to changes in fuel cycles (more complicated fuel design, higher burnup, perspective use of thorium and actinides transmutation) and life-time prolongation.

Best-estimate simulation tools are considered key elements of NPP safety assurance. Such a tool – the three-dimensional reactor dynamics and core design code DYN3D has been and is being developed at Helmholtz-Zentrum Dresden-Rossendorf. DYN3D is able to calculate the steady-state of a reactor core, including parameters important for safe and economical operation, such as the power distribution and reactivity coefficients, and to simulate transients and accident scenarios. The present work is part of a continuous effort to improve DYN3D and describes a method of increasing the accuracy of nodal cross section treatment by taking into account burnup spectral history effects.

Cross sections (XS) for the same fuel with the same burnup level (measured in terms of produced energy) could differ even if the instantaneous local conditions are the same. This is mainly due to differences in the plutonium buildup and uranium depletion rates that change with the neutron spectrum. The operational parameters (moderator density, fuel temperature, boron acid concentration, etc.) define the local spectrum, and thus their history influences nuclide content of the burned fuel, foremost actinides concentrations.

Actinides have high neutron absorption and fission microscopic cross sections, therefore the local burnup history has the strongest influence on the homogenized absorption and fission cross sections. Deviations of these XS values for nodes with different burnup history grow with burnup and can be higher than 10% for burnup levels of 50 MWd/kgHM. Deviations in multiplication factors reach 3% for the same burnup level.

DYN3D, as well as many other nodal codes, estimates nodal XS using a XS-library prepared by the lattice code. The change of nuclide content during fuel depletion is calculated by a lattice code in a single-assembly depletion calculation applying a single set (usually, core- and cycle-averaged values) of operational parameters. This approach cannot represent effects of local (nodal) spectral history and leads to an error in XS estimation which is growing with burnup.

A series of lattice code single-assembly depletion calculations for the same fuel model but with different sets of operational parameter have been performed and analyzed. Results have shown that changes of different actinides concentrations in off-nominal depletions are related with each other. Furthermore, the proportionality between history-originated changes of nodal cross sections and deviation in plutonium-239 concentration has been found and used in the method proposed here. The correction for nodal cross sections is proportional to the deviation of the nodal ^{9}Pu

concentration from the value in the reference depletion. All additional data necessary for correction calculation is stored in a "historical sub-library", which is generated once for each fuel type by a lattice code.

This method has been implemented in DYN3D and tested in single-assembly, whole-core steady-state, burnup and transient calculations.

A verification of the new cross section estimation procedure was performed by single-assembly calculations for PWR UOX, UOX with burnable absorber and MOX fuel assemblies. A special DYN3D model was developed to make possible a direct comparison of the XS calculated by DYN3D and the lattice code HELIOS. The application of the developed ^{9}Pu-correction reduces the error in the XS estimation by more than a factor 10, and for the multiplication factor k-infinity – down to deviations less than 100 pcm at a burnup level of 50 MWd/kgHM. Similar results were achieved in single-assembly calculations for TWSA fuel assembly with hexagonal geometry for VVER-1000 reactor.

Whole-core steady-state, burnup and transient calculations of PWR were performed to investigate the influence of history effects. Three modes of DYN3D calculations were compared: without history consideration, with ^{9}Pu history indicator and with Ad-Hoc history parameters.

The most significant effect of the application of historical correction in full-core burnup and steady-state calculations is the change in axial power and burnup redistribution and fuel cycle length.

History corrections shift the power distribution from the lower to the upper part of the core during the whole cycle. The increase of relative power in the middle of the upper part of the core and decrease in the middle of the lower part are about 3% for the whole core at nominal power and about 5% for some assemblies with high burnup. For hot zero power level the differences in axial relative power reach even 10%. Axial power redistribution causes axial redistribution of the burnup, the upper part of the core is depleting faster which leads to partial self-compensating of history effect. Resulting axial burnup and power distributions are more uniform (bottom peak is lower) at the end of cycle which decrease neutron leakage through the bottom border of a core. Improved neutron balance results in higher critical boron concentration and longer fuel cycle. The equilibrium cycle of the considered PWR is about 10 days (~3%) longer in both calculations with history corrections.

Thermo-hydraulic parameters of fuel like fuel and cladding temperatures, cladding surface heat fluxes, DNBR, etc. are determined by nodal power and power redistribution leads to respective redistribution of these parameters. The historical corrections result in 30-50 K (about 2-3%) higher fuel temperatures in the upper part of the core and lower temperatures in the lower part.

The axial flux shift due to history effects has also some influence on the differential weight of control rods. Integral core characteristics like reactivity coefficients are not sensitive to axial power

redistribution and therefore to history corrections. The obtained results are in good agreement with previously published investigations.

In order to investigate the influence of historical corrections on transients, hypothetical control-rod-ejection accidents were chosen. No significant influence of history effects on reactor dynamics was found, apart from effects of axial power and burnup redistribution in the initial steady-state before the transient. The peak values of safety-relevant parameters like fuel and cladding temperatures and DNBR are decreased if the peak occurs in the bottom of the core or increased if the peak occurs in the upper part of the core. The change of the peak values is the same in calculations with and without historical correction.

As a "side product" of this research, the "Ad-Hoc parameters" history correction methodology was extended to burnup calculations, which makes the AdHoc-method an independent option of DYN3D. The results obtained using the AdHoc- and plutonium-correction are similar in relevant cases (like fuel cycle length and axial power and burnup distribution). The main advantage of the developed Pu-correction method over the AdHoc-methodology is the ability to consider history effects like the presence of a control rod, the influence of poisoning and the influence of neighboring nodes on the local spectrum.

The method of taking into account history effects by following the local ^{9}Pu concentration has been developed, implemented in the reactor dynamic and core design code DYN3D and verified in this study. Test calculations for single assemblies, as well as full-core steady-state, burnup and transient calculations have proven its effectiveness for western-type PWR and VVER reactors.

Possible directions of further development could be:

- the extension of methodology to the multi-group solver;
- the correction of kinetic parameters (inversed neutron velocities and delayed neutron fractions);
- the inclusion of other actinide isotopes to improve the method accuracy;
- the extension of this method to Boiling Water Reactors, and, maybe, to some of the innovative reactor concepts;
- the further validation of the Pu-correction method in code-to-code comparison with coupled Monte-Carlo-thermodynamics codes or in comparison with high-quality plant measurements.

Nomenclature

Abbreviations

2D, 3D	Two, and three Dimensional
^{5}U	Uranium isotope 235
^{8}U	Uranium isotope 238
^{9}Np	Neptunium isotope 239
^{9}Pu	Plutonium isotope 239
ADF	Assembly Discontinuity Factors
BA	Burnable Absorber
BOC	Beginning Of Cycle
BWR	Boiling Water Reactor
CCCP	Current Coupling Collision Probability Method
DNBR	Departure From Nucleate Boiling Ratio
DYN3D	Dynamical 3-Dimensional code for Light Water Reactors
DYN3D-AdHoc	DYN3D with Ad-Hoc-based XS correction
DYN3D-Pu	DYN3D with ^{9}Pu-based XS correction
ENDF	Evaluated Nuclear Data File (Nuclear Data Library)
EOC	End Of Cycle
FA	Fuel Assembly
FP	Full Power
FPD	Full Power Days
GRS	Gesellschaft für Anlagen- und Reaktorsicherheit
HZDR	Helmholtz-Zentrum Dresden-Rossendorf
HZP	Hot Zero Power
IAEA	International Atomic Energy Agency
JEF	Joint Evaluated File (Nuclear Data Library)
LWR	Light Water Reactor
MOX	Mixed Uranium-Plutonium Oxide Fuel
MW	Mega Watt
MWd/kgHM	Energy in Megawatt*day produced in fuel per kilogram of initial Heavy Metal
NEACRP	OECD Nuclear Energy Agency Committee on Reactor Physics
NEM	Nodal Expansion Method

OECD	Organization for Economic Co-operation and Development
pcm	per centomille, 1 pcm=1^{-5}
ppm	parts per million
PWR	Pressurized Water Reactor
SCRAM	Emergency shutdown of a nuclear reactor
SSTC NRS	State Scientific and Technical Center for Nuclear and Radiation Safety, Ukraine
TWSA	Fuel assembly with hexagonal geometry
UOX	Uranium Oxide Fuel
VVER	Water-Water Energetic Reactor (Russian type PWR)
XS	Assembly-homogenized few-group macroscopic cross sections

Symbols

B	burnup	MWd/kgHM
C_B	boron acid concentration	ppm
D	diffusion coefficient	cm
E	neutron energy	eV
G	number of the neutron energy groups	
HC_B	burnup-weighted local boron acid concentration	ppm
HR_M	burnup-weighted local moderator density	g/cm^3
HT_F	burnup-weighted local fuel temperature	°C
J	neutron current	cm^{-2}s^{-1}
k	history coefficient	
k_∞	multiplication factor of infinite system	
n	neutron density	cm^{-3}
N	number density	atoms/cm^3
P	pressure	MPa
$\vec{r}$	position vector	
R	reaction rate	cm^{-3}s^{-1}
SH	spectral history	
SI	spectral index	
t	time	s
T_F	fuel temperature	°C
T_M	moderator temperature	°C
v	scalar neutron velocity	cm/s

V	volume	cm^3
λ	decay constant	s^{-1}
ρ_M	moderator density	g/cm^3
ν	number of neutrons released per fission	
$\overline{\mu_0}$	mean cosine of the scattering angle	
σ	microscopic cross section	barn
Σ	macroscopic cross section	cm^{-1}
φ	angular neutron flux	$cm^{-2}s^{-1}sr^{-1}$
ϕ	neutron flux	$cm^{-2}s^{-1}$
χ	fission spectrum	
$\vec{\Omega}$	direction vector	

Indexes

a	absorption
c	capture
f	fission
g	neutron energy group
r	removal
s	scattering
t	total

References

Aragonés, J.M., Ahnert, C., Cabellos, O., (1996) Methods and Performance of the Three-Dimantional Pressurized Water Reactor Core Dynamics SIMTRAN On-Line Code, Nuclear Science and Engineering vol.124, pp.111-124.

Bahadir, T., Lindahl, S. Ö, Palmtag, S.P., (2005) Microscopic Depletion Model In SIMULATE-4, American Nuclear Society Transactions vol.92, pp.635-636.

Bahadir, T., Lindahl, S. Ö, Palmtag, S.P., (2005a) SIMULATE-4 Multigroup Nodal Core with Microscopic Depletion Model, American Nuclear Society Topical Meeting in Mathematics & Computations, Avignon, France.

Baturin, D.M., Vygovskii, S.B., (2001) Taking account of the spectral history of fuel burnup during the preparation of the neutron-physical constants for VVER-1000 fuel assemblies, Atomic Energy vol.90(4), pp. 267-272.

Bilodid, Y., Mittag, S., (2008) Spectral-History Modeling in DYN3D Burnup Calculations, Proceedings of 18th Symposium of AER, Eger, Hungary, pp. 467-481.

Bilodid, Y., Mittag, S., (2010) Use of the local Pu-239 concentration as an indicator of burnup spectral history in DYN3D, Annals of Nuclear Energy vol.37, pp.1208-1213.

Bilodid, Y., Mittag, S., (2011) Influence of spectral history on PWR full core calculation results, Proceedings of 21th Symposium of AER, Dresden, Germany.

Bilodid, Y., Ovdiienko, I., Mittag, S., Kuchin, A., Khalimonchuk, V., Leremenko, M, (2012) Assessment of spectral history influence on PWR and WWER core, Kerntechnik vol.77(4), KT11025.

Borland, R., Fu, H. (1995) Evaluation of Spectral History Effects in B&W PWRs Using Studsvik CMS, American Nuclear Society Transactions vol.73, p.382.

Cabellos, O., Aragonés, J.M., Ahnert, C., (1999) Generalized Effects in Two-Group Cross Sections and Discontinuity Factors in the DELFOS Code for PWR Cores, Proceedings of the Int. Conf. on Mathematics and Computation, Reactor Physics and Environmental Analysis in Nuclear Applications, Madrid, Spain, vol. 1, pp. 700-709.

Cacuci, D.G., (2010) Handbook of Nuclear Engineering, vol. 2, Springer Science + Business Media LLC.

Carlvik I. (1965) A method for calculating collision probabilities in general cylindrical geometry and applications to flux distributions and Dancoff factors, U.N. Intl Conf. on the Peaceful Uses of Atomic Energy, Geneva, pp.225-231.

Chauliac, C., Aragones, J.M., Bestion, D., Zimmermann, M., Cacuci, D., Crouzet, N. (2009) NURESIM Project Final Activity Report.

Croninget, J.T., Smith, K.S., Ver Planck, D.M. (2005) SIMULATE-3 Methodology, Advanced Three-Dimensional Two-Group Reactor Analysis Code, Studsvik of America, Newton, USA, STUDSVIK/SOA-95/18-Rev0.

DOE, (1993) Fundamentals Handbook. Nuclear Physics And Reactor Theory. DOE-HDBK-1019/2-93. U.S. Department of Energy.

Downar, T.J., Kozlowski, T., et. al. (2002) PARCS: Purdue Advanced Reactor Core Simulator, Proceedings of the PHYSOR Conference, Seoul, Korea.

Duderstadt, J., Hamilton, L., (1975) Nuclear Reactor Analysis, John Wiley & Sons,Inc.

Finnemann, H., Galati, A. (1992) NEACRP 3-D Core Transient Bencmark, NEACRP-L-335, OECD Nuclear Energy Agency

García-Herranz, N., Aragonés, J.M., Cabellos, O., Ahnert, C., (1999) Dependence of the Nodal Homogenized Two-Group Cross Sections on Intranodal Flux-Spectrum, Burnup and History, Proceedings of the Int. Conf. on Mathematics and Computation, Reactor Physics and Environmental Analysis in Nuclear Applications, Madrid, Spain, vol. 1, pp. 127-138.

Gavin, P., (1995) Explicit treatment of spectral history Effects in PWR Design. American Nuclear Society Transactions, vol.73, p. 381.

Grundmann, U., Lucas, D., Rohde, U. (1995) Coupling of the Thermohydraulic Code ATHLET with the Neutron Kinetic Core Model DYN3D, Int. Conf. on Mathematics and Computations, Reactor Physics, and Environmental Analyses, Portland, Oregon, Proc. vol. 1, p. 257

Grundmann, U. (1995a) The Code DYN3DR for Steady-State and Transient Analyses of Light Water Reactor Cores with Cartesian Geometry, Rossendorf, Report FZR-114

Grundmann U., Hollstein F., A (1999) Two-Dimensional Intranodal Flux Expansion Method for Hexagonal Geometry, Nuclear Science and Engineering, vol. 133, pp.201-212.

Grundmann, U., Rohde, U., Mittag, S. (2000) DYN3D – three-dimensional core model for steady-state and transient analysis of thermal reactors, Proceedings of the 2000 ANS International Topical Meeting on Advances in Reactor Physics and Mathematics and Computations into the Next Millennium PHYSOR 2000, Pittsburgh, Pennsylvania, USA.

Grundmann, U.; Kliem, S.; Rohde, U. (2004) Analysis of the Boiling Water Reactor Turbine Trip Benchmark with the Codes DYN3D and ATHLET/DYN3D, Nuclear Science and Engineering, vol. 148, pp. 226-234.

Grundmann, U., Rohde, U., Mittag, S., Kliem, S., (2005) DYN3D version 3.2 – code for calculation of transients in light water reactors (LWR) with hexagonal or quadratic fuel elements. Description of models and methods, Report FZR–434, ISSN 1437-322X, p.140, Rossendorf.

Heinrich, H. (1981) NESSEL-4 - a code for computation of local burnup in H2O-moderated nuclear reactors, Kernenergie vol.24, pp.465-471.

Herman, M., Trkov, A. (2009) ENDF-6 Formats Manual – Data formats and procedures for the Evaluated Nuclear Data File ENDF/B-VI and ENDF/B-VII (Document ENDF-102), Tech. Report BNL-XXXXX-2009, National Nuclear Data Center, Brookhaven National Library, Upton, New York, USA.

HELIOS Methods, (2003) Studsvik Scandpower.

Ivanov, B.D., Ivanov, K.N., Stamm'ler, R.J.J. (2004) Helios, current coupling collision probability method, applied for solving the NEA C5G7 MOX benchmark, Progress in Nuclear Energy vol.45, pp.119–124.

Iwamoto, T., Yamamoto, M. (1999) Advanced Nodal Methods of the Few-Group BWR Core Simulator NEREUS, Journal of Nuclear Science and Technology, vol.36:11, pp.966-1008.

Kotlyar, D., Fridman, E., Shwageraus, E., (2009) Coupled neutronic thermo-hydraulic analysis of full PWR core with BGCore system, Proceedings of Annual Meeting on Nuclear Technology, Dresden, Germany.

Lee, C.H., Kim, Y.J., Song J.W., and Park, C.O., (1995) Determination of Local Power Distribution Considering Spectral History Effect in Nodal Method, Proceedings of the Int. Conf. on Mathematics and Computation, Reactor Physics and Environmental Analysis, Portland, p.1034.

Lee, C.H., Kim, Y.J., Song J.W., and Park, C.O., (1996) Incorporation of a New Spectral History Correction Method into Local Power Reconstruction for Nodal Methods, Nuclear Science and Engineering, vol.124, pp.160-166.

Leppänen, J., Pusa, M., (2009) Burnup Calculation Capability in the PSG2 / Serpent Monte Carlo Reactor Physics Code. In Proc. M&C 2009. Saratoga Springs, NY.

Lötsch T., Khalimonchuk V., Kuchin A., (2009) Proposal Of A Benchmark For Core Burnup Calculations For A VVER-1000 Reactor Core, Proceedings of the 19th Symposium of AER on VVER Reactor Physics and Reactor Safety, Varna, Bulgaria

Lötsch T., Khalimonchuk V., Kuchin A., (2010) Corrections And Additions To The Proposal Of A Benchmark For Core Burnup Calculations For A VVER-1000 Reactor, Proceedings of the 20th Symposium of AER on VVER Reactor Physics and Reactor Safety, Espoo, Finland

Manera, A., Rohde, U., Prasser, H.-M., van der Hagen, T. H. J. J. (2005) Modeling of flashing-induced instabilities in the start-up phase of natural-circulation BWRs using the code FLOCAL, Nuclear Engineering and Design, vol.235, pp.1517-1535

Mittag, S., Nuding, M., Grundmann, U., (2006) FZR-interner Arbeitsbericht: Vergleichsrechnungen DYN3D-SIMULATE, Rossendorf.

Nam Zin Cho (2005), Fundamentals And Recent Developments Of Reactor Physics Methods. Nuclear Engineering and Technology, vol.37, pp.25 - 78

NEA, (2010) JANIS 3. Java-based Nuclear Data Display Program. http://www.nea.fr/janis/

Petkov, P. T., Christoskov, I. D., Kamenov, K., (2002) Generation of a library of two-group diffusion and kinetics parameters for DYN3D. Proceedings of 12th AER Symposium, Sunny Beach, Bulgaria, pp.179-190.

Petkov, P. T., Mittag, S., Christoskov, I. D., Kamenov, K., Antov, A., Bakalov, I., Wehner, H., (2003) A new DYN3D library for the WWER-1000 reactors, Proc. of 13th Symposium of AER, Dresden, Germany, 22-26 September 2003.

Rhodes, J., Smith, K., Lee, D. (2006) CASMO-5 Development and Applications, PHYSOR-2006, ANS Topical Meeting on Reactor Physics, Vancouver, Canada

Ronen, Y., (1986) CRC Handbook of Nuclear Reactors Calculations. Vol.1, CRC Press. Inc.

Sanchez, R., Mondot, J., Stankovski, Z.,Cossic, A., Zmijarevic, I., (1988) Apollo-II - a User-Oriented, Portable, Modular Code for Multigroup Transport Assembly Calculations. Nuclear Science and Engineering, vol.100, p.352.

Sissaoui, M.T., Marleau, G., Raozon, D., (1999) CANDU Reactor Simulations Using the Feedback Model with Actinide Burnup History, Nuclear Technology, vol. 125.

Smith, K. and Forget, B., (2013) Challenges in the Development of High-Fidelity LWR Core Neutronics Tools, Proceedings of the M&C 2013 conference, Sun Valley, Idaho, USA, pp.1809-1825

Stacey, W.M., (2004), Nuclear Reactor Physics, Wiley-VCH Verlag GmbH & Co. KGaA.

Stamm'ler, R.J.J., Abbate, M.J., (1983), Methods of Steady-State Reactor Physics in Nuclear Design, Academic Press Inc.

Teschendorff, V., Austregesilo, H., Lerchl, G. (1996) Methodology, status and plans for development and assessment of the code ATHLET. Proc. OECD/CSNI workshop on transient thermal-hydraulic and neutronic codes requirements, Annapolis, USA

Villarino E A, Stamm'ler R J J, Ferri A A And Casal J J (1992) HELIOS: Angularly dependent collision probabilities, Nuclear Science and Engineering vol.112, pp.16-31.

Watson, J.K., Ivanov, K.N., (2002) Improved cross-section modeling methodology for coupled three-dimensional transient simulations. Annuals of Nuclear Energy vol.29(8), pp.937-966.

Wikipidea, (2010) Minor Actinides. Wikipedia. http://en.wikipedia.org/wiki/Minor_actinides

List of Figures

List of Tables

Appendix A

A.1 Case C2 at BOC. Periphery-rod ejection.

Results of control-rod ejection at the full power level at the beginning of fuel cycle from a periphery assembly are illustrated in Fig. A.1-A.9.

The rod is ejected from the assembly #170, which is located in the upper-right quarter of core, so the power production after ejection is asymmetric (see Fig. A.5) with the maximum in this quarter. The course of transient is generally the same as in the central-rod ejection case described above. The maximum local power appears in assembly #129 at the moment 0.12 sec and the maximum fuel temperature – in assembly #113 at the moment 3.15 sec.

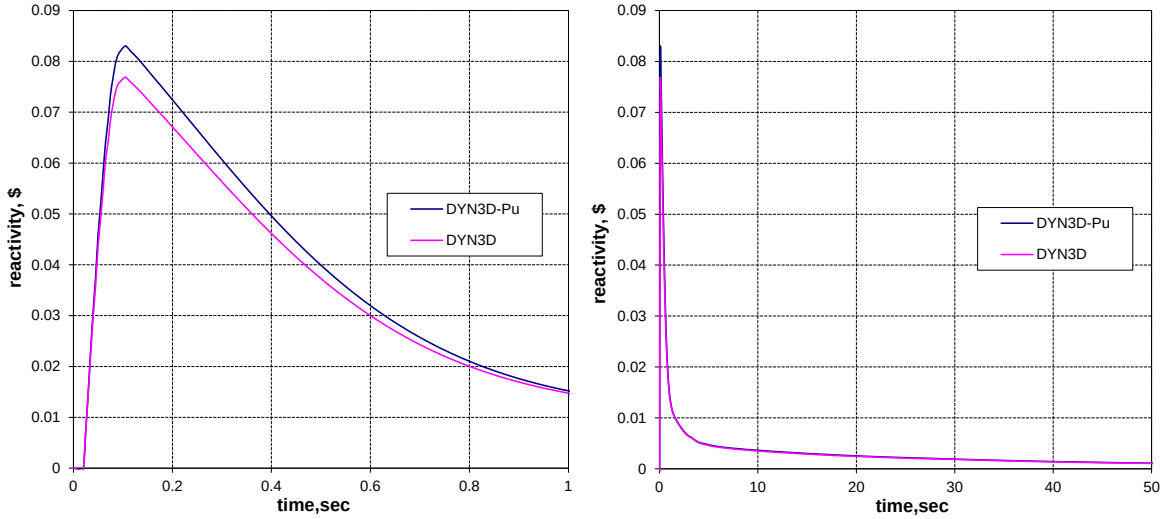

Fig. A.1 Change of reactivity during the transient.

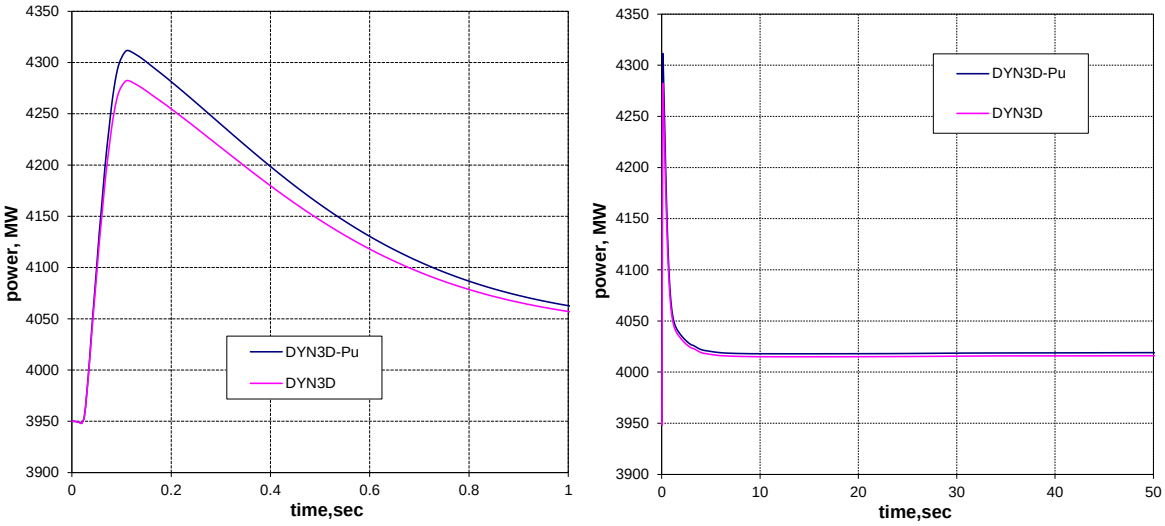

Fig. A.2 Change of reactor power during the transient.

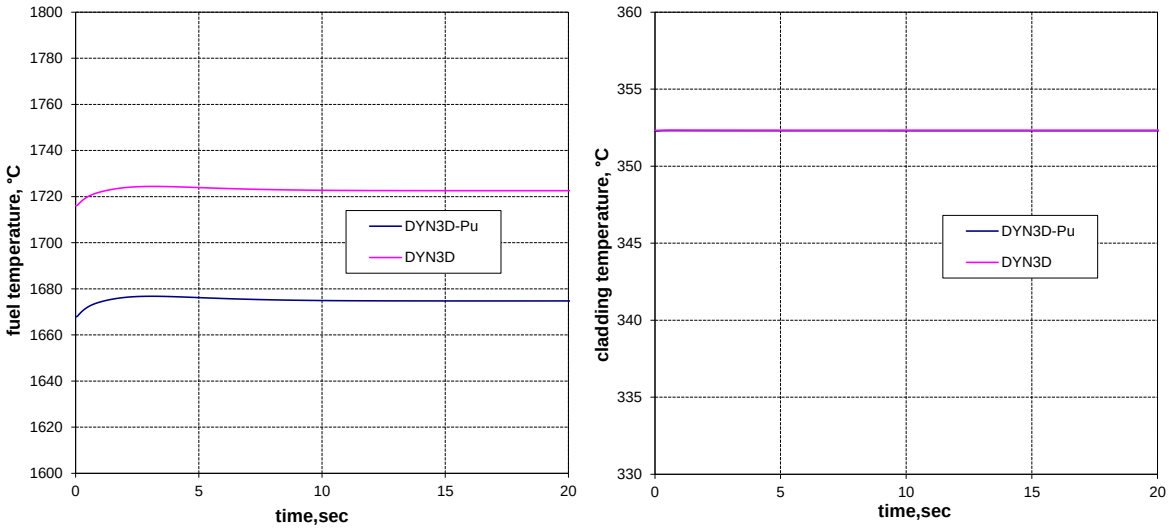

Fig. A.3 Change of fuel center line and cladding temperatures during the transient.

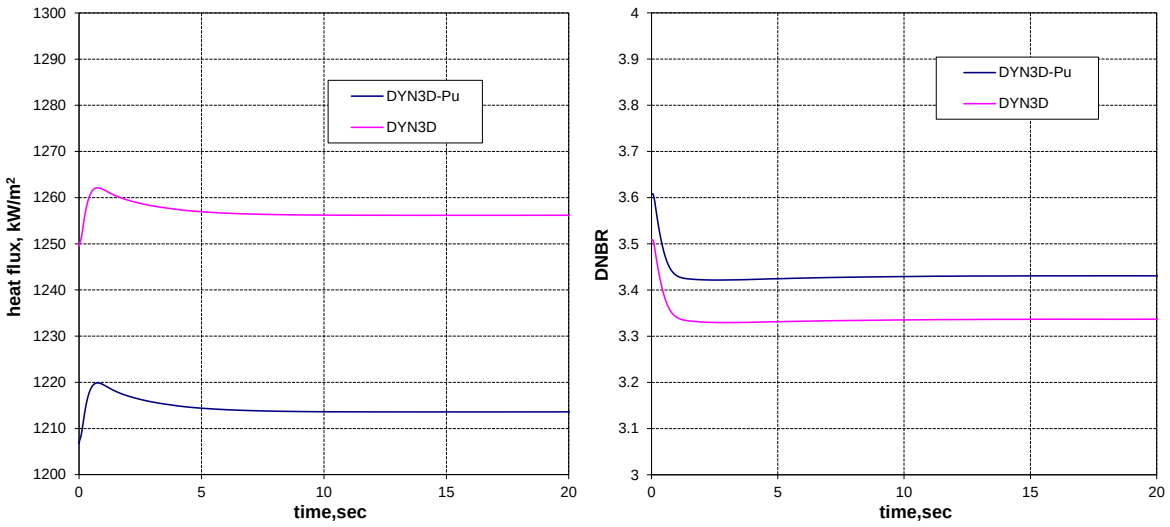

Fig. A.4 Change of heat flux and DNBR during the transient.

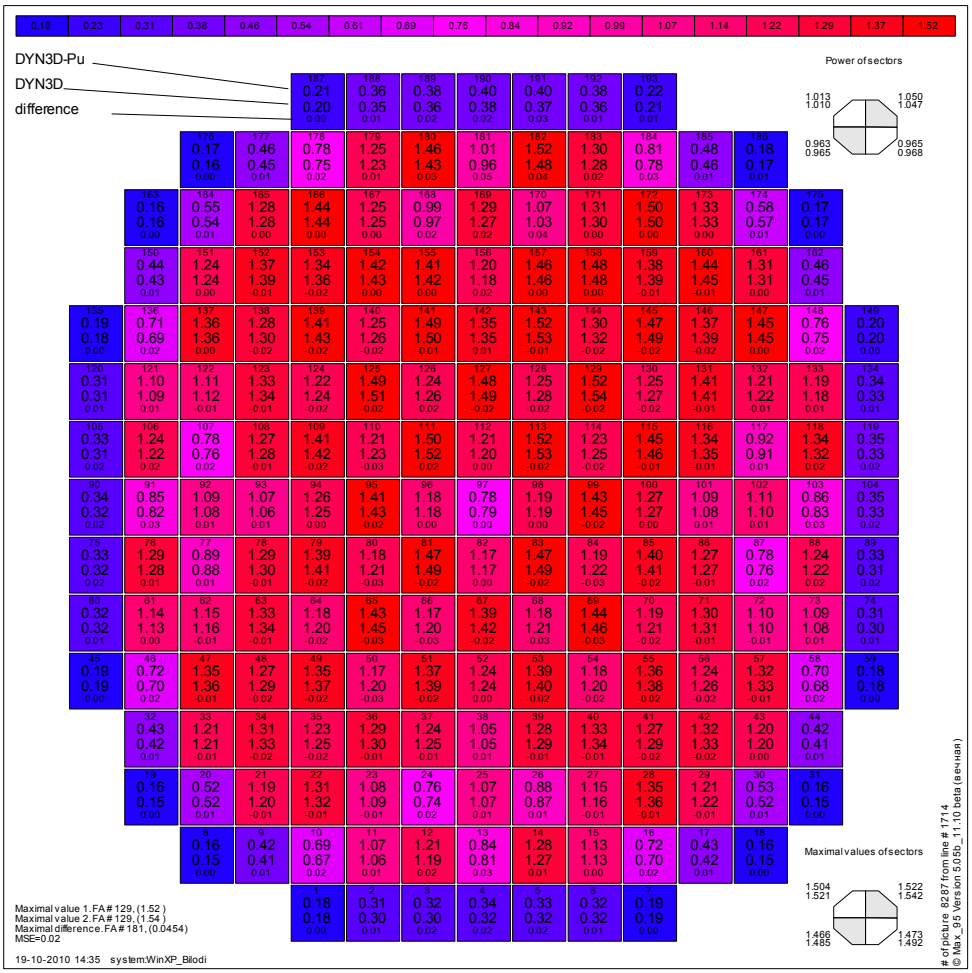

Fig. A.5 Relative power distribution at 0.12 sec.

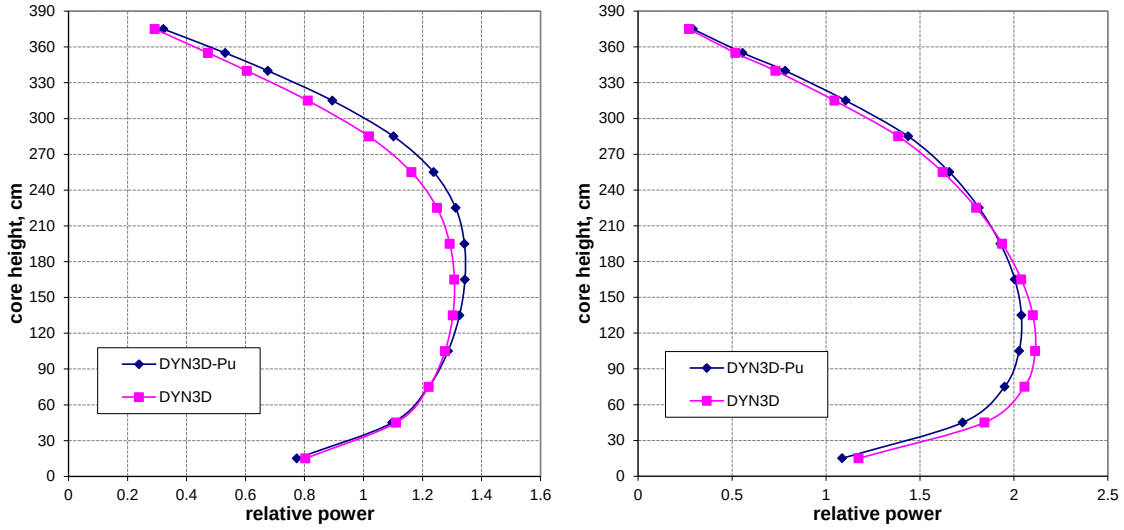

Fig. A.6 Axial power distribution in fuel assembly #170 (left) and assembly #129 (right) at time 0.12 sec.

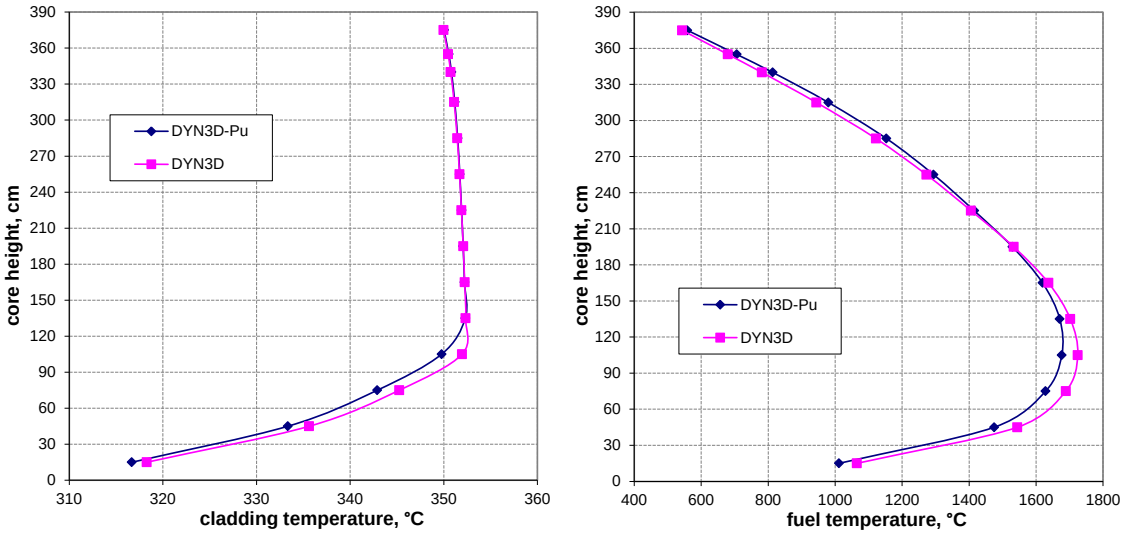

Fig. A.7 Axial fuel and cladding surface temperatures distributions in fuel assembly #113 at time 3.15 sec.

A.2 Case C1 at EOC

Case C1. The initial state

The initial power distribution is illustrated in Fig. A.8. The initial axial power distributions for assemblies #97 and #145 are shown in Fig. A.9.

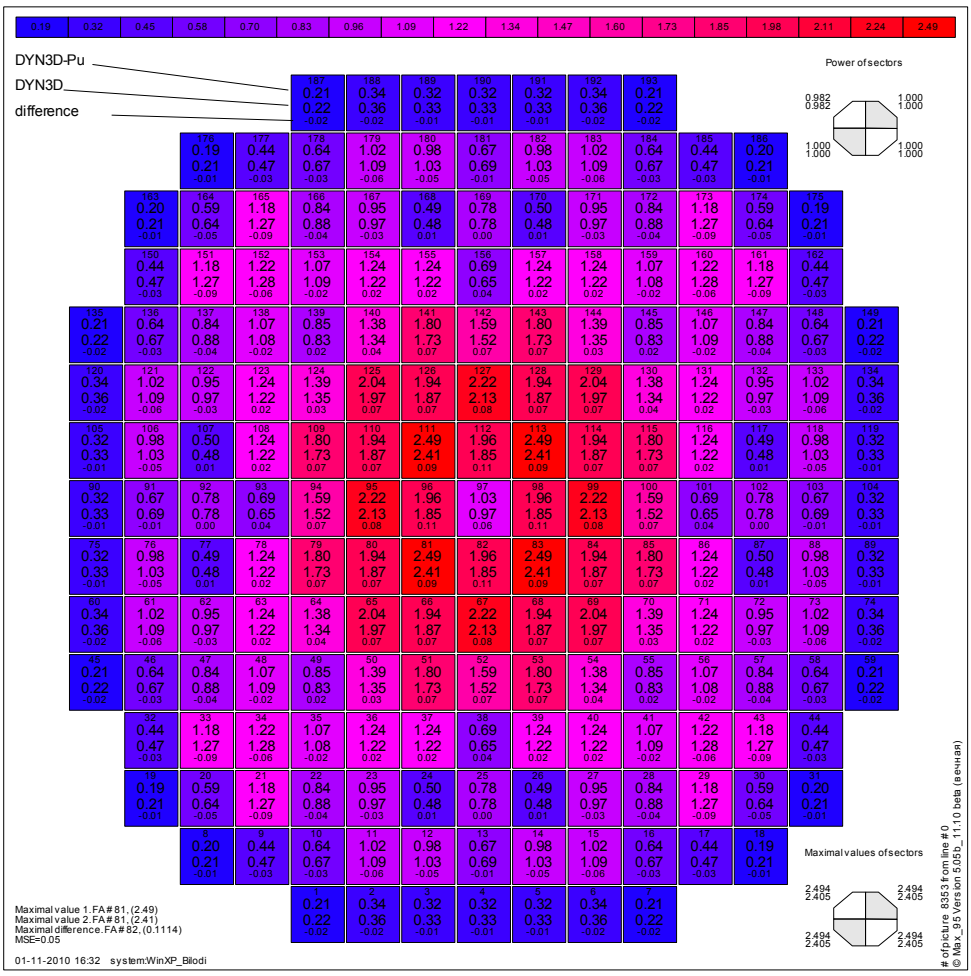

Fig. A.8 Relative power distribution in the initial state at the end of equilibrium cycle.

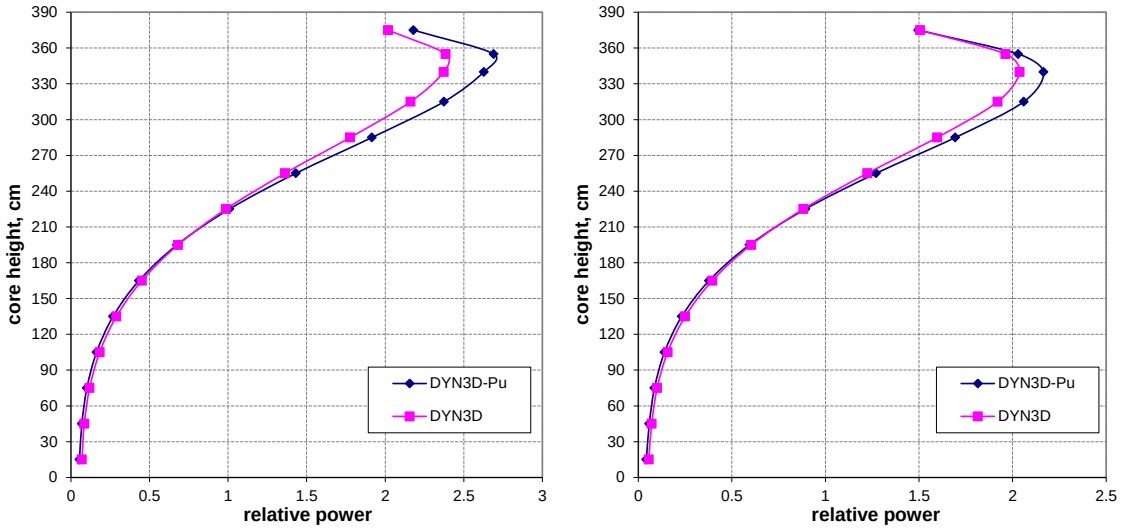

Fig. A.9 Axial power distribution in the central fuel assembly #97 (left) and assembly #145 (right) in the initial state.

Case C1. Central-rod ejection.

Results of control-rod ejection at the hot zero power level at the end of fuel cycle from the central assembly simulation are illustrated in Fig. A.10-A.17 and safety-relevant parameters are summarized in Table 7.4. The course of transient is generally the same as at the beginning of cycle. The reactivity reaches its maximum at the moment ~5 sec, the maximum local power and fuel temperature appear in assembly #81 at the moment 200 sec.

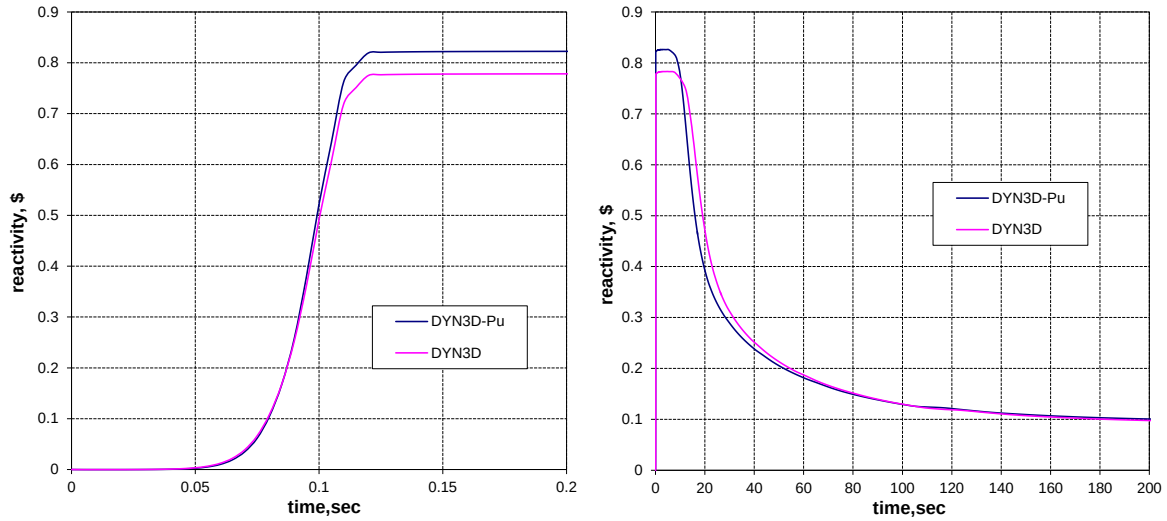

Fig. A.10 Change of reactivity during the transient.

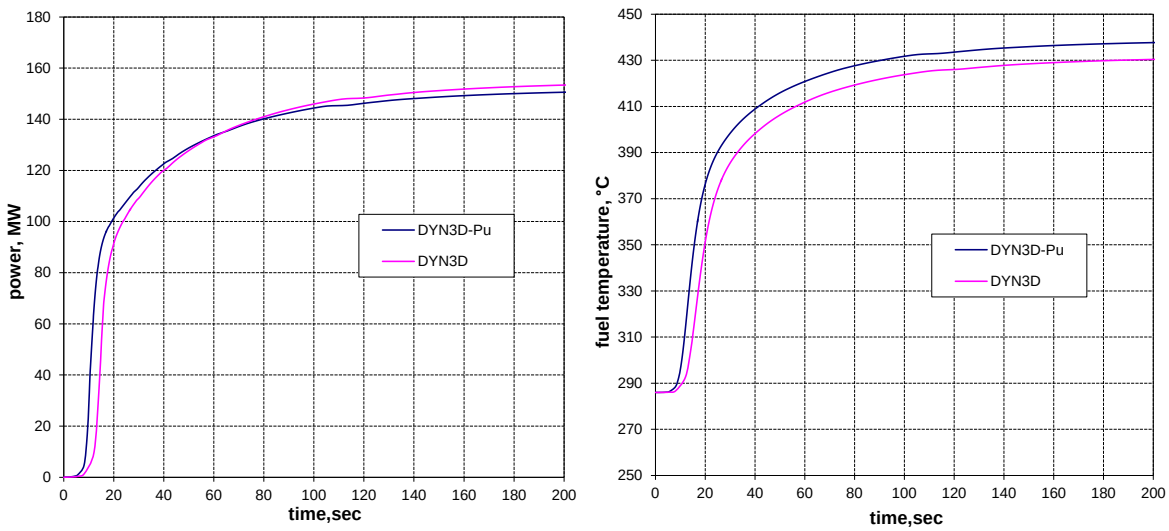

Fig. A.11 Change of reactor power and maximum fuel centre line temperature during the transient.

The maximum value of fuel temperature during the transient is shown in Fig. A.11, while maximum values of heat flux and cladding temperature are in Fig. A.12.

The radial power distribution at the moment 5.0 sec (reactivity maximum) is shown in Fig. A.13 and at 200 sec (power maximum) – in Fig. A.15.

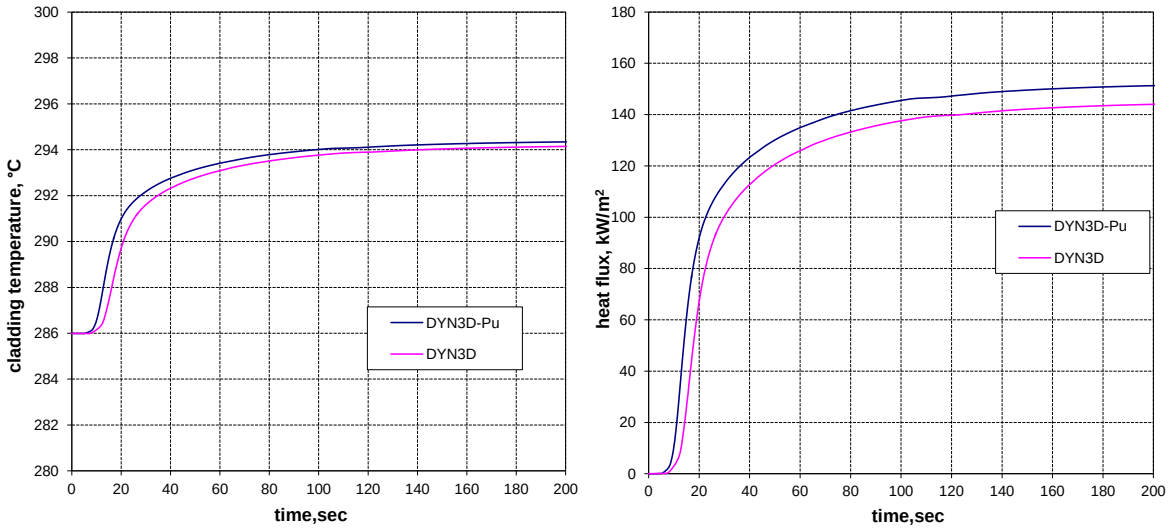

Fig. A.12 Change of maximum cladding temperature and heat flux during the transient.

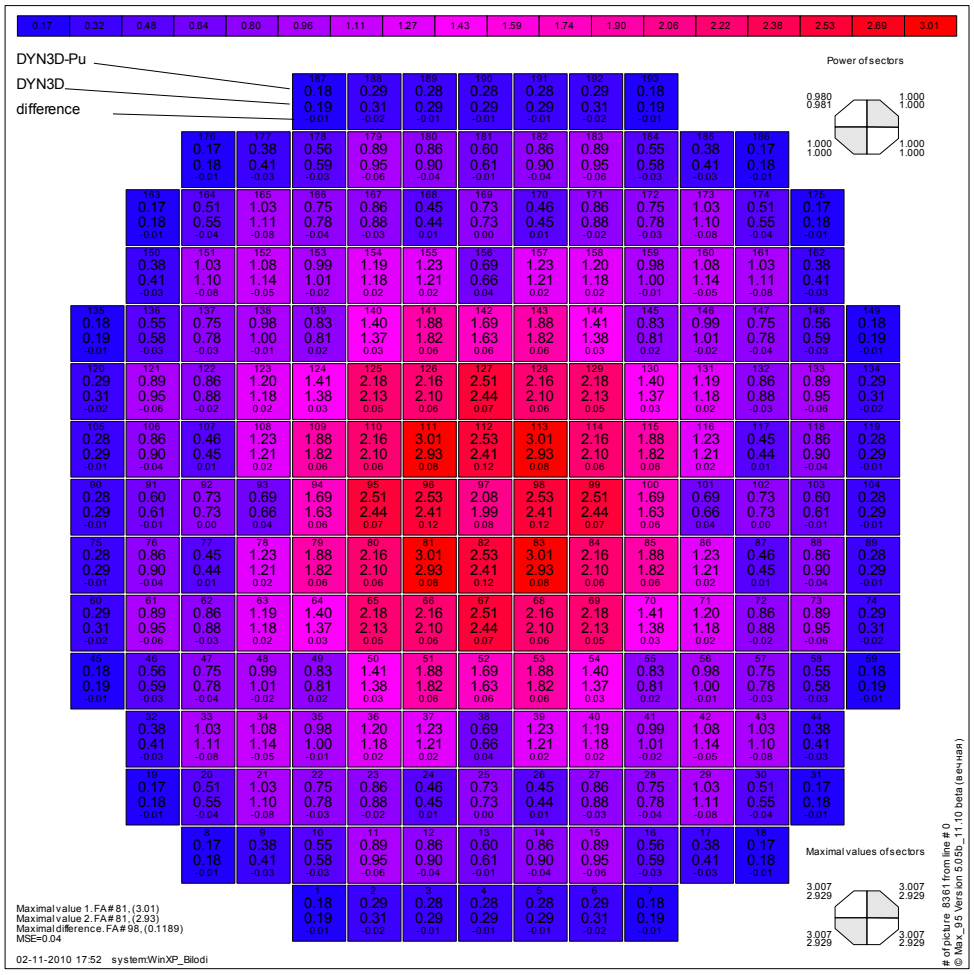

Fig. A.13 Relative power distribution at 5.0 sec.

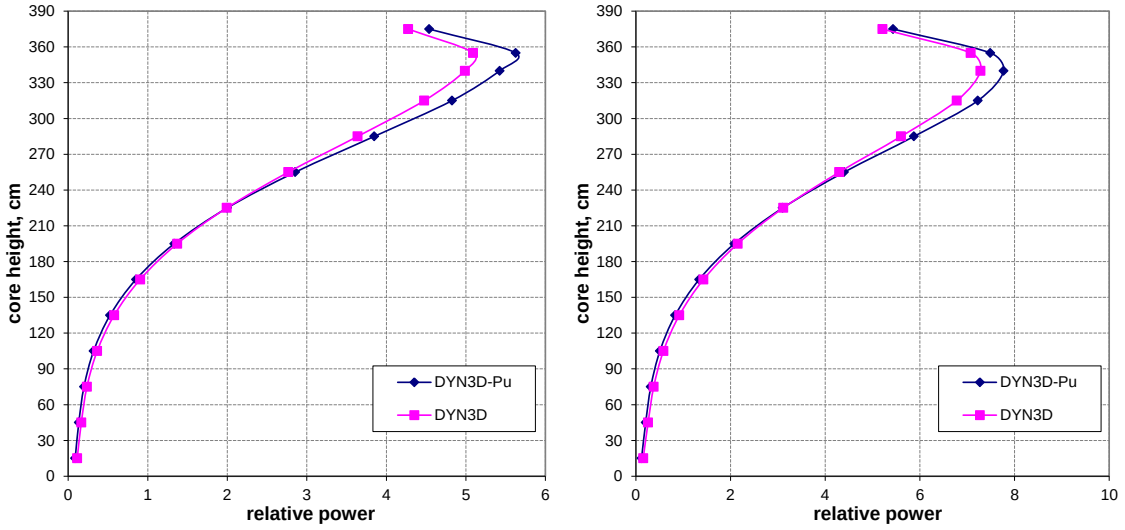

Fig. A.14 Axial power distribution in the central fuel assembly #97 (left) and assembly #81 (right) at time 5.0 sec.

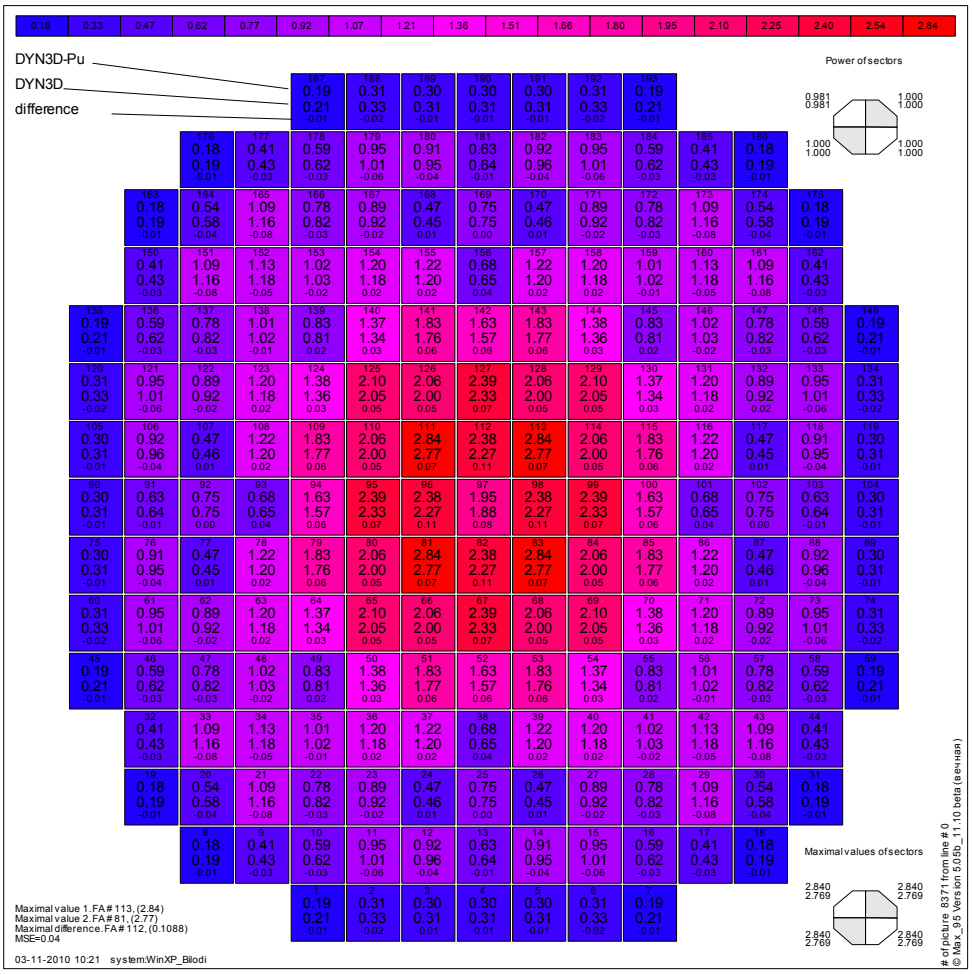

Fig. A.15 Relative power distribution at 200.0 sec. Comparison between DYN3D-Pu and DYN3D.

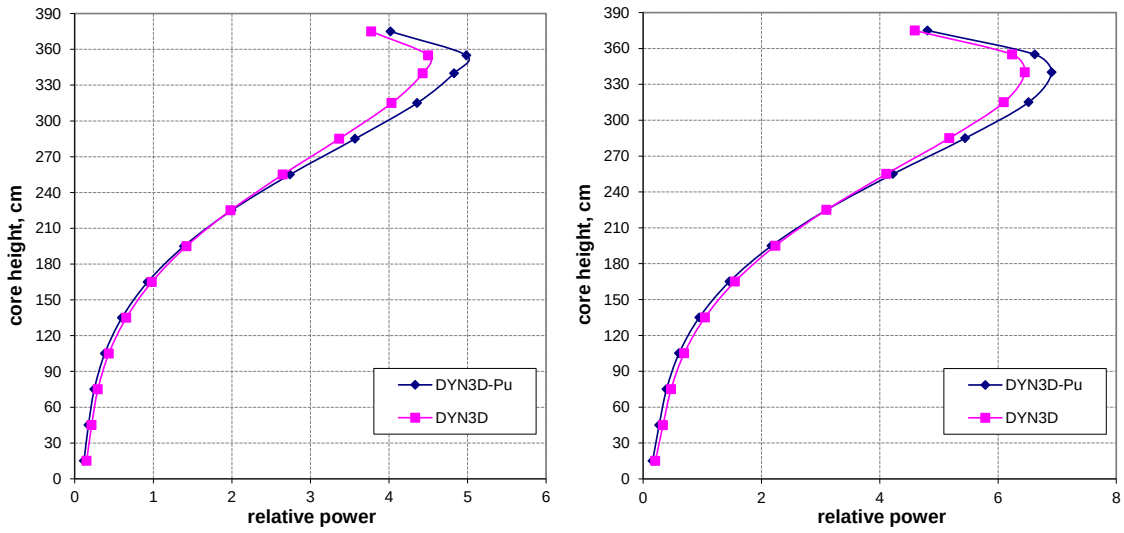

Fig. A.16 Axial power distribution in the central fuel assembly #97 (left) and assembly #81 (right) at time 200.0 sec.

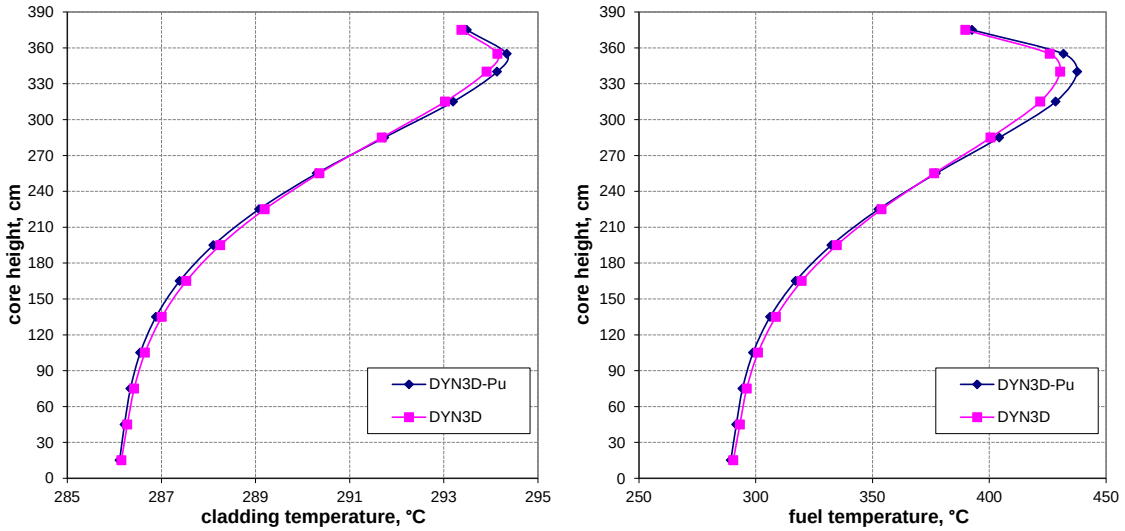

Fig. A.17 Axial fuel and cladding surface temperature distributions in fuel assembly #81 at time 200 sec.

Case C1. Periphery-rod ejection.

Results of control-rod ejection at the hot zero power level at the end of fuel cycle from a periphery assembly are illustrated in Fig. A.18-A.25 and safety-relevant parameters are summarized in Table 7.10. The reactivity reaches its maximum at the moment ~7 sec, the maximum local power and fuel temperature appear in assembly #129 at the moment 200 sec.

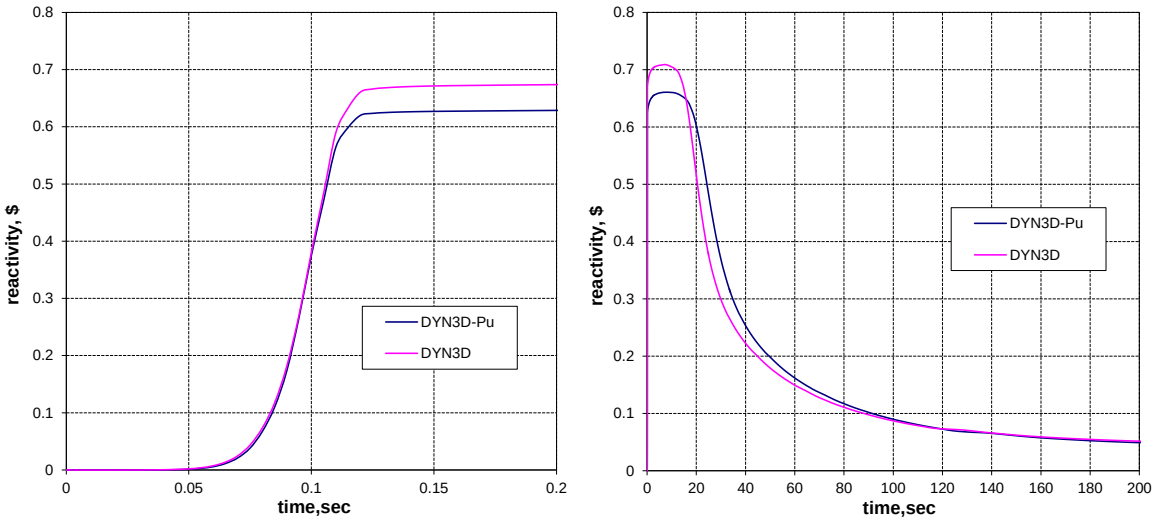

Fig. A.18 Change of reactivity during the transient.

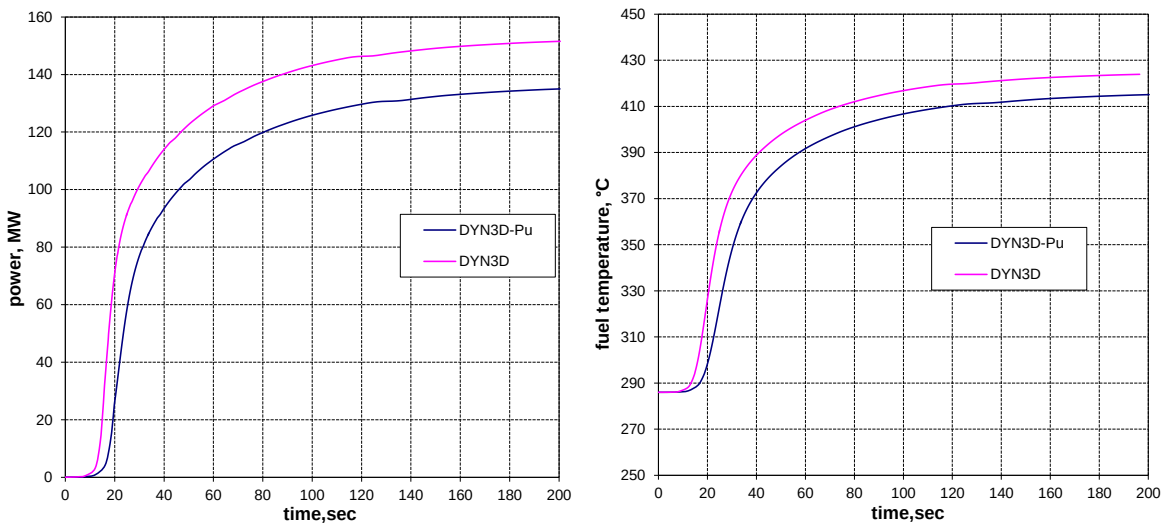

Fig. A.19 Change of reactor power and maximum fuel center line temperature during the transient.

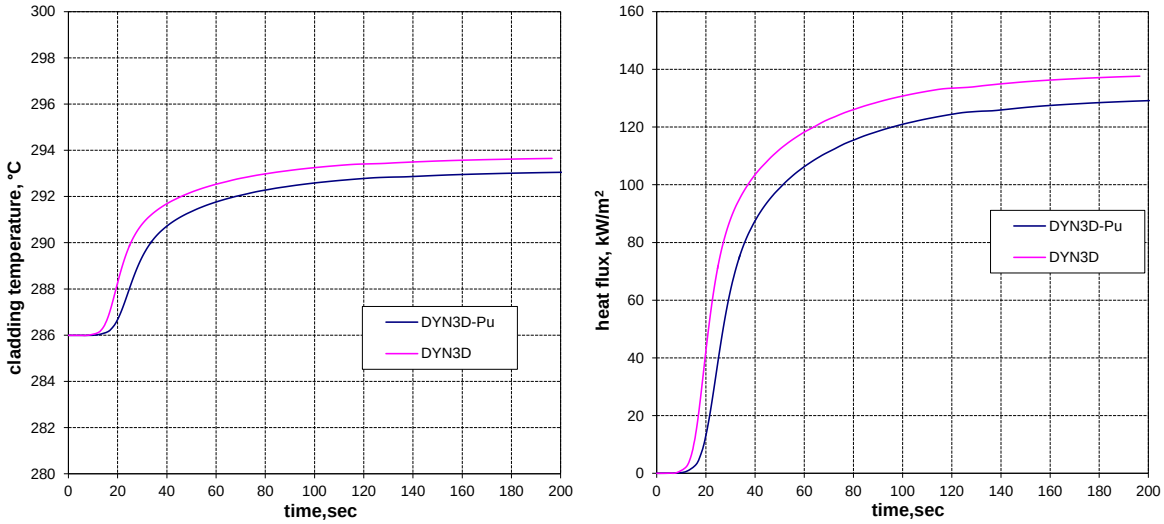

Fig. A.20 Change of maximum cladding temperature and heat flux during the transient.

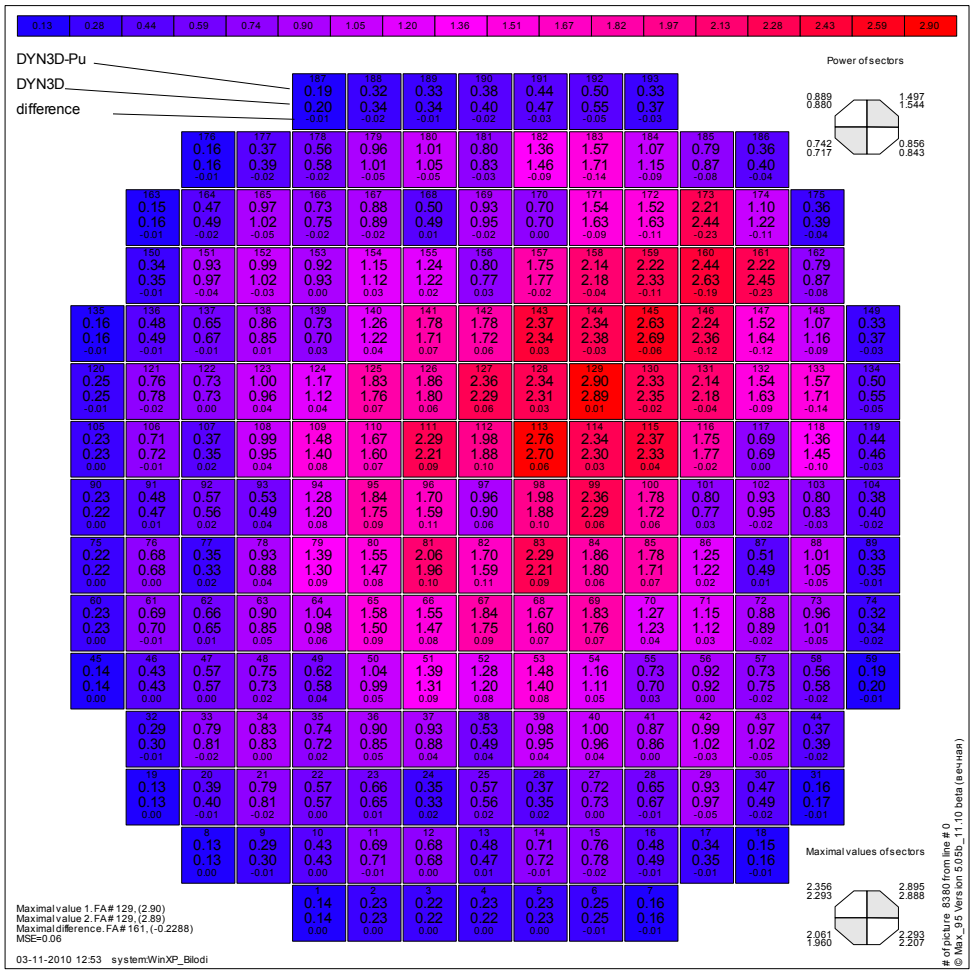

Fig. A.21 Relative power distribution at 7.0 sec.

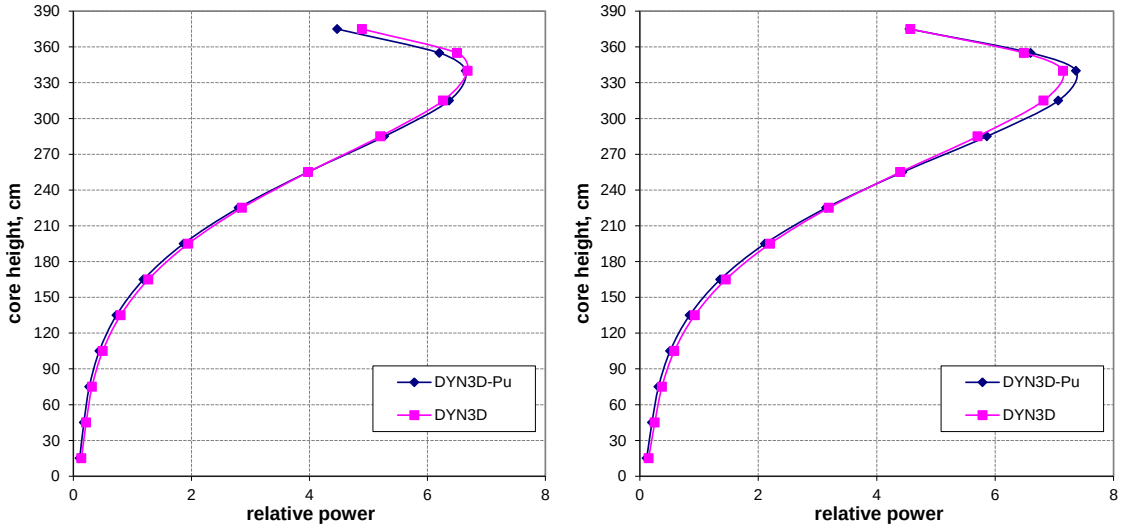

Fig. A.22 Axial power distribution in the assembly #145 (left) and assembly #129 (right) at time 7.0 sec.

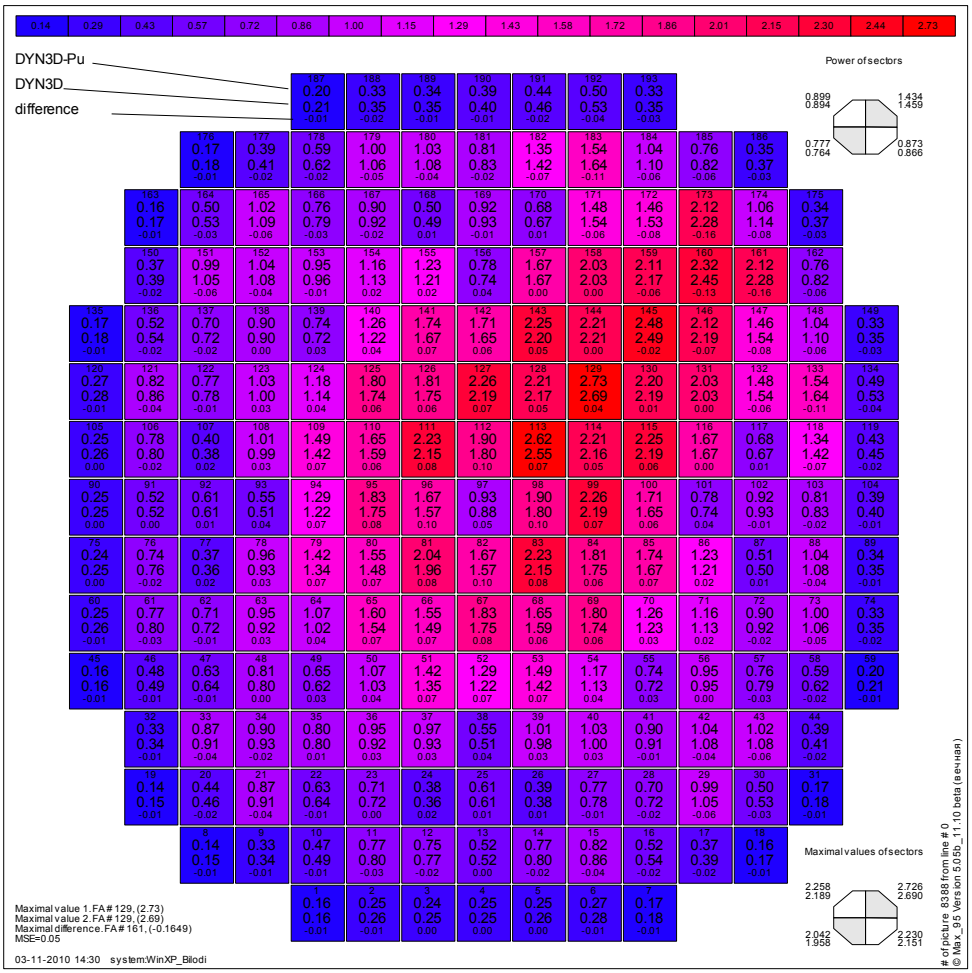

Fig. A.23 Relative power distribution at 200.0 sec.

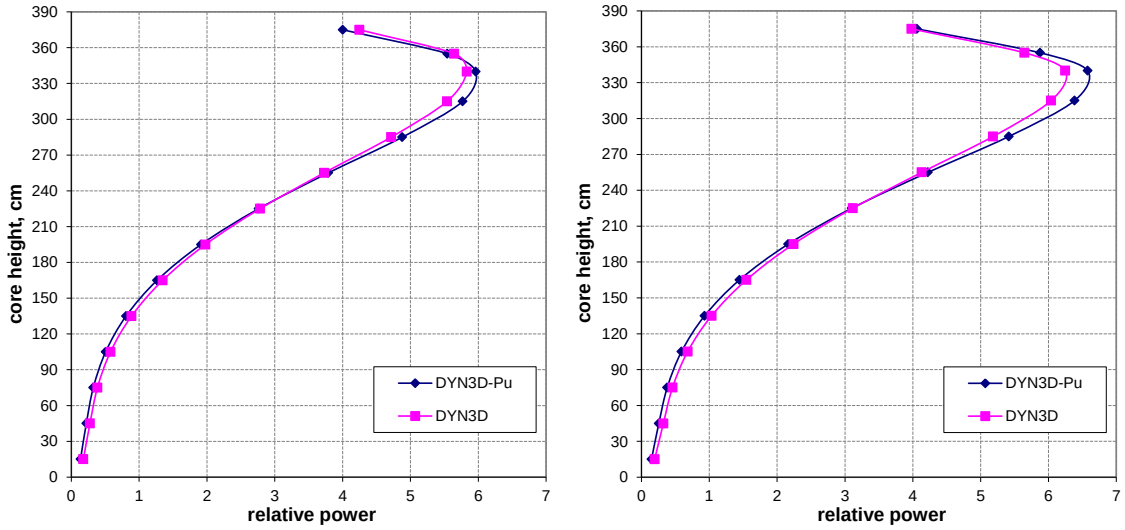

Fig. A.24 Axial power distribution in the assembly #145 (left) and assembly #129 (right) at time 200.0 sec.

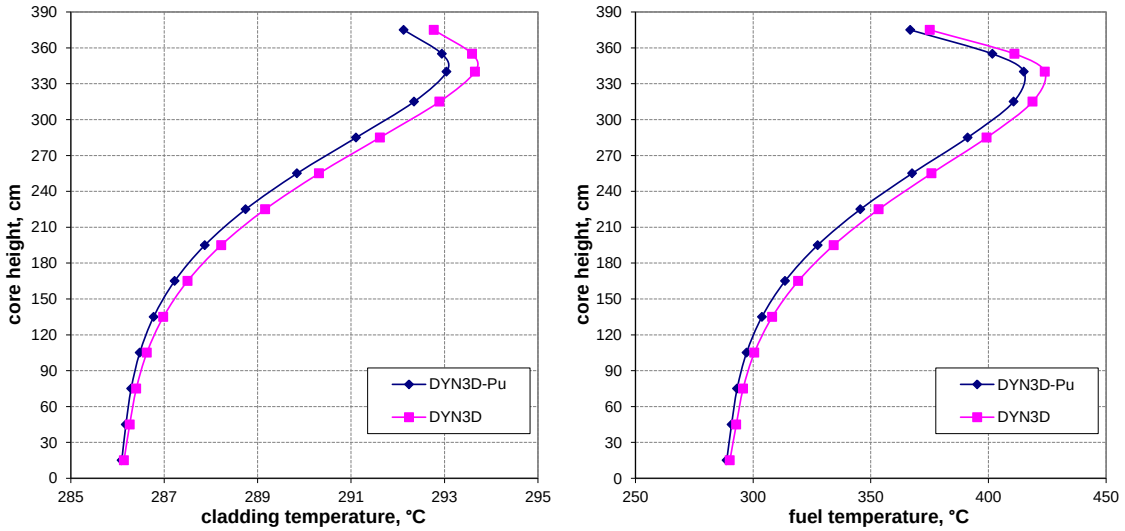

Fig. A.25 Axial fuel and cladding surface temperature distributions in fuel assembly #129 at time 200 sec.

A.3 Case C2 at EOC

Case C2. The initial state

The initial power distribution is illustrated in Fig. A.26. The initial axial power distributions for assemblies #97 and #170 are shown in Fig. A.27.

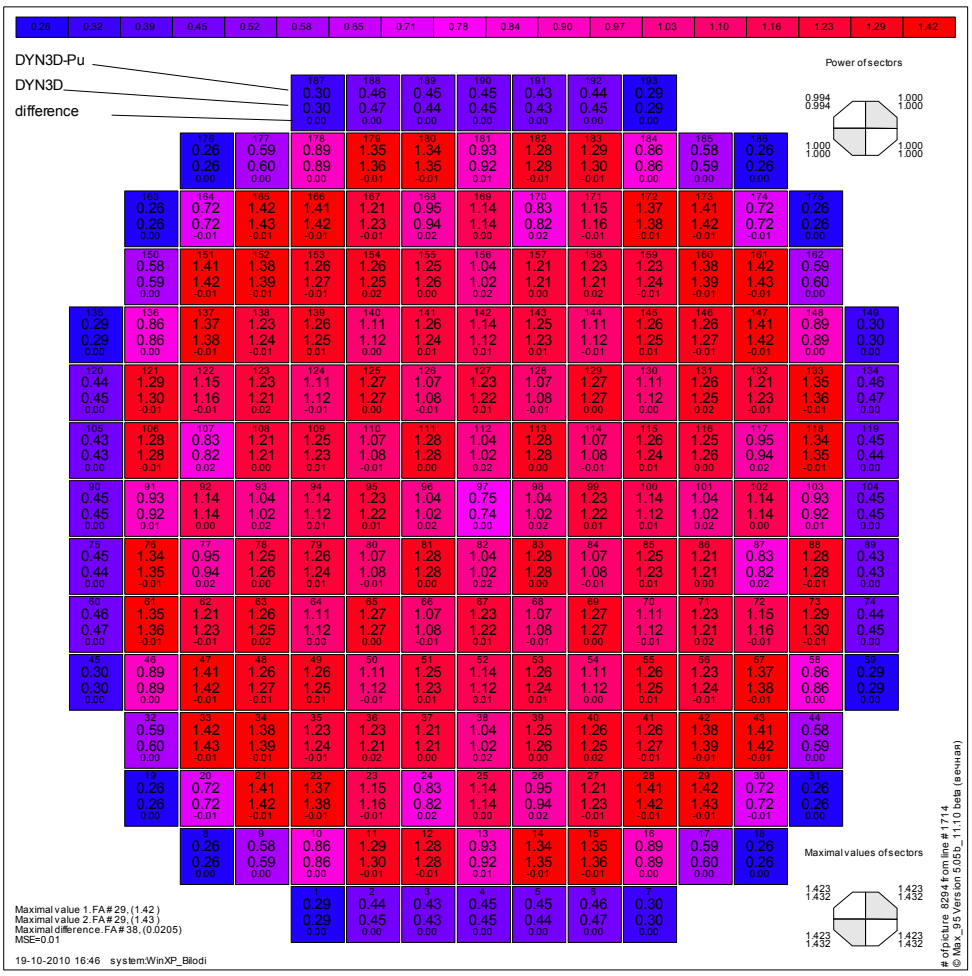

Fig. A.26 Relative power distribution in the initial state at the end of equilibrium cycle.

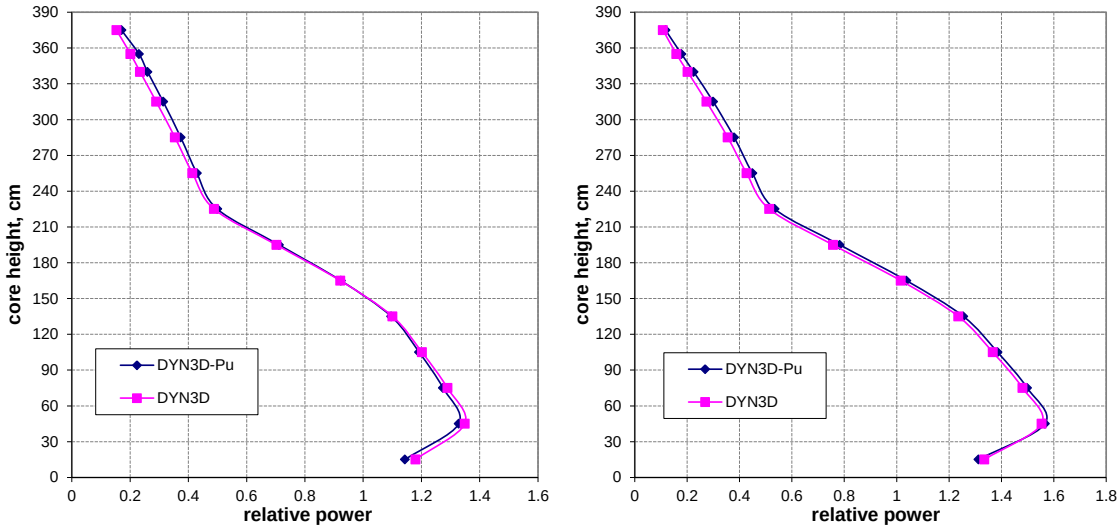

Fig. A.27 Axial power distribution in the central fuel assembly #97 (left) and assembly #170 in the initial state.

Case C2. Central-rod ejection.

Simulation results of control-rod ejection at the full power level at the end of fuel cycle from the central assembly are illustrated in Fig. A.28-A.34 and safety-relevant parameters are summarized in Table 7.9. The course of transient is generally the same as at the beginning of cycle. The maximum local power appears in assembly #29 at the moment 0.12 sec and the maximum fuel temperature – in assembly #29 at the moment 1.77 sec.

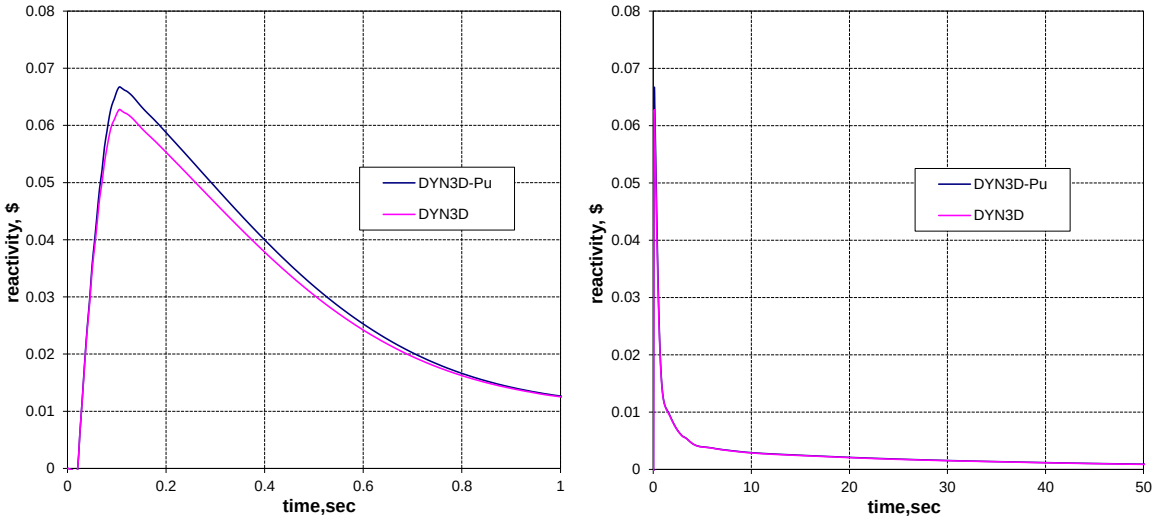

Fig. A.28 Change of reactivity during the transient.

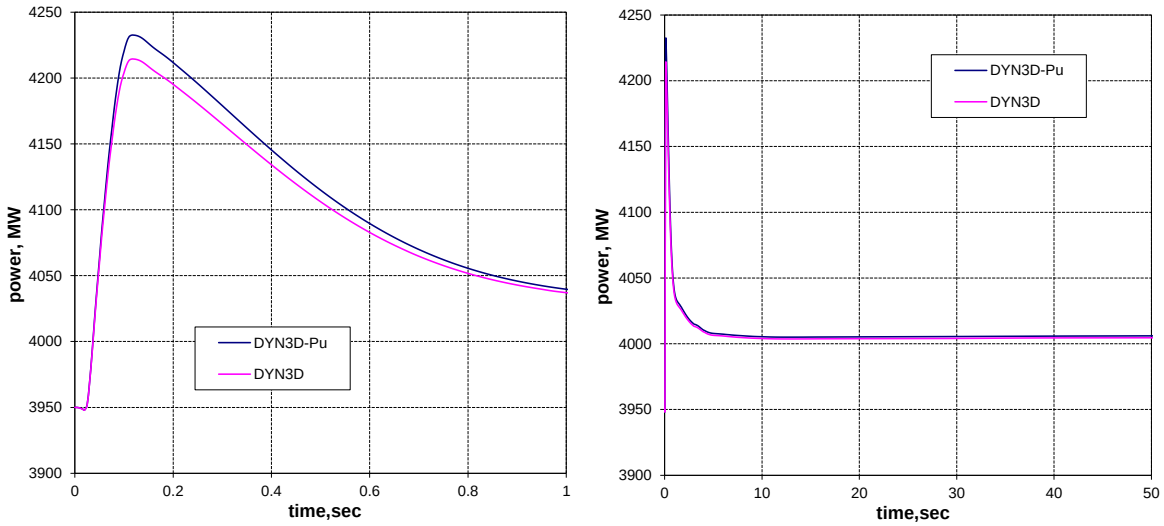

Fig. A.29 Change of reactor power during the transient.

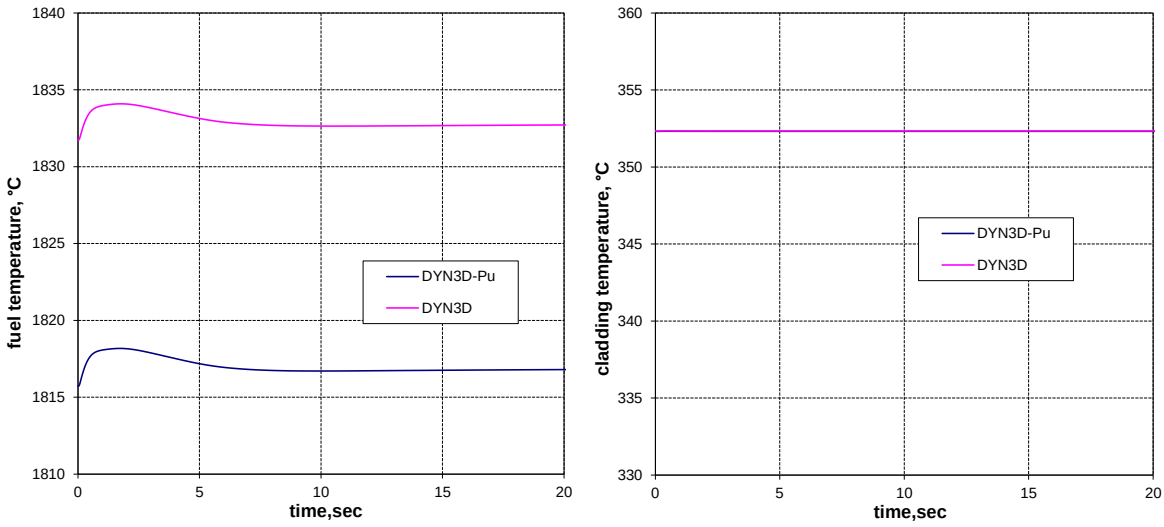

Fig. A.30 Change of fuel center line and cladding temperatures during the transient.

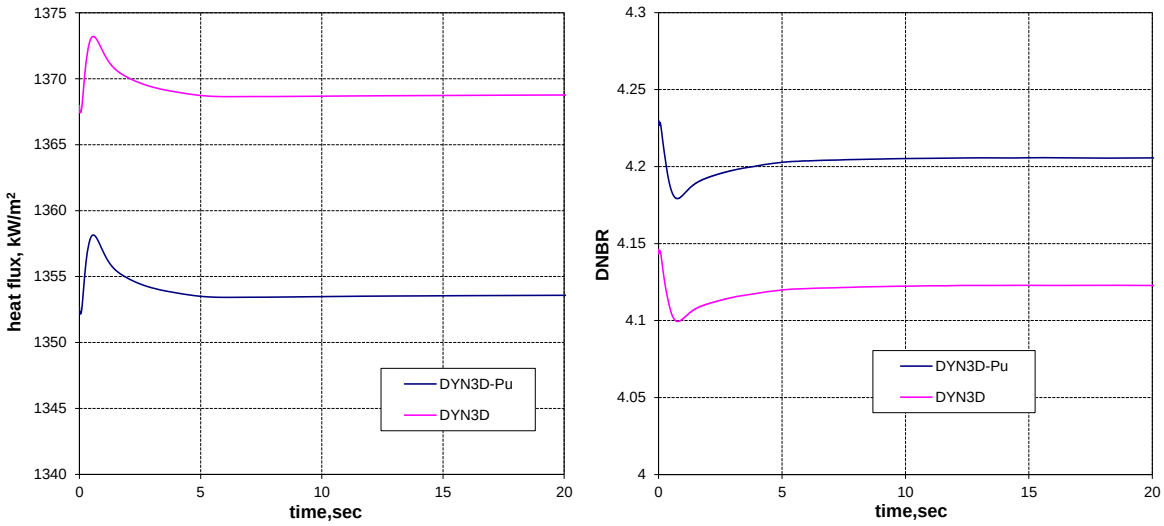

Fig. A.31 Change of heat flux and DNBR during the transient.

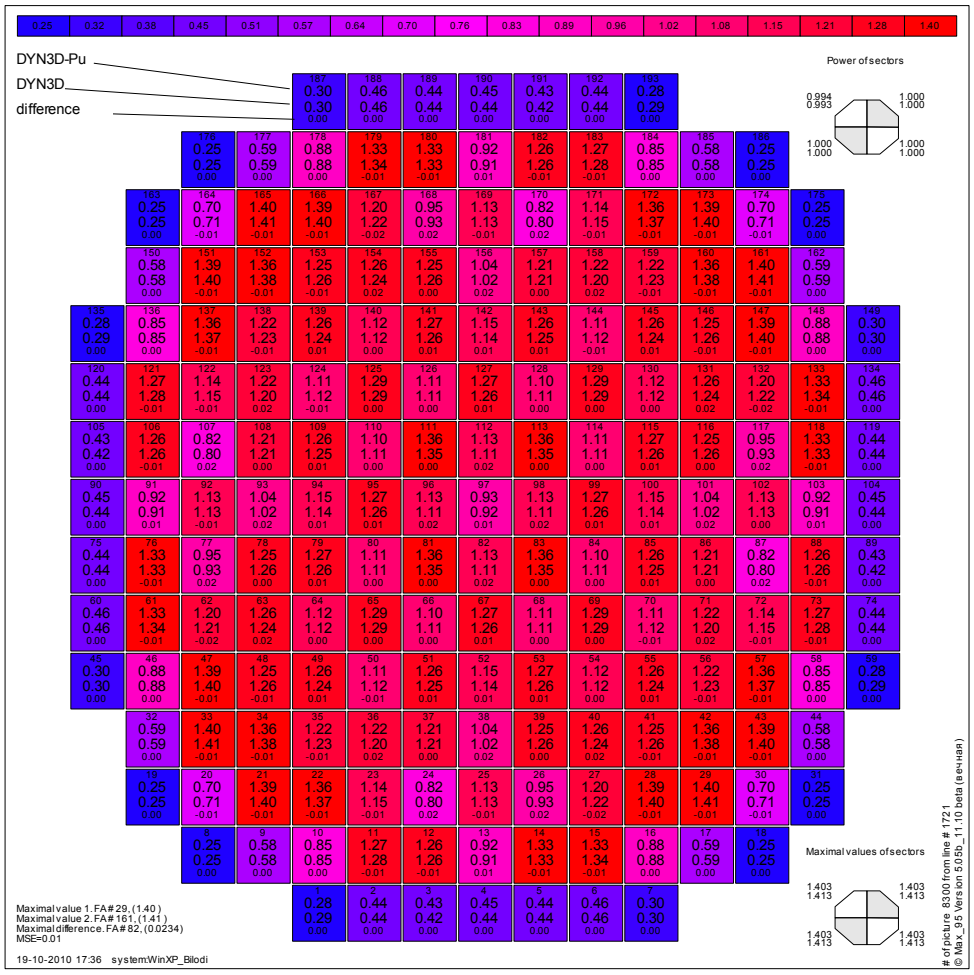

Fig. A.32 Relative power distribution at 0.12 sec.

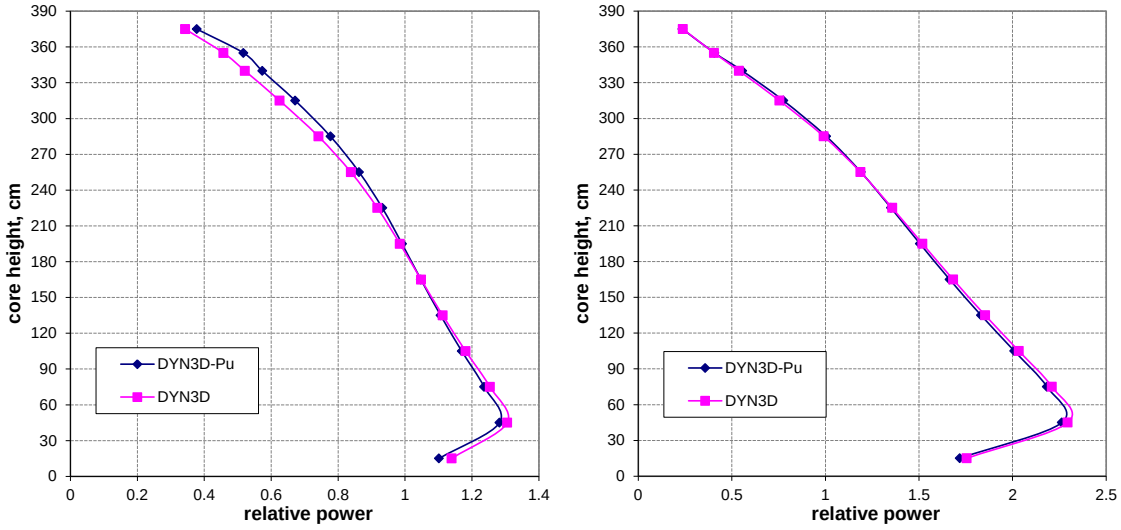

Fig. A.33 Axial power distribution in the central fuel assembly #97 (left) and assembly #29 (right) at time 0.12 sec.

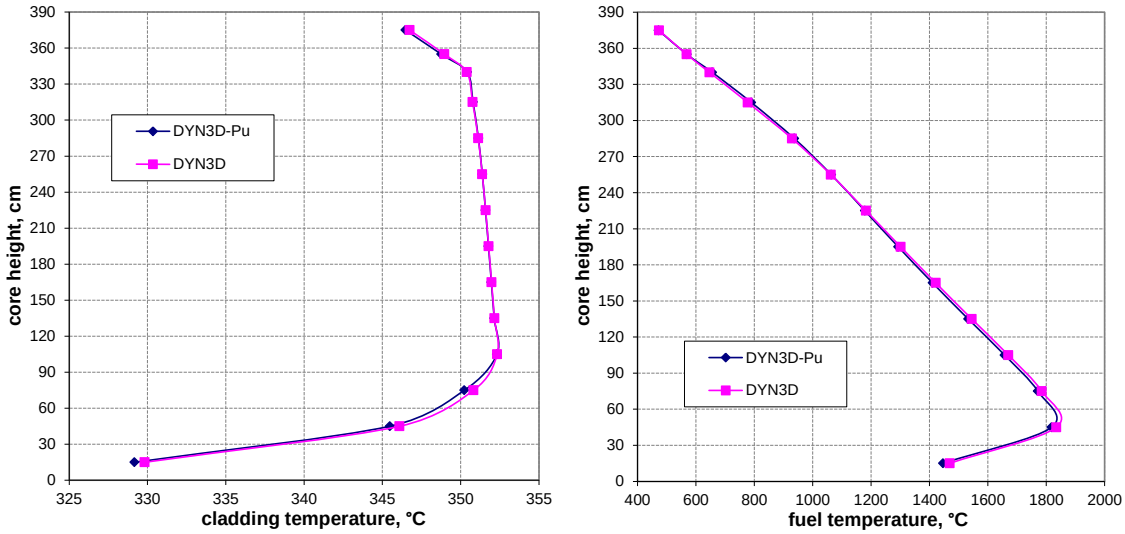

Fig. A.34 Axial fuel and cladding surface temperatures distributions in fuel assembly #29 at time 1.77 sec.

Case C2. Periphery-rod ejection.

Results of control-rod ejection at the full power level at the end of fuel cycle from a periphery assembly are illustrated in Fig. A.35-A.41 and safety-relevant parameters are summarized in Table 7.10. The maximum local power appears in assembly #182 at the moment 0.12 sec and the maximum fuel temperature – in assembly #161 at the moment 2.3 sec.

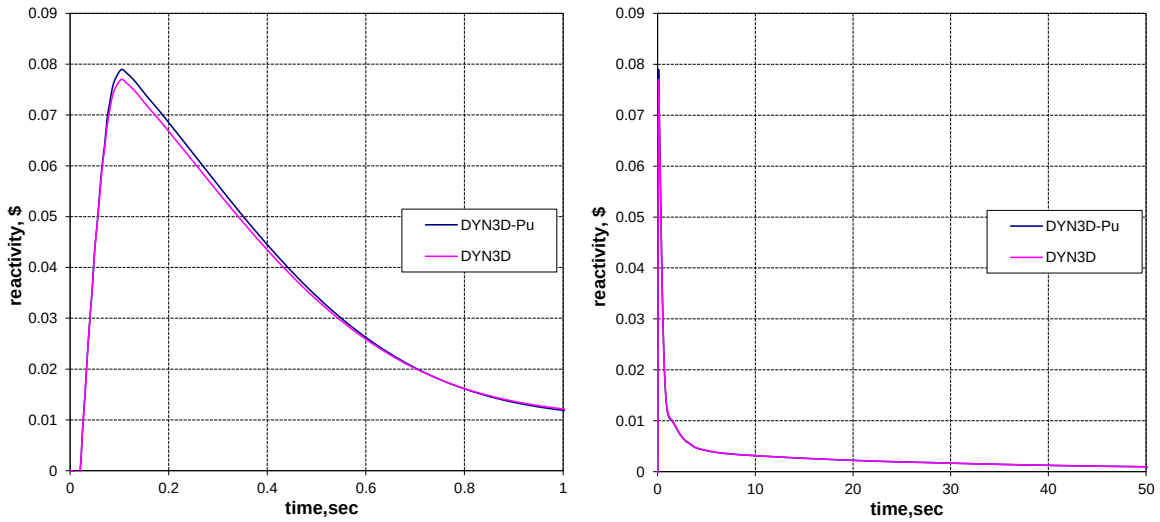

Fig. A.35 Change of reactivity during the transient.

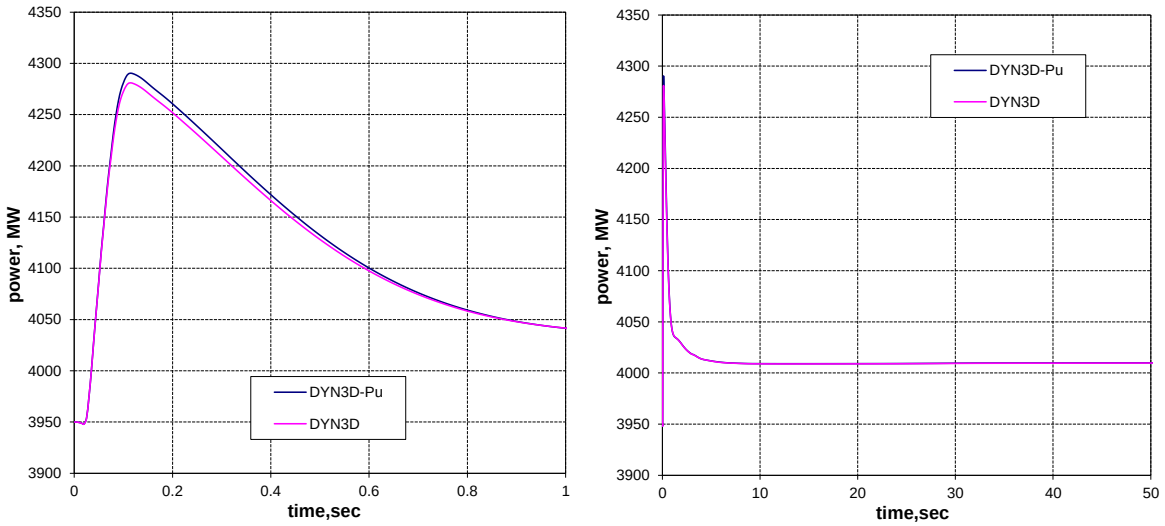

Fig. A.36 Change of reactor power during the transient.

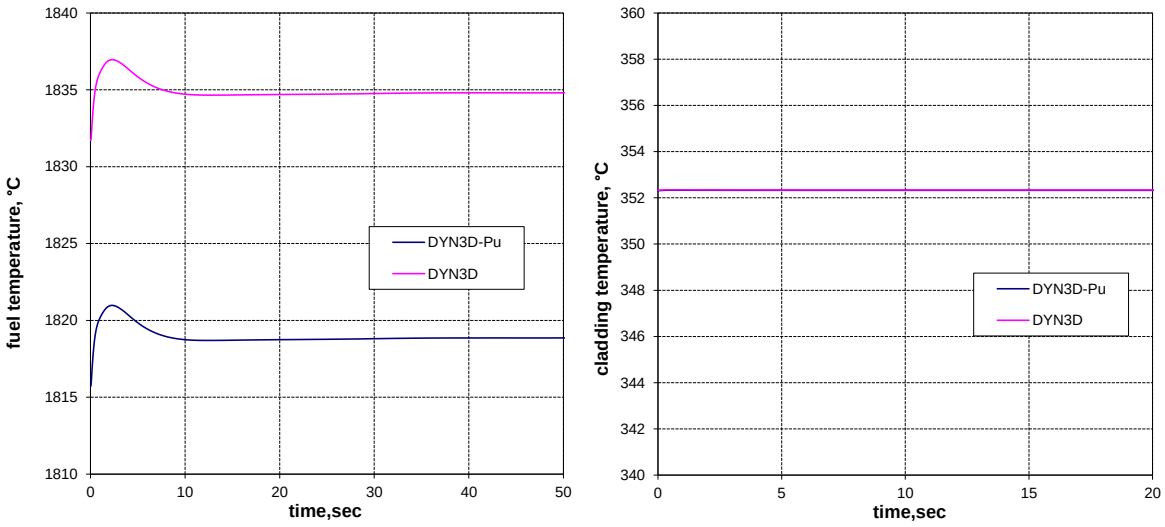

Fig. A.37 Change of fuel centre line and cladding temperatures during the transient.

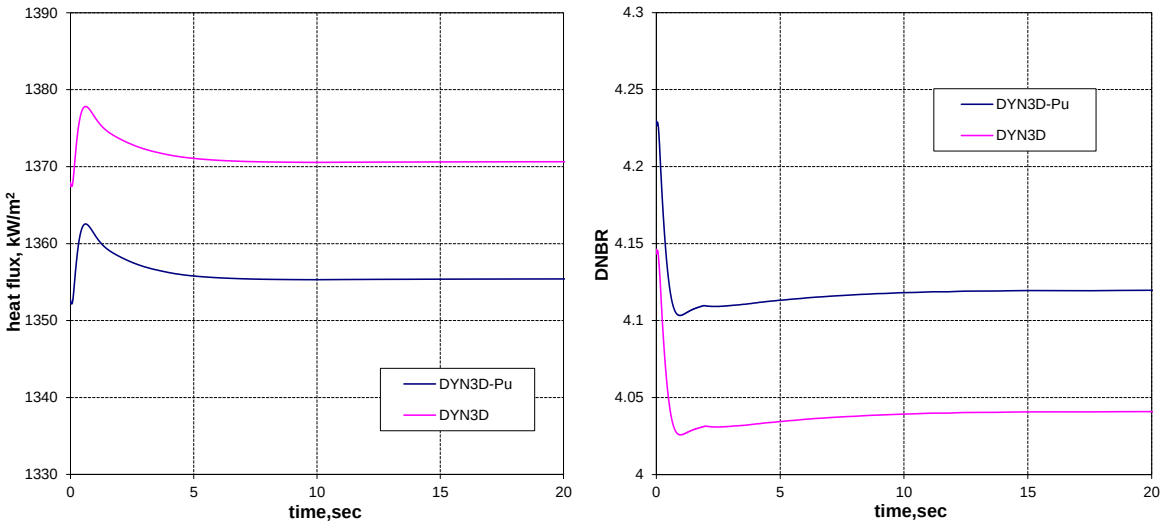

Fig. A.38 Change of heat flux and DNBR during the transient.

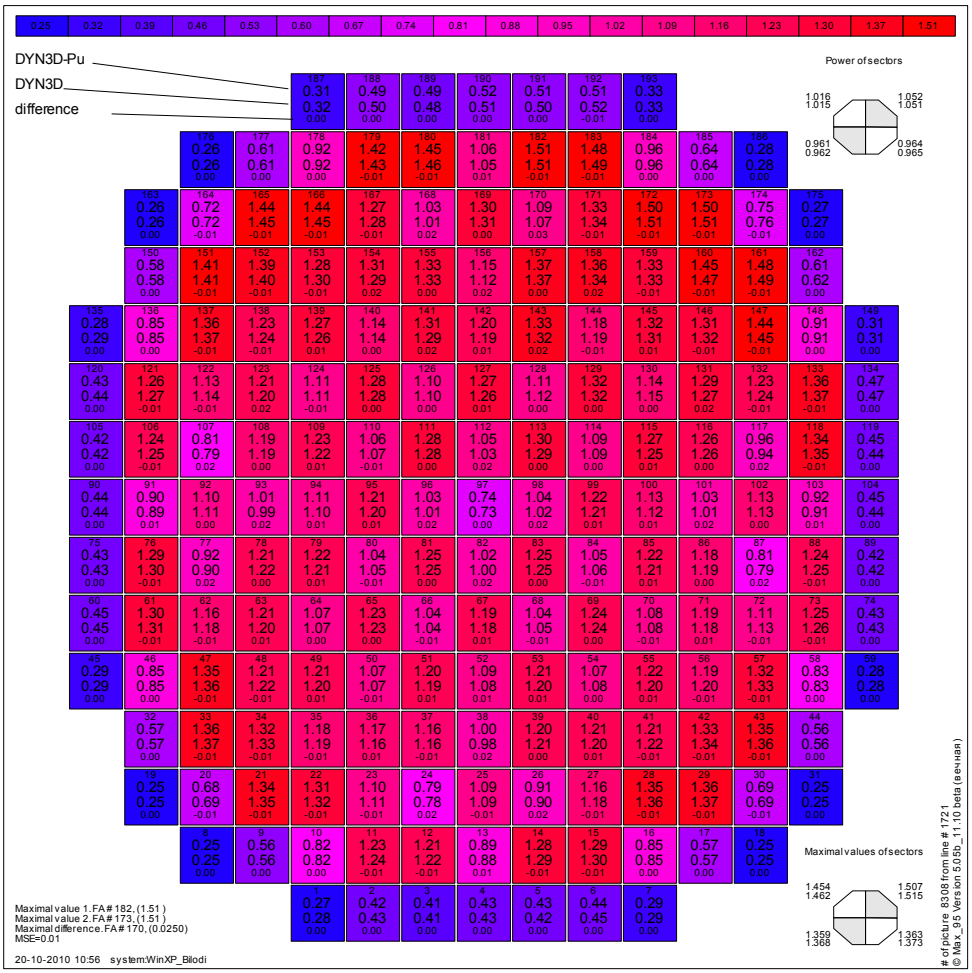

Fig. A.39 Relative power distribution at 0.12 sec.

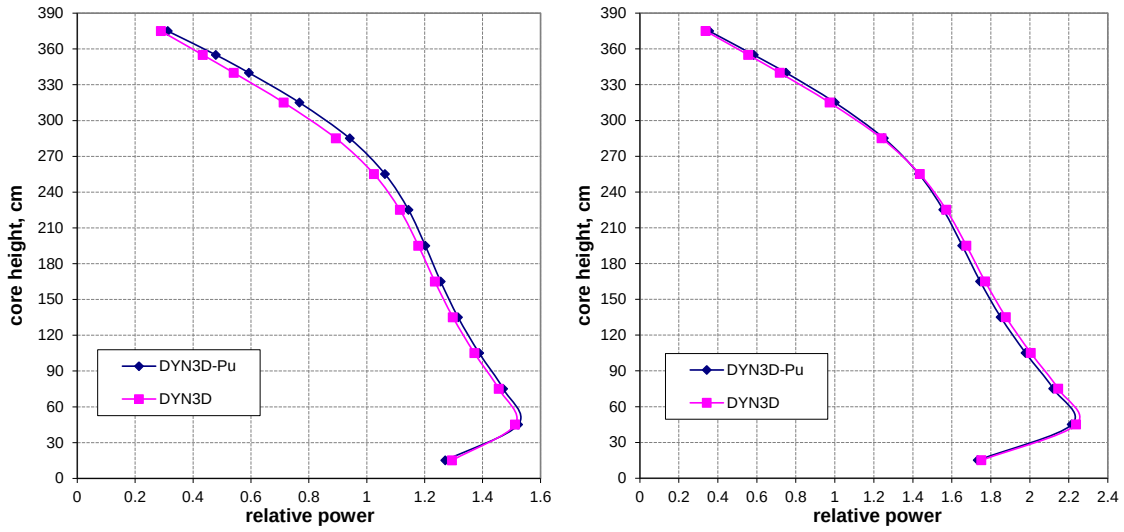

Fig. A.40 Axial power distribution in fuel assembly #170 (left) and assembly #182 (right) at time 0.12 sec.

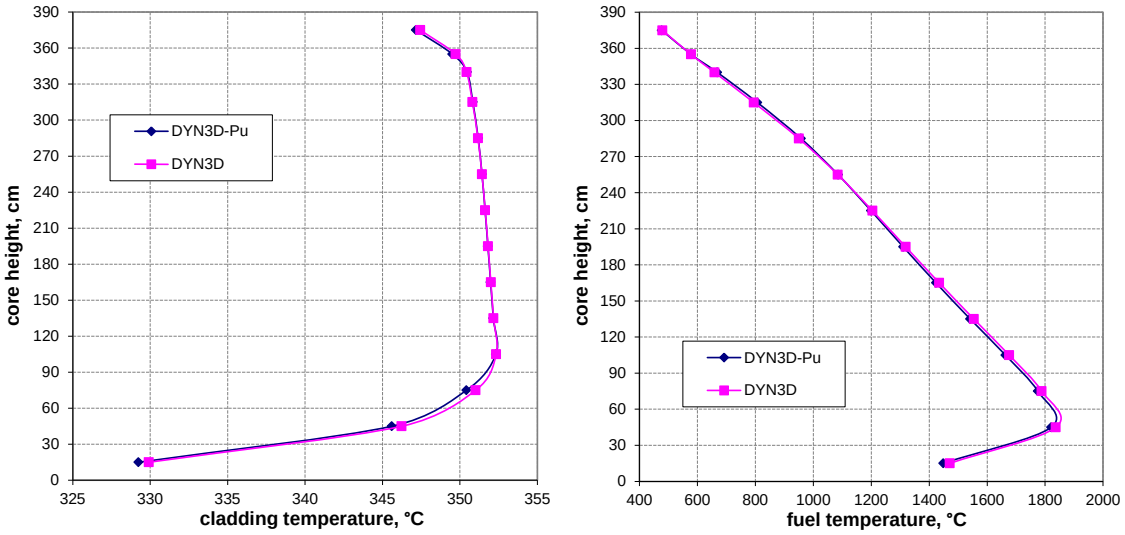

Fig. A.41 Axial fuel and cladding surface temperatures distributions in fuel assembly #161 at time 2.30 sec.

Acknowledgments

First of all I would like to express sincere thanks to my supervisors Dr. Siegfried Mittag for scientific support, discussions and ideas.

I am deeply grateful to my scientific adviser Prof. Dr. Frank-Peter Weiß for valuable advices and numerous important corrections to my work. I wish to thank Prof. Dr. Antonio Hurtado for the review and friendly support, Dr. Ulrich Rohde and Dr. Sören Klim for very helpful and valuable comments.

I am very thankful to my colleges from SSTC NRS, Kyiv and especially to Dr. Volodymyr Khalimonchuk and Alexander Kuchin, who have encouraged me to make PhD in Rossendorf.

I would like to thank all colleges from Reactor Safety department who made my work in Rossendorf very comfortable and interesting. Special thanks to Dr. Polina Tusheva, Dr. Susan Dürigen, Andre Gommlich, Torsten Berger, Dr. Emil Fridman, Evgeny Nikitin, Dr. Roland Rzehak and Daniela Baldova for our everyday little talks at lunch time.

Many thanks to my climbing and skiing friends for great time we spent together outdoors.

Finally, I want to thanks my family for continuous support and especially my wife Valentyna, who bring love and sense to everyday life and all what I am doing.

HZDR
HELMHOLTZ ZENTRUM DRESDEN ROSSENDORF

Bautzner Landstr. 400
01328 Dresden, Germany
Tel. +49 351 260-2020
Fax +49 351 260-12020
y.bilodid@hzdr.de
http://www.hzdr.de